University of Bath

PHD

Mechanical properties of clay and fibre reinforced clay-based ceramics

Papargyris, Athanasios D.

Award date:
1994

Awarding institution:
University of Bath

Link to publication

Alternative formats
If you require this document in an alternative format, please contact:
openaccess@bath.ac.uk

Copyright of this thesis rests with the author. Access is subject to the above licence, if given. If no licence is specified above, original content in this thesis is licensed under the terms of the Creative Commons Attribution-NonCommercial 4.0 International (CC BY-NC-ND 4.0) Licence (https://creativecommons.org/licenses/by-nc-nd/4.0/). Any third-party copyright material present remains the property of its respective owner(s) and is licensed under its existing terms.

Take down policy
If you consider content within Bath's Research Portal to be in breach of UK law, please contact: openaccess@bath.ac.uk with the details. Your claim will be investigated and, where appropriate, the item will be removed from public view as soon as possible.

Download date: 04. May. 2023

MECHANICAL PROPERTIES OF CLAY AND FIBRE REINFORCED CLAY-BASED CERAMICS

submitted by
ATHANASIOS D. PAPARGYRIS
BSc, M.Sc

for the Degree of PhD
of the University of Bath
1994

COPYRIGHT

Attention is drawn to the fact that copyright of this thesis rests with its author. This copy of the thesis has been supplied on the condition that anyone who consults it is understood to recognise that its copyright rests with its author and that no quotation from the thesis and no information derived from it may be published without the prior written consent of the author.
This thesis may be made available for consultation within the University Library and may be photocopied or lend to other libraries for the purposes of consultation

Signed

Athanasios D. Papargyris

UMI Number: U064437

All rights reserved

INFORMATION TO ALL USERS
The quality of this reproduction is dependent upon the quality of the copy submitted.

In the unlikely event that the author did not send a complete manuscript
and there are missing pages, these will be noted. Also, if material had to be removed,
a note will indicate the deletion.

UMI U064437
Published by ProQuest LLC 2013. Copyright in the Dissertation held by the Author.
Microform Edition © ProQuest LLC.
All rights reserved. This work is protected against
unauthorized copying under Title 17, United States Code.

ProQuest LLC
789 East Eisenhower Parkway
P.O. Box 1346
Ann Arbor, MI 48106-1346

LIBRARY BATH
25 03 MAY 1995
Ph D
5090504

ABSTRACT

The present thesis is the result of research on mechanical properties of heterogeneous polyphase ceramic and ceramic fibre composite systems carried out in the School of Material Science of the University of Bath during the period October 1989 to December 1994 under the supervision of Dr. R.G.Cooke.

A series of experiments, examinations and analyses, including three point bending of notched and un-notched specimens, acoustic emission, dynamic testing of elasticity modulus, thermogravimetry, differential thermal analysis, X-ray diffraction, X-Ray fluorescence, scanning electron and optical microscopy, Weibull and Neville statistical analysis have been conducted on clay, clay-fly ash, pottery mixture and brick-clay heterogeneous ceramics after sintering at various temperatures. In a similar way, a series of clay based fibre composites with fibres such as alpha and delta alumina, mullite and XAS graphite fibres, sintered at different sintering temperatures, have been tested. Some specimens of glass and cement and cement-fly ash composites have also been produced, tested in compression and bending and analysed using the above methods for comparison.

Measurement of MOR (Modulus of Rupture), K_{IC} (Fracture Toughness) and E (Modulus of Elasticity) show them to be material parameters with a close relation to the structure of the ceramics.

Acoustic emission in most of the examined cases shows that subcritical activity (crack growth activity) is present, in the whole ceramic body from the beginning of

the stress application up to the highest values, just before fracture. Generally, acoustic activity increases with increase of sintering temperature and fibre content. The Kaiser effect was evident in all cases except glass, showing that the processes preceding fracture are not the same in all brittle materials. SEM examination shows that the point of fracture initiation is not evident in most of the cases and any point could equally be responsible for it. SEM examination shows also that the fibre-matrix interface plays a fundamental role in fracture processes and mechanical properties of fibre-ceramic composites.

Investigation on the statistical distribution of MOR and K_{IC} values of the above ceramic systems, by using Weibull two and three parameter functions and Neville two parameter function , show that both functions have limitations. It is argued that since in some cases other distributions give better results, there is not a universal function describing statistical distribution in heterogeneous brittle materials.

Fracture mechanics is a recognized tool for characterising toughness of homogeneous materials like metals, despite the fact that there is not an entirely satisfactory explanation for the influence of structure on the crack tip processes. The addition of heterogeneity and anisotropy as in case of ceramics, probably precludes the practical application of fracture mechanics in these systems.

ACKNOWLEDGEMENTS

The author wishes to express his sincere thanks to many people who helped him to complete this research project. In particular to

Dr R.G.Cooke for his supervision, continued guidance, encouragement, and cooperation throughout the period of this research. The many hours of discussion and helpful advice were greatly appreciated.

Professors B.Harris, B.McEnaney and V.D.Scott, for both making available the laboratory facilities and occasional formal and informal discussions.

Dr. R.Russell-Floyd for his assistance with AE experiments and Dr. Peter Vandor for his great physical and emotional support throughout this work.

I would like also to thank Mr. B.Chapman in X-ray Crystallography Laboratory and Mr. H.Perrot in Electron Optics for their help in XRD and SEM examination, and all the technical and secretarial Staff of the School of Materials Science, for providing a friendly environment for my research work.

Finally I would like to thank my colleagues in Technological Institute of Larissa for their support and the Greek Ministry of Education for giving permission for this research.

Last but not least, I would like to express my gratitude to my beloved family Penelope, Sophie and Dimitris, to whom this work, with all my love, is dedicated.

CONTENTS

LIST OF ABBREVIATIONS

AE Acoustic Emission

ALF Aluminosilicate Fibres

AVG Average

CMC Ceramic Matrix Composite

CVD Chemical Vapour Deposition

DTA Differential Thermal Analysis

EDXRF Energy Dispersive X-ray Fluorescence analysis

FA Fly Ash

IR Infra Red

MAS-NRM Magic Angle Spinning NMR

MOR Modulus of Rupture

NMR Nuclear Magnetic Resonance

OM Optical Microscopy

OPC Ordinary Portland Cement

PAN Poly-Acrylo-Nitrile

SEM Scanning Electron Microscopy

TEM Transmission Electron Microscopy

TG Thermogravimetry

WLT Weakest Link Theory

XRD X-ray Diffraction

XRF X-Ray Fluorescence

LIST OF SYMBOLS

Note: f,m,c subscripts generally denote fibre,matrix and composite respectively unless otherwise stated.

Greek alphabet

α notch or precrack length in a fracture toughness test

α_d atomic displacement corresponding to theoretical strength

α_{fa} Expansion coefficient of fibre in axial direction

α_{fr} expansion coefficient of a fibre in radial direction

α_m Expansion coefficient of matrix

a_o,a1 constants

$\alpha,\gamma,\delta,\eta$-alumina structures

β_d number of events with amplitude larger than V_a

β_r total number of AE events

γ_o thermodynamic or surface energy per unit area

γ_f,W_f Work of fracture

γ_i effective surface energy for fracture initiation

γ_p plastic work of fracture term

ΔT temperature difference

ϵ strain

λ angular frequency or wavelength

ν Poisson's ratio

o_i observed frequencies of values

ρ radius of curvature at crack tip

ρ_o population correlation coefficient

π 3.14

σ tensile stress

σ_c compressive strength

σ_f fracture stress

σ_{max} maximum stress at the crack tip

σ_o, x_o Weibull scaling factor (normalising factor)

σ_{th} theoretical stress

σ_{tip} stress at crack tip

σ_u minimum stress (threshold stress)

σ_x, σ_y stress in x or y direction

ΣN Cumulative counts

Φ thermal expansion mismatch parameter

x measured variable

x_u a value of x where the function is vanished

Latin alphabet

A Area

A_o constant in AE testing

B_p scale parameter in Neville function

B_w weight of specimen

b,B width of specimen

b_o constant in AE testing

D,d	density
d_p	distance between planes in XRD
D_p	shape parameter in Neville function
c	size of defect or flaw, or crack length
c_E	equivalent elastic crack length
c_o	constant in AE testing
c_V	coefficient of variation
D_l	deflection
d_f	depth of field in OM
E	Young's modulus,Modulus of Elasticity
E_b	Young's modulus from bending tests
E_d	Young's modulus from dynamic testing
e_i	expected frequencies of values
f	frequency
F	force
F(V)	cumulative distribution function of the apparent AE amplitude V
f(x)	probability density function
f(a)	geometrical factor of crack size and shape
f(a/w)	geometric term of crack size/width of specimen
i	the ith (ranked) order of failure
G	Energy release rate
G_c	critical energy release rate

$g(x)$ function represending the number of flaws per unit volume or area

K stress intensity factor

K_{IC} critical stress intensity factor

K_{min} minimum stress intensity factor

K_o constant

l, l_c mean length and critical fibre length

L specimen length or span length in a 3-point bending test

m Weibull modulus (shape parameter)

n constant

N sample size

n_e number of detected events

N_o constant in AE testing

N_r number of ringing down counts

M bending momentum

P fracture load in 3-point bending or compression

P_f Probability of failure

P7,P8,P9 sintering programmes

r interatomic distance

r_e equilibrium interatomic distance

R_{AE} Felicity ratio

r_W correlation coefficient for Weibull function

$r_o, r1$ correlation coefficients for 2- or 3- parameter Weibull functions resp.

r_N correlation coefficient for Neville function

P,P_f or $P_{(x)}$ Probability of failure

r_s resolution in OM

r_a radius of cylindrical specimen

R or ρ radius of curvature at the crack tip, or radius of spherical particle

r_o equilibrium interatomic distance

s stiffness

s_l true slope of the stress-strain curve in 3-point bending

S sampling in Neville function

S_{std} standard deviation

T_c critical temperature

t time

U internal energy

U_e stored elastic energy

U_m strain energy within matrix

U_p strain energy within particle

v crack velocity

V volume of specimen

V_a peak amplitude

v_{avg} average crack velocity

V_c constant in AE testing

V_i input voltage in AE testing

V_f output voltage in AE testing

V_o reference unit volume

V_p peak voltage

V_s scale parameter in AE testing

V_{th} threshold voltage

w or W height of specimen

W_f work of fracture

X_{avg} average value

Y,Z dimensional terms depending on crack depth and test geometry

LIST OF TABLES

LIST OF FIGURES

CHAPTER 1. INTRODUCTION

Structural ceramics are generally brittle composite systems, having a coarse structure and consisting of two or more phases. They are very useful materials with attractive properties such as good mechanical characteristics, low density, good corrosion and high temperature resistance. Their structure is influenced by their chemical and mineralogical composition and also by their particle size distribution, sintering temperature and time, which result in various structures.

The application of stress on ceramics results eventually in fracture with energy consumption, ideally required for the formation of new surfaces. In reality energy is also required for other absorbing processes since the main mode of failure of ceramics is by brittle fracture with no yielding or plastic flow .

In accordance with linear elastic fracture mechanics as applied to homogeneous monophased materials, fracture starts at some flaw and in this respect is flaw dependent. Flaws in ceramic bodies are introduced during fabrication and manufacturing and can cause a scatter on mechanical properties as high as 100%, no matter how well the specimens were produced.

For the above reasons the use of only mean values in ceramics is insufficient and several attempts have been made to develop statistical functions describing mechanical property variation.

The aims of this project fall into the following areas :

a. The experimental investigation of mechanical properties of various

heterogeneous coarse grained polyphase ceramic and fibre-ceramic composites and the relation of these properties to structure, using a variety of electron-optical methods.

Clay based ceramics like kaolin, a pottery mixture, a brick clay, and kaolin-fly ash composites were used to provide a range of different ceramic structures. The above materials were chosen to represent coarse grained ceramic materials, because of their abundant availability and relative ease in manufacturing many samples.

A number of oxide fibres (α-Al_2O_3 , δ-Al_2O_3 and mullite) and a graphite (Grafil XAS) fibre mixed with kaolin as a ceramic matrix were used to produce random oriented short fibre-composites. The effect of structure and fibre content on the mechanical properties of composites were examined.

In both cases slip casting was the main production method used for specimen preparation and three-point bending of notched and un-notched specimens was the main fracture test.

Cement and cement-fly ash composites and glass specimens were used tested and examined in the same way as the other ceramics in order to provide comparison systems of different nature.

b. The examination of applicability of linear elastic fracture mechanics for describing failure processes in brittle polyphase coarse ceramic systems which present under stress, sub-critical activity before fracture. Crack growth was monitored by the use of acoustic emission techniques.

c. The examination of applicability and validity of statistical theories and functions (Weibull and Neville functions) on the analysis of flexural strength (MOR) and stress intensity factors (K_{IC}) from brittle ceramic systems.

CHAPTER 2. LITERATURE REVIEW

2.1 MATERIALS

2.1.1 CLAYS

2.1.1.1 Introduction

Clay minerals are most important naturally occurring substances for industrial use. They are found in many parts of the world (e.g. England, USA, Germany) and are classified in two main groups, the kaolins (which include kaolinite, nacrite, dickite, and halloysite) and the montmorillonites (which include montmorillonite, nontronite, beidellite, hectorite, saponite).

From geological point of view the clays are classified in two types: residual and sedimentary [1]. Residual clays (e.g china clays) are those which have remained in their place of origin, and sedimentary (e.g. ball clays, brick-clays, fire- clays) are those that have been removed from their original places.

Transportation makes sedimentary clays contain impurities and to be finer than residual clays because of mechanical abrasion.

Kaolins and kaolinitic clays are used as they are or in mixtures in industrial applications for production of structural ceramics and may also be used in the production of advanced ceramics. As an example, Higgins and Hendry [2,3] studied the mechanism of formation of β-sialons ($Si_{6-z}Al_zO_zN_{8-z}$ from oxides and by

carbothermal reduction of kaolinite through an idealized reaction:

$$3(2SiO_2.Al_2O_3.2H_2O)+15C+5N_2 \longrightarrow 2\,Si_3Al_3O_3N_5+15CO+6H_2O$$

2.1.1.2. Chemical Composition

The kaolins in their pure form contain 39.5% Al_2O_3, 46,5% SiO_2 and 14% H_2O and have the formula $Al_2Si_2O_5(OH)_4$ and their structure is not three-dimensionally homogeneous. They have a layer structure [4], a combination of an $(Si_2O_5)n$ layer of SiO_4 tetrahedra joined at the corners with an $AlO(OH)_2$ layer of alumina octahedra as shown in Fig.1. The montmorillonites contain 28% Al_2O_3 66.5% SiO_2, 5.5% H_2O and have the formula $Al_2Si_4O_{10}(OH)_2$ and the structure of a AlO(OH) layer between sheets of Si_2O_5, [5].

English china clay (found in Devon and Cornwall) with a 46.5% SiO_2 and 39.5% Al_2O_3 content, alkalis less than 2% and iron oxide less than 1.2%, is one of the purest sources of kaolinite. The refined clay consists of lamellar crystals or platelets with size of about 2 μm. The main minerals are approximately 85% kaolinite and about 12% mica.

Ball clays are always secondary residuals and contain 40-60 % SiO_2 25-40 % AL_2O_3, up to 4% Fe_2O_3, up to 4% K_2O and up to 0.75%Na_2O. Brick clays usually have high SiO_2 content (45-75 %),and low Al_2O_3 content (10-35 %). They also contain usually considerable amounts of iron oxide (4-9 %), calcium carbonate up to 10 % as CaO), potassium oxide (up to 4 %) and low content in sodium oxide (up to 1 %), titanium oxide(up to 2%) and sulphades (up to 2 % as SO_3).

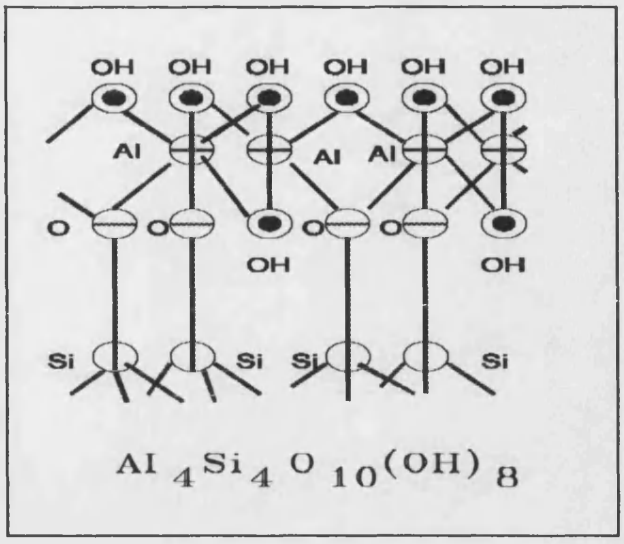

Fig 1. Schematic representation of kaolinite srtucture.

The main minerals in brick-clays are kaolinite and chlorite with illite, quartz and organic matter. Because of the chlorite content (uncertain composition) rational analysis for brick-clays is difficult.

The phase diagram of the SiO_2-Al_2O_3 system (fig. 2) shows a eutectic temperature of 1547°C [6] (or 1587°C [5,7]) at 5.5% Al_2O_3, which means that no liquid is produced below this temperature [7]. Heating a mixture of silica and alumina at temperatures over 1000 °C, produces a mixture of cristobalite (SiO_2) and mullite ($3Al_2O_3.2SiO_2$) or mullite and alumina, formed if there is time for equilibrium to be established [8,9]. The phase diagram also shows that the proportion of mullite in the final product is increased as alumina is added up to about 73%. At this percentage the mixture theoretically will give 100% mullite.

The presence of oxide impurities (Fe_2O_3, CaO, MgO, K_2O, Na_2O) (fluxing oxides), lowers the eutectic temperature in the region of 1200°C or less depending on the amount of the fluxing agents. Peters and Iberg [10], suggested that on firing of

clays, gas evolution and liquid formation starts below 900°C. Khalil and Korashy [11], examining the characteristics of calcareous clays found that increase of the amount of fluxing agents increased the liquid phase formed during sintering.

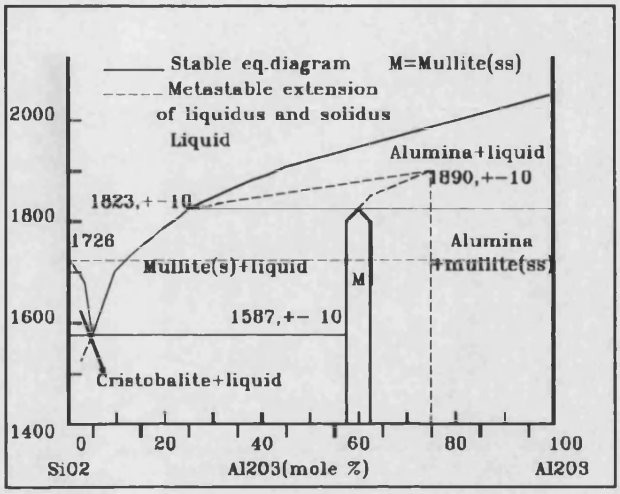

Fig.2 Phase Diagram of the SiO_2-Al_2O_3 system.

They also found that increase of the sintering temperature improved the compressive strength of the fired clay-bodies up to 1050°C, after which a dramatic drop was attributed to breakdown of the crystalline phases (gehlenite ,wollastonite and plagioclase).

2.1.1.3 Firing reactions of clays

Heating kaolinite in the range of 400-1200°C results in atomic rearrangements between the main elements present.

The firing reactions of clays (china, kaolinite, ball clays etc) have been the

subject of various studies and are generally the same,[12-18] . There is still the uncertainty about the cause of the 980°C exotherm and the composition of the formed spinel phase [e.g 19-25]. The main reactions which take place during firing of kaolinite are presented in Table 1. According to these reactions, at 500°C metakaolin is formed which at 950°C is transformed to a two phase mixture with another final transformation at higher temperatures to mullite.

Most hydrated minerals lose water when they are heated. During reaction No1 at 480°C kaolinites start to loose their combined water, and the water loss being less than 1.4 % of the total weight of the clay. Dehydroxylation is almost completed at 700°C (slow evolution continues up to 900°C) where the weight loss is increased to about 14 % [26]. The theoretical weight loss is 13.9% for a pure kaolinite clay specimen on a dry weight basis.

However, there is a disagreement about the cause of the exothermic reaction No2 (Table 1) and the composition of the 980°C spinel phase. Some workers [27] considered that metakaolin first forms γ-Al_2O_3 and amorphous silica in accordance with the reaction:

$$Al_2O_3.2SiO_2 \longrightarrow \underset{\gamma\text{-alumina}}{Al_2O_3} + 2SiO_2$$

Brindley and Nakahira [19], examining the high temperature phases of the kaolinite-mullite reaction series, reported an Al-Si spinel phase with $2Al_2O_3.3SiO_2$ chemical composition. Sequit and Anderson [28], examining two clays, have found dependence of the mullite formation temperature on the source and purity of the clay.

In the purer clay a temperature of 1300°C was necessary for mullite formation, while in the less pure clay mullite was observed at 1200°C, probably as a result of the fluxing properties of the impurities.

1. $Al_2O_3.2SiO_2.2H_2O$	ca 500°C ——————> $Al_2O_3.2SiO_2 + 2H_2O$ meta-kaolin
2. $2(Al_2O_3.2SiO_2)$ meta-kaolin	ca 950°C ——————> $2Al_2O_3.3SiO_2 + SiO_2$
3. $3(2Al_2O_3.3SiO_2)$	1200-1400°C ——————> $2(3Al_2O_3.2SiO_2) + 5SiO_2$ mullite

Table 1. Reactions taking place during sintering of kaolinite

Percival and Duncan [29], using infrared spectroscopy, found evidence of metakaolin decomposition to γ-alumina and amorphous silica as temperature was raised from 500 to near 900°C. At 900°C reaction No 2 products transformed to mullite (and probably some spinel at higher temperatures). At 1100°C excess secondary mullite and cristobalite was formed. These results are in agreement with other reports, although 1100°C is a low temperature for secondary mullite formation.

Chakraborty and Ghosh [22] and Chakraborty [30], examined the kaolinite-mullite reactions by firing kaolinite and synthetic gel, and proposed a

$3Al_2O_3.2SiO_2$ composition for spinel phase. X-ray diffraction measurements have shown that a small amount of mullite is produced during reaction No 2 [31-34].

X-ray diffraction first gives evidence of mullite formation at about 1000°C although it is not visible in SEM examination until about 1200°C [19,35,36]. Lach [36], proposed three stages in mullite formation. First, at 1000°C, the formation of isometric small crystals, second the growth of these crystals and third, at about 1400°C the formation of well developed mullite. Bulens et al. [37], suggested that the relative ratio of spinel to mullite depends on the origin of the kaolinite and the impurity oxides. They reported that addition of CaO promotes mullite formation and MgO promotes the spinel formation.

Hoffman et al. [38], synthesized a single-phase xerogel and a diphasic gel. Analysing the gels, using DTA analysis and diffractometry, they found in the single phase (but not at the diphasic gel) a 960°C exotherm and a weakly crystalline mullite formed at 1015°C. They concluded that the exotherm was due to mullite formation.

Brown et al [14], using Magic-Angle Spinning (MAS)-NMR examination reported that a maximum of 19% spinel phase was formed at 980°C, comprising of γ-alumina without any detectable, with this technique SiO2 content [39].

Chakraborty and Ghosh [17], re-examined the results of Hoffman et al. [38], by synthesizing and characterizing a freshly prepared Al-Si gel and found XRD peaks of Al-Si spinel along with peaks of weakly crystalline mullite. They concluded that it was unjustifiable to ignore the presence of spinel formation as a contribution to exothermic peak.

Okada et al. [40], and Okada and Otsuka [41], characterising the spinel phase formed by firing of SiO_2-Al_2O_3 xerogels and kaolin minerals respectively, used X-ray

quantitative analysis, lattice constant determination and chemical analysis by analytical TEM. They reported a 92% γ-Al_2O_3 + 8% SiO_2 spinel phase. They also reported that the mullite coexisting with spinel phase differed between the mineral species due to retention of metakaolin structures. Sonuparlak et al. [42], isothermally heat-treating Georgia kaolinite and using DTA, X-ray diffraction and TEM examinations, concluded that the 980°C exothermic peak was due to γ-Al_2O_3 spinel formation only. They proposed a less than 10% SiO_2 content of the spinel.

Sanz et al. [43], examining a high-purity kaolinite from Spain, and using high-resolution Aluminum-27 and Silicon-29 MAS-NMR techniques, found that amorphous silica, spinel phase and nuclei of mullite were produced at 980°C giving the exotherm. They assigned the exothermic peak at 980°C to the transformation of the coordination of the Al from the pentahedral or tetrahedral form of the metakaolinite to the more stable octahedral form and concluded that it was not associated with the formation of a particular crystalline phase.

Today it is generally accepted that spinel and mullite are formed simultaneously during the 980°C exothermic reaction. Recently, Chakraborty and Ghosh [25,44], concluded that the key target in the determination of the cause of 980°C exotherm is to identify what phases crystallize at the 980°C peak. They underlined that both spinel and mullite could be responsible for the 980°C exotherm and only in cases of absence of one of the above phases the cause could be attributed only to one phase.

At 1100°C the bulk of the secondary mullite is formed and amorphous silica is transformed into cristobalite. Again, kaolins with well developed crystalline network present a delay of the second reaction during which also a rapid shrinkage

occurs.

Research on the change of crystallite size of mullite with temperature and sintering time, [45], showed that the increase of sintering time and temperature increase the crystallite size and leads to crystal growth of mullite crystallites.

2.1.1.4 Thermal analysis methods of clays

The study of clays using thermal analysis methods is well covered in the literature [46-49], based on the observation and measurement of physical and/or chemical changes which happen in a material when it is heated or cooled. The main techniques used in the examination of clays and generally of ceramic materials are Thermogravimetry (TG) and Differential Thermal Analysis (DTA).

In thermogravimetry the weight change of a material in powder form, during heating and cooling is recorded and information about the relation between weight and temperature changes, about thermal stability and the substances produced during heating is gained.

The main reactions and changes which can be detected using this technique include dehydrations, decompositions, reductions, oxidations, and gas evolutions [50]. Clay minerals loose water and other volatile substances (e.g. carbonates) when heated at temperatures which can characterise the minerals.

During Differential Thermal Analysis measurements, a sample to be analyzed and an inert substance are heated up in a furnace simultaneously under the same conditions and the temperature difference in relation to time or temperature is recorded. The DTA curves present peaks related to absorption or desorption of heat

as a result of energetic changes in the samples. DTA records all the enthalpy changes independently of weight changes. When crystallisations, oxidations or decompositions take place, exothermic curves are formed. Other changes such as phase transformations, dehydrations and reductions cause endothermic effects [46]. Generally physical changes are endothermic and chemical changes can be endo-and/or exothermic. The main physico-chemical phenomena detectable by DTA analysis are presented at Table 2.

Kaolinites usually present an endothermic peak in the region of 100°C when desorption of the absorbed water takes place. TG and DTA measurements showed [51], that the magnitude of this peak is dependent upon the particle size (surface area) and the crystallinity of the clay. The more crystalline the clay the lower the endo-peak.

At higher temperatures in the region of 400-700 °C a large endothermic peak is formed (for kaolins usually around 480°C) as a result of dehydration of combined water (dehydroxylation of the silicate lattice) and decomposition of the clay [47]. Dilatometric experiments showed that kaolinites expand when heated in the region of 450-500°C and contract in the region of 500-600°C as a result of the -OH group detachment [52].

The temperature of dehydroxylation depends on the degree of the arrangement of the structure. Well developed kaolinite networks seems to be more stable and present a thermal delay and a more distinct reaction in - OH detachment. Well crystallized kaoline specimens (API standard) show a peak minimum at 540°C [51].

The weight loss produced from dehydroxylation in the region of 500°C, is about 1.4% and could be used for quantitative measurements of kaolinite content of

a clay, provided there are no other substances present which loose weight at the

Phenomenon	Endothermic change	Exothermic change
Physical	Crystalline transition	Crystalline transition
"	Vaporisation, Fusion	
"	Sublimation	
"	Desorption, Adsorption	Adsorption
"	Curie point transition Liquid crystal trans.	
Chemical		Chemisorption
"	Desolvation	
"	Dehydration	
"	Decomposition	Decomposition
"		Oxidation
"	Reduction	
"	Redox reactions	Redox reactions
"		Combustion
"		Polymerisation, resin curing
"		Catalytic reactions

Table 2. Detectable phenomena by thermal analysis

same temperature. At higher temperatures and till 700°C the total weight loss is about 14% [26].

At higher temperatures (900-1000°C), a relatively strong exothermic peak due to a crystallization phenomenon is formed as a result of mullite formation [20,31-34] and/or γ-alumina and silicon spinel formation [19,27]. A second exothermic peak at

1250°C is attributed to mullite crystallisation.

A similar thermal behaviour was found during examination of illites [52]. They expand till 500°C and loose their hydroxyl groups in the region of 520-550°C. At higher temperatures (about 750°C) their crystalline network is destroyed. XRD measurements show that at 700°C all the peaks from the clay minerals have disappeared. At 850°C a spinel starts to form and this continues until 1200°C. At the same temperature silica and alkalies from the interpacked layers begin to form uncrystallized glass, which results in rapid contraction of the clay. At higher temperatures the formed glass dissolves the spinels formed earlier.

The fired colour of the clays depends mainly on their iron oxide content and also on the state of oxidation of the iron, the degree of sub-division, the kind of the firing atmosphere (oxidizing or reducing), and the temperature and duration of firing. Other oxides such as calcium oxide and magnesium oxide produce more white fired clays and organic matter lighten the colour by keeping the iron in the ferrous state. Oxidizing atmospheres and higher temperatures darken the colour of the fired brick-clays from light red to dark red or brown.

As it was shown in experiments on the preparation of glass from quartz-porphyrite sands (73% SiO_2, 15% Al_2O_3) [21], that when iron oxide is present in the fired bodies, it can produce extensive bubble formation at 1300°C, due to reduction of Fe_2O_3 to Fe_3O_4, according to reaction:

$$3Fe_2O_3 \longrightarrow 2Fe_3O_4 + 1/2\ O_2$$

After sintering (firing), clay ceramics are very brittle materials [e.g. 53] and

up to about half of their melting temperature, fracture occurs without plastic flow at the crack tip.

2.1.2.6. Fly Ash and Fly Ash Bricks

Fly Ash (FA) is a product (about 15% of the coal) of the combustion of sub-bituminous or lignitic coal of modern electric power stations.

In countries where coal is used as energy source, there is a considerable interest in using fly ash (FA) as additives of cement. However, FA utilization in the commercial markets is still limited, [54],(e.g. in U.S.A. is about 20% of the available ash) despite the fact that FA is an inexpensive material and its disposal causes environmental problems. Other uses of FA in industry, [55], include, fabrication of mineral wool when the chemical composition falls within certain limits, high flexural strength ceramics from fired mixtures of FA, glass scrap and clay, wall tiles from pure FA, and ash bricks.

Mineralogical analyses of several fly ashes performed by Mehta [56], revealed the following:

a. Crystalline silica in the form of quartz is present in all FAs.

b. Crystalline aluminosilicate in the form of mullite was not present in high calcium fly ashes.

c. Crystalline C_3A, a highly reactive compound and anhydride CS^-, were found in all high calcium FAs.

d. Fe_3O_4 and periclase (crystalline MgO) were present.

e. Quantitative mineralogical analyses showed also that the non crystalline

matter (glass) content, was high in all the examined FAs.

The fly ashes in mixtures with P.C. act as active additions , due to their ability to react with lime and produce hydraulic compounds . The suitability of a FA to be used in cement industry depends mainly on its chemical and mineralogical composition. It was also found [57] that the presence of a refractory phase e.g. mullite, influence the crystallization of the clinker minerals.

FAs are pozollanic materials. This means that they give the pozollanic reaction in which particles of FA react with water and lime to form cementitious products (calcium silicate hydrates -C_xSH_y) in a similar way to cement hydrates. With respect to particle morphologies and composition, fly ashes consist of various particles with different morphology and chemical composition. As a result even adjacent FA particles of similar size may vary in glass content and composition and content and type of crystalline matter included, a fact which influences reactivity at later stages of FA reaction in cement and concrete [58,59]. From morphological point of view the finer particles of FA are in the form of plenospheres while the coarser ones are pebble-like and porous [60].

FA produced during combustion of all kinds of coal, can also be used as a substitute of clay in bricks [61-64] and also as a starting material in mixture with other materials for the production of e.g. mineral wool, high strength ceramics, ceramic glazed wall tiles etc. Actually these uses are more important than those of cement mixtures, because they could result in appreciable reduction of existing large stockpiles of FA as they are larger volume applications.

Bricks are normally manufactured from clays, an inexpensive material which however may not be always available from local sources and it needs expensive

processing (excavation, milling etc) to be suitable for use. The manufacture of bricks from FA is not new. A number of research centres on this subject exist in Holland [62], India [63] and USA [64]. Day et al, [65], used western Canadian FA, in mixtures with binders (e.g. sodium silicate) to produce superior ceramic material, as an interesting alternative to standard clay brick, with strengths adequate for masonry elements.

Their main characteristic was the low density (typically 1.7 g/cm^3 compared to 2.27 g/cm^3 of clay bricks) and durability in freezing and thawing. They also needed less energy for production, requiring lower firing temperatures (900°C-1000°C) and shorter duration (3 hours was adequate to reach the desired strength level). They could solve the problem of elimination of the waste product and environmental pollution, as well as conservation of natural resources.

2.1.2 COMPOSITES

2.1.2.1. Introduction

Although ceramic materials have useful physical, chemical and mechanical properties, their use is restricted by their brittle behaviour. In order to overcome this deficiency composite ceramic materials have been developed and new avenues to production of advanced engineering systems have been opened.

The idea of developing composite materials is not new. The first fibrous material, used some 2000 years ago for thermal insulation purposes, was the greek-named asbestos, a natural ferro-magnesian silicate material. The first man-made

fibres, were coloured glass threads and produced for decorating purposes [66]. In 1930's glass fibre production improved and composite materials (synthetic resins and polymers) with glass-fibre reinforcements became useful. Later the development of ceramic fibres was stimulated by the need for high-temperature reinforcing fibres in aerospace applications.

Ceramics reinforced with a fibrous phase with high aspect ratio (length/diameter) have been developed in situ as precipitates in the host matrix. However, since the volume fraction was low and the interface between the phases too strong to act as an effective crack deflector, the reinforcement was low. Several composite systems of ceramics have been developed [67] where the toughening agent is particulate matter platelets, whiskers and fibres. A schematic representation of the fibre composites is shown in fig. 3.

The fabrication of short random oriented fibre composites and whisker reinforced ceramics can utilise all the conventional production methods (e.g slip

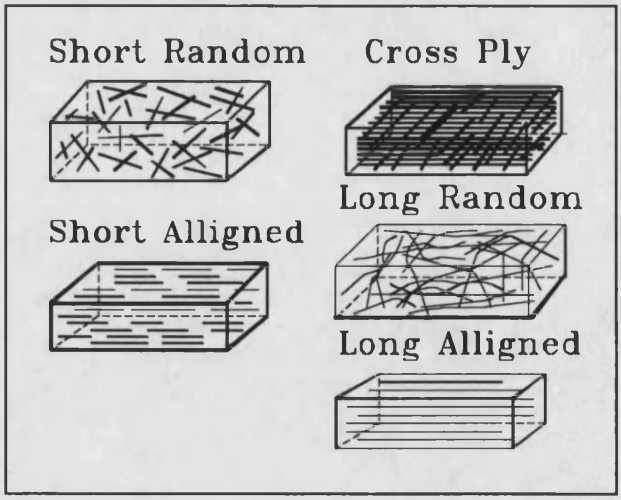

Fig.3 Representation of fibre-composite systems.

casting, injection moulding etc), while fabrication of continuous composites follow other methods (e.g. slurry infiltration with hot pressing, sol-gel melt infiltration etc).

Since only random orientated short fibre composites were examined in this thesis, a brief review of the discontinuous ceramic composite literature was considered and included here . Extensive analysis in the theory of engineering ceramic and metal composite materials can be found in the literature e.g. Watt et al, [68], Hull, [69], Kelly and Rabotinov [70], Harris [71], Johnson and Sowman [66], Warren [67]. It must be mentioned that during the literature review on CMCs and fibres for the present thesis, the majority of information was about aligned long fibres and that much of it was found in the form of patents or proprietary methods. Similarly, Schioler and Stiglich [72] in a literature review of the ceramic matrix composites developed in USA , indicated that much of the work in this field is proprietary in nature and thus is not referenced in the usual sources.

2.1.2.2 Ceramic fibres

The commercially available fibres are divided in four categories with respect to chemical composition: the oxide fibres (e.g alumina, aluminosilicate, glass etc.), the non-oxide fibres (mainly carbon, boron, SiC, etc.) the polymeric fibres (e.g. polyethylene, kevlar etc.) and the metallic fibres (e.g steel, tungsten). The majority of commercial fibre refractories are based on alumina or aluminosilicate fibres. Hybrid fibre composites consisting of two different fibres have also been developed in an attempt to tailor properties in accordance to specific requirements. The fibres are grouped according to structure in amorphous, single crystal, polycrystalline and

multiphase. Their usual fabrication processes include plastic forming, slip casting, cold pressing and sintering, and hot-pressing.

With respect to their length they are divided, again, in two types : the discontinuous (short) fibres and the continuous (long) fibres. A useful review on fibres and their composites is given by Watt, Harris and Ham (eds) in the proceedings of the Royal Society of London [68].

2.1.2.2.1 Alumina fibres

Three are the main production processes for the manufacture of polycrystalline oxide fibres, [70] :

a) The relic process (where an organic filament is soaked in an inorganic salt solution, then is dried and finally is calcined to produce a relic of the original fibre).

b) The extrusion of slips (where a suspension of an oxide in water is forming a "slip" which is the extruded, dried and calcined to form a fibre), and

c) The spinning of viscous solutions (where an aqueous solution of an oxide is transformed to a viscous solution which is then extruded as a filament).

Oxide inorganic fibres [73] comprise mainly combinations of aluminium oxide (alumina) and silicon dioxide (silica) in various proportions , and in lesser extent zirconium oxide (zirconia) and boric oxide, e.g.Al_2O_3-SiO_2, Al_2O_3, Al_2O_3-ZrO_2, Al_2O_3-B_2O_3-SiO_2 and ZrO_2-SiO_2.

Generally alumina fibres are cheap, have high Young's modulus (over 300 GPa), good chemical resistance but also high density (over 3 g/cm^3) and low tensile strength which result in inferior specific mechanical properties when compared to

other fibres.

A little more information will be given for the first two types of fibres which have been used in the present thesis.

a. Aluminosilicate fibres (ALF)

They contain about 45-60% alumina and the rest is silica and minor constituents iron titanium and calcium oxides, produced mainly from kaolin. Also in this category are the mullite fibres.

These are used in composite fabrication and as a substitute for asbestos in insulating applications.

As was shown by XRD, DTA, and IR spectroscopy, [74], Triton Kaowool, and Fiberfrax ALF fibres (with impurities of iron, titanium sodium, and potassium) transform to mullite when they are fired at temperatures at about 1000°C, the quantity of mullite increased with time. No indication of cristobalite formation was found even after long time firing at 1050°C for the first fibre. However the second fibre, which had a higher oxide content, showed transformation to cristobalite after long firing at the same temperature. These results show that oxide impurities can accelerate conversion of mullite to cristobalite. Other workers [75] reported similar transformation to beta cristobalite from devitrified commercial grade aluminosilicate zirconia refractory fibres. The main production routes of these fibres starts with melting of the raw mixture and continues with compressed gas separation to form fibres or with the use of a rotating disk from which fibres are produced by centrifugal force.

b. High alumina fibres

The main production methods include the slurry process in which an aqueous stabilized slurry is extruded into air and sintered at high temperature, and the sol-gel spinning method in which aluminium compounds, precursors to the oxide, are dried and heat treated to form fibres. Alumina is usually produced by heating $Al(OH)_3$ to above 1000°C. Alpha-alumina has the more stable structure of all the alumina oxides [76], with a hexagonal close-packed unit cell (with interstices filled with aluminium atoms), of high density (3.97 gcm^{-3}). As the temperature is increased (above 1100°C) alpha-alumina acquires larger crystal grains. The main features (advantages and drawbacks) of using alpha-alumina fibres in composites are shown in Table 3, [76]:

In aqueous solutions alumina fibres have positive or low negative surface charge, [70], as demonstrated by zeta potential at pH 5.5 (e.g. Saffil fibres (delta structure) have +28 mV and aluminosilicate fibres -4mV).

ADVANTAGES	DISADVANGAGES
a. High temperature stability up to 1100°C	a. High densities (heavier than gamma-alumina, glass and carbon fibres)
b. Stability in molten metals.	b. Not so high UTS (as above)
c. Electrical inertness	
d. High Modulus of elasticity	

Table 3. Characteristics of alpha-alumina fibres.

2.1.2.2.2 The Saffil fibres

The Saffil, short polycrystalline alumina fibres, produced as short staple by the centrifugal spinning of a solution of aluminium compounds (aluminium chlorohydroxide $AlCl_x(OH)_y$, silica, organic polymer and water) followed by drying in a high velocity gas stream and heat treatment to transform the fibres in α, γ, δ, η, and θ, structures of alumina, have been developed by ICI PLC. Initially they were used as a high temperature furnace insulation, but later improved grades (e.g. RF grade) were used in metal matrix composites mainly for automotive applications [77-79]. Saffil RF fibres have a fine grained mainly delta alumina microstructure developed by the use of about 4% silica and careful production control. The production method employed minimizes also, the non-fibrous materials and give a quite thin uniform mean diameter of about 3 microns [80].

2.1.2.2.3 Carbon fibres

The non-oxide fibres include carbon, carbide and nitride fibres. The structure properties and thermal stability of carbon fibres are well documented by Watt and Perov [70].

Carbon fibres are the only class of reinforcing agents that retain their stability to temperatures above 1500°C. Unfortunately, they have a limited lifetime in oxidizing atmospheres at medium temperatures, since carbon is readily oxidized at temperatures higher than 400°C. Carbon fibres of high strength and Young's modulus are important reinforcing agents in modern technological applications.

High modulus carbon fibres are produced [81] by:

a. pyrolysis of cellulose in inert atmosphere (cellulose method).

b. polyacrylonitrile (PAN) fibre conversion .

c. low-melting point isotropic pitches transformation.

d. Pyrolytic deposition of hydrocarbons from the gas phase.

The carbide and nitride fibres are produced by pyrolysis of polymers or by chemical vapour deposition (CVD).

2.1.2.3 Compatibility of fibres and matrixes - The fibre-matrix interface

The structure and properties of the fibre-matrix interface play an important role in the properties of composites. Generally, the lower strain to failure of the matrix in comparison to that of the fibres, indicates that the mode of fracture depends on the bonding between fibres and matrixes.

There are two main types of matrix-fibre interfaces which play an important role in the mode of fracture:

a. Strong interfaces when there is high chemical compatibility and strong bonding between fibre and matrix as, for example, in the case of mullite-mullite composites or, generally, oxide ceramic-oxide fibre systems. In this case a crack propagating in the matrix may pass through fibres and matrix resulting in catastrophic failure.

b. Weak interfaces when there is no chemical compatibility and the bonding between matrix and fibres is weak, as in the case of oxide ceramic-carbon fibre

systems. In this case debonding of the fibres may occur allowing the fibres to slide through the matrix to bridge the cracks. This mechanism leads to load transfer from the matrix to fibres and theoretically results in improvement of the mechanical characteristics of composites, determined by the frictional effects between matrix and fibres.

Additionally the interfaces within the matrix of polycrystalline and/or polyphase composites are important, especially at elevated temperatures where e.g. softening of a glass phase can result in change of the load transfer mechanism and fracture behaviour of the composite.

In order for a fibre to form a useful composite [82] with a given matrix, three main parameters must be examined: (a) The thermal expansion coefficients, (b) The elastic moduli, (c) The chemical compatibility under the fabrication and usage conditions.

Several simple theoretical formulae (e.g. [83],[84]) have been proposed to predict the matrix stresses due to thermal mismatch in aligned fibre systems with reasonable success. However, in random oriented systems the complexity of stressing allows only qualitative comparisons. Thermal mismatch cracking in short random fibre systems is more extended than in similar continuous unidirectional ones [82].

The expansion coefficients of fibres, α, are not equal in radial and axial direction, particularly those of carbon fibres [82]. So the differential values $\Delta\alpha_r$ (radial) and $\Delta\alpha_a$ (axial) may not be equal.

When matrix cracking due to thermal expansion mismatch occurs during cooling, in random short fibre composite systems, cracks are formed in all directions and the expected result is the weakening of the composite. Sambell et al.[85], gave

the following (Table 4) comparison of the damage due to thermal expansion mismatch in some carbon fibre reinforced systems. The thermal expansion mismatch parameters Φ_α (axial) and Φ_r (radial) are given by the following equations :

$$\Phi_\alpha = \frac{(\alpha_m - \alpha_{fa})\ \Delta T E_m}{\sigma_m}$$

(eq1)

$$\Phi_r = \frac{(\alpha_m - \alpha_{fr})\ \Delta T E_m}{\sigma_m}$$

where α_m , α_{fa} and $\alpha_{fr,}$ are the mean expansion coefficients of matrix ,fibre in axial and fibre in radial directions respectively.

ΔT, is the temperature difference from the critical temperature T_c

σ_m , E_m , are the stress and the Young's modulus of the matrix

The critical temperature T_c is defined as the temperature below which little stress relaxation can take place. σ_{fa} and σ_{fr} in Table 4 are the axial and radial stresses in fibres respectively.

Improvement of strength and toughness in a composite requires a relatively low-toughness interface between matrix and fibres, when debonding and sliding take place in order for the fibres to bridge the crack surfaces, [85]. When there is no bonding at the interface (as in case of non-compatible matrix-fibre interface), sliding is resisted by friction.

An important factor which must also be taken into account in relation to compatibility is that fibres could not retain their integrity if they reacted chemically, or were soluble or formed low melting eutectics at sintering temperatures.

MATRIX	α_m x10^{-6}	T_c °C	E_m GPa	σ_m GPa	σ_{fa} GPa	σ_{fr} GPa	Φ_α	Φ_r	Damage
MgO	13.6	1200	300	0.2	4.9	2	25	10	Severe cracking
Al_2O_3 80% dense	8.3	1400	230	0.3	2.66	0.097	9	0.3	Severe cracking
soda-lime glass	8.9	480	60	0.1	0.26	0.026	2.6	0.3	Localized cracking
borosilicate glass	3.5	520	60	0.1	0.11	-140	1.1	-1.4	Un-cracked
glass-ceramic	1.5	1000	100	0.1	0.15	-650	1.5	-6.5	Un-cracked

Table 4. A comparison of the damage due to thermal expansion mismatch in carbon-fibre reinforced composites, [85].

2.1.2.4 Ceramic Matrix Composites (CMC's)

The need for high-temperature high toughness and strength materials prompted in early 1980, the research and development on ceramic matrix fibre composites (CMC).

The ceramic matrix composites can be classified in two large categories: the glass and glass-ceramic matrices reinforced with continuous or short fibres, (e.g.[86,87]) and the polycrystalline ceramic matrices reinforced with whiskers (e.g. [88,89]).

The main methods of CMCs production include:

a. Continuous-fibre reinforced glass-ceramic and glass systems produced by a solid state slurry impregnation followed by hot-pressing.

b. Infiltration of woven-fibre preforms with a ceramic matrix by a gas or liquid route.

c. Hot-pressing whisker toughened ceramics.

As Harris indicated [71], simple models can be used for elastic properties prediction. However accurate strength prediction is more difficult, since strength is dependent not only on the properties (strengths and elastic moduli) of the composite constituents, but also on the development of damage on the microscopic scale, so the formation of a crack and the control of its growth is controlled by the heterogeneous nature of the composite (effect of relative thermal expansion coefficients, porosity etc). This difficulty is more important in the case of short random oriented fibres where there is also the additional effect of fibre length and orientation. Phillips [82], reviewing short fibre composites, underlined that these systems are weak and, sometimes, even weaker than the matrix itself. Harris [71], indicated that elastic moduli in parallel and series composites can be calculated using the Voigt and Reuss models respectively:

$$E_c = E_m V_m + E_f V_f \quad \textit{Voigt parallel model} \qquad \textbf{(eq.2)}$$

$$\frac{1}{E_c} = \frac{V_m}{E_m} + \frac{V_f}{E_f} \quad \textit{Reuss series model}$$

where E_c , E_f and E_m are the Young's moduli of composite, fibre and matrix and V_m and V_f are the volume fractions of matrix and fibres respectively.

Phillips [82], also indicated that deviation from the above Voigt model needs to allow for presence of porosity and the E_m value must be corrected in accordance

to Mackenzie's relation: $E_m = E_{mo}(1-1.9P+0.9P^2)$ where E_{mo} is the Young's Modulus at zero porosity.

Research in continuous carbon aligned fibre reinforced borosilicate glass [90], has shown an initial increase of strength with volume fraction of fibres, but with higher fibre volume (over 55%) a dramatic decrease attributed to increased porosity.

Sambell et al. [85], examined the properties of a number of ceramic fibre (zirconia or carbon) composites with oxide (MgO or Alumina) or glass matrix, produced by hot pressing mixtures of fibres with powdered matrix material. They found that alignment increased fracture strength. On the other hand, randomly dispersed fibres decreased fracture strength. They suggested that main reason for this behaviour was mismatch of thermal expansion coefficients and the nature of the interface. They also reported [91], that in an aligned continuous carbon fibre composite strength increased with fibre content as predicted by the rule of mixture, until above 40% volume content of fibres, when the flexural strength was decreased.

The work of fracture was increased in all cases. They suggested that a number of reasons could be responsible for this, such as, deflection of a propagating crack (in aligned fibre-composites) and/or fibre pull-out (since it dissipates energy and can result in high works of fracture). SEM examination had shown that fibres pull out was the main mechanism. Generally, a number of toughening mechanisms exist in short fibre-ceramic matrix composites [67] :

a. Load transfer from the matrix to reinforcing fibres when the matrix fail.

b. Fibre pull out (requires weak whisker/matrix interfacial bonding, and energy is absorbed during pull out).

c. Crack deflection or arrest at the interface .

d. Fibre bridging (un-fractured fibres bridge the crack behind the crack tip.

e. Microcracking (decreasing stress intensity at main crack tip).

The above mechanisms are synergetic, i.e. they can be additive and complement each other. A schematic illustration of the last two toughening mechanisms are shown in fig.4.

Strengthening of ceramics with dispersion of particles (as in the case of metals) cannot be done through dislocation blocking since dislocation mobility is already extremely low or nil [92], but may be achieved through reduction of the Griffith flaw size, thereby raising the stress for initiation and propagation of cracks (e.g [93,94]).

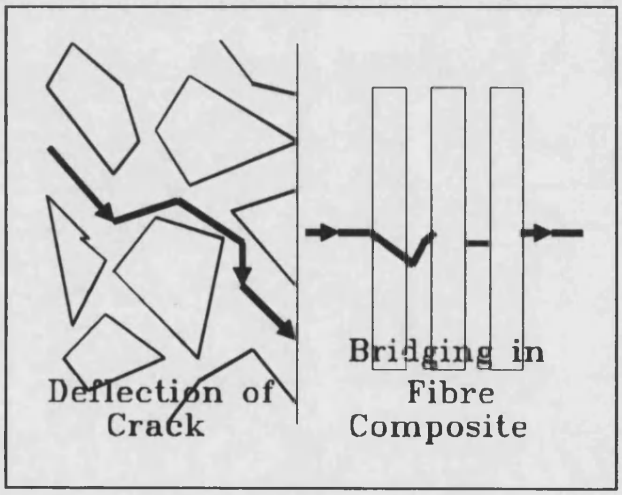

Fig.4 Graphic representation of deflection and fibre bridging mechanisms.

An important factor affecting the strength of both continuous and discontinuous fibre-composites is the presence of microstructural defects and especially the occurrence of voids, since a small fraction of voids can have a drastic effect on strength [81].

The theory of the fibre reinforcement indicates that two requisites exist for strengthening of ceramics [84]. It will only occur:

a. If the elastic modulus of the fibres is greater than the elastic modulus of the matrix; and

b. If tensile stresses can be transmitted to fibres.

When the fibres have lower modulus, the fracture stresses will be reduced, because a reduced cross section must carry the applied load. In case of continuous fibre reinforced composites, the rule of mixtures may be applied.

In discontinuous fibre composites, the strength of a fibre can only be utilized if it is parallel to the tensile axis and its length exceeds a critical length. In randomly oriented fibres the proportion of the fibres capable of being loaded to their fracture stress will be reduced and the strength of the composite will be lower than that of an aligned system.

However, several random oriented fibre-systems show an increase in strength, a classical example is the cement composites (e.g. [95]). Strengthening is also observed in glass-alumina fibres and special porcelain-alumina fibres systems with zero differential thermal expansion ($\Delta\alpha$) (the difference between the thermal expansion coefficient between fibres and matrix). The differential thermal expansion determines the residual stress-strain distributions after fabrication and is considered very important for the mechanical properties composite systems [84].

Phillips [96], measured the fracture energy by the work of fracture technique in carbon-fibre reinforced glass composites. He found meaningful material properties only when crack propagation was controlled throughout failure.

Phillips [82], also indicated that improvement of strength in short fibre

systems can be expected when it is used as a low temperature fabrication technique in order avoid thermal mismatch stresses, or by using a very weak matrix. He also indicated that alignment of the short fibres can improve the strength of the composite.

Rice and Freiman [97], in a survey on the properties of particle disperse or fibre ceramic composites, reported that although K_{IC} was found often to be improved, strengths changes depended on the relative size of matrix flaws and particle or fibre spacings. Analysis showed that strengths decreased with increasing fibre or particle content in cases where the flaw size of the matrix was smaller than the spacing between the fibres or the particles and that strengths increased in the opposite situation. They also indicated that internal stresses due to phase mismatch in composites, could be a limiting factor in the strength of composites.

Sheldon and Lewis [98], investigated a short random oriented mullite-mullite fibre (Fiberfrax H) composite sintered at 1500°C (with 40% porosity). They found improvement of MOR at 3.5% fibre content, but gradual decrease with higher fibre additions. They also reported increase of modulus of elasticity with increase of fibre content. They explain the increase of Young's modulus as a result of load transfer through the fibres and the effect of fibres on crack growth halting or slowing. However they did not give an explanation for strength reduction with higher fibre contents.

Wang et al. [99], studied short polycrystalline α-alumina (5-10 microns in diameter and 50-100 microns in length) fibre-reinforced mullite composites prepared with pressureless sintering. They used indentation techniques on sintered die-pressed pellets for toughness evaluation and found a high increase in toughness (a 20% volume composite gave a three times increase of the initial toughness). They

considered this to be due to interaction between fibres and cracks and a combination of toughening mechanisms such as load transfer, fibre debonding and pull out and crack deflection and bridging taking place.

They also examined the change of the sintered density and shrinkage as a function of the volume content of the alumina fibres and showed that up to about 5% vol. fibre content, the density and the shrinkage was about the 90% of the theoretical value. At higher fibre contents a drastic decrease was observed. They concluded that high alumina fibre loading of the mullite matrix will result in a 3-dimensional fibre network formation where agglomeration is unavoidable resulting reduction in density and shrinkage.

A similar behaviour was observed in Ce-PSZ, CeO_2-ZrO_2 composites materials which have high strength and toughness and good stability in humid atmospheres. Maschio and Lucchini [100], in an examination of mechanical properties of a composite containing short α-alumina (Saffil) fibres in ZrO_2/12% mol CeO_2 matrix containing also MnO_2, tested in 4-point bend tests, showed initially (with about 5% vol. fibres for composites containing 1% and 3% MnO_2) an increase in density and modulus of rupture and then linear decrease for both characteristics.

Ruh et al. [101], examined the mechanical and microstructural properties of several mullite matrix whisker reinforced composites. They found that mullite-SiC whisker composites increase their strength with increase of the volume content of whiskers up to about 20%. After this percentage a decrease in strength was observed. The same behaviour has been also reported by other investigators [102]. Fracture toughness measurements of the same composites showed a trend of increase as whisker content was increased. However, no explanation was attempted for this

composite behaviour.

A similar effect of fibre volume on strength was observed also in concrete. Mashima et al. [103] examining the effect of fibre volume in reinforcing concrete reported that although the compressive strength was initially increased with increase in fibre content up to 20%, later a drastic decrease was found. They attributed this behaviour to void inclusion in the composite.

Pabst [104], commenting on strength characterisation by a fracture mechanics approach, divided ceramic composites in two categories with respect to behaviour: the macro-mechanically isotropic and homogeneous systems containing second phases, and the macroscopically anisotropic systems as in case of fibre-composites. He underlined that fibre reinforced brittle composites are macroscopically anisotropic structures and a reliable crack length definition is difficult for them. The compliance method cannot be used unless if the crack path is visually detected. As a result of the poor knowledge of crack character, life prediction and reliability in brittle composites is questionable.

In a similar way, Harris et al [105], in a survey of the tensile strength and toughness of carbon fibre reinforced epoxy or polyester composites, with various kinds of lay-up, found a linear relationship between strength and K_{IC}, regardless the structure, composition and manufacturing process. They underlined that this would, in accordance with LEFM, indicate that all composites contained a defect of the same order of 1 mm in length, which is a rather unlike possibility. They concluded that K_{IC} is meaningless for such materials, where fracture path proceeds through combinations of fibres, matrix and interface. Probably factors such as heterogeneity and anisotropy make the practical application of LEFM to composites invalid.

Habib, Cooke and Harris [106] investigated the mechanical properties of SiC fibre and carbon fibre-Pyrex composites. They found that matrix cracking starting at the onset of load resulted in non-elastic response, and concluded that cracking in brittle matrix composites has serious implications for the meaning of conventional engineering properties measured by standard methods.

2.2 FRACTURE

2.2.1 INTRODUCTION

After the Industrial Revolution, which resulted in a high increase in the use of materials, a high number of accidents from material failure involving, railway equipment, steam boiler explosions, structural components like bridges, all welded designs by liberty ships and tankers had shown that not only poor design but also pre-existing flaws in materials could initiate cracking and fracture.

Material failures under load can be by yield or fracture. The existence of defects is important in both types of failures, although the types of defects which are important in each case are different. A complete understanding of the failure processes within ceramic materials has been the target of many studies over a considerable period of time. Nowadays three main directions of research on fracture processes of heterogeneous materials [107] are:

a. Phenomenological analysis

b. Statistical studies ; and

c. Structural analysis

Phenomenologal analysis, based on Linear Elastic Fracture Mechanics (LEFM) do not analyze the physical reasons which lead to fracture but examines only the results considering fracture as an instantaneous process where defects (cracks or generally discontinuities) are formed or pre-exist in an elastic continuum and propagate to final fracture.

Statistical theories analyze fracture on the basis that the strength of a material

is determined by the strength of the weakest primary element, not taking into account factors such as actual structure, stress state near pores and cracks, cracks between binding components etc. Finally, structural theories cannot explain the way the stresses form the first cracks and therefore they do not provide an entire description of fracture process, but analyse the physical behaviour of materials under load showing that cracks must be formed mainly near structural defects and inclusions.

Fracture mechanics examines the fracture-dominant failures. The first analysis of a fracture problem was conducted by Griffith in 1920, with the examination of crack propagation in glass. Griffith was the first to suggest that the discrepancy between theoretical predictions and observed strength values in brittle materials was due to the existence of small flaws in the body of these brittle materials. He assumed that a simple energy balance exist between the energy needed for formation of new crack surfaces and the elastic strain energy decrease as a crack extends. Later, Irwin, Orowan and others contributed in advancing the knowledge of fracture mechanisms in materials. Important books on Fracture Mechanics e.g. from Knott [108] Broek [109], and Ewalds [110], are very informative and give a detailed analysis of the fracture mechanics concepts. Only the basic necessary information for brittle fracture was included in the present thesis.

2.2.2 THEORETICAL STRENGTH

The application of an external force on a body results in deformation. This deformation may be elastic if it disappears, or plastic if it remains, on removal of the external force. Brittle materials like ceramics, usually behave at ambient

temperatures in an elastic manner and fracture occurs, without plastic deformation, when the stress on them exceeds a critical value. At higher temperatures (near softening temperature) brittle materials, e.g. glass, may present plastic deformation under stress. On the other hand many metals deform plastically before fracture at all temperatures.

Generally, when a uniform rod of cross-sectional area A is under tensile stress σ and a strain ϵ is produced the following relationship exists:

$$\sigma = \epsilon E \qquad \textbf{(eq.3)}$$

where E is proportionality constant (Young's Modulus)

The theoretical strength, σ_{th}, of a material, i.e. the strength due to chemical bonds can be estimated by energetic considerations, [111]. The internal energy, U, of a crystal, considering only the chemical bonding forces, is a sum of two components: an attractive term related to the bond type, and a repulsive term related to overlapping of neighbouring electron clouds. The potential between two atoms can follow a function similar to that shown in fig.5.

The force F, between atoms is equal to dU/dr and the theoretical cleavage stress is:

$$\sigma_{th} \sim \frac{F}{r_e^2} \qquad \textbf{(eq.4)}$$

where r_e is the equilibrium interatomic distance between two atoms in absence of any external stress.

Since it is difficult to estimate the exact force-displacement curve Orowan

[112], estimated the theoretical cleavage or tensile strength, σ_{th}, assuming a simple sinusoidal function. He related stress to displacement with the expression:

$$\sigma=\sigma_{th}\sin\frac{\pi(r-r_e)}{2\alpha_d} \qquad \textbf{(eq.5)}$$

where α_d, is the atomic displacement corresponding to theoretical strength σ_{th} and r, is the interatomic distance

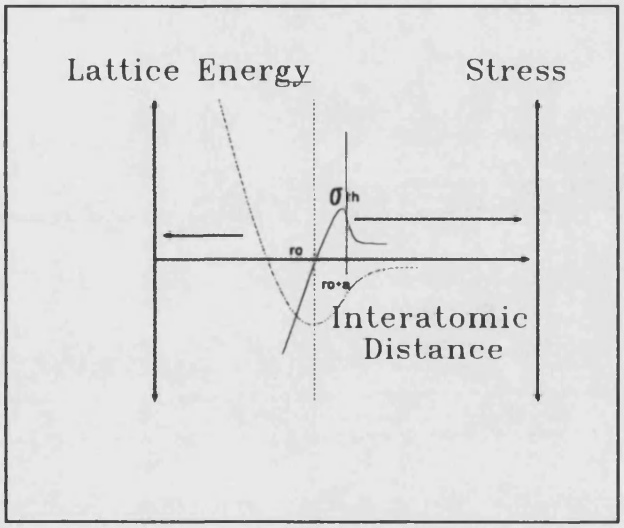

Fig.5 Variation of lattice energy and stress with interatomic distance.

Since the Modulus of Elasticity, the Young's modulus, E, is equal to $d\sigma/d\epsilon$ (where ϵ is the strain), for isotropic materials at small strains, the theoretical strength will be, [111], :

$$\sigma_{th}=\frac{2E\alpha_d}{\pi r_e} \qquad \textbf{(eq.6)}$$

Orowan also assumed that the work done in stressing a material to theoretical strength must be equal to the energy required to produce the two new fracture surfaces. If the surface energy per unit area is γ_o, integration of eq.5 from (r_e) to ($r_e+2\alpha_d$) and substitution of σ_{th} from eq.6 will result in the following expression :

$$\gamma_o = \frac{4 E \alpha_d^2}{\pi^2 r_e} \qquad \textbf{(eq.7)}$$

2.2.3 TYPES OF FLAWS

Ceramic materials are brittle in nature and their strength characteristics are mainly controlled by the stress concentration at flaws. So, it is of great importance to know the characteristics and main types of flaws.

The structural defects of ceramics can be identified and classified into the following categories, [113,114]:

a. Large surface and internal flaws formed during fabrication.

b. Cracks resulting from thermal mismatch of adjacent grains and/or phases.

c. Surface and internal pores formed during fabrication.

d. Stepped flaws found in the surface with a step-like appearance. Fracture in these, occurs by linking the flaws in two or more different planes parallel to fracture surface.

e. Penetration flaws, resulting probably from surface damage in a plane that is intersected by a fracture surface.

It must be underlined that the shape and the way one flaw influences the others

may alter the stress field inside the material and change its fracture characteristics.

2.2.4 BRITTLE FRACTURE

Brittle fracture is the fracture which happens from the elastic state without general yielding. Brittle materials, like ceramics, are unable to disperse stress concentrated areas and fail with no yielding or plastic deformation. In brittle fracture the energy involved is used for creating new surfaces, [115]. Surface or internal flaws and/or cracks can act as stress intensifiers and result in material failures at stresses far below the intrinsic strength of the material.

Substituting in eq.6, $\alpha_d = 0.14 r_e$ [111] shows that the theoretical strength (in ideal solids) is equal about 0.1 E and the ratio σ_f /E (which expresses the strain) is equal to about 0.1 (which means that, theoretically, materials fail at about 10% strain). Very thin fibres of some materials, glasses and hard drawn steel have strengths approaching the theoretical value E/10, but the majority of real materials have usually a ratio σ_f /E of 0.05 times and in some cases (e.g engineering ceramics) 0.001 times of the theoretical values, [116], (see Table 5). According to Davidge, [111], practical engineering ceramics have strengths ranging from 0.001-0.005E. Astbury [117] analysed failure data from a wide range of ceramics and found strengths in the range of 0.0005-0.002E.

The main reasons for deviation from ideal behaviour is the presence of a number defects or imperfections in real materials, e.g point defects, dislocations , voids, pores, inclusions, segregations, cracks, grain boundaries, which act as stress intensifiers.

Ref	Material	E_{th} GPa	σ_{th} GPa	E_{th} / σ_{th}	E Gpa	σ_f GPa	Actual E/σ_f
1	Alumina Al_2O_3	460	46	10	364	0.48	757
1 2	Magnesia MgO	245	37	6.6	210	0.103	2038
1	Si_3N_4				310	0.68	456
2	Mullite porcelain				69	0.069	1000
2	Firebrick clay				96	0.05	1920
1	Concrete				19	0.019	1000
3	Portland cement				7-28	0.003-0.014	2000-2300
1	Glass				90	0.69	768

Table 5. Strength characteristics of selected ceramic materials.

Ref. 1. Jayatilaka Ayal de S., [116]

2. Kingery et al, [5]

3. The Concrete Soc. [118]

Other factors, such as surface cracks from contact damage, residual stresses chemical and stress corrosion chemical embrittlement are also very important. However the fracture determining factors are the dislocations for ductile materials and the cracks for brittle materials.

Measurement of fracture strength in ceramics, because of their brittleness, is usually performed by modulus of rupture testing (three or four point bending). The values recorded by this testing are usually higher than that of fracture strength by a factor of two, due to the fact that a bend specimen is subjected to the maximum tensile stress over only a thin layer on its surface, whereas a tensile specimen is subjected to this stress over its entire volume, [119]. The probability that a large flaw is to be found is higher when the volume stressed is increased. Thus the difference between MOR and σ_f is a result of the statistical distribution of flaw sizes within the material or on its surface.

2.2.5 STRESS CONCENTRATION IN CRACKS

Flaws and cracks formed in materials during fabrication or developed in service can grow under load in a slow and steady way, until a critical value is reached. Beyond this value unstable fracture occurs, the functional relationships of which are described by Linear Elastic Fracture Mechanics (LEFM) [113].

The magnitudes of stresses concentrated at flaws can be estimated based on the initial work of the father of Fracture Mechanics, Inglis in 1913 [120].

A hole of elliptical cross section passing through a thin plate which is subjected to uniform tensile stress applied perpendicular to the major axis of the

ellipse is shown in figure 6.

Inglis investigated the distribution of stresses around elliptical holes which, if there are infinitesimally narrow, can be considered as cracks. For an elliptical centre crack of length 2c extending through the thickness of a thin plate subjected to uniform tensile stress, the stress at crack tip , σ_{tip}, will be:

$$(a) \quad \sigma_{tip} = \sigma\left(1+2\sqrt{\frac{c}{\rho}}\right) \qquad \text{(eq.8)}$$

$$(b) \quad \sigma_{tip} = 2\sigma\sqrt{\frac{c}{\rho}}$$

where ρ, is the radius of curvature at the crack tip , and

c, is half length of the crack

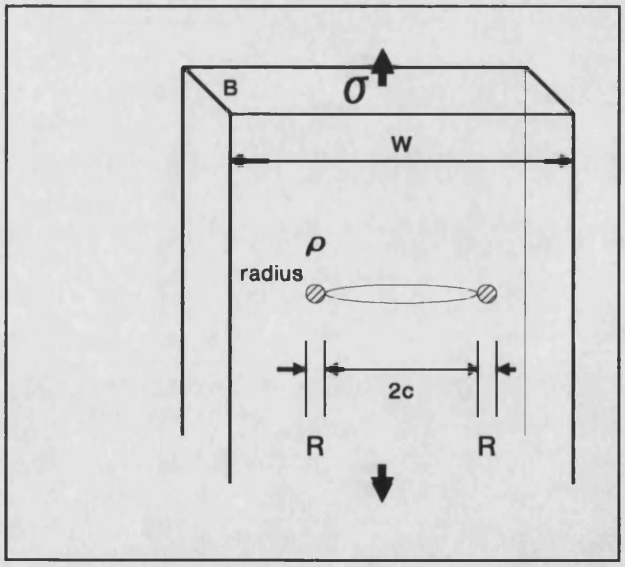

Fig.6 Stress concentration in an elliptical hole under tensile stress.

Eq.8(b) applies to stress at the tip of a narrow crack , under plane stress conditions and is a simplification of eq.8(a) made by neglecting the first term , since for small radii of curvature the first term is small.

The assumption which is sometimes made that the radius of the curvature is one half of the interatomic distance, giving very high stress concentration factors (about 1000) whereas values of 20-50 are more near reality, in accordance to available data [113].

Assuming that fracture will occur, when the stress at the tip of the crack reaches the theoretical strength and substituting in the above equation, Orowan's equation for theoretical strength (eq.6) and the surface energy equation (eq.7), gives:

$$\sigma_f = \sqrt{\frac{E\gamma_o\rho}{4cr_e}} \qquad \textbf{(eq.9)}$$

If further it is assumed that the curvature is half the atomic spacing , the above equation is simplified to:

$$\sigma_f = \sqrt{\frac{E\gamma_o}{8c}} \qquad \textbf{(eq.10)}$$

Tetelman and Evans [121] used an energy approach to estimate the critical condition at a crack tip for unstable fracture and a factor K, the stress intensity factor, which describes the magnitude of the elastic stress field at the crack tip (K will be discussed later).

They considered a plate of thickness B and width W containing a sharp crack of length 2c and a tip radius ρ. Under gross tension stress σ (less than the gross yield

stress σ_y) and assuming a perfect elastic material the stress intensity factor K will be [122]:

$$K=\frac{\sigma_{max}}{2}\sqrt{\pi\rho} \qquad \textbf{(eq.11)}$$

where σ_{max} is the maximum stress in the tip of the crack as the root radius ρ goes to zero.

Since the stress at the tip is equal to maximum stress, substitution of eq.8 , in the above equation, results in equation 12:

$$K=\sigma\sqrt{\pi c} \qquad \textbf{(eq.12)}$$

For edge cracks (with length 2c) Griffith, [123], indicated that the above equation must be modified to:

$$K=1.586\,\sigma\sqrt{\pi c} \qquad \textbf{(eq.13)}$$

From the above it is evident that edge cracks reduce strength by a factor of 1.59 when compared with similar cracks inside the ceramic body. On the other hand, for penny-shaped flaws with 2c diameter totally embedded in a large block of brittle material the Sack equation, [124], gives:

$$K=\sigma\sqrt{\pi c}\,\frac{\sqrt{4(1-\nu^2)}}{\pi} \qquad \textbf{(eq.14)}$$

The above equation for $\nu=0.25$ gives an increased strength by factor of 1.62 compared with that of a through crack.

Kendal et al. [125] underlined that comparing the three cases of cracks (centre-through, edge and penny- shaped) the net result is a factor of about one (1.59 almost off-sets 1.62), when, and if, there is a symmetric fraction of the above flaws in the brittle body.

Generally the stress intensity factor is a function of the applied stress and crack length, and for any crack shape and loading mode the function becomes:

$$K=\sigma\sqrt{\pi c}\, f(a) \qquad \textbf{(eq.15)}$$

where f(a) is a geometrical factor of the order of 1-2 which can be determined analytically for a given crack and structural shape.

Tetelman and Evans [121] used also an energy approach to estimate the critical condition for unstable fracture. According to their approach, unstable fracture occurs when the work, G, done at the crack tip of a crack, reaches a critical value G_c i.e when K reaches the critical value K_c).

Under critical conditions, the fracture stress σ_f for a wide plate containing a centre crack of length 2c [f(a)=1], using eq15, will be:

$$\sigma_f=\frac{K_{ic}}{\sqrt{\pi c}} \qquad \textbf{(eq.16)}$$

The energy release rate G, i.e. the work done in opening the crack , [126], is:

$$G=\frac{(1-\nu^2)K^2}{E} \qquad \textbf{(eq.17)}$$

Substituting K_{IC} from eq.15, will result:

$$\sigma_f = \sqrt{\frac{E G_c}{\pi c (1-\nu^2)}} \qquad \textbf{(eq.18)}$$

If in the last equation G_c is substituted by $2\gamma_i$ where γ_i is the energy required to produce a unit area of fracture surface, the relation becomes the same as that proposed by Griffith (described later in the energetic approach).

In metals, due to extensive plastic deformation before the unstable crack propagation, G_c is found to be several orders of magnitude larger than the thermodynamic surface energy γ_o. In ceramics G_c is much closer to γ_o, usually varying between about 2 and 100 times γ_o depending on the microstructure and temperature [121].

2.2.6 CRITICAL CONDITION FOR FRACTURE

Several criteria have been proposed to describe the condition for unstable fracture. The three main approaches include:

a. The Energetic or Thermodynamic (or Griffith) Approach.

b. The Elastic Stress Field Approach; and

c. The Stress Intensity Approach, which is essentially a combination of the other two.

These three approaches will briefly discussed here.

2.2.6.1 The Energetic or Thermodynamic or Griffith Approach

This approach is named after Griffith,who in two classic papers [123,127] proposed a criterion for crack propagation based on energetic and thermodynamic considerations.

In accordance with Griffith's theory the fracture strength is flaw size dependent. He based his approach on the concept that when a crack is formed or a pre-existing crack propagates, an amount of energy must be added proportionally to the area of the new surface without change of the total potential energy of the system. The original material used by Griffith to demonstrate that the fracture strength of a brittle material is a function of $\sqrt{c}$, where c is half the length of a pre-existing sharp crack, was glass, a material with structure consisting of irregular networks of silica tetrahedra bonded together with covalent bonds.

In order to demonstrate the effect of scratches as stress intensifiers he analysed the conditions of stresses in slit like cracks of glass spheres and cylinders as shown in fig.6. The basic idea was the following. A slit through-the-thickness crack of length 2c, having nearly the shape of a narrow ellipse, is considered present in uniform isotropic sheet of a brittle material subjected to a biaxial stress applied in the plane of the sheet at its outer edge. At remote points the stresses will be parallel or perpendicular and equal. He premised that a crack can propagate if the stored energy released is greater than the surface energy of the created new surfaces. He has shown that microscopic flaws could be present in apparently flaw-free materials, act as stress raisers and produce locally high stresses.

Griffith calculated the elastic strain energy release during grow in length of

the crack (dU/dc) from the results of Inglis [120] for the distribution of stresses in a cracked plate and proposed an energy balance criterion for predicting the propagation of a crack, in terms of the fundamental energy theorem of classical mechanics and thermodynamics:

a. Under plane stress condition, i.e. under bi-axial stress condition as in thin sheets or plates:

$$\sigma_f = \sqrt{\frac{2E\gamma_o}{\pi c}} \qquad \textbf{(eq.19)}$$

Comparing the above equation with that of Orowan's (eq. 10) it follows that this gives higher values of strength (about double).

b. Under plane strain condition:

$$\sigma_f = \sqrt{\frac{2E\gamma_o}{(1-\nu^2)\pi c}} \qquad \textbf{(eq.20)}$$

where: γ_o is the thermodynamic surface energy called also surface energy per unit area, since it is associated with the formation of unit area of new surface.

E, is the Young's modulus

v, is the Poisson's ratio (the ratio of contraction to extension when a specimen is under tension). Its value for ceramics is around 0.25, and c is the half length of the elliptical crack.

Griffith's series experiments in glass specimens showed good agreement with

his theory. This is an indication that possibly his theory is valid in cases where fracture occurs without prior plastic deformation near the crack tip.

Griffith's theory does not provide information about the way that cracks propagate and its main advantage is that a detailed understanding of the stresses in the vicinity of the crack tip is not required. However the energetic approach does not provide a measure of the stresses at the crack tip , which must be high enough to cause fracture. As a result it is possible that although there is adequate strain energy in the system to fracture, the stress concentration in the crack tip to be insufficient for crack propagation.

Hasselman et al [128], discussed the criteria for global instability (the system is considered as a whole and only a single site is under failure stress) and local instability (any site within the structure is under failure stress) of mechanical structures. They indicated that the Griffith criterion represents a necessary but not sufficient condition for catastrophic fracture. They suggested that, a brittle material with a microcrack will have:

a. A lower critical fracture stress which corresponds to the Griffith criterion for reversible fracture and represents the minimum stress level for slow crack growth by a reversible thermally activated process; and

b. A higher critical fracture stress which corresponds to the stress required for irreversible catastrophic fracture.

Finally they additionally concluded, as a consequence of the irreversibility of catastrophic fracture, that the surface free energy cannot be measured by a fracture test.

Theoretical analyses of the stresses at the tip of a crack have shown that under

the stress condition of the Griffith criterion, the stress at the crack tip is approximately equal to theoretical strength of the material (the interatomic cohesive stress). But when limited plasticity occurs at the crack tip the thermodynamic surface energy is often many times higher than the actual surface energy estimated by other methods [116].

Irwin [129] and Orowan [112], proposed a simple modification of Griffith's criterion to account for plastic deformation in metals. When there is no plastic deformation the work of fracture is equal to thermodynamic surface energy.

They introduced the work of fracture γ_f, and a plastic work term γ_p:

$$2\gamma_f = \gamma_p + 2\gamma_o \qquad \textbf{(eq.21)}$$

After this transformation the Griffith's criterion for plane stress becomes:

$$\sigma_f = \sqrt{\frac{2E\gamma_f}{\pi c}} \qquad \textbf{(eq.22)}$$

and for plane strain:

$$\sigma_f = \sqrt{\frac{2E\ \gamma_f}{(1-\nu^2)\pi c}} \qquad \textbf{(eq.23)}$$

The work of fracture sometimes is also called work for fracture crack initiation or effective surface energy for fracture initiation with the symbol γ_i . According to Davidge and Evans [130], the following general relationship exists between σ_f and γ_i:

$$\sigma_f = \frac{Z}{Y}\sqrt{\frac{2E\gamma_i}{c}} \qquad \text{(eq.24)}$$

where: γ_i is the effective surface energy for fracture initiation and considers contributions due to work consumed by plastic flow, the work needed to create cleavage steps [131,132] the work used in creating secondary cracks [133] and original γ and, Y and Z are dimensional terms which depend on the crack depth and test geometry.

2.2.6.2 The Elastic Stress Field Approach

This approach [110,134] can be applied if the following two requirements are fulfilled:

a. The stresses applied in a body are in equilibrium.

b. The strains produced by the stresses do not destroy the elastic continuity of the material. This is also known as compatibility condition.

A requirement resulting from the compatibility condition is that the material is considered as a continuum and not as resulting from construction of discrete particles e.g. atoms, molecules, crystals or crystallites.

Considering the more simple two dimensional case, in order to avoid complexity, Airy demonstrated that there exist a function $\Phi(x,y)$ which satisfy the equilibrium equations of stresses. The stresses σ_x, σ_y and τ_{xy} are defined as :

$$\sigma_x = \frac{\partial^2 \Phi}{\partial y^2}$$

$$\sigma_y = \frac{\partial^2 \Phi}{\partial x^2} \qquad \textbf{(eq.25)}$$

$$\tau_{xy} = -\frac{\partial^2 \Phi}{\partial x \, \partial y}$$

The compatibility equation of strains is satisfied by the following biharmonic equation:

$$\nabla^4(\Phi) = \frac{\partial^4 \Phi}{\partial x_1^4} + \frac{\partial^4 \Phi}{\partial x_1^2 \, \partial x_2^2} + \frac{\partial^4 \Phi}{\partial x_1^4} \equiv \qquad \textbf{(eq.26)}$$

$$= \nabla^2(\nabla^2 \Phi) = 0$$

where ∇ is the Laplace operator

Every function $\Phi(x,y)$ which satisfies the above equation is called an Airy stress function [110]. Except ideal cases the boundary conditions impose severe difficulties in the solution of the above equations.

Considering now a biaxially loaded infinite plate containing a slit crack (fig.7) quite complex mathematical analysis shows that the stresses will be :

$$\sigma_x = \frac{\sigma\sqrt{\pi c}}{\sqrt{2\pi r}} \cos\frac{\theta}{2}\left(1 - \sin\frac{\theta}{2}\sin\frac{3\theta}{2}\right) \qquad \textbf{(eq.27)}$$

$$\sigma_y = \frac{\sigma\sqrt{\pi c}}{\sqrt{2\pi r}} \cos\frac{\theta}{2}\left(1 + \sin\frac{\theta}{2}\sin\frac{3\theta}{2}\right)$$

$$\tau_{xy} = \frac{\sigma\sqrt{\pi c}}{\sqrt{2\pi r}} \sin\frac{\theta}{2}\cos\frac{\theta}{2}\cos\frac{3\theta}{2}$$

The above equations show that the stresses tend to infinity as r goes to zero (the crack tip) and they are all products of a common factor $\sigma\sqrt{\pi c}$ which determines the magnitude of the elastic stresses in the crack tip field and a geometrical position factor $[1 / \sqrt{(2\pi r)}]\ f(\theta)$.

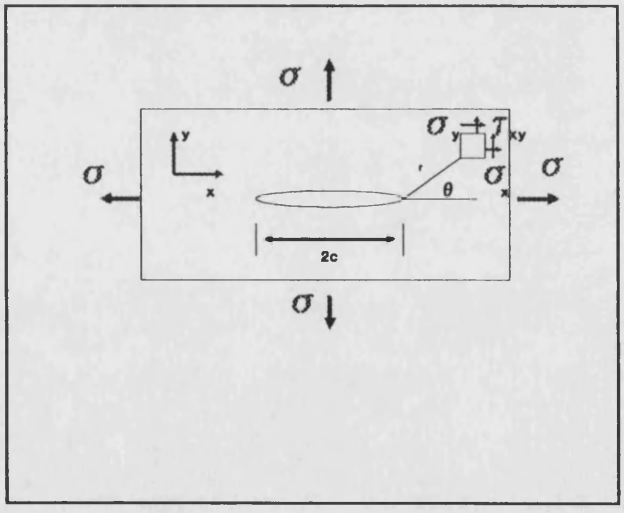

Fig.7 Stress distribution in a biaxially loaded infinite plate containing a slit crack.

2.2.6.3 The Stress Intensity Approach

Before the analysis of the stress intensity approach it should be necessary to define the three basic, technologically important modes of crack surface displacement which can occur under conditions of combined loading (fig.8) [126].

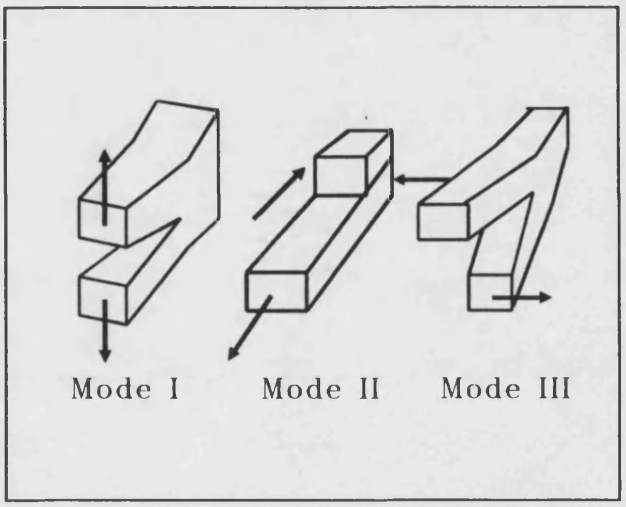

Fig.8 The three modes of loading

The elastic stresses and strains produced ahead of the crack tip differ in each mode. In the mode I, the crack surface displacements are perpendicular to the crack plane, tending to open the crack. In mode II the displacements occur perpendicular to crack front, tending to shear the crack. In mode III, the displacements occur parallel to the crack front, tending again to shear the crack.

Each displacement mode is associated with a stress intensity factor (K_I,K_{II}, K_{III}). The technologically most important type is the mode I and the main fracture mechanics test methods are designed to measure the mode I fracture only.

The stress intensity approach which is a combination of the previous two

approaches was originally suggested by Irwin in 1958.

Since, in many cases, the processes which happen at the crack tip are not known and, in order to avoid this need for detailed knowledge, the so-called stress intensity approach was developed which introduced the stress intensity factor K_{IC}. This factor describes the magnitude of the elastic stress field in the crack tip.

Toughness of a material is defined as the resistance of a material to growth of cracks. In practice it is measured in a number of ways, [82], such as impact testing, work of fracture and linear elastic fracture mechanics techniques (the K_{IC} method). The stress intensity factor K_I, can be related to the applied stress σ and the crack length, by the following equation [111]:

$$K_I=\sigma Y\sqrt{c} \qquad \textbf{(eq.28)}$$

where Y is a dimensionless constant which depends on the geometry of the loading and the crack configuration.

Relation of the above equation with Griffith's equation gives the following relation [135] (for critical K_I for fracture, K_{IC}) which is **the general fracture equation**:

$$\sigma_f=\frac{K_{IC}}{Y\sqrt{c}}=\frac{1}{Y}\sqrt{\frac{2E\gamma_o}{c}} \qquad \textbf{(eq.29)}$$

where Y is a geometrical constant

The result is that K_{IC} is equivalent to $(2E\gamma_o)^{1/2}$ for ideal fracture when the principles of L.E.F.M. apply. It follows that:

$$\gamma = \frac{K_{IC}^2}{2E} \qquad \text{(eq.30)}$$

Both parameters (K_{IC} and γ) can be considered as material parameters. Typical values of fracture toughness from various ceramics and glass are given in Table 6 [136,137].

Davidge, [135], indicated that although LEFM has been used in a wide range of materials for describing the strength, the complexity of the fracture process changes when materials like glass, ceramics, cement, or brittle polymers are considered. He also underlined that in practice, fracture toughness or fracture surface energy, is rarely a material constant as could expected by LEFM.

For cracks opening under the influence of tensile stress (Mode I crack opening), modification of the above "general fracture equation " to account for flaw shape gives the equation [138,139]:

$$\sigma_f = \frac{Z}{Y}\sqrt{\frac{2E\gamma_i}{c}} \qquad \text{(eq.31)}$$

or

$$K_I = \frac{Y}{Z}\sigma_f\sqrt{c} \qquad \text{(eq.32)}$$

where, Z is the shape parameter depending on the crack shape [138]
Y is a geometrical factor adjusting the relative sizes of the crack and the specimen, γ_i is the fracture surface energy; and c is half the crack depth.

Material	K_{IC}, MPa.$m^{1/2}$
Alumina (Al_2O_3)	3-5
Soda glass (Na_2O-SiO_2)	0.7-0.8
Cement	0.2
Mullite	1.8-2.5
Porcelain (electrical)	1
Silicon nitride (Si_3N_4)	4-5
Partially Stabilized ZrO_2	9
Magnesia (MgO)	3
Silicon carbide (SiC)	3

Table 6 Typical Values of K_{IC} for various ceramics and glass [136,137].

In accordance to the above equations, a blunt crack with small c, will fracture at high stress and relatively high K_{IC}. But high K_{IC}, results when there is high effective surface energy, even though there is no physical relationship between bluntness and surface energy. In a analogous way sharp cracks will fracture at low stresses leading to low values of γ. K_{IC}, the characterizing parameter for crack extension is the fundamental principle of Linear Elastic Fracture Mechanics (LEFM).

2.2.7 EFFECT OF MICROSTRUCTURE ON MECHANICAL PROPERTIES

The microstructure of ceramics is generally a combination of their original chemical and mineralogical composition and fabrication history.

In accordance with Linear Elastic Fracture Mechanics (LEFM), K_{IC} in brittle

materials can be connected to microstructural changes. Evans and Tappin [139] examined the effect of grain size on the appearance of the fracture surfaces of slip cast polycrystalline aluminas and they found that fine grain alumina (about 3 μm) gave a large number of pull outs about 40 μm deep, intermediate alumina (about 30 μm) gave a small number of pull outs about 90 μm deep and large number of grain sized pull outs and, finally, coarse grained alumina (about 100 μm) gave no indication of the point of fracture initiation but showed many surface cracks none of them larger than the grain size. They concluded that, in absence of large flaws, catastrophic failure occurs with the linking of existing flaws a fact which makes the description of the strength in terms of fracture mechanics insufficient.

Claussen et al. [140], examined the influence of microstructure of sintered and hot pressed Al_2O_3 and ZrO_2 ceramics on K_{IC} using the notch beam test. They observed a different behaviour with respect to fracture path. When intercrystalline fracture occurred, K_{IC} was decreased as grain size was increased.

When the fracture path changed to transcrystalline the K_{IC} was increased with increase in grain size. They also examined the temperature dependence of K_{IC}. Experiments with pure alumina, showed decrease of K_{IC} with increase of temperature. However, mixtures of alumina and 3% silica showed increase of K_{IC} in the range of 700-960°C and decrease in higher temperatures. At room temperatures the glassy phase was brittle and the fracture mainly intercrystalline.

Finally they concluded that:

a. Notch width sensitivity was low with very porous alumina.

b. The relative notch depth had no significant effect on K_{IC} for types of Al_2O_3 over a wide range of a/w ($0.1 < a/w < 0.6$),

where w is the height of the specimen.

c. The scatter in K_{IC} depended mainly on microstructure.

As Davidge and Tappin [141] explained, the increase in K_{IC} can be attributed to drop of viscosity at temperatures above 700 °C . As a result more energy can be dissipated by deformation of this phase. At higher temperatures, the very low viscosity does not offer a resistance to fracture and K_{IC} is reduced.

Alderson [134], reviewed the historical development of stress analysis, as applied in brittle materials obeying the laws of linear elasticity, for the solution of stress functions in cracks and flaws. He examined, theoretically and experimentally, in coarse polyphase clay based ceramics, the influence of material structure on stress analysis. He found that LEFM parameters such as the fracture stress σ_f the critical stress intensity K_{IC}, and the modulus of elasticity E vary with clay composition and structure.

Buresch [142], indicated that the toughness of ceramics is controlled by micromechanical features which occur in the process zone (having a size of 0.1-1 mm for many fine and coarse-grained ceramics) during stress redistribution. Factors affecting K_{IC} include the notch radius in connection to microstructure, and specimen geometry.

Cooke [143], underlined that flaws formed during microcracking from thermal mismatch stress relaxation develop this process zone (mentioned by Buresch) in front of the crack tips, and their statistical distribution controls the strength by a Weibull function. In heterogeneous ceramics the flaws that determine strength are microstructurally dependent and their development has been modelled to predict strength statistics.

Dalgleish et al. [144], examined the fracture toughness-microstructure relationship of alumina based ceramics using 3-point bending and acoustic emission techniques in order to detect subcritical crack growth during testing. They concluded that small grain size, high density and rounded pores, resulted in good mechanical properties.

2.2.8 SURFACE ENERGY

More than twenty years prior to Orowan, Griffith, [123,127] first applied energy considerations to the fracture of materials. During the application of stress on a material strain energy is stored in it, until fracture. When fracture occurs this energy is released and the work of fracture done is equal to thermodynamic surface energy of the formed surfaces. If γ_o is the thermodynamic surface energy per unit area, relation of equations (6) and (7) gives Orowan's equation for theoretical strength σ_{th} with relation to surface energy, E and r_e:

$$\sigma_{th} = \sqrt{\frac{E\gamma_o}{r_e}} \qquad \textbf{(eq.33)}$$

It is evident that materials have high strength when they have high surface energy and stiffness and small lattice spacings.

The experimental surface energies for cleavage of single crystals are very close to the theoretical ones (differing by a factor of 2), except for aluminum oxide, where because of the difficulty to produce good cleavage planes, the difference is from 10-30 times. However, the experimental surface energy values for glasses,

which are non-crystalline solids with high hardnesses and high elastic moduli, is very small [135].

Early work on glass [145], tested in flexure, revealed that the fracture face of glass specimens partially consists of a smooth, mirror-like area, and that a relation exists between the "mirror surface" area and the fracture stress. Noone and Mehan [146], examining ceramic materials suggested that the increasing fracture energies which were observed with increasing grain size was a consequence of the increasing tortuous fracture path and multiple secondary crack branching observed with increasing grain size. Fracture of ceramics near room temperature is dependent mainly on grain boundary mechanisms and the effects of local inhomogeneity and anisotropy, while in metals multiple slip is the primary mechanism of energy absorption. They indicated that the fundamental energy relations of fracture mechanics are based on linear elastic behaviour of homogeneous and isotropic materials and some inconsistencies arise when LEFM is applied to polycrystalline ceramics. They used Paris and Sih's formula to compute K_{ic} and the following formula to compute γ for Lucalox alumina specimens:

$$\gamma = \frac{(1-\nu^2) K_{IC}^2}{2E} \qquad \textbf{(eq.34)}$$

They concluded that the K_{IC}= 3.96 MPa.m$^{1/2}$ and γ= 19.3 J/m^2 values were similar to those from other measurements.

There are large differences between fracture energies and thermodynamic surface energies. Fracture energies are usually several times larger than thermodynamic surface energies (e.g. three times for glasses). Polycrystalline fracture

energies are typically three to ten times more that of single crystal fracture energies.

Rice [147], reviewed the microstructural dependence of the fracture energy and especially the effect of porosity, grain size and shape effects. Generally fracture energy and strength decrease with increasing porosity. A surface energy-porosity exponential relation was proposed by Rice et al., [148]. They, examining the microstructural dependence of fracture mechanics parameters in ceramics, concluded that the fracture energy relation to porosity (p) is:

$$\gamma = \gamma_o e^{-bp} \qquad \textbf{(eq.35)}$$

where b is a constant depending on the character of porosity.

2.2.9 ACOUSTIC EMISSION AND K_{IC}

Tetelman and Evans [121] reviewed some of the principal correlations between acoustic emission and fracture mechanics parameters, as applied to brittle structural materials.

Acoustic emission measurements [121,149,150] have shown that the acoustic emission rate dN/dt is related to the stress intensity factor K_{IC}. Acoustic emission is a result of three entirely separate processes near the crack tip which may have a separate dependence on K, i.e the growth of plastic zone (in metals), microcracking in the zone near the crack tip and extension of the primary crack. As was shown by Evans and Linzer [149], during slow crack growth, as the crack grows to its critical size, the crack velocity is dependent on the applied stress intensity factor and the following empirical relation exists:

$$v=\frac{dN}{dt}=c.K_I^n \qquad \text{(eq.36)}$$

where, v is the crack velocity, c is the crack length, and n is a constant

Dunegan et al. [151], proposed that the cumulative AE counts are directly proportional to $(K_I)^q$ where q=4 (from theoretical analysis). Lloyd and Tangri, [152], found for Al_2O_3 a relation between ΣN (Cumulative counts) and K_{IC} of the form:

$$\sum N=A\,K_{IC}^n \qquad \text{(eq.37)}$$

where A and n are constants (n = 2 to 3).

Evans and Linzer [149], found a linear relationship between acoustic emission event rate and log-time in porcelain depending on the stress level.

2.2.10 SUB CRITICAL CRACK GROWTH

In many cases of fracture surface energy measurements a lower value of surface energy than the expected one is taken. This could be attributed to sub-critical crack growth which changes the shape of the crack making it more severe. In this case the flaw shape parameter, Z, increases (eq.32), K_I decreases and a lower apparent surface energy is recorded. Subcritical crack growth is also responsible for the failure of loaded structures. The subcritical crack growth rate u is related to the stress intensity factor K_I with a power law (see 2.4.6).

Dalgleish et al, [144], indicated that AE prior to fracture in notched alumina specimens depends on the extent of sub-critical crack growth which in turn is

dependent on the grain size and porosity. They also indicated that AE from MOR specimens is due to a linkage process of flaws, while AE from notched specimens is due to sub-critical crack growth of pre-existing cracks. Since they did not detected AE counts in MOR testing they concluded that the unit step in the linkage process AE is smaller than that in notched specimens.

Davidge [135] underlined the complications when the flaw sizes are comparable in size to microstructural features and when there is high density of inherent flaws. The surface energy for a grain size crack should be similar to grain cleavage or boundary surface energy which is at least an order of magnitude less than the effective surface energy for macroscopic fracture. This means that fracture may be preceded by a period of subcritical crack growth. Furthermore the Weibull theory (which will be discussed later in sub-chapter 2.3) assumes that flaws do not influence each other, an assumption which does not stand when the crack size is similar to crack spacing. As Okada and Sines [153] have shown a relatively high density of active microcracks in polycrystalline alumina and a number of close and small microcracks can coalesce and lead to failure.

As Davidge [135] pointed out similar effects are expected in porous materials (porosity in ceramics larger than 5-10% is of the open connected type) where pores act as connected flaws and the whole specimen can be considered as perforated by a single large flaw.

Strong uniformly structured ceramics behave differently compared to weaker coarse structured materials. Cooke [154] discussed the mechanical, acoustic and microstructural observations on ceramic systems with varying heterogeneity on the basis of mechanisms of failure. He pointed out that fine grained (about 1 μm particle

size) materials like glass and quartz are "quiet" from AE point of view and show failure as a result of a single flaw propagation, while coarser ceramics (with grain size of about 100 μm) show significant sub-critical activity. He indicated that in heterogeneous materials in addition to difficulties in identification of the flaw size and the surface energy, there is one more, namely the non-linearity of the transmission of load to various components of the heterogeneous structure (in LEFM it is assumed that the load is transferred to the crack tip by a uniform elastic field whose properties are given by the bulk elastic moduli).

He also underlined that taking into account the critical strain, introduced by Astbury [117], which is about 1 millistrain for all ceramic materials, the difference in critical flaw size between e.g. 20 μm for Refel SiC [155], and 300 μm for fired clay, gives a scaling factor for the homogeneity of the microstructures.

Cooke [156] also investigated the strength and toughness of coarse structured ceramics and compared with that of model systems (e.g. NaCI/NaF). He concluded that changes in microstructures result in changes of sub-critical acoustic activity and of mechanical properties. He underlined that although there is a linear load-deflection relationship and the materials could be considered as fully brittle, acoustic emission indicates sub-critical activity and concluded that changes in microstructures result in changes of sub-critical acoustic activity and of mechanical properties.

2.2.11 LIMITATIONS IN APPLYING LEFM TO CERAMICS

Rice and Lewis [157] presented a summary of the limitations in applying continuum based fracture mechanics to ceramics and ceramic composites. They

indicated that much of the early work on ceramics was on glasses or fine grain polycrystalline materials, which are " very near" the idea of LEFM and that a number of microstructural features can modify the fracture behaviour of ceramics and result in large discrepancies between experimental results and LEFM predictions. There are actually large differences between LEFM and actual values in strength and Young's modulus predictions.

They pointed out that the main effects of microstructure on LEFM as applied to ceramics include:

a. Effects of pores

Widespread pores of various shapes and sizes and spatial distributions occur in ceramics as a result mainly of incomplete densification during processing or from gas bubbles from reaction with impurities and other reasons. These pores individually or as clusters act as fracture origins [e.g. 148,158] and there are uncertainties about the form of the interaction between these pores and cracks.

b. Effects of grains and particles

Microcracking is usually associated with large grains or second phase particles usually as a result of thermal expansion anisotropy [159]. Microcracking can exist before any application of stress and problems arise from the relation between crack size and scale and distribution of microcracks and the existence or not of interaction between microcracks. Another microcrack problem, often associated with high technology ceramics, is the generation of additional or totally new microcracks in the high stress field of a highly stressed crack tip.

They concluded that the two basic factors needing analysis are:

a. Kinking, jogging and mixed mode aspects of fracture; and

b. Statistical effects of pore, particle and microstructural stress.

Many "classic" and "new" ceramic materials can be considered as particulate composites, where a particulate phase is dispersed in a polycrystalline matrix [160]. When a particulate composite ceramic is cooled from its fabrication temperature (firing or sintering temperature) stresses are produced, due to different thermal expansion of particles and matrix.

Lange [160] used an energy balance approach to determine the conditions under which crack extension and arrest will take place within the residual stress field formed in a ceramic material when second phase particles are embedded within its matrix. He concluded that the criterion of crack instability is governed mainly by the following factors: (a) particle size of second phase, (b) maximum stress, (c) elastic properties of the two phases, (d) surface energy of the cracked phase, (e) size of pre-existing crack. He also concluded that as an implication of the above, the second phase particles are not necessarily crack precursors if these particles are very small.

It has been shown [161,162] that during cooling, cracks are formed near to the larger particles, a fact which is inconsistent with the Griffith fracture equation according to which, since the maximum tensile stress is independent of particle size, cracks should be observed to all particles. Davidge and Green [162] explained this inconsistency indicating that the stresses around particles are highly localized and crack extension is due to a limited amount of stored strain energy.

According to their results the strain energy within a particle, U_p, and the strain energy within the matrix, Um, are equal to:

$$U_p = 2\pi \frac{\sigma^2(1-2\nu_p)}{E_p} R^3 \qquad \textbf{(eq.38)}$$

and

$$U_m = \pi \frac{\sigma^2(1+\nu_m)}{E_m} R^3 \qquad \textbf{(eq.39)}$$

where E and v are the elastic constants of matrix (subscript m) and particle (subscript p), σ is tensile stress and R is the radius of a spherical particle

Thus, the total stored strain energy (the sum of U_p and U_m) is a function of σ^2 and R^3.

Gupta [163] has shown that toughness in ceramics can be best described in terms of critical strain energy release rate G_c and presented a model for development of tough ceramics based on the concept of stable crack propagation as developed by Glucklich and co workers for cement composites [164,165,166]. According to this concept crack arresters in a brittle matrix result in a non-linear relation between energy for crack propagation and crack length in contrast to linear Griffith relation which applies in single phase homogeneous materials. The non-linearity arises from the ability of the second phase to stabilize a growing crack. As an example , a crack developed in a weak matrix (e.g. alumina dispersed glass composite) which has a low critical strain energy release rate G_c , may as it propagates to meet a zone of tougher second phase with higher G_c. The crack could detour around the obstacle or go by cutting through it. Whatever happens an increased energy demand will result, crack propagation will be halted and the composite toughness will be increased [167].

However, increase in strength as well as in toughness, require a good bonding between the dispersed phase and the matrix at least as strong as of the matrix itself.

2.2.12 STRENGTH OF SHORT FIBRE CERAMIC COMPOSITES

Typically, fibre ceramic composites are divided in two large categories : those where there is a strong interface between matrix and fibres, which usually occur when oxide fibres form composites with similar oxide matrices, and those where there is a weak interface between matrices and fibres which have no chemical similarities and there is no chemical bond between them.

In order for fibre ceramic composites which form a strong interface to develop a higher strength than the ceramic matrix, loads must be transferred to fibres which normally have better mechanical characteristics. While this is quite easily attained in unidirectional long fibre-composites, in short fibre composites loading cannot be applied at the fibres ends and stress must be transferred by shear forces at the fibre-matrix interface [71]. So, the fibre ends play an important role in these composites since the load carried by the fibre, build up from the ends. According to Cox [168] a short fibre in a matrix which is under tensile stress will have a tensile stress variation along its length and a shear stress at the interface, like the one shown in fig.9, under the assumptions that fibre and matrix are elastic, the interface is thin, the bond between matrix and fibre is perfect, and the material near the fibre is identical and has the same properties as the bulk matrix material.

Shear stress will be maximum at the fibre ends and minimum (zero) at the fibre centre. The reinforcing efficiency of short fibres is less that of long fibres since

there are regions at the ends of the fibres that do not carry the full load, and decreases as the average fibre length decreases.

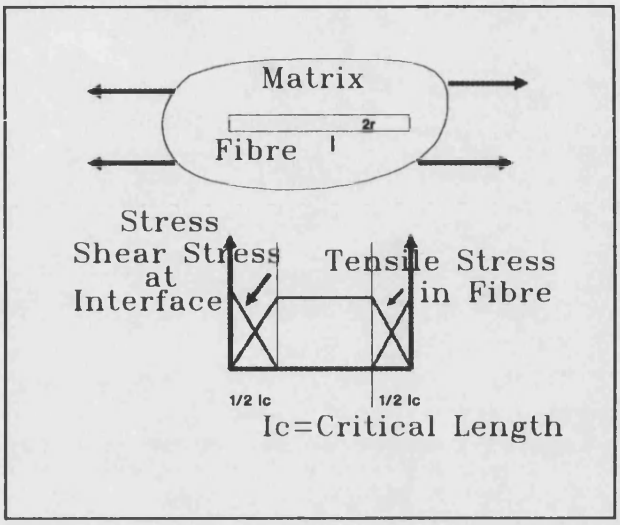

Fig.9 Variation of tensile and shear stresses along a fibre embedded in a matrix subjected to tensile load.

In accordance with Cox's analysis, shear stresses are high at the interface (near the fibre ends) and zero at the centre and tensile stress has been transferred to the fibre when it has sufficient length larger than l_c (critical length). The aspect ratio l/2r influences the effect of fibre ends, the higher the ratio the less important the effect [69].

Harris [71] indicated that a minimum fibre length l_c (critical length) is necessary in order the fibre to carry the maximum fibre breaking stress (fig.10). When fibres are shorter than l_c, they cannot be broken by direct stress transfer from the matrix. A transformed "rule of mixtures" for calculation of composite strength in a short fibre composite with aligned fibres [69,71], taking into account the average

tensile stress carried by the short fibres, is as follows:

$$\sigma_c = \sigma_f V_f (1 - \frac{l_c}{2l}) + \sigma_m (1 - V_f) \qquad \textbf{(eq.40)}$$

where σ_c ,σ_m, σ_f, are the strengths of composite, matrix, and fibres respectively, V_f is the volume fraction of fibres, and

l, l_c are the mean length and critical length of fibres respectively.

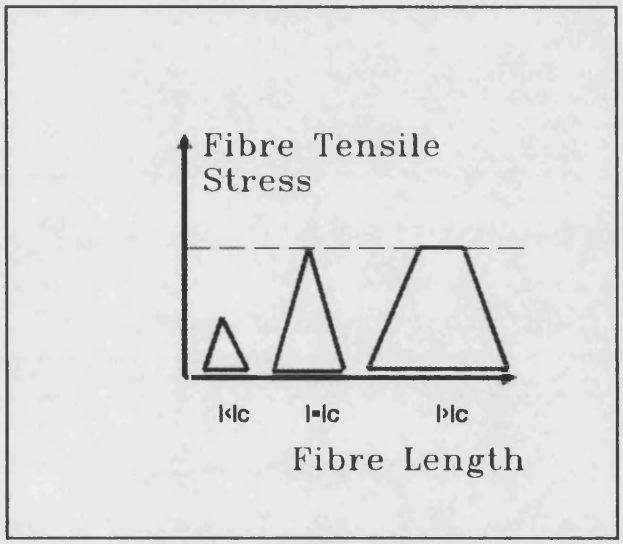

Fig.10 Variation of tensile stress in a short fibre as function of fibre length.

Calculation of composite strength [71], in accordance to the above equation, shows that when $l = 10l_c$ the short aligned fibre composite has about 95% of the strength of the continuous fibre composite. However when the short fibres are not aligned the composite strength is much lower influenced by three parameters: (a) the fibre length, (b) the lower levels of V_f and (c) the fibre mis-orientation. The strengths of such systems are difficult to be computed because of the combination of variables.

In the case of fibre composites with weak fibre-matrix interfaces the work of fracture depends on the amount of pull out and on V_f. The work of fracture increases with fibre length [69], has a maximum when the length of the fibres is equal to a critical length l_c and then drops rapidly because fibres fracture for $l > l_c$ before complete fracture and the amount of pull out decreases.

2.2.13 MEASUREMENT OF SURFACE ENERGY AND EQUIVALENT CRACK LENGTH

Surface energy can be estimated by determination of K_{IC} with the help of a notched specimen, under 3 or 4 point bending and use of the formula :

$$\gamma = \frac{K_{IC}^2}{2E} \qquad \textbf{(eq.41)}$$

Davidge and Tappin [141] introduced a method for determination of Griffith flaw size or equivalent elastic crack c_E. Using notched and un-notched bars they measured K_{IC} and σ_f respectively. The formula connecting the two parameters is :

$$\sigma_f = \frac{1}{1.92}\sqrt{\frac{K_{IC}^2}{c_E}} \qquad \textbf{(eq.42)}$$

where c_E is the equivalent crack length

From the above equation it is obvious that the strength of a ceramic can be improved by increasing toughness and reducing the flaw sizes. Toughness can be improved probably through composite production (see sub--chapter 2.1.3). Flaw sizes

can probably be controlled through changes in manufacturing processes (e.g. sol-gel processes).

Alford et al [169] measuring the dimensions of surface defects using image analysis and optical microscopy methods, estimated, using the above equation, the strength of fine-grained commercial alumina ceramic produced by a colloidal process and found that it was in agreement to that of three-point bending tests.

2.2.14 MEASUREMENT OF TENSILE STRENGTH IN CERAMICS

Ceramic materials have much greater compressive strengths than tensile, by a factor of 10-15, as a result of the behaviour of their pre-existing flaws and the different mode of failure [170]. As a consequence, failure in bending is tensile.

In tensile testing, the most favourably oriented crack propagates unstably almost vertically to loading axis when K_{IC} is reached, whereas in compressive testing a large number of cracks oriented at an angle to compression axis propagate stably parallel to the loading axis, leading to failure by crushing at higher fracture stresses, [170].

The standard measurement of tensile characteristics in materials, by pulling a specimen after gripping it with a pair of jaws, cannot be used in ceramics because in most cases the specimen will break during alignment and positioning it on the grips. The usual way to measure tensile strength in ceramics is by three or four point bending, provided that simple beam theory can be applied. In three point bending, a specimen is placed in two supports and is pressed by a third edge in the middle between the other two. The three point bending load application shear stress and

moment and diagrams resulting from this system are shown in fig. 11 (A, B and C). As indicated, [171], the maximum stress occurs along a line on the specimen side opposite the single central support.

The main advantage of 3-point bending test is its relative simplicity and the main disadvantages are that the maximum stressing of the specimen is confined only on a small area and there exist stress gradients along the specimen's length and thickness. However, these disadvantages could turn to be desirable in cases where manufacturing flaws must be avoided and a maximum stress in a limited area can be used.

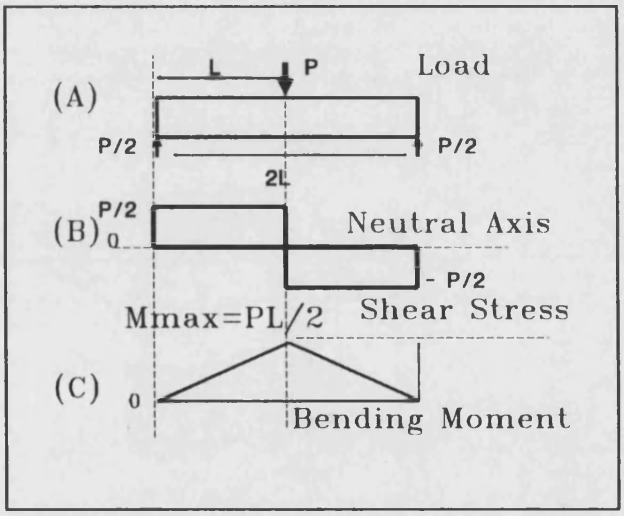

Fig.11 Load, Shear stress and Moment diagram in three point bending

In four point bending the specimen is placed in two supports and then is pressed by other two inner supports in a symmetrical way. This test has the advantage of having an almost uniform applied stress over the length between the two inner supports. However, the probability to find a significant manufacturing flaw in this test is greater than in three point bending, because larger specimen volume is under

maximum stress. As a result strengths in 4-point-bending are lower than that in 3-point bending, for the same material [172]. The probability of failure is higher when the stressed volume is larger, since the probability of finding a critical flaw is increased.

The calculation of failure stress and strain in a beam in bending is simple if it is assumed [172] that:

a) the stress-strain behaviour in tension and compression is identical.

b) the beam is bent into an arc of a circle between the supports, and

c) friction at contact points is negligible.

Typical bending strength of ceramic materials are given in Table 7 [137].

2.2.15 EXPERIMENTAL DETERMINATION OF FRACTURE MECHANICS PARAMETERS

Fracture surface energy, γ_i, the energy term in the Griffith's criterion for crack instability, and the critical stress intensity factor K_{IC} can be measured by the Notch-Beam Technique (NBT) [138,173]. In accordance with this method, a crack of known dimensions and orientation, much larger than the inherent flaw size, is induced in specimen of various geometries and loading configurations. The most common and simple specimen is the single-edge notched beam specimen (SENB) which is then loaded in three or four point bending and the fracture stress is recorded. Bansal and Duckworth [173] reported that this technique gives valid fracture surface energy values on ceramic materials.

The determination of mechanical properties of ceramics using the principles

Material	Bending strength, MPa
α-Al_2O_3, porosity $<4\%$, polycrystalline	300-450
mullite	220-240
porcelain	63-76
silica glass	72
Carbon fibre-silica glass matrix composite (35% volume fraction of fibres)	600-625

Table 7. Typical bending strength of ceramic materials

of fracture mechanics, can be achieved by experimental determination of effective surface energy, γ_i, and stress intensity factor K_I. The methods used for determination of the above parameters are :

a. The Compliance analysis

This method does not require the knowledge of stress distribution in the specimen and the parameters are estimated directly from the force-deflection measurements of the specimens with a wide range of crack sizes. Nakayama [174] and Tattersall and Tappin [175] described similar methods of measurement of the work of fracture, based in the following experimental procedure.

When a centre-notched specimen, with a narrow notch sharp at the tip is tested in three point bending, the crack area A and the force -deflection relations will be:

$$A=2ba \quad and \quad F=sD_l \qquad \textbf{(eq.43)}$$

where b is the width, α is the notch depth of the specimen, F is the applied force, s, is the stiffness and D_l is deflection of the specimen.

At fracture the stored elastic energy U_e , since $dU_e/dA = \gamma_i$ will be equal to :

$$U = F\frac{D}{2} = \frac{sD^2}{2} \quad or \quad \frac{dU}{dA} = \gamma_i = -\frac{D^2}{2}\frac{ds}{dA} \qquad \textbf{(eq.44)}$$

Typically, the work of fracture [82] for non-reinforced ceramics and glasses range from a few Jm^{-2} to a few hundred Jm^{-2} , while for fibre composites it can be increased to 10^4 Jm^{-2} . The work of fracture for various types of materials is given in Table 8.

Davidge and Tappin [178], measuring the effective surface energy of brittle materials have shown that the stiffness s is proportional to α/w (notch to depth ratio) and that ds/dA can be determined as a function of crack area. Testing a variety of brittle materials (alumina, PMMA {poly-methyl-meth-acrylate}, soda-lime glass graphite) in three-point bending, found that there was no systematic variation of the effective surface energy at the initiation of fracture (γi), with the notch depth using the modified Griffith treatment and the compliance analysis method.

They suggested that for a given material the effective surface energy (γ) was not necessarily the same at all stages in the fracture process and could be

distinguished by γ_i, related to the initiation of fracture and γ_f applying to average energy over the whole fracture process.

They also used the work of fracture method [174,175] and calculated the values of γ_f, (obtained by measuring the work which has be done during complete fracture) in notched specimens from the equation:

$$\gamma_f = \frac{U}{2B(W-\alpha)} \qquad \textbf{(eq.45)}$$

where, U is the strain energy, and B,W,α are the width, height and notch depth of the specimen respectively.

Material	Work of fracture, J/m^2	References
Copper	5×10^4	(1)
Polystyrene	10^3	(1)
Firebrick	20 - 70	(1)
Alumina (polycrystalline)	40 30 15-40	(1) (2) (3)
Magnesia	10	(1)
Kaolinite	20-25	(4)
Carbon fibre-lime -soda matrix 40% vol.fract.	2200-3100	(5)
Glass (lime-soda)	0.5 8 3	Griffith (2) (5)

Table 8. Work of fracture of various materials

1.Tattersall and Tappin [175], 2. Davidge [176]
3. Meredith and Pratt [177], 4.Alderson [134], 5. Pambuch [137]

They found that γ_f decrease with increase in depth of notch as the fracture process becomes more controlled.

b. Analytical methods

The Stress Intensity factor can be calculated using a formula suggested by Paris and Sih [126], which connects K_{IC} with bending momentum M and since (M=PL/4) with load during bending tests:

$$K_{IC}=\frac{6M}{B(W-a)^{3/2}} f(a/W) \qquad \textbf{(eq.46)}$$

where M is the bending momentum at the centre of the beam [For three point bending: M= PL/4, P is the load in MN, L is the span length in m, B is the thickness of the sample in m, W is the total width of the specimen in m, α is the crack depth in m, and f(a/W) is a geometric term.

Brown and Srawley [179] proposed the following empirical equation for experimental determination of K_{IC} using the bending moment of precracked specimens:

$$K_{IC}=\frac{M}{BW^{3/2}}\sqrt{\frac{126.8(a/W)-259.2(a/W)^2+844(a/W)^3}{[1-\nu^2]}} \qquad \textbf{(eq.47)}$$

Graham and Alers [180], performing AE measurements in polycrystalline ceramics under slow crack growth conditions, determined the critical load for crack initiation and calculated the fracture mechanics parameters K_{IC} and γ. They found good agreement for fracture surface energy values estimated with Srawley and Brown's equation in comparison with values from other tests but the data agreed better with the shape of the curve given by Paris and Sih's equation.

2.3 THE STATISTICAL APPROACH TO BRITTLE FRACTURE

2.3.1 INTRODUCTION

The statistical approach to brittle fracture is another method to analyse fracture data (The deterministic or phenomenogical approach to brittle fracture was analysed in the previous sub-chapter 2.2). Brittle materials, like ceramics, under stress cannot deform plastically to dissipate stress concentrations in numerous small (10-100 μm) flaws and stress raisers. As a result, failure occurs at stresses about one hundred times lower the theoretically predicted based on the crystalline structure.

Variations in the measured material properties are mainly due to the following reasons:

a. Those due to experimental errors (mainly in measurements) which are generally reasonably small when testing is carefully carried out. Furthermore according to the central limit theory [181] the errors of a set of measurements are normally distributed if several small errors contribute to the total error.

b. Inhomogeneity and structure variations.

c. Variations in different batches due to variations in production parameters.

The most important of the above sources, for brittle materials and especially for ceramics, is inhomogeneity and structure variations, since even identical specimens produced under the same conditions and from the same batch after complete mixing and identical conditions in different parts of the batch, show a wide scatter of fracture stresses and generally a large variation in mechanical properties.

In order for ceramic materials to be used as engineering materials, their

reliability must be assessed and their mechanical properties must be characterized. So research on the fracture processes of heterogeneous materials includes statistical analysis. Several statistical analysis methods have been developed. Two of them will mainly be analysed: the most widely used Weibull probability distribution which is very general in nature, and the recently developed Neville statistical distribution which has a theoretical basis with respect to materials. Other mathematical distribution functions [182] (e.g. normal, log-normal etc.) seem not to be capable of characterizing brittle fracture.

Statistical fracture theories do not examine the fracture processes, or specify the nature of the flaws and characterize the stress state in the crack front. They consider the material flaws as a fundamental property and give the distribution of fracture strengths with respect to probability of failure or reliability of a number of specimens.

2.3.2 THE WEAKEST LINK THEORY (WLT)

Weibull based his empirical function on the assumption that the strength of a body is determined by the strength of the weakest primary element, in analogy to the way that the strength of a chain is dependent on the strength of its weakest link (the weakest link theory WLT). In accordance with this theory when a test specimen is loaded and a critical stress (capable to propagate a crack) at the most severe flaw is first reached, fracture occurs. From an engineering point of view, when the weakest link theory is applied to ceramics, the number of specimens having strength lower than a desired strength is more important than the average strength obtained.

In WLT and in accordance with the Griffith concept that a brittle material has many flaws, it is assumed that fracture results from flaws of unspecified nature and unknown sensitivity to the direction of the stresses. Furthermore in homogeneous materials, e.g. glass, fracture occurs at the flaw whose stress intensity factor first reaches the fracture toughness of the material.

WLT theory implies that:

a. The mechanical test results will have a considerable variability.

b. There is a size effect which means that large specimens are expected to be weaker than small specimens.

c. The final failure of a complex mechanical system will not necessarily happen at the point of maximum nominal stress.

Davies [183], supporting this theory, indicated that while in ductile materials the central tendency of the flaw distribution is important, in brittle materials the main concern is in extreme values. He also underlined the problems which arise in complex stress conditions.

Batdorf [184] pointed out that this theory does not give information about poly-axial fracture statistics.

While WLT is a logical probabilistic approach to explain the scatter in strength and other mechanical characteristics of brittle materials, it is also rather arbitrary and other approaches have also been proposed. Mihasi and Wittmann [185] have developed a stochastic theory of fracture of concrete. According to this theory which contains the WLT as a limiting case a stable crack can exist before final fracture.

Hu et al.[186] pointed out that, although for homogeneous materials WLT may apply, this may be not so for less homogeneous materials e.g. ceramics, cement etc,

where the first crack does not necessarily lead to immediate fracture. They developed a theory based on a model proposed by Wittman [187], applied in materials where a strong phase is dispersed in a weak matrix, e.g. concrete, and a stable crack can be formed. In this theory fracture initiated at an internal flaw in the matrix may grow to form a penny shape crack and may be arrested at a tougher second phase or propagate in another direction. This model predicted the decrease of bending to tensile strength with decrease in size for any flaw size distribution. However this model has limitations and needs further development.

Lamon [188] summarised the main statistical approaches to brittle failure based on the weakest link concept (Weibull, Batdorf and elemental strength approach) and pointed out that the Weibull approach is limited by its inability to predict failure of large components. He suggested that under multi-axial stress state, the elemental strength approach [189,190], is a more physical approach to failure based on the assumption that a body contains a distribution of cracks that can be characterized by their flaw extension stress and the Batdorf approach [191,192] which is based on the same assumption but is mathematically more complex.

Another statistical model of brittle fracture which considers that principal stresses act independently, is the PIA model, [193]. This approach may lead to serious undep-estimates of failure probabilities since it neglects the interaction of combined principal stresses.

In continuous fibre reinforced composite materials the WLT concept is opposed by the less known "parallel or bundle model theory" [194,195] in which the failure in "one chain" causes redistribution of load in the other chains until the whole system becomes able to withstand the external load.

2.3.3. THE WEIBULL FUNCTION

The statistical function most commonly used in analysis of strength data of ceramics is the cumulative distribution function proposed by Weibull [196,197], using the theorem of the product of independent event probabilities (the probability of an event comprising a number of independent events is equal to the product of the probabilities of the individual events considered separately).

The distribution of extreme values is influenced by the type of the function used to manipulate the data. Three types of asymptotic Extreme Value distributions have been developed, [198]. The type I is unbounded in the direction of extreme value, the type II do not possess finite moments, and the type III is bounded in the direction of extreme value. The Weibull function use extreme value statistics and is a type III asymptotic extreme value distribution also known as Fisher-Tipper Type III distribution of smaller values and as the third asymptotic distribution of smallest extreme value, [199]. Kittl and Diaz [200] proposed five mathematical ways for deduction of this function.

Weibull proposed the use of his function in a wide range of applications (e.g. from strength of steels to statures of adult males in the British Isles). However he also admitted that his function was not necessarily always valid. For brittle solids, Weibull theory assumes that they are: (a) homogeneous, (b) isotropic, (c) contain uniformly distribute randomly oriented flaws, (d) the strength of the solid is that of the weakest unit. In a general form the "chain" probability of survival will be [201,202]:

$$P_{survival} = \exp\left[-\int g\,(x\,)dV\right] \qquad \textbf{(eq.48)}$$

or

$$P_{survival} = \exp[-A\, g\,(x\,)] \qquad \textbf{(eq.49)}$$

where $P_{survival}$ is the probability of survival, g(x) is a function representing the number of flaws per unit volume or area (cumulative number of flaws of strength less than x per unit volume or area), V, is the volume of the material; and A, is the surface area of the material.

Weibull assumed the simple empirical form for function g(x):

$$g(x) = \left(\frac{x - x_u}{x_o}\right)^m \quad for\ x > x_u \quad and \qquad \textbf{(eq.50)}$$

$$g(x) = 0 \quad for\ x \le x_u$$

Generally, the Weibull function , is a three parameter equation and it has the following form :

$$P_f = 1 - e^{-\int_x (\frac{x - x_u}{x_o})^m dy} \quad for\ x > x_u \qquad \textbf{(eq.51)}$$

$$P_f = 0 \quad for\ x \le x_u$$

where : P_f is the distribution function of a variable x (probability of failure), x is the measured variable, x_u is a value of x where the function is vanished, x_o and m are function parameters (scale and shape parameters respectively); and y is the area or the volume of the specimen. The integral is defined as the risk of fracture, $R_{fr.}$

The integration may be carried out over the volume or the surface area of the

specimen depending on the type of the failure-determining flaws.

In the case of fracture strength and taking into account the volume of the material, the Weibull function giving the fracture probability can be written [198]:

$$P_f=1-\exp\left[-\frac{V}{V_o}\left(\frac{\sigma_f-\sigma_u}{\sigma_o}\right)^m\right] \qquad \textbf{(eq.52)}$$

where: P_f is the cumulative failure probability, V is the volume of the specimen, V_o is the reference unit volume, σ_f is the fracture stress, m is the Weibull modulus (shape parameter with values 5-20 for ceramics), σ_o is the Weibull scaling factor which is a function of specimen size and stress state (normalising factor); and σ_u, is the minimum stress (threshold stress,below which the probability of failure is zero).

In a similar way the Weibull function can be used for calculations of the statistical distribution of fracture toughness (in this case $x=K_{IC}$) and the function has the form:

$$P_f= 1-\exp\left[-\frac{V}{V_o}\left(\frac{K_{IC}-K_{IC_u}}{K_{IC_o}}\right)^m\right] \qquad \textbf{(eq.53)}$$

The probability density function (p.d.f), f(x) of the Weibull function (defined as dP_f/dx), assuming x_u is zero, is:

$$f(x)=\left(\frac{m}{x_o}\right)\left(\frac{x}{x_o}\right)^{m-1}\exp\left[-\frac{x}{x_o}\right]^m \qquad \textbf{(eq54)}$$

where $x, x_o, m > 0$

The Weibull function can be considered as a specific case of other functions (e.g. for values of m=3.44 and m=1 give respectively the normal and the true exponential distribution curves, [203]. For large values of m (m>40), the strength of materials becomes deterministic.

Assuming that x_u is equal to zero, and taking the logarithm of $[1/1-P_f]$ twice the Weibull equation is transformed to:

$$lnln\left[\frac{1}{1-P_f}\right] = m\,lnx - m\ln x_o \qquad \textbf{(eq.55)}$$

This is a linear equation with slope equal to the shape parameter m . If $x=x_o$ then, $\ln\ln[1/(1-P_x)]=0$ and $P_x=0.63$.

Taking the mean strength close to the median strength which is given by the value of σ at $P_f=0.5$, and $\sigma_u = 0$ the following equation is taken which shows the effect of specimen volume on mean strength:

$$\ln\bar{\sigma}=\ln\sigma_o + \frac{1}{m}\ln\left(0.693\frac{V_o}{V}\right) \qquad \textbf{(eq.56)}$$

Considering the stress-probability Weibull curve it can be seen that the curve at one end is limited to zero probability of failure (100% probability of survival) for zero strength, which is the physical lower bound of stress and at the other end, is limited to 100% probability of failure with the possible upper bound of theoretical stress.

As Neville indicated [204], the shape parameter m determines mainly the

skewness of the function (whether the majority of the values are above or below the mean), and the scale parameter σ_o influences the standard deviation and mean of the function.

Trustrum and Jayatilaka [205], using the above equation, related the mean failure stresses σ_1 and σ_2 of two specimens with respective volumes V_1 and V_2 with the formula:

$$\frac{\overline{\sigma_1}-\sigma_u}{\overline{\sigma_2}-\sigma_u} = \left[\frac{V_2}{V_1}\right]^{\left(\frac{1}{m}\right)} \qquad \textbf{(eq.57)}$$

When m and σ_u are known for a material, mean failure stress for a large volume V_2 can be estimated from observed failure stress of smaller volume V_1 specimen.

The σ_u value is usually taken as zero in order to avoid under-estimation of failure probability. The Weibull modulus m characterize the variability of test results. The higher the value of m the less variable the test results. A low modulus represents a wide scatter of data. When m=0 there is a constant probability for failure at any strength. When m=infinity a single value deterministic strength exist. Changes in manufacturing techniques affect the values of modulus m and the factor σ_o, [201].

In the Weibull equation it is assumed that: (a) Compressive stresses do not contribute to fracture (since brittle materials are much stronger in compression than in tension), (b) The failure initiating flaws are volume distributed and that the tensile stress is constant in the volume.

The Weibull approach is a pure statistical method without a physical meaning (the strength is considered as a variable and it does not take into account that the

flaws are distinctive elements, [190,206]. Its limitations become obvious when larger sizes and more complex stresses are used. Quoting Evans, [190]," This approach does not recognize the flaws as being unique entities operated on by the multi-axial stress".

Jayatilaka and Trustrum [195], indicated that m is a material characteristic (expressing the "brittleness" of a material) with no real relation to micro or macro-structure of the material, and using the WLT developed a general expression for failure probability using a flaw size distribution ($f(c) = k.c^{-n}$) and the stress necessary to fracture an inclined crack in homogeneous brittle materials. They connected m with the rate n of which probability density of the semicrack length f(c) tends to zero with the expression:

$$m = 2(n-1) \qquad \textbf{(eq.58)}$$

According to their theory : (a) Weibull function is a particular solution of the general case, (b) In materials with low m, a large crack is more likely to be present, the strength for a given volume is less and the materials are more brittle,
(c) Below a certain number of cracks the Weibull analysis is not valid.

In a more recent paper, [207], the same authors admitted that it is possible for different materials or even for the same material prepared in different ways to have differing crack size distributions. They concluded that, since their results supported the use of Weibull analysis for all the flaw size distributions the failure stress distribution can be considered insensitive to the flaw size distribution. They also admitted that m may or may not be a material constant depending on the flaw size distribution.

McClintock [189] proposed a new extreme value statistical distribution of

strength, derived from a statistical model of occasional cracked grain boundaries under the assumption that there is no crack interaction. However, he indicated that an improvement of his model should take into account the crack interaction and that would make more complicated the analysis. He also underlined the fact that acoustic emission and petrographic experiments on rocks indicate that brittle fracture is not the result of the first crack growth (as the weakest link theory suggests) but rather a combined result of crack growth over a number of elements.

Batdorf [184,191,192,208] also underlined that WLT does not necessarily apply in all situations and suggested that ideally fracture statistics should be based on three elements: (a) Extreme value statistics, (b) Fracture mechanics, and (c) Material microstructure. Batdorf and Crose [191] proposed a physically based statistical theory describing material strength by a flaw density function. This approach is mathematically complex and required extensive numerical analysis. Furthermore it failed to predict biaxial failure.

Evans [190] and Lamon and Evans [209] underlined that statistical analysis of bending strengths from brittle materials is a multiaxial fracture problem. They tested in three point bending porcelain cylinders with different span lengths in order to take results under predominantly uniaxial stresses and under appreciable shear stresses (when span length is large uniaxial stresses determine fracture while when it becomes short shear stresses dominate fracture). They identified two concurrent flaw populations (internal and surface) under multi-axial stresses and concluded that only the multi-axial elemental strength model is appropriate for handling multi-axial fracture.

Lamon [188] explained that this model "is based upon a non-coplanar failure

criterion and considers the combined effect of stress components and accounts for compressive stresses ". However, even in this case, the $\ln\ln[1/1-P_f]$-$\ln\sigma$ distribution does not give an absolutely straight line.

Pankow and Finnie [201] reviewed also the attempts to provide insight into the statistical fracture mechanics. They tested the Weibull function in cases of blunt notches in polycrystalline alumina and found that LEFM analysis is better in sharper notches. As Davidge indicated [135] comparison of the K_{IC} measurements in polycrystalline alumina specimens with sharpened notches (20μm), with strength results from smooth beams in three point bending has shown a four times less scatter of K_{IC} values. This probably indicates that scatter in strength data is mainly due to variations in the largest flaw size.

Richerby [210] proposed also a modified version of Weibull"s function introducing a stress dependent correction term. He indicated that this term is negligible when failure originates from a flaw of relatively large size but becomes significant as the flaw size is reduced.

Four-point bend strength- Weibull probability distribution plot for alumina data reported by Petrovic and Stout [206], show considerable deviation from the expected sigma curve (P_f-σ_f) mainly in the lower and upper parts of the curve.

Wallin [211] examined the scattering in K_{IC} results and evaluated test results from sharp crack, carbide induced brittle fracture of steel, using the Weibull distribution and a function similar to Weibull with shape parameter equal to four:

$$P_f = 1 - \exp - \left[\frac{K_{IC} - K_{\min}}{K_o - K_{\min}} \right]^4 \qquad \textbf{(eq.59)}$$

where K_{min} and K_o are the limiting K value and a constant respectively.

He concluded that the same result is produced using the effective volume hypothesis or the WST model [210]. In this model the macroscopic fracture is supposed to nucleate in a volume extending from the crack tip to the elastic-plastic boundary. Criticizing the shape parameter of four, Neville [212], indicated that extension of the Weibull models to materials with many cracks, as in case of microcracked ceramics, is not in agreement with evidence where good quality ceramics have a shape parameter of 10 or more.

Phani and Maitra [202] examining borosilicate glass rods tested under three point bending found a deviation of linearity of the lnln [1/1-P] versus $\ln\sigma$ plot. They indicated that since the histogram of failure stresses show a unimodal distribution, the bi-modal function and generally the Weibull model in not applicable in the analysis. They suggested that a beta function give better results.

Wu and Qiu [213] underlined the fact that the Weibull model does not take into account the interaction between the material elements and the possible existence of nonuniform stress field, and so results in errors. In order to correct the above insufficiency, they took into account the mutual actions of adjacent elements along one direction. Their results, based also on the "chain model " were more accurate but the used formulas more complicated. However, even with these formulas their results show the same per cent error as with the use of Weibull equation.

The Weibull unimodal or multimodal function has been also used in statistical strength analysis of fibres. Scott and Gaddipati [214], analyzing data from 119 silica glass fibre specimens, found no satisfactory results using the Weibull equation and assumed that the curvature in the $\ln\ln[1/1-P]$-$\ln\sigma$ line could be a result of overlapping

of a bimodal distribution, that is the underlying population is a mixture of two distinct populations [198]. They concluded that direct fractography would indicate different types of flaw origins.

Goda and Fukunaga [215], analyzing data from SiC and alumina fibres and examining fracture surfaces by SEM, found surface and inner flaws and used a bi-modal Weibull distribution function for strength evaluation:

$$P_f = 1-\exp\left[-\left(\frac{\sigma}{\sigma_{o1}}\right)^{m_1}-\left(\frac{\sigma}{\sigma_{o2}}\right)^{m_2}\right] \qquad \textbf{(eq.60)}$$

where m_1, σ_{o1} and m_2,σ_{o2} are respectively the shape and scale parameters for the two defect sub-populations.

They concluded that the bi-modal function gave better results than the single Weibull distribution.

Asloun et al. [216], estimating the tensile strength of high strength carbon fibres at short lengths, found unimodal and in some cases also a bi-modal behaviour. In a similar way a recent examination of SiAlON specimens [217] has shown a 25% strength improvement by minimizing the surface flaws (in this case the volume flaws dominate the fracture process). In a recent paper Masson and Bourgain [218] gave some guidelines for a consistent use of the Weibull statistics with ceramic fibres, indicating that the validity of a fitting model without physical background can be misleading. Finally, Kim et al [219], in a study of the fracture strength of delta-alumina Saffil RF fibres with variable diameters and lengths, reported a large scatter in strengths and dependence of fracture strength on the specimen volume. Using Weibull analysis, a Weibull modulus of 2.2 was found.

2.3.4 THE NEVILLE FUNCTION

A critical examination of Weibull function was performed in a series of papers by Neville [220-223]. He indicated that the Weibull function applied for fitting of toughness data, even when three parameters are used, shows a systematic deviation. He showed [221] that when considering the mean as fundamental characteristic of the function, the use of Weibull function results in non-conservative toughness and defect sizes estimations. Furthermore, he underlined the lack of any theoretical grounding of Weibull function to suit the situation near sharp cracks and concluded that probably there exist many materials for which the Weibull function is unsuitable.

Neville tried to develop a theoretically based function taking into account the behaviour of stress and strain near crack tips. He introduced a new statistical distribution function for fracture toughness, [223,224], applicable to ceramics and steels, based on following assumptions:

a. Brittle materials contain many cracks and remain macroscopically linearly elastic, when the non linear region near the tip of a crack is small with respect to the sizes of the piece, the crack and the distances between cracks.

b. Failure near the crack tip leads to total failure along the whole crack front.

c. The variability of strength is due to microstructural inhomogeneity.

He considered [220,223] that in a piece of material containing many microcracks, the failure-prone volume will increase in direct proportion to load. The failure-prone volume near the tip of the short length of crack front, δl, is linearly proportional to K^4, (K=stress intensity factor), or P^4 (P= load), and he expressed it as sampling S [$S=P^4$.(volume of piece), when all the pieces in a set have the same

sizes $S=P^4$]. Neville considered a cumulative failure probability depending on the size of the surviving population and on some function g(S). He supposed that his function has the following form:

$$g(S)=\left(\frac{S}{B_p}\right)^{D_p} \qquad \textbf{(eq.61)}$$

Neville developed the following expression as a simple statistical criterion for the failure of pieces containing microcracks, supposing that failure will take place when sampling is sufficiently reached. This sufficiency of sampling is statistically distributed according to the function :

$$P_f=\frac{\left(\frac{S}{B_p}\right)^{D_p}}{1+\left(\frac{S}{B_p}\right)^{D_p}} \qquad \textbf{(eq.62)}$$

where: P_f is the cumulative probability of failure, S is the sampling, always linearly proportional to the actual amount of material loaded at greater than a given stress or strain. (It is defined as Ki^4, Ji^4, COD^2, and its effect, g(S) is equal to $(S/B_p)^{Dp}$, B_p is a scale parameter which can change with temperature and which normalizes S (it is actually the median value of S for all values of D_p), D_p, is a shape parameter which allows the shape to change with temperature. Different D_p values for a given material are also expected for different distributions of stresses.

Neville considers that this theory is applicable to all materials regardless of mechanism of failure. Plots of $\ln[P_f/(1-P_f)]$ against ln(S) in accordance with this

theory must give straight lines.

This function may also be applied to failure stresses for tests on materials containing many crack-like defects [204,223], instead of one large crack but in this case (and if all the pieces in a set are of the same size) the load at failure in the fourth power is used rather than the sampling S ($S=P^4$).

Neville used also other worker's strength data from glass tested under impact loading bricks, Refel-SiC ceramic, concrete in compression [202,225, 226] and concluded that his function with only two parameters gave better fits than that of Weibull with three parameters. He also examined the effect of outliers of the two functions and concluded that the removal of an outlier has little or no effect on Weibull function but is the source of lack of straightness in his function.

Pineau and Mudry [227], criticised the Neville's statements on non-conservatism of the Weibull Function when applied to statistics of toughness, indicating that the non-conservatism is not necessarily very clear when applied to a statistical property.

2.3.5 CORRELATION THEORY

Transformation of the Weibull and Neville functions to their linear form allows the use of correlation theory in order to examine how well the variables satisfy the proposed equations. This theory examines the degree of relationship between variables. When all variables satisfy exactly an equation, there exists a perfect correlation.

In both cases the correlation of the variables is positive. The least squares

regression line is: $Y = a_0 + a_1.X$ with the constants a_o and a_1 equal to :

$$a_o = \frac{(\sum Y)(\sum X^2) - (\sum X)(\sum XY)}{N\sum X^2 - (\sum X)^2} \quad and$$

$$a_1 = \frac{N\sum XY - (\sum X)(\sum Y)}{N\sum X^2 - (\sum X)^2} \qquad \textbf{(eq.63)}$$

2.3.6. THE CHI-SQUARE TEST

The discrepancy between the experimental values of a material property e.g strength, toughness etc., and the theoretical values produced from the application of a statistical function e.g. Weibull, Neville, Normal or any other function, can be measured by the use of the statistic χ^2 (chi-square) value given by the expression:

$$\chi^2 = \sum \frac{(obs.value - expect.value)^2}{expected\ value} \quad or$$

$$or\ \chi^2 = \sum \frac{o_i^2}{e_i} - N \qquad \textbf{(eq.64)}$$

where : o_i the observed frequencies, e_i the expected frequencies ; and

N the total number of frequencies.

The larger the value of χ^2 the greater the discrepancy between the observed and the expected frequencies.

2.3.7 TESTING THE FITS OF THE TWO FUNCTIONS

The difference in quality of fits to data of two functions can be tested

statistically by using the correlation coefficients r, which can be estimated with the product-moment formula, [181]:

$$r = \frac{N\sum XY - (\sum X)(\sum Y)}{\sqrt{[(N\sum X^2 - (\sum X)^2][N\sum Y^2 - (\sum Y)^2]}} \quad \textbf{(eq.65)}$$

where: N is the sample size, and X and Y, are the values of the least square line $Y = a_o + a_1 X$.

The least quare lines for the two functions will have the following variables:

(a) For the Weibull function: $Y = \ln\ln[1/1-P_f]$ and $X = \ln(\sigma_f$ or MOR or $K_{IC})$.

(b) For the Neville function: $Y = \ln[P_{(x)}/(1-P_f)]$ and $X = \ln[S]$ where $S = K_{IC}^4$, σ^4, MOR^4 etc.

The r_W and r_N correlation coefficients have values between -1 and 1. The closer to 1 or -1 the higher the functional linear relation of the variables X and Y. The closer the coefficient to zero, the less possible the variables to be correlated.

Using the correlation coefficients r_W and r_N, the corresponding values of z_W and z_N of a variable z are calculated according to Fisher's Z transformation, **[181]**:

$$z_W = \frac{1}{2}\ln\frac{(1+r_W)}{(1-r_W)}$$

and **(eq.66)**

$$z_N = \frac{1}{2}\ln\frac{(1+r_N)}{(1-r_N)}$$

This distribution is approximately normally distributed with standard deviation

STD_z and mean μ_z equal to :

$$STD_z = \frac{1}{\sqrt{N-3}} \qquad \mu_z = \frac{1}{2}\ln\frac{(1+\rho_o)}{(1-\rho_o)} \qquad \textbf{(eq.67)}$$

where ρ_o, is the population correlation coefficient

The number j of standard deviations between z_W and z_N is:

$$j = |z_W - z_N| \,(STD_z) \qquad \textbf{(eq.68)}$$

When the Weibull function fits the data, the corresponding coefficient r_W is representative of the population, and the likelihood l that r_N is different from r_W is the same with the likelihood that a value from a normal distribution is j or more standard deviations from the mean on one side. If for example, r_W is smaller than r_N and l is 0.01 then there is 1% likelihood that this is purely by chance and 99% confidence that the Neville function is better.

2.3.8 AVERAGE AND STANDARD DEVIATION

The measured values of strength, toughness etc., can be assumed to fall into some form of the Normal or Gaussian Distribution curve. The most common functions of the Normal Distribution are: (a) the average value X_{avg} (or arithmetic mean) which is a measure of the central tendency, (b) the standard deviation S_{std} , which shows the dispersion of data, and (c) the coefficient of variation C_v, which is a measure of the relative dispersion, since the significance of the standard deviation is depended on the arithmetic mean.

The closer to average the measured values the taller and narrower the Normal curve. As the variation in strength increases the values spread and the curve becomes low and elongated. The coefficient of variation can be expressed as a percentage and is useful in comparing distributions where the units are different. The lower the coefficient, the more homogeneous the values of the variable.

The average value X_{avg} is given by the formula:

$$X_{avg}=\frac{X_1+X_2+.....X_N}{N} \qquad \textbf{(eq.69)}$$

This value is very sensitive to extreme measured values, in cases where they are not balanced on both sides of it.

The standard deviation S_{std} is given by the formula:

$$S_{std}=\frac{\sqrt{(X_1-X_{avg})^2+(X_2-X_{avg})^2+....(X_N-X_{avg})^2}}{N} \qquad \textbf{(eq.70)}$$

The coefficient of variation C_v is defined as :

$$C_v=\frac{S_{std}}{X_{avg}} \qquad \textbf{(eq.71)}$$

where X_1, X_2....X_n are the values of the individual strength , toughness or other tests, and N, is the number of the tested specimens.

Generally in brittle materials and especially in ceramics variation of strength of specimens exist even when the specimens are produced within the same batch, after complete mixing and identical conditions in different parts of the batch.

When the weakest link theory is applied to ceramics, the number of specimens having strength lower than a desired strength is more important than the X_{avg} obtained.

Laboratory testing of strength of glass present a large scatter that makes the average value practically non usable. Kies [228], examining the strength of soda-lime glass filaments, indicated that the measured average strength was of little engineering use and concluded that for sufficiently large size specimens the use of the Weibull function for representation of the effect of flaws on the breaking strength based on the WLT was adequate.

2.3.9 ESTIMATION OF THE WEIBULL PARAMETERS

Many methods have been used to estimate Weibull parameters [183,198,205, 228,229] e.g the linear plotting between lnln $[1/1-P_f]$ and lnx, the maximum likelihood method (ML), the non-linear least squares estimation. The problem is that none of the used methods was found to be the best under all circumstances.

Before the estimation of Weibull parameters the data must be examined for outliers, that is data values far from the rest of the sample.

2.3.9.1 Linear Plotting

Probably the best technique for estimating the scale and shape parameters in Weibull statistics is the linear plotting method because of its simplicity. The linear plot can be expressed by the equation: $y=mx+b$

where $y=\ln\ln[1/(1-P_f)]$ and $x=\ln(\sigma$,MOR or $K_{IC})$, m=shape Weibull parameter and $b=-m\ln\sigma_o$.

The least squares analysis allow to obtain the line of the best fit with slope m. Typical formulations for m and b are:

$$m = \frac{N\sum x_i y_i - \sum x_i \sum y_i}{N\sum x_i^2 - \sum x_i \sum x_i}$$

$$b = \frac{\sum y_i \sum x_i^2 - \sum x_i y_i \sum x_i}{N\sum x_i^2 - (\sum x_i)^2} \qquad \textbf{(eq.72)}$$

The linear plot shows in a visual way the suitability (or not) of the Weibull model in a brittle fracture examination.

Extensive data on glass fibres reported in the literature [214,231-233] show a lack in linearity of such plots. Scott and Gaddipati [214] indicated that the appearance of a curvature instead of linear plot probably indicates the need of a third parameter or a bimodal or a multimodal population.

Snowdon [233] indicated that strict application of the Weibull distribution presumes a single mode failure and suggested that a beta distribution can describe better the strength distribution.

2.3.9.2 The Maximum Likelihood Method

The least squares analysis is a particular case of the maximum likelihood method. The Maximun Likelihood (ML) method estimates the values of the Weibull parameters σ_o and m with minimum error when the number of flaws in the sample

is large [183], but seriously underestimates m is cases of abnormally high strength values. In this method, the likelihood function for the observed failure stresses $\sigma_1, \sigma_2 \ldots \sigma_n$ is:

$$L = f(\sigma_1) f(\sigma_2) \ldots\ldots\ldots f(\sigma_n)$$

(eq.73)

$$where \quad f(\sigma) = \frac{dP_f}{d\sigma}$$

Substituting the probability density function with its equivalent expression shows that the likelihood of the sample failure data $\sigma_{f1}, \sigma_{f2}, \ldots$ is a function of the Weibull parameters m and σ_o. The maximum likelihood estimates are the maximum values of m, σ_u and mean σ that maximize L. The Maximum Likelihood estimates of m and x_o for Weibull function can be found from the expressions,[198]:

$$\left[\frac{1}{N}\sum_{i=1}^{N} \ln x_i\right] + \frac{1}{m} = \frac{\left[\sum_{i=1}^{N} x_i^{\,m} \ln x_i\right]}{\left[\sum_{i=1}^{N} x_i^{\,m}\right]}$$

(eq.74)

and

$$x_o = \left[\frac{1}{N}\sum_{i=1}^{N} x_i^{\,m}\right]^{\left(\frac{1}{m}\right)}$$

The above estimates can be obtained by trial and error using a graphical estimate as a starting value or other methods.

Somerville and Bean [229] compared the least squares analysis and ML and concluded that when the data fit the Weibull distribution, both methods give actually

the same results.

2.3.9.3 The non-linear least squares analysis

Davies [183] used the Non-linear Least Squares estimation using the exponential equation of Weibull probability in order to improve the fit. The problem is that this estimation needs the use of a computer program which may not be readily available.

2.3.10 ESTIMATORS

In order the fracture probability to be expressed an estimator must be used. The expected values of the probability of failure P_f can be obtained from the two estimators used by Trustrum and Jayatilaka, [205]:

$$P_f = \frac{i}{(N+1)} \quad and \quad P_f = \frac{(i-0.5)}{N} \qquad \textbf{(eq.75)}$$

where i, is the ith (ranked) order of failure; and N, is the total number of specimens experimentally tested.

They demonstrated that when less than 50 specimens are used for statistical analysis, the first of the above estimators give a more biased m. Other proposed estimators, (used also by Neville in his calculations [204]), follow the expressions [203,234,235]:

$$P_f = \frac{i-0.3}{(N+0.4)} \quad and \quad P_f = \frac{i-\frac{3}{8}}{(N+\frac{1}{4})} \qquad \textbf{(eq.76)}$$

The first estimator corresponds to the median probability of failure.

Examination of the statistical properties of the four estimators using Monte-Carlo simulation technique have shown that the popular $P_f=i/(n+1)$ estimator gives the more biased m. This value of m gives a more conservative probability of failure and from engineering point of view is the best choice in reliability prediction [235] and is used in many statistical applications, [236]. The second formula gives for n more than 20, the less biased m values and probably is the most preferable from a materials science point of view. Asloun et al. [216], using the above estimator , have shown that the estimator and the sample size when it is higher than about 20 do not influence the results.

Results from flexural and tensile strength measurements on a carbon fibre-borosilicate composite [237] showed a poor fit of Weibull statistics, which was attributed to the small number (12) of tested specimens. Research has shown [203,218] that a sample size of about 30 specimens is acceptable for estimating Weibull parameters in ceramics and generally brittle materials.

2.3.11 STATISTICS IN COMPOSITES

Weibull theory and generally statistical theories for strength evaluation does not apply in composites since composites have a changing (increasing) flaw population

with load application, in contrast to Weibull model where the flaw population is considered unchanged until the moment to failure. Fibre ceramic composites present extensive sub-critical activity and, as Pabst [104], indicated statistical considerations which account for the volume effect of brittle structures do not consider subcritical crack extension behaviour. Since the strength of fibres is statistical in nature, statistical theories (bimodal or multimodal Weibull functions) can apply to fibres (e.g.[215,238,239]) or whiskers, which are used as reinforcements, with a similar success to that in brittle materials. As an example, Bourgain and Masson [238], examining high-modulus carbon fibres and taking into account their heterogeneity and resulting residual stresses, developed a multimodal Weibull distribution. Similarly, Warren and Anderson examining Nicalon (SiC) fibres [239], showed a quite high scatter of results which could only be explained if a bimodal behaviour was accepted.

Kendall et al. [125] examined the influence of toughness on the Weibull Modulus and concluded that in truly brittle materials, toughness improvement does not influence the Weibull Modulus, as expected in Griffith materials.

They indicated that if σ is the fracture strength of a material and since the probability of failure is equal to n/k+1, where n is the number of samples with strength σ or less and k is the total number of tested specimens, the above equation is transformed to:

$$lnln\frac{1}{1-\frac{n}{k+1}} = m\ln\sigma - m\ln\sigma_o$$

or **(eq.77)**

$$lnln\frac{1}{\frac{k+1-n}{k+1}} = m\ln\sigma - m\ln\sigma_o$$

According to statistical theory for the minimum strength σ_{min} recorded in a series of k specimens, the value of n is equal to 1, and $P_f=1/k+1$, and for the maximum stress σ_{max} n=k and $P_f=k/k+1$.

Substitution of the above strengths in equation 77, gives the following expression (eq.78) for the Weibull Modulus m :

$$lnln\frac{(k+1)}{k} = mln\sigma_{min} - mln\sigma_o$$

or

$$lnln(k+1) = mln\sigma_{max} - mln\sigma_o$$

(eq.78)

or

$$m = \frac{lnln(k+1) - lnln\frac{(k+1)}{k}}{\ln(\frac{\sigma_{max}}{\sigma_{min}})}$$

This transformation indicates that when Griffith equation applies (Griffith materials), the Weibull modulus depends only on the ratio of the maximum to minimum strength and the number of the tested specimens and does not change with toughness.

On the other hand addition of fibres to a ceramic generally improves m modulus but

sometimes causes a reduction of m. They suggested that the increase of m can be attributed to R-curve behaviour (increase of toughness with increase of the crack length) which is often observed in ceramics. R is equal to dU/dc and is the crack resistance to propagation in plastically deforming materials where an increase in strength results in additional crack extension under stable situation. R is a function of crack length attributed to plastic zone development at the crack tip which enlarges as the crack elongates. No explanation was given for reduction of m modulus with the addition of fibres.

In a recent paper Lamon and Guillaumat, [240], described the contribution of interfacial failure expressed as debond length to mechanical behaviour of microcomposite CMC specimens using a statistical probabilistic approach. They considered, that matrix failure and finally fibre failure are non interactive brittle events and the weakest link theory can be applied.

They introduced two equations for the probability of the occurrence of the n^{th} matrix crack and the probability of fibre failure in the presence of (n-1) matrix cracks as functions of the debond length associated to the i^{th} matrix crack.

They concluded that their approach permitted prediction of features of the mechanical behaviour of microcomposites, e.g. the matrix cracking process is limited by the weak interfaces (large debond length), while when strong interfaces are present (shorter debond length) the matrix cracking process is limited by fibre failure.

Petrovic et al. [89], evaluating the tensile mechanical properties of silicon carbide (SiC) whiskers have found a positive effect in use of them as short-fibre reinforcement elements for ceramic matrix composites. Another important result was the considerable deviation from linearity when the weibull probability of fracture was plotted against fracture stress for whiskers.

2.4 ACOUSTIC EMISSION

2.4.1 INTRODUCTION

Acoustic emission (AE) (also sometimes called stress-wave emission) may be defined as the high frequency stress waves (within the range of 50 kHz to 10 MHz) which are produced as a result of released energy that occurs within a material during dynamic processes as a consequence of structural changes [241]. Examples of such changes are crack propagation in ceramics, fibre breakage in composites or twinning in metals.

Acoustic emission differs from other sound dependent NDT tools (e.g.ultrasonics) in the source of the emission. In AE analysis the material itself gives off stress waves as a result of dynamic generation and growth of defects, while in NDT acousto-ultrasonics testing, the waves are produced by the testing instrument and give information about the static presence of defects.

The first observation of acoustic emission in materials was probably in "tin cry" where the audible emission was produced by mechanical twining of pure tin during plastic deformation.

There were three early experiments performed under controlled conditions, not in order to study the AE phenomenon itself, but to detect AE. The first was conducted in Germany in 1936 by Forster and Scheil, during the study of martensitic transformation in nickel steel [242], the second in USA in 1948 by Mason et al.[243], during observation of moving dislocations in pure tin and the third in England in 1950 by Millard during twining experiments on single crystals [244].

The first who used AE in order to study the phenomenon was the German scientist J.Kaiser in 1950 [245] and the first who used AE to study composite materials (GRP filament) were Green et al. in 1961 [246]. Today, there is a lot of commercial AE equipment, books and several ASTM publications on AE. Drouillard [247] has published a bibliography with about 2000 references on acoustic emission and a comprehensive guide to the literature on AE of composites [248]. Detailed bibliography and review papers have shown that the total number of publications on AE exceeded, in 1987, the vast number of 5000 [247,249-253].

The main areas of AE utilization, due to its ability to detect the energy released by flaw evolution include [121,252]:

a. Use as a research tool to investigate and characterize fracture processes.
b. Use as a continuous monitor of slow crack growth of structural components (e.g. in power plants, nuclear stations, pressure vessels etc.).
c. Use as a monitor in deformation, stress corrosion cracking, fatigue and other processes.

2.4.2 TYPES OF ACOUSTIC EMISSION

Research in the field of AE has shown that there are two main types of AE [249-254]: the continuous and the burst type. AE associated with plastic deformation, movement of dislocations and phase transformations, is usually continuous and has normally low amplitude. The AE rate increases, presents a peak AE rate near the yield stress of the material and then decreases exponentially. This type of AE is usually observed in tension tests of unflawed metal specimens. AE from crack growth

is intermittent (burst type) and has high amplitude [255]. The released energy may originate from stored elastic energy as in crack propagation and plastic deformations or from stored chemical free energy as in phase transformations [256]. In this type the count rate increases rapidly as failure is reached [151].

In composite and multiphase materials the two types of emission are most likely to happen simultaneously. Fibre fracture produces high energy burst events whereas matrix deformation and fibre debonding produces continuous AE events. In addition to the above, the material structure through which the AE propagates affects the characteristics of AE, e.g. by absorbing, scattering or dispersing the stress waves. Furthermore, the coupling agent, the type of the transducer and other factors affect the characteristics of AE events.

2.4.3 FACTORS AFFECTING ACOUSTIC EMISSION

Dunegan and Green [257] have studied the acoustic emission from various materials and summarised the factors which affect this emission. The factors which affect AE response from materials can be divided in two categories [254,257]:

a. In the first category which contains factors not related to the material, belong the presence of flaws and notches (possibly produced during manufacturing), the thickness, the density and others. The higher the thickness the higher the AE amplitude when a material is tested under load.

b. In the second category which contain the material related factors, belong mainly characteristics such as crystal structure, homogeneity and material history (mechanical working, heat treatment, stress relief etc.). The higher the anisotropy of

the crystalline structure the higher the AE amplitude. The presence of inclusions, or combination of different materials, as in case of ceramics and composites results in an entirely different acoustic behaviour.

2.4.4 KAISER EFFECT - FELICITY RATIO

The first systematic investigation of AE phenomenon was carried out by J.Kaiser in 1950 in Germany [177,258,259]. Kaiser's observations on the irreversibility of AE have been confirmed by many investigators and are known as " Kaiser effect".

According to this effect, when a material is loaded to a given stress level and then unloaded, no emission will be observed upon immediate reloading until the previous load has been exceeded. Many workers investigated and confirmed this property in various materials [e.g. 256].

Kerawalla [260], working on ferrous materials under cyclic tensile loading, has shown that the Kaiser effect is not universal. It is associated only with continuous type emission and is not evident for loads below the upper yield point. Spanner [261] indicated that annealing processes remove most of the Kaiser effect and that some metals and alloys do not present any measurable Kaiser effect.

Examination of AE from chopped glass fibre reinforced SMC composites showed no Kaiser effect after reloading [262]. Fuwa et al. [263] reported first and later Phillips and Harris [264] that in composite materials there is a ratio (Felicity ratio) between the first maximum loading stress and the lowest reloading stress at which AE starts again (Felicity effect). This ratio, R_{AE}, could be used as an "index of the damage" within the material. By definition R_{AE} is equal to:

$$R_{AE} = \frac{L_{ini}}{L_{\max}} \qquad \textbf{(eq.79)}$$

where L_{ini} is the load at which acoustic activity restarts during reloading; and L_{max} is the maximum load applied before reloading

The acoustic behaviour of materials has been also investigated in relation to another phenomenon called the " Bauschinger effect ". This is a general phenomenon observed in polycrystalline metals [265], according to which, when a ductile specimen is plastically strained first in tension and then in compression, deformation in compression starts at lower yield stress and a discrepancy at the start between the two stress-strain curves exists. Orowan [266] attributed this effect to movement of dislocations. Sankar [267] reported that in materials that show "unload" acoustic emission, that is acoustic emission during unloading, there is no detectable Kaiser effect.

Frederic and Felbeck [268], reported that materials in which AE is detected when the applied stress is removed, (unload emission) showed a considerable Bauschinger effect.

2.4.5 AE ANALYSING METHODS

A number of AE analysing methods have been used in order to decode the information that possibly the AE events carry with them. The main methods include [266,269,270]:

a). Ringdown counting

Ringdown counting is the counting of the ringing of the transducer to give a measure of the pulse signal size. This method of counting is a relatively simple technique of analysing an AE event. Brindley et al. [271] described the principles, advantages and limitations of ring-down counting. The principle of this method is to count the number of times the signal exceeds a threshold voltage, (fig.12). A fast circuitry is necessary for counting.

The number of ringing-down counts N is proportional to the natural logarithm of the initial voltage and equal to:

$$N = \frac{\lambda}{2\pi\beta} \ln \frac{V_p}{V_{th}} \qquad \textbf{(eq.80)}$$

where : λ is the angular frequency, β is the damping constant

V_p is the peak voltage, V_{th} is the threshold voltage

The higher the amplitude of an event, the higher the energy content of the events and the higher the number of ringdowns. The main advantages of this method include the "weighting effect" of events of higher energy, i.e. counting increases with amplitude, and the improvement of noise rejections.

The main limitations of this analysis is the difficulty of distinguishing the energy levels of individual events and the lack of absolute indication of the number of source events [270]. As a result it is usually impossible to relate micromechanical damage events with the emission data. A single high energy event may produce many ringdown counts which could equally well be produced by low energy events each producing only one count.

b). Event counting

This is a more complicated method of AE analysis than ringdown analysis, and gives more precise information but it looses all the amplitude information. An event is defined a group of threshold crossings separated from the next group of crossings by a period known as dead time. The dead time (usually 100 μsec) sets a limit on the maximum count rate but in most cases is never reached. Idealised acoustic emission events are shown in fig.12.

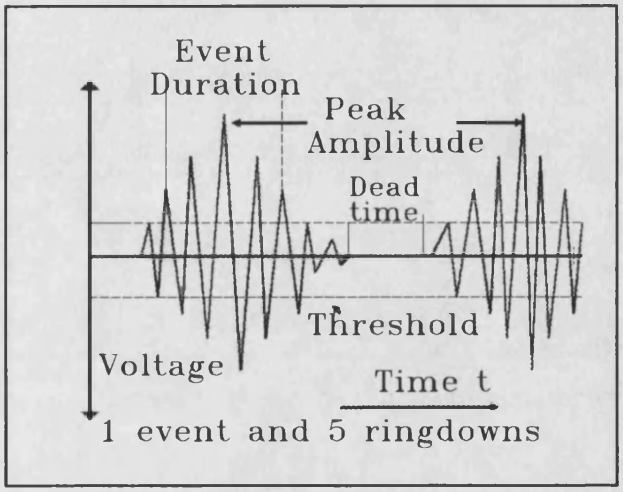

Fig.12 Characteristics of AE events

This technique was developed in order to be possible to connect the micromechanical failure steps inside a material with the AE signals produced. However, since the propagation of the AE could follow several different paths, a number of separated acoustic emission signals could be produced by only one event, or two events overlapping in time could give a composite signal. Nevertheless, in tests on systems where the AE signals could be attributed to discrete events, e.g. in

the case of breaking fibres in composite fibre materials, event counting is one of the best analysis methods, [254].

In practice the experimental data are largely dependent upon the equipment used and the selected settings. It is usual to find in the literature count rates as low as a few events per deformation increment and as high as 10^5 events per second.

c). Frequency analysis

Event and ringdown counting give no information about the specific characteristics (e.g. frequency and amplitude) of the AE events. So, in order to collect information from e.g. matrix cracking and fibre fracture in a composite material, other analysing methods must be used.

In frequency analysis the frequency content of an event is analysed. Unfortunately, this method is usually complicated and has certain limitations. Curtis [272] suggested that in practice, the AE pulse loses its frequency identity when passing through a material. This method also needs more advanced electronics.

d). Amplitude analysis

In this technique an amplitude distribution of the AE events is received by classifying after amplification AE signals in a series of channels each of which has a standard bandwidth. The absolute determination of acoustic emission amplitude, although possible in principle, is rather difficult in practice since it is affected by a number of variables, such as resonances, losses, position of transducers etc. The use of amplitude analysis has shown that event amplitude and production of high amplitude events increase with deformation [273-{276].

Peaks in the amplitude distribution could be attributed to specific failure micromechanisms. As an example, high amplitude events in a test of fibre composite

could indicate the growing of a crack. However, geometric effects and interferences could alter the analysis.

Lorenzo and Hahn [277] examined unidirectional composites (glass/epoxy and graphite/epoxy), using simulation and experimental work. The effect of source amplitude location and attenuation, on the apparent AE amplitude distribution recorded by a transducer was reported. The amplitude simulation was based on the assumption that the acoustic activity of the composite is a result of fibre breakages only, with a relationship of one AE event to one fibre breakage. The source amplitude was considered to be the amplitude that the AE system shows when the transducer was placed right over the breaking fibre.

The final simulated cumulative distribution F(V) for the apparent AE amplitude V_a, was fitted by a two parameter Weibull distribution of the form:

$$F(V) = 1 - \exp\left[-\frac{V_a}{V_s}\right]^m \qquad \textbf{(eq.81)}$$

where m and V_s are correspondingly the shape and scale parameters.

They compared the results of the simulation and the experiments and concluded that the amplitude distribution at the source is closely related to the apparent amplitude distribution and that the position of fibre break and the attenuation affect amplitude distribution. They indicated that changes in material properties (e.g. type of fibres, ductility of matrix, etc.) result in different amplitude distributions.

Evans and Linzer [269] and others [278-280] used the peak voltage of the acoustic emission as an amplitude parameter.

2.4.6 ACOUSTIC EMISSION FROM CERAMIC MATERIALS

Lord [253], in a review on Acoustic Emission, indicated that in a large number of materials including flawed and unflawed metal specimens, rocks, composites, concrete, ceramics, ice, soils, wood, acoustic emission can be used to investigate processes such as fracture welding, corrosion, martensitic transformations, slope stability of soils, magnetic effects, structural integrity etc.

Clarke [281] proposed a mechanism for crack nucleation based on internal stresses in polycrystalline ceramics originating from anisotropic thermal contraction or radiation-induced anisotropic expansion and spontaneous intergranular cracking was observed in BeO after irradiation [282].

Romrell and Bunnell [283] used acoustic emission to monitor crack growth in ceramic tubes due to thermal shock and corrosion. They found a correlation between microscopic observation and AE results and indicated that cracks in ceramic materials can be readily detected by AE both during the early stages of crack growth and during catastrophic failure and are associated with crack growth.

Gatti et al. [284] examined AE from transparent ceramic Lucalox alumina and special spinels specimens under 4-point bending and found that Lucalox was much noisier. The crack growth was monitored photographically and there was not a simple correlation between AE and the crack surface generated. Wright [285] studying the acoustic emission of a polycrystalline aluminum titanate ceramic, found that acoustic events resulting from microcracking during cooling of the ceramic, corresponding to thermal expansion hysteresis behaviour.

Tetelman and Evans [121] discussed the nature of information which can be

gained from AE testing and the applicability of AE in failure prevention and reviewed some of the principal correlations between AE and the processes of flow and fracture in structural materials as expressed by the fracture mechanics parameters. In two phase solids, the acoustic activity during testing is more than that from single-phase solids.

Examination of AE in polycrystals shows higher activity than that produced from single crystals or glasses [146,180]. Evans and Linzer [150] found two types of AE investigating the possibility of failure prediction in structural ceramics (e.g. porcelain). The first type was attributed to slow growth of fracture initiating flaws and the second type to the presence of second phase particles like quartz. They proposed the use of the effect of thermal anisotropic stresses in order to increase the AE of a "quiet" matrix. They concluded that AE activity in composite materials such as porcelain can be increased by incorporating second phase particles. They also found that the emission rate during the fracture of porcelain was a function of the stress intensity factor K_{IC}. The presence of particles like SiC in Si_3N_4 matrix will enhance AE [167], and even improve the mechanical strength of the matrix [286]. When a load is applied the particles will fracture giving AE which can be used for failure prediction.

Schuldies [287] examined the AE response, from polycrystalline lithium-aluminum- silicate ceramic bars made by slip casting and sintering, during testing in four point bending. He found a three stage AE response to stress, initially a high number of cumulative counts, followed by an almost constant rate and finally near fracture an exponentially increase in AE counts with increase of load and a strong Kaiser effect during reloading of previously loaded specimens. He also noted that the

AE response to stress presented a precursor to failure implying a transition from microcracking to unstable macrocracking and concluded that additional testing was necessary in order to be established a relationship between events and mode of failure.

Graham and Alers [180] tried to determine the conditions under which AE is generated in various ceramics prior to failure and to relate the produced AE signals with the microstructure. They used various techniques of loading (three and four point bending, pressing with a spherical or cylindrical intender and fatigue loading) in various materials (glass , MgO single crystals and polycrystalline ceramics. They concluded that AE signals precede failure in polycrystalline ceramics and in single MgO crystals undergoing deformation by slip, while in glass no emissions were observed prior its fracture or during slow crack growth under a Hertzian load. They also found that for samples with small grain size (30 μm) one AE event corresponded approximately with each broken grain, while this was not observed for samples with larger grains (100 μm). They suggested that in the later case the crack growth was controlled by other morphological feature such as pore distribution.

Noone and Mehan [146] studied the crack propagation in polycrystalline ceramics (magnesium aluminate spinel and Lucalox from Gen.Electric Corporation) under four point bending and its relationship to AE. The examined polycrystalline ceramics had high degree of optical transparency, were suitable for window applications resistant to ballistic impacts and had the advantage of direct observation. They concluded that acoustic activity was an indication of sub-critical crack growth and it was greatest in materials which were either coarse grained and particularly highly anisotropic multi-phased inhomogeneous or pre-flawed. The large grains

emphasised the effect of thermal expansion anisotropy and generated strains in the grains and the grain boundaries which separated under the applied load forming cracks. They also reported that glass fused silica and glass-ceramic specimens showed no acoustic activity before fracture.

Evans and Linzer [269], reviewing the acoustic emission in brittle materials, underlined its increased practical application and concluded that although the understanding of the basic mechanisms in AE is limited, the phenomenological description of AE is easier and is based on the fact that the emission amplitude is a statistically distributed quantity.

They suggested that the main sources of AE in brittle materials are:

a. Macrocrack propagation, with average velocity U_{avg} connected with the applied stress intensity factor K_{ic} with the formula:

$$U_{avg} = A K_{IC}^{n} \qquad \textbf{(eq.82)}$$

where A and n are constants.

b. Microcracking, general or localized near crack tips, resulting from precursors (e.g. pores or inclusions) and activated by large local strains resulting from contraction anisotropy and elastic mismatch. For most materials microcracking is time and stress dependent.

c. Plastic deformation, with acoustic emission resulting mainly from dislocation motion and amplitudes smaller than those from fracture processes.

Cooke [288], comparing the acoustic behaviour of coarse polyphase ceramics (type I materials) and uniform fine-grained ceramics (type II materials), reported that

type I materials present large number of sub-critical events before fracture compared with that of type II materials which are acoustically "quiet". He concluded, that strength and toughness results for the coarse grained ceramics [289] were not consistent with the concept that failure is due to stresses concentrated to a single critical value in front of a particular single flaw as LEFM implies. In these materials a number of microscopic fracture events (sub-critical activity) occurs before overall fracture. Especially in clay ceramics, strength and fracture toughness showed similar changes related to microstructure and not only to flaw distribution. On the other hand, failure of the "quiet" fine grained materials at loads calculated from LEFM shows that the concept of critical stress concentration in front of single critical flaws and statistical theories of strength based of distribution of these flaws are acceptable.

Nemets et al.[107] studied the AE activity and tried to explain the fracture processes under thermal loading (1000°-20°C) in a two-phase aluminosilicate refractory, a composite reinforced aluminosilicate ceramic and a periclase ceramic . They found in the coarse-grained aluminosilicate refractories high AE event rate during cooling from 1000°C in two regions, one in the range of 800-700°C due to stresses between the matrix and the filler and another one in the region 600-450°C due to polymorphic transformations of quartz. They concluded that the study of fracture processes should take into account not only mechanical models (e.g. crack nucleation and propagation) but also structural models, and that the AE methods are very suitable for investigating cracking kinetics in ceramics.

Glass, the material which Griffith used to test his LEFM considerations, is relatively "quiet" material, compared with other ceramics. Nadeau [290,291], investigated the origins of acoustic emission, during double torsion loading of notched

at one end in order to initiate cracking, 6mm thick soda-lime silicate float glass plates. His principal aim was to find a relation between the ring-down counting and the events at the crack tip. He recorded the data and using ringdown analysis he found that the event rate for the same crack velocity was two orders of magnitude lower than in ceramics probably because of their more heterogeneous structure. He found also that unabraded specimens presented very low AE, only slightly above the background noise level of the testing system.

He suggested that acoustic emission in glass plates, after formation of artificial microstructures (flaws) on them results from successive pinning and breakaway produced by interaction of the microstructures with the main crack. He found that a flaw (a groove) of about 4 μm deep was capable of producing one AE count.

It must be underlined that ceramics are heterogeneous multicomponent mixtures with a complex structure. Because of this, the fracture mechanics of ceramics differs significantly from that of homogeneous materials such as metals, glasses etc.

2.4.7 ACOUSTIC EMISSION FROM COMPOSITE MATERIALS

Acoustic emission differs depending on the type of material and in composites can be used as a tool for distinguishing the source of emission. There are many possible stages in the deformation of composites which can be distinguished by acoustic emission: (a) matrix cracking,(b) fibre fracture, (c) debonding, (d) delamination between layers of the fibres, (e) fibre pullout and (f) final fracture.

Lloyd and Tangri [152] investigated the AE rates amplitudes and frequencies

of AE from Al_2O_3 and Al_2O_3-Mo fibre composites during three point bending. It was shown that:

a. AE due to crack growth was present prior to fracture of alumina and alumina-fibre composites containing 6, 23 and 20% volume Mo fibres.

b. The acoustic activity, with different amplitudes rates and frequency, continued after the macroscopic crack formation, as the Mo fibres crossing the crack were deformed.

c. The amplitudes, event rates and frequencies presented differences in early and later stages of the tests.

d. Fibre composites showed higher activity than pure Al_2O_3.

e. Frequency analysis could be used to connect AE events and fracture steps.

Becht et al. [292], using amplitude analysis, found that fibre fractures produced high amplitude, high energy events. AE produced from fracture of fibres during testing of fibre-reinforced composites is different from that of the matrix.

Many investigators have tried to correlate amplitude distribution with specific failure micromechanisms in composites. In resin fibre composites Brecht [293] found a correlation between the slope of the curve of log cumulative counts versus amplitude and the operation of specific failure mechanism. However Gouid et al. [294] have shown that the amplitude of the signals depend on the condition of the fibre/resin interface and other factors.

Duke [262] examined randomly distributed short glass fibre SMC (Sheet Moulding Compound) composites in uniaxial tension, using various quality control NDE techniques. He found that acoustic emission started early and increased as the load was increased. Reloading of the specimens resulted in fracture at values slightly

less than the maximum value attained in previous loading. He found also that the Kaiser effect was not present for the loads used in his study.

Berthelot [295] examined the usefulness of the amplitude analysis as a tool for the explanation of the failure mechanisms in discontinuous fibre composites. During flexural tests he observed three types of emission:

a. Discontinuous distributions from steel fibre-epoxy composite.

b. Continuous distributions from Sheet Moulding Compounds-SMC of low interlaminar rupture and glass fibre-polyamide injection composites; and

c. Intermediate distributions from SMCs having a good interlaminar adhesion.

He indicated that the energy released during fracture of composites depends:

a. On the fracture process (fibre breakage, matrix cracking etc.).

b. On the nature of the created fracture surface.

c. On the interaction between cracking and surrounding part.

Caneva and Mazzola [296] investigated the use of AE in modelling the AE emission from composite materials during testing in tension. They concluded that AE permits quantitative evaluation of the parameters characterizing the fracture of composite materials.

CHAPTER 3. EXPERIMENTAL DETAILS

3.1. MATERIALS

A series of brittle ceramic materials such as Remblend China Clay from ECC International [297], a pottery mixture, a brick clay mixture used in production of roof-tiles and bricks, white Ordinary Portland Cement (O.P.C), Fly Ash powder from a Thermo-electric Power Plant and also a number of short fibres such as, Denka B-80 mullite and B-95 alpha alumina fibres, Saffil RF delta-alumina fibres and Grafil XAS PAN carbon fibres were used for manufacturing all the test specimens. Some common laboratory glass rods and rectangular glass plates were also used as test specimens in 3-point bending and acoustic emission measurements, for comparison.

3.2 FABRICATION OF SPECIMENS

The flow diagram for specimen preparation and testing of ceramics and composites is shown in fig.13. Sambell [298], reviewed the basic fabrication processes used in ceramics. Two techniques used for fabrication of the ceramic samples in the present work: (a) slip casting (main production method for ceramic mixtures and fibre-composites) and (b) hydroplastic extrusion (limited to a number of brick-clay samples for comparison of results).

a). Slip Casting

In slip casting the ceramic materials wet with water formed a plastic dough.

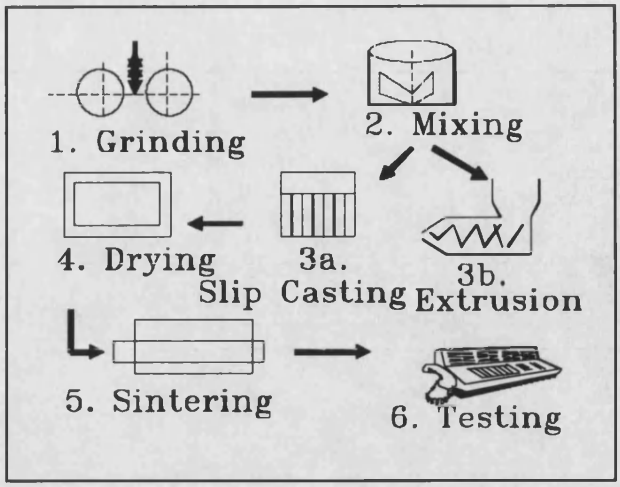

Fig. 13 Flow diagram for specimen preparation and testing of ceramics and composites.

Although the water content was not critical with respect to the properties of the final specimens, it was critical for the ease of workability of the dough. If too much water is added, the dough is sticky and is difficult to work with it. It was found by trial that the optimum total (humidity and added) water content was about 28%.

In the case of fibre-composites the first step which has a great effect on fibre-composite quality is the uniformity of dispersion of the fibres in the matrix, [96,298,299]. The problem in dispersion is the low hydrodynamic forces of the mixture and the high physical interaction between fibres. In the case of limited dispersion of the fibres and formation of agglomerates, the densification process which take place during sintering is obstructed and microstructural defects such as porosity and cracking result. The powdered matrix material was added simultaneously with small portions of fibres in water under continuous blending with a Galtenkamp

Silverson stirrer Model L2R first at minimum speed and after the final addition at medium speed (positions 5-6) for a number of hours. Several trials performed in order to find the optimum time required for complete and uniform mixing. For production of a 500 g dough about 12 hours were needed for addition of fibres and about 48 hours for complete mixing. Carbon fibres presented higher difficulty in mixing, than oxide fibres, since their larger length forced them to lie side by side and form discrete bundles.

Slip casting (fig.14) was used for the production of rectangular test specimens in moulds measured 75X19X9mm (length X width X height) by spreading the dough into the mould with a spatula and removing the excess mixture from the surface. A second spatula was used at the open end of the mould to close it during the filling process. The mould was sprayed with a silicone release agent before casting in order to make easy the removal of the samples.

b). Hydroplastic extrusion

In the hydroplastic extrusion the malleable mixture extruded through a die orifice by means of a rotating screw (fig.15).

All the samples were left to dry naturally for about twenty four hours covered with absorbent paper in order to reduce the surface drying rate and to avoid cracking. At the end of this time the specimens were dry enough to be removed easily from the mould.

About 1000 specimens were produced from each ceramic mixture (china clay -Kaolinite, the pottery mixture) which were divided in two lots (for notched and un-notched testing) of 300 pieces. A larger number of brick clay specimens was produced in order to study also the size effect on statistical analysis and the effect of

soaking time at the firing temperature. A number of about 100 specimens were produced from each composite system.

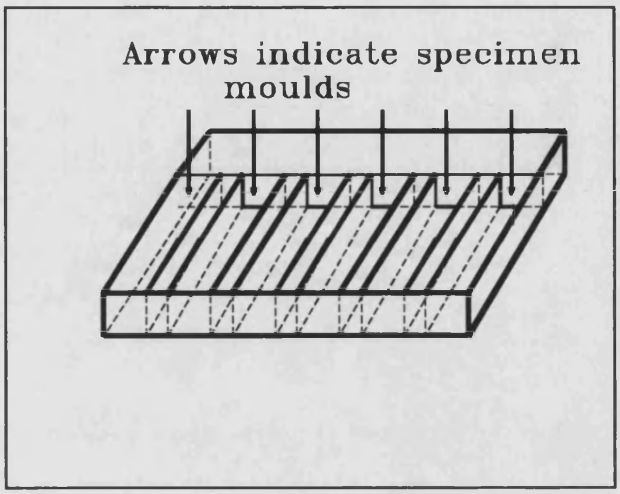

Fig.14 Slip Casting mould

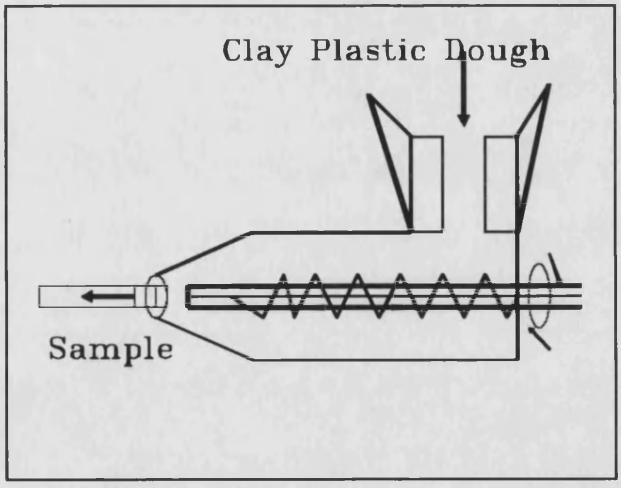

Fig.15 Extrusion casting

A level notch of uniform depth was made in the K_{IC} samples by inserting a razor blade into the test piece to a depth of about 5mm (fig.13).

In most of the reported K_{IC} results in the literature the specimens are produced from solid materials such as alumina, by sawing the notch. Simpson [300], concluded that for a valid K_{IC} determination the sawn crack should produce at its root a crack with length more than half the radius of the notch.

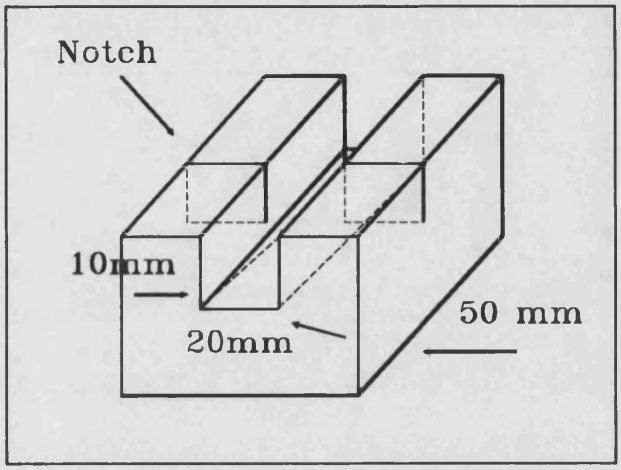

Fig.16 Specimen K_{IC} preparation by slip casting

Alderson [134], indicated that in the case of notch insertion before sintering when glass is formed during sintering, sharp cracks are formed at the base of the notch as result of thermal stresses during cooling. Since in all the tested ceramic materials in this work, glass formation was evidenced by SEM, the determined K_{IC} results must be acceptable. Furthermore Cooke, [289] indicated that after firing extension due to contraction during cooling produces sharp cracks for accurate K_{IC} measurements.

Each lot of notched and un-notched samples were left flat on a board piled in stacks to dry for another 24 hours. Before firing the specimens dried further in an oven at 105°C for about one hour, in order to ensure complete removal of

moisture.

For sintering of all china-clay , pottery , brick -clay and composite specimens computerised Carbolite furnaces (maximum 1300°C) and Carbolite RHF furnaces (maximum 1500°C) in air atmosphere were used. In the case of carbon-fibre composites a tube furnace and an atmosphere of argon with sufficient gas flow to avoid oxidation of fibres were used.

The specimens were laid flat inside the furnace. The temperature inside the furnaces in the area of the specimens, was monitored during the experiments and was found only +/- 1°C fluctuating from the set temperature. The temperature raise was adjusted to 5°C per minute. About 4 hours were needed for attaining the sintering temperature. Three pairs of notched and un-notched specimens were fired for 24 hours at temperatures from 1100 to 1500°C (Kaolinite) and 900-1300°C (pottery mixture) and 900-1150°C (brick-clay). An additional number of 110 brick-clay samples fired at 900°C. Kaolin-Fly Ash composite specimens sintered at 1000°C. Fibre composite specimens sintered at various temperatures from 1000 to 1300°C.

Another number of brick-clay specimens fired at three different sintering programs in a computerized Nabertherm furnace with a C-8 Program Controller. Schematic representation of the special sintering programs coded under the names : P7; P8 and P9 are shown in fig.17. All programs had a common first step up to 500°C, which the brick specimens reached in about 5 hours (rate 1.7°C/min) followed by further heating up to 850°C (P7), 950°C (P8) and 1050°C (P9) at a rate of about 4.5 °C/min. At the maximum temperatures the specimens remained for 15 minutes and then furnace-cooled to room temperature (24 hours).

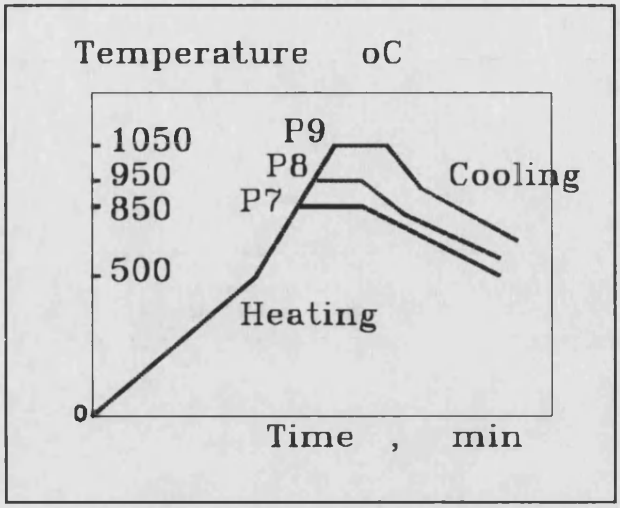

Fig.17 Special sintering programs P7,P8,P9 of brick-clays

3.3 TEST METHODS

3.3.1 CHEMICAL ANALYSIS OF MATERIALS

X-ray fluorescence techniques (XRF) have been applied to the analysis of ceramics, cements and related materials (e.g. F.A.) for the past 20 years or more, mainly using wavelength dispersive XRF spectrometers. The development of solid state Si(Li) detectors allowed analysis by energy-dispersive XRF spectrometry which give excellent precision, provided that proper specimen preparation had been followed [301,302]. The free lime content can be found by extraction with hot ethanediol, [303].

Energy Dispersive X-ray fluorescence (EDXRF) technique have been applied to the analysis of the materials (ceramics and fibres) used in the present thesis . The

main advantage of this technique is its ability to give quick and accurate quantitative results. Advanced computer programs (e.g. QMS,[304]) can overcome problems such as overlapping, low concentrations of light elements etc.

The principle of this technique is the following. When a sample is bombarded with high energy electrons, x-rays are emitted, characteristic of the atoms in the sample and having an intensity analogous to the concentration of the chemical element present. Energy dispersive spectrometry collects and analyses the x-ray data in terms of x-ray energy, using a semiconductor crystal for detection of the x-rays, [305]. In the detector a number of semiconductor electrons, proportional to incoming x-ray energy, is excited to the semiconductor conduction band and a proportional current which can be amplified flows [304,306]. In a screen peaks of characteristic energies show the presence of chemical elements whereas the peak height informs about the quantitative chemical composition of materials. Wavelength dispersive spectrometry has similar capabilities.

An XR300 Energy Dispersive X-ray Fluorescence Spectrometer from LINK Analytical with a lithium doped silicon semiconductor Si(Li) as detector, a 30KV max x-ray tube with a Rh(rhodium) anode and a vacuum of 10^{-3}bar was used. In order to minimize the particle size effects on calibration, fine grinding was employed. Pelletizing pressure of 25 tons/square inch was used for all materials [301]. The analytical parameters were :(a) Anode voltage: 15KV, (b) Anode current: 100uA, (c) Livetime: 500 sec, (d) Filter: none, (e) Atmosphere: vacuum.

3.3.2 MECHANICAL TESTING OF SPECIMENS

Ceramic materials and especially clay ceramics, clay fibre composites and cement based composites, have mainly two types of flaws: inherent flaws and manufacturing flaws. The inherent flaws result from changes inside the ceramic during heating and cooling and in most instances cannot be avoided. The manufacturing flaws are produced during manufacturing and include pores and voids from trapped air and are large in comparison with the inherent flaws.

The higher the area under maximum stress the higher the possibility for a manufacturing flaw to be present. So, in order to limit the area under maximum stress and to avoid fracture due to the presence of a manufacturing flaw three point bending was selected for mechanical testing.

As a result of high resistance to slip, ceramics have low, about 1/20 of that of metals, fracture toughnesses and critical stress intensities.

Flexure testing, is used extensively in monolithic ceramics as a substitute of the difficult and expensive tensile test. The same type of testing continues to be used also in composites since it is simple, inexpensive, and requires small specimens. However, Larsen and Stuchly [307], analysing the mechanical behaviour of CMCs underlined that since there is a nonuniform stress state and a brittle matrix, redistribution of stresses takes place when the matrix fails on the tensile side of the flexure beam, and the span length must be considered and at least a higher span to depth ratio must be employed to reduce the chance of shear failures.

All the mechanical testing results to be reported were obtained in three-point bending tests (flexure testing). Additionally, some testing results were obtained from

cylindrical cement specimens tested in compression. The tests were performed at am Instron model 1195 testing machine using an Instron Tension-Compression Load Cell type 2577, or a LLOYD 2000R testing machine with a 1000N load cell, at a constant crosshead speed of O,5 mm/min. A paper chart speed of 50-100 mm per minute was found to be suitable for measuring the slope and other characteristics of the stress-strain curve.

a. Three point bend testing

The flexural modulus and strength of powder ceramics and composites after sintering were assessed, using three point bending tests. The specimens were placed in the three point bend loading rig (fig.18) and the span (L) was adjusted at 50mm for the un-notched specimens and 35 mm for the notched specimens (in order to have a length to height ratio of 4). No difference in the calculated values of fracture stress was found either the top or the bottom of the specimen with respect to mould was placed down. As the load was applied to the specimen, a "settlement" was frequently occurred on the supports with no effect on the curve, since the slope was remained un-altered before and after each "jump".

In order to permit sensitive AE monitoring, the supports of the bend rig (10mm steel bars) were covered with neoprene rubber to reduce the possibility of recording noises from the machine and from metal-ceramic contact points .

b. Toughness (Stress Intensity) testing

In the case of K_{IC} specimens the notch was downwards i.e in the opposite side of the single support of the bend rig, (fig 19).

c. Compressive testing of cement (see APPENDIX I)

Cement is a brittle material very weak in tension which traditionally is used

in compression. The compressive strength of cement and cement mixtures, is usually measured after 3,7, and 28 days. In the present work the strength was measured after 28 days. Typically a value of 24 MPa is required for compressive strength of P.C. type I after 28 days in accordance to ASTM, [308].

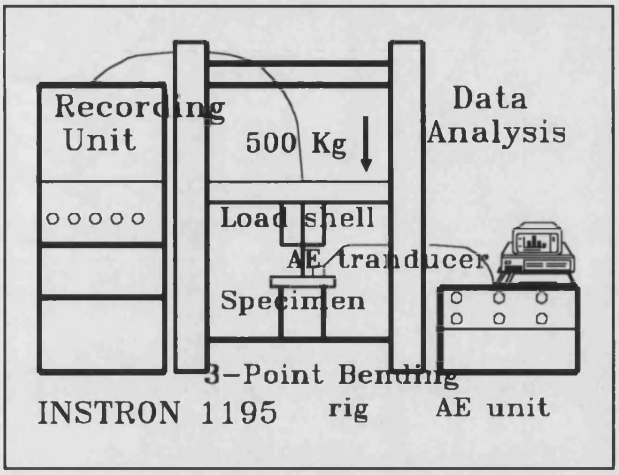

Fig.18 Three point bend testing in an Instron 1195 machine using also an AE Marandy recording unit.

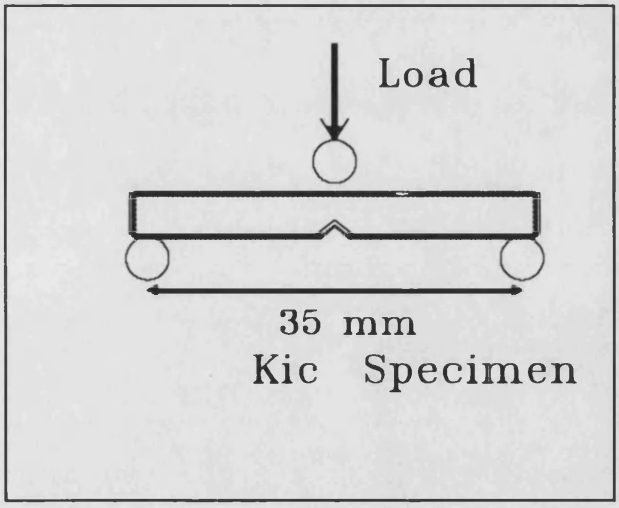

Fig.19 K_{IC} testing

3.3.3 REJECTION OF SPECIMENS

A number of the fabricated specimens was rejected for the following reasons:

a. Visual observation revealed abnormally large fabrication defects e.g. large cracks, holes, foreign particles.

b. The fracture stress was abnormal (deviated more than two standard deviations from the mean).

c. The set of test pieces had a rejection rate more than 10% . The usual rejection rate was less than 10%; and

d. Inadequate mixing and uniform dispersion of constituents especially in composites.

3.3.4 CORRECTION FOR TEST MACHINE COMPLIANCE

In order to measure accurately the slope of the stress-strain curve for Modulus of Elasticity calculations the stiffness of the test machine must taken into account. Any lack of stiffness, will result lower values of E since it will give lower values of slopes. The true slope of the stress-stain curve was found using the formula, [134]:

$$True\ slope = \frac{Mach.slope\ x\ Meas.slope}{Mach.slope - Meas.slope} \qquad \textbf{(eq.83)}$$

The machine slope (lack of stiffness of test machine and load cell) was measured by driving the central point bend test rig against the base of the rig which was bolted to the base of the machine.

3.3.5 MEASUREMENT OF DYNAMIC MODULUS OF ELASTICITY

A simple method and instrument were used for dynamic modulus of elasticity, E_d, measurement [309,310]. The principle of the method is the following: Stimulating vibrations are produced in a specimen and the velocity of propagation of longitudinal waves is measured. The radius of the specimen must be small compared with wavelength. Since the wavelength λ of a vibration induced in a specimen of length L is equal to $\lambda=2L$, the velocity v of the propagation of the longitudinal wave will be equal to $v=\lambda.f$, where f is the frequency. By substitution it is taken $v=2Lf$. The velocity is also equal to :

$$v=\sqrt{\frac{E}{d}} \qquad \textbf{(eq.84)}$$

where E, is the Modulus of elasticity (Young's modulus) of the specimen, and

d, is the relative bulk density of the material.

The Dynamic modulus of elasticity was measured using a Model PUNDIT from CNS Electronics ltd instrument. A bar of known wave velocity was used for instrument calibration. The tested specimen was placed between two transducers and the time needed for a wave to cross the known length of the specimen was read in the digital screen of the instrument. A silicon grease was used to couple the transducers on the tested specimen surface in order to improve the contact. The density of the material was found by measuring its dimension and weight. The dynamic E modulus, E_d, was estimated then by the formula:

$$E_d = \frac{2LB_w}{t^2 wb} \qquad \text{(eq.85)}$$

where B_w is the weight, 2L the length, w the height, b the width of specimens respectively, and t is the time needed by the wave to cross the specimen's length.

3.3.6 THERMAL ANALYSIS

Thermal analysis (T.A) , as defined by ICTA and ASTM E-473 [311,312],is " a group of techniques in which a physical property of a substance , is measured as a function of temperature while the substance is subjected to a controlled-temperature program ". Between the most common T.A techniques are:
(a). Thermogravimetry (TG), measuring changes in mass as a function of temperature increase; and (b). Differential Thermal Analysis (DTA) where the difference in temperature between the sample and an inert reference material is measured as a function of temperature while the sample and the reference material are subjected to a controlled temperature program. These two methods were used in the present thesis.

Cements are a suitable mixture for thermal analysis application since large energy changes occur both during manufacture and use and the hydration reactions of cement minerals in the presence or absence of other materials are of considerable interest. The application of DTA to building research and especially to cements has been reviewed by Webb [313], Ramachandran [314], Webb and Kruger [315], and more recently by Ben-Dor [316]. Thermogravimetric analysis is a widely used accurate method for the determination of crystalline CH content in cement and

cement-fly ash mixtures [317,318]. This determination is useful in recording the progress of pozzolanic reaction.

Marsh and Day [319] found that the way in which ash/cement mixtures hydrate depends on the type of FA high calcium lignite ash /cement mixtures, which produces a significant amount of hydrate by reaction of ash with water.

The diagrammatic representation of the thermal analysis equipment used is shown in fig. 20. For the thermal analysis measurements of the materials examined in this work a Computer operated, high accuracy (with post amplification) Linseis L81/65 Vertical Thermobalance was used with a heating rate of 10°C/min in air atmosphere, [320].

The ceramic sample powders and the inert substance (Al_2O_3) in crucibles of platinum were positioned in a L81/431 sample holder of sintered alumina mounted with PtRh(10)/Pt thermocouples which were connected against each other so that

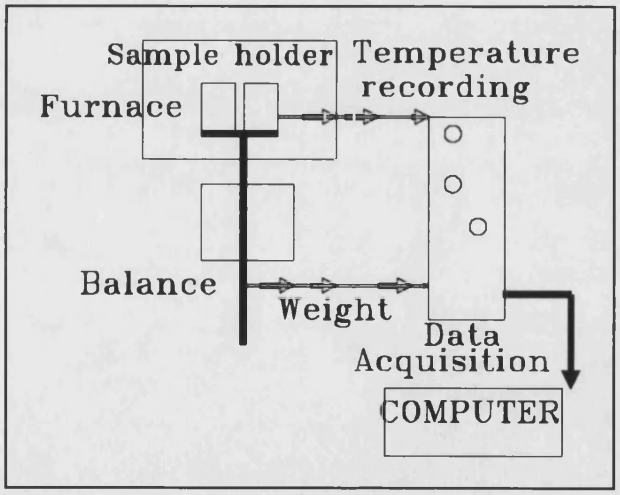

Fig. 20 Schematic representation of Thermal Analysis System.

the difference between sample and inert substance was measured. When the temperature of the sample is lower than that of the inert substance, an endothermic reaction is taking place.

The temperature difference is converted to an equivalent voltage difference which finally is transferred to a recorder. On the other hand when an exothermic reaction is taking place the temperature of the sample is higher and an opposite deflection curve is recorded.

Changes in weight of the sample cause a displacement in the Linseis L81 vertical mode thermobalance, built using the zero balance principle which is sensed by inductive transducers which regulate the current in the compensating magnetic coils. The current is proportional to the weight change and after amplification produce a TG and DTA signal.

Electronic differentiation allowed the simultaneous measurement of the time derivative of the TG signal (DTG).A computer controlled measuring and evaluating system was used for calculation of results.

3.3.7 FROST RESISTANCE TESTING

A limited number of brick-clay specimens, for comparison reasons, were used for Frost resistance testing. The Frost Resistance (DIN 52252 DIN 52253) of building clay ceramic materials is a measure of the capability of these materials to withstand weathering during their use [321]. Duc to water absorption during the

hydration testing cycle (soaking in water 25 °C, cooling at -15 °C after absorption) the strength behaviour of the specimens (MOR) crack formation etc, were largely dependent on the firing program and the initial chemical composition of the powders.

The frost resistance testing comprised of 5 cycles and was performed in an ANGELANTONI CLIMATIC SYSTEM apparatus with the following steps (fig.21): (a) Water immersion at room temperature for 72 hours, (b) Cooling down to 0°C in about 110 min, (c) stay for an hour at 0°C, (d) further cooling to -15°C and stay at that temperature for an hour, (e) quick heating to room temperature and stay for an hour at 20°C.

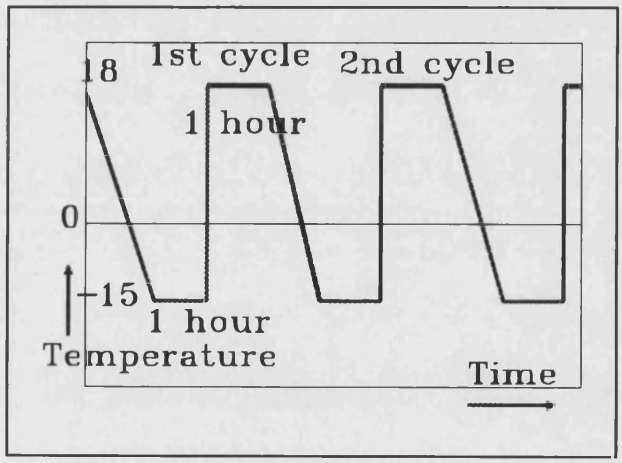

Fig.21 Frost resistance testing cycles

3.3.8 ACOUSTIC EMISSION TESTING

Acoustic emission (AE) is a dynamic process, which indicates the existence of sub-critical activity when a ceramic material is stressed. AE measurements have been also used to study micro and macrocracking in concrete and cement [322].

In a number of the tested specimens (approximately half from each type) Acoustic Emissions (AE) produced during three point bending were also detected by an AE amplitude distribution analysing system. Diagrammatic representation of the system [255] is shown in fig.22.

The AE system used in the present thesis was a Marandy MR1004 system, which is widely used in the University of Bath for examination of a variety of materials (e.g. [106,323, 324]). Two sets of data, acoustic emission and load, are fed in the unit. The number of events, their amplitude and the number of ringdown counts of each event are recorded.

The stress waves, generated when a material reacts in order to decrease internal energy, travel as acoustic signals in all directions and are detected by a mounted

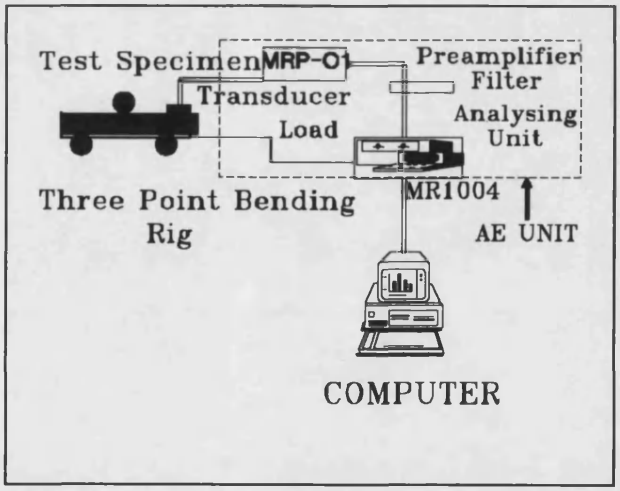

Fig.22 Diagrammatic representation of the Marandy AE system

piezoelectric PZT transducer. These transducers are the most popular, because of their high sensitivity and moderately flat frequency response. The piezoelectric

transducer converts the acoustic waves into sinusoidal decaying electrical voltage of low amplitudes. A silicon grease was used to couple the transducer on the tested specimen surface. The transducer employed for the sensing of AE was a single ended lead-zirconium titanate (PZT), u30D-108 PAC transducer with resonant frequency of 275 KHz($\pm$10%)and a near flat response between 100 and 1000 KHz with a high electromechanical coupling coefficient.

The output from the transducer was first amplified by a low noise MRP-01 MARANDY preamplifier with 60 dB gain, filtered to cut off unwanted low frequency noise below around 100 kHz, produced from vibrations from mechanical equipment, and processed to give a recording. Amplification was necessary because the voltages produced are of very low amplitude.

The following formula exist between amplification and input (V_i) and output (V_f) voltages [270,291]:

$$Gain(db)=20\log\left(\frac{V_f}{V_i}\right) \qquad \textbf{(eq.86)}$$

Thus for the 60dB amplifier the imput voltage is amplified by 1000.

Processing of the amplified signals was done by a MARANDY/ MR 1004 amplitude analysis system which stores the digital AE data as a function of time together with A-D converted load signals. The system provides information about the peak amplitude of each event and the number of ringdowns per event. The peak amplitude is the maximum AE signal relative to 10mv. The number of ringdowns per event is the number of times the signal amplitude exceeded the threshold level.

The amplitude detector of the unit sorted the peak amplitude of the AE events into 25 levels each 2.4 dB wide. Channel 0 had a threshold of 10 mV and channel 25, 7586 mV.

An AE event in this unit is defined in terms of the threshold voltage and a fixed dead time (i.e the time which if passed without a threshold crossing, while the next threshold crossing defines the beginning of a new event) of 100 microseconds. This means that each time the AE signal exceeds 10 mV an event is recorded and a following event will be recorded if within 100 microseconds there is no other threshold crossing. One memory of the system counts and records the ringdown events while another stores the highest amplitude ringdown. The maximum ringdown number per event defined by the system's processor is 256.

The results were analysed and plotted with the aid of software developed for this purpose [325] and also using conventional spreadsheet software.

3.3.9 OPTICAL MICROSCOPY

Reflected light optical microscopy was used as a first tool in surface examination of the specimens in etched and un-etched condition. In this technique the light reflected from the specimen surface forms a magnified image in the viewing plane.

Generally two factors limit the magnification in optical microscopy [e.g. 326, 327]: resolution, i.e. the ability to distinguish two close points as separate objects and the depth of the field, i.e. the ability to see sharp and in focus areas of different depth at the same setting of the microscope. The resolution r_s , and the depth of the field

d_f are given by the formula:

$$r_s = 0.61\,\lambda(\mu \sin a)^{-1} \quad and$$

$$d_f = k(\lambda sina)^2 \qquad \textbf{(eq.87)}$$

where λ is the wavelength , (λ sinα) is the numerical aperture, μ is the refractive index, and k is a constant.

It is obvious that a compromise between the two factors is necessary. In practice the optical microscopy useful magnification is about 1000X and resolution cannot be improved below about 200 nm (0.2 μm). Other problems connected with optical aberrations, astigmatism, distortion etc also exist and if corrected, increase the cost of a high quality microscopical system.

A Macro Zeiss optical microscope, with an eyepiece micrometer with 0.1 mm divisions, was used for: (a) macro examination of the fractured surfaces for gross defects such as large pores, holes, or manufacturing defects, and (b) measurement of the dimensions of the test piece (width, height, depth of notch) at its point of fracture.

Distortion produced during drying and sintering made the fractured surfaces quite irregular for measurement of the above dimensions and some judgement was necessary. Although the judgement was unavoidably subjective, the fact that all the measurements were made by the author and repeated at least three times in a period of four years with only very minor changes, indicated a constant standard.

High quality optical microscopes (ARISTOMET Leizt and Zeiss ICM 405) with a magnification range of 40X to 1000X were used for metallographic

examination of the specimens.

Metallographic preparation of the specimens was as follows. Samples were cut with a resin bonded diamond cutting wheel using Aquicut cutting fluid for cooling and lubrication. The samples were initially mounted in resin, grinded and polished and then etched using 15%HF solution for 60 sec. The grinding and polishing steps in order to prepare the samples, was performed in an automated Buhler Motopol 12 machine. The following five steps were followed:

a. Grinding in resin bonded diamond wheel, at 120 rpm, contra, with 5 lbs per sample, until no more resin exists on the surface.

b. Grinding in ceramic plate (Metlap 10 of Buhler) and spraying with 30 μm diamond slurry at the same as above variables.

c. Grinding in Polymet with 15 μm suspension at 240 rpm, complementary, with 5 lbs per sample.

d. Polishing in Texmet with 1 μm diamond suspension at the same as in (c) variables.

e. Polishing in Texmet with colloidal silica, at 100 rpm, contra, with 2.5 lbs per sample.

3.3.10 SCANNING ELECTRON MICROSCOPICAL EXAMINATION

Scanning Electron Microscopy (SEM) is a valuable tool in the study of structural ceramic clay ceramics and composites as it can be used in the examination of the effect of firing temperature and sintering time on the structure of the final products (e.g the pore and glassy phase topography, composite interface appearance

etc).

SEM is also the main research tool in examination of fractured ceramic and composite surfaces offering advantages in depth of focus and preparation [328]. As an example this technique has been used in studying the microstructure of clay and soil beds and the transformation of clays to bricks [329]. It has been also extensively used in the examination of cement hydration and hardening reactions and hardened fractured surfaces. The large number of reports on SEM or TEM (e.g. Diamond [330], Williamson [331]) show that electron-optical methods, have been widely used to study the formation of hydration products in cements and samples made from pure or cement mixtures, due to their ability of observation of details in the 1-0.01 μm range,. Generally the morphology of the C-S-H gel depends on the w/c ratio and the age of the cement sample [332,333]. The large depth of focus, the ease of specimen preparation and the ability for direct observation have made SEM a suitable instrument for examination of fibre composites.

In SEM (fig. 23) an electron beam produced from a heated tungsten filament (thermionic emission) is accelerated to an energy level of 2 to 40 keV. The electron beam is condenced passing through a series of electromagnetic lenses and focused on the surface of the specimen as a spot of diameter between 2 and 10 nm [306,326]. The secondary electrons emitted from the examined area are detected by a detector, amplified and an image of the surface under examination is formed on a cathode ray tube (CRT). SEM has high resolving power and can give magnifications from 50X to 200000 times. The high depth of field permits examination of rough surfaces as in the case of fractured surfaces. Typical calculated values of depth of field at 1000X magnification are in reflected optical microscopy 1 μm and in electron microscopy

40 μm [306].

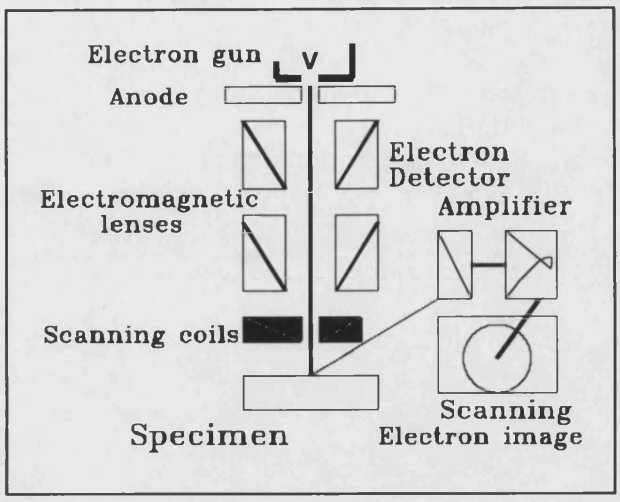

Fig. 23 SEM schematic diagram.

Fractured surfaces from K_{IC} and MOR specimens cut by means of a water-cooled diamond saw were both examined in etched (15%HF for 60 sec) and un-etched condition from each formulation and firing temperature in a JEOL T-330 scanning electron microscope with resolution 4.335 nm at 25KV accelerating voltage. The aim of etching was to remove, the amorphous glass phase by dissolution without affecting the crystalline one. A number of trials showed that about 60 seconds were enough etching time for glass removal. Etching for less time produced only shallow etch while longer time degraded the crystalline phase (usually mullite).

In order to establish the distribution of fibre aspect ratio (length to diameter) small portions of each kind of fibres was dispersed in water filtered with a filter paper and rinsed off the paper with ethanol on to aluminium 35mm disks. After evaporation of ethanol in an oven the aluminium disks were sputter coated (the procedure as

explained below) with conducting gold film and examined in SEM.

In order to avoid charging effects from the non-conductive ceramic surfaces and fibres, [328], a thin coating was applied under low pressure argon gas using a "cool" Edwards S150B Sputter Coater. Moisture removal in order to avoid water decomposition to oxygen which reduces the deposition rate of gold, was necessary in all cases. Usually a layer of 200-400 A was able to solve the charging problem. In the sputter coater a high voltage accelerates gas atoms in the gold target, causing sputtering and deposition of some gold atoms on the specimen surface. The gold film does not affects resolution because it copies the surface details. A conductive paste was also used to mount the specimens in the right position in the specimen holder during the SEN examination.

3.3.11 X-RAY DIFFRACTION ANALYSIS

X-ray Diffraction (XRD) analysis is a valuable tool in determination of original mineralogical and phases formed during sintering of ceramics and composites and hydration and hardening of cements. X-ray diffraction (XRD) is used for phase identification in portland cement clinker as a supplement to microscopy [303]. In the case of kaolinites it shows the formation of mullite at lower temperatures than those observed in SEM.

X-ray diffraction analysis is based on the following principle [334]. Monochromatic x-rays when meet a crystalline material are diffracted by the crystal planes according to Bragg's equation:

$$2d_p \sin\theta = n\lambda \qquad \textbf{(eq.88)}$$

where d_p is the distance between the planes, θ is the angle between the plane and the x-ray beam, n is a whole number, and λ is the wavelength (for copper Kα =1.541819 Å).

The specimen in a powder form is placed in the centre and the x-ray detector on the circumference of the camera. For a known wavelength, the d spacings are recorded as a function of angle. Each peak in the diffraction intensity can be attributed to a lattice d spacing. Using index cards containing data on d spacings and taking into account the chemical analysis, the phases and chemical compounds present can be determined.

A few chippings from test pieces of each material and firing temperature were ground in an agate pestle and mortar. The grinding was carried out under alcohol to retain the powder formed. For practical reasons it saved time to crush the chippings between two filter papers before grinding. The grinded powder passed through a 100 mesh (150 μm) sieve and was examined in an X-ray Philips diffractometer with a PW1820/00 vertical goniometer and a PW1710 micro-processor based control and measuring system. The powdered materials were exposed to Kα (λ=1.541819 A) radiation from a copper target (a nickel filter was used to absorb Kβ and background radiation). The recorded results (every 0.02°) were for a 2θ scan from 4° to approximately 70° which covered all the major lines. Tabulated cards with the major and minor peaks of X-ray diffraction were used to identify the phases which were present in the materials examined in this thesis. Quantitative estimation of the phases

was not attempted.

In the case of portland cement (see APPENDIX I) X-ray diffraction (XRD) is used for phase identification as a supplement to microscopy [303]. Alite is identified by the peak at 29.45° 2θ and belite by the weak peak at 31° 2θ . Tricalcium aluminate (C_3A) is identified by the peak at 33.25° 2θ, and calcium aluminoferrite has diffraction peaks moving from 33.0° 2θ to 33.7° 2θ depending on iron oxide content. The examination of the aluminate and ferrite phases is easier if the silicates are first removed from the sample by salicylic acid dissolved in methanol.

CHAPTER 4 RESULTS

4.1 CHEMICAL ANALYSIS

Quantitative XRF chemical analysis results from the ceramic materials examined in the present work are given in Table 9.

Chemical compound weight %	Remblend China clay	Pottery mixture	Brick clay	Fly Ash
SiO_2	48.2	59.7	50.6	34.4
Al_2O_3	37.1	25.5	20.1	19.6
Fe_2O_3	1.0	1.5	6.7	4.1
TiO_2	0.05	1.6	1.2	0.5
CaO	0.07	3.1	3.8	32.2
MgO	0.3	0.2	3.4	1.9
K_2O	2.0	1.9	3.2	0.7
Na_2O	0.1	0.1	2.1	0.4
L.O.I.	12.1	9.5	9.9	6.0

Table 9. Chemical analysis of ceramic materials.

(L.O.I. = Loss of ignition)

EDXRF spectra after 500 seconds exposures 15kV voltage, 100 μA current,

under vacuum, are shown in figures 24. The calculated rational mineralogical composition for the Remblend china clay, [297], is: 83 % kaolinite, 13 % micaceous material 2 % feldspar and 2 % other minerals.

Quantitative XRF chemical analysis and characteristic properties of the fibres [66,71,80,335,336] used in the present work are given in the following Table 10.

4.2 MECHANICAL TESTING

4.2.1 MATHEMATICAL FORMULAE

(a). Fracture stress (Modulus Of Rupture, MOR)

The tensile (fracture) strength of ceramics is not usually measured by tensile testing, because of their brittleness and the high possibility of breaking in the grips. The test usually used is the three or four point bending test which give the Modulus Of Rupture (MOR). According to Timoshenko beam theory the fracture stresses(MOR or σf) can be calculated from the formula [119,337,338]:

$$MOR = \frac{6M}{bw^2} \qquad \textbf{(eq.89)}$$

or:

$$MOR = \frac{3PL}{bw^2} \quad in \quad MPa \qquad \textbf{(eq.90)}$$

where: M is the maximum moment, P is the fracture load in MN ,

L is half of the span between the supports of the bend rig in m

b is the width and w, is the height of the specimen in m

In the case of circular section specimens, as in rods the above formula is expressed as:

$$MOR = \frac{16PL}{\pi D^3} \qquad \textbf{(eq.91)}$$

where D is the diameter of the circular rods

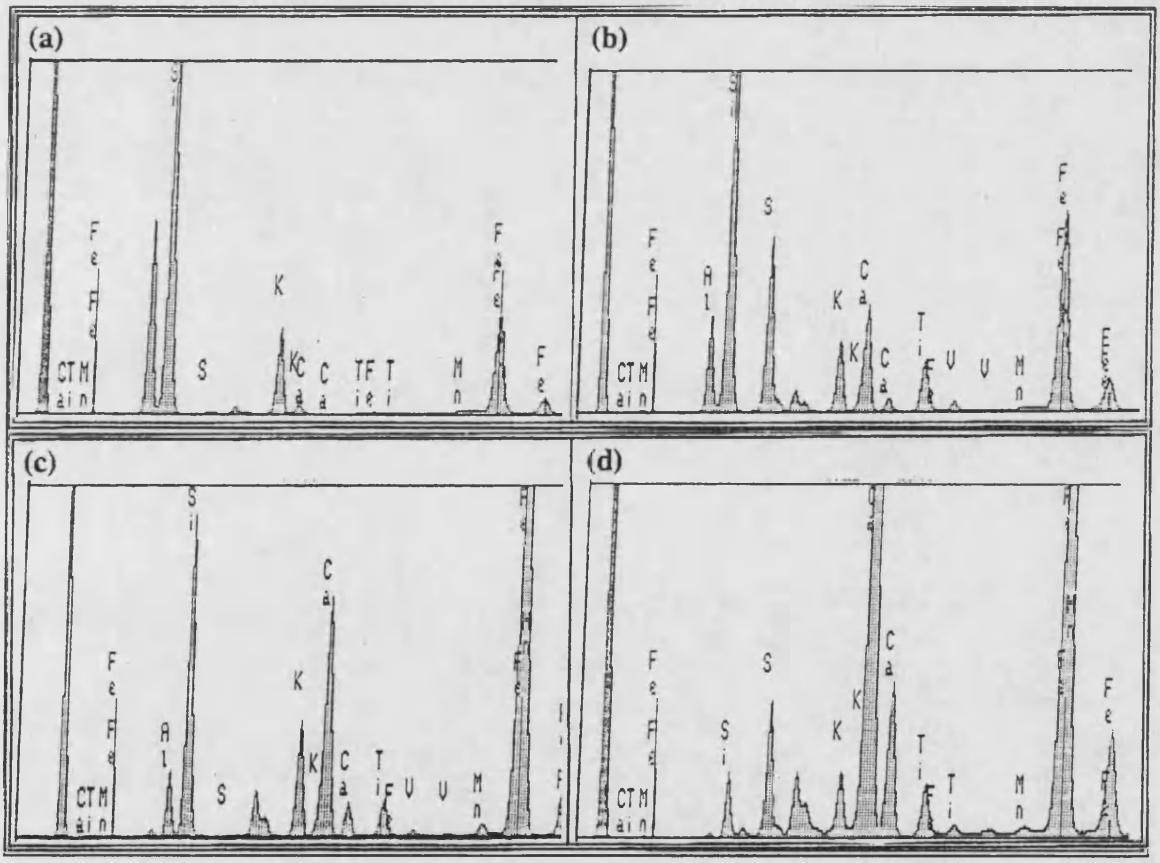

Fig.24 EDXRF spectrums from: (a) Kaolin, (b) Pottery mixture

(c) Brick-clay and (d) Fly Ash in as received condition.

Characteristics	Denka B-80 mullite short fibres (Ref.362)	Denka B-95 alpha-alumina short fibres (Ref.362)	Saffil RF delta-alumina short fibres (Ref 109)	Grafil XAS PAN short fibres
Classification temperature °C	1650	1600	> 1000	
True density, g/cm^3	3.3	3.5	3.3	1.79
Chemical composition Al_2O_3 SiO_2 $Al_2O_3+SiO_2$ Other	 80 20 99.7 0.3	 95 5 99.7 0.3	 96-97 3-4	 graphite
Crystallinity ratio α-Al_2O_3 mullite	 5 >, = 50 <, =	 30-65 5 >, =		
Filament Diameter, μm	2-5	2-5	3.4 (1-10)	
Strength Mpa	1670		2000	4480
E, GPa	167		300	227
Colour	white	white	white	black

Table.10 Characteristic properties of fibres used in the present work

(b). Modulus of Elasticity, E_b or E_d

The modulus of Elasticity from bending tests, E_b, was calculated from the formula:

$$E_b = \frac{2L^3}{b w^3} s_l \qquad \textbf{(eq.92)}$$

where S_l is the true slope of the stress-strain curve (see 3.3.4 Correction of the test machine compliance).

The modulus of Elasticity from dynamic testing E_d was calculated from eq.85.

(c). Stress Intensity Factor, K_{IC}

Stress intensity factors (K_{IC}) were calculated using the formula **[116,134,179]**:

$$K = \left(\frac{3PL}{BW^{3/2}} \right) Y \quad [MPa.m^{1/2}] \qquad \textbf{(eq.93)}$$

where Y is a compliance factor equal to:

$$Y = 1.93\left(\frac{a}{w}\right)^{\frac{1}{2}} - 3.07\left(\frac{a}{w}\right)^{\frac{3}{2}} + 14.53\left(\frac{a}{w}\right)^{\frac{5}{2}}$$

$$-25.11\left(\frac{a}{w}\right)^{\frac{7}{2}} + 25.80\left(\frac{a}{w}\right)^{\frac{9}{2}}$$

(eq.94)

where a is the notch depth and $0.4 < a/W < 0.6$

d). Work of Fracture

The work of fracture was calculated from the formula:

$$W_f = \frac{K_{IC}{}^2}{2E_b} \quad in \quad \frac{J}{m^2} \qquad \textbf{(eq.95)}$$

e). Compressive strength

The compressive strength of cement and cement-fly ash mixtures (see APPENDIX 1) was calculated from the expression , **[339]**:

$$\sigma_c = \frac{P_{max}}{\pi . r^2} \qquad in \qquad MPa \qquad \textbf{(eq.96)}$$

where $L_{max,}$ is the maximum applied load in MN: and r, is the radius of the cylindrical specimen

f). Density

The apparent density of the specimens was calculated by dividing the weight with the volume (dimensions measured with a SIVAC digital caliper).

4.2.2 MECHANICAL TESTING RESULTS

The measured characteristics of E_b, E_d, MOR, K_{IC} are presented with Average (AVG), Standard Deviation (STD) and Coefficient of Variation (Cv) values . The work of fracture W_f is presented as average values as it is a result of computation of other average values (K_{IC} and E_b). The density values D are also presented as average

values since the STD values were always less than 0.035 and the coefficient of variation less than 2%.

Mechanical characteristics of following ceramic systems at various sintering temperatures are presented in Tables 11-19 :

a.Table 11: Kaolin sintered at 1000°C, 1100°C, 1200°C, 1300°C, 1400°C and 1500°C.

b.Table 12: Pottery Mixture sintered at 900°C, 1000°C, 1050°C, 1100°C, 1150°C and 1300°C.

c.Table 13: Brick-clay sintered at 900, 1000, 1050, 1100 and 1150°C.

d.Table 14: Brick-clay produced by extrusion and sintered at special sintering programmes P7, P8, P9 (sint.programmes are explained in fig.17).

e.Table 15: Kaolin+5% and 10% (W/W) Fly Ash composite sintered at 1000°C.

f.Table 16: Kaolin+ 4.7, 9.2 and 14 vol alpha-alumina (B95) Denka fibres sintered at 1000,1200 and 1300°C.

g.Table 17: Kaolin+4.5, 9.7 and 14.75% vol.delta-alumina Saffil fibres, sintered at 200 and 1300°C.

h.Table 18: Kaolin+9.7% vol. mullite (B80K) Denka fibres, sintered at 1000 and 1200°C.

j.Table 19: Kaolin+8.55 and 16.6% vol. Graphite (Grafil-XAS) fibres sintered at 1000, 1200 and 1300°C.

Graphical representations of the effect of sintering temperature on mechanical characteristics of the tested ceramics and composites are presented in most of the cases in two groups of data. In the first group, moduli of elasticity E_b ,E_d and density, and in the second MOR,K_{IC} and W_f, are presented as a function of sintering temperatures as follows:

a.Fig.25: Kaolin. b.Fig.26: Pottery mixture. c.Fig.27: Brick-clay.

d.Fig.28: Kaolin+Fly Ash.

e.Figs29-31: Kaolin+4.7, 9.2 and 14 α-AI_2O_3 B95 Denka fibre composite rsp.

f.Fig.32-34: Kaolin+4.5,9.7 and 14.75% δ-AI_2O_3 Saffil fibre composite rsp.

g.Fig.35: Kaolin+9.7% mullite B80-K Denka fibre composite.

h.Fig.36,37: Kaolin+8.5 and 16.5% Graphite Grafil fibre composite.

The flexural strength and toughness variation with sintering temperatures of various ceramics and composites with the same matrix (kaolin) are presented in a graphical way in fig.38 and 39.

In a similar way the effects of α-AI_2O_3 (B-95), δ-AI_2O_3 (Saffil) and graphite (Graffil) fibre content on mechanical properties at different sintering temperatures are presented in figures 40, 41 and 42.

4.3 S.E.M AND OPTICAL EXAMINATION

A sample from a large number of mostly SEM (Scanning Electron Microscopy) and some OM (Optical Microscopy) micrographs from the examined ceramics, fibres and composites is presented in figures 43-54. All the SEM micrographs are from fractured notched specimens. All the OM micrographs are taken from composite specimen surfaces after grinding and polishing. The selected micrographs attempt to represent some typical areas of the examined specimens (but not all) are shown as follows:

Fig.43 (a) to (h): Kaolin sintered at 1000°C , 1100°C, 1200°C, 1300°C, 1400°C and 1500°C.

Fig 44 (a) to (f): Pottery Mixture sintered at 900°C, 1000°C, 1050°C, 1100°C

1150°C and 1300°C.

Fig.45 (a) to (j): Brick-clay sintered at 900°C, 1000°C, 1050°C, 1100°C, 1150°C and sintering programs P7, P8, P9 (fig.17).

Fig.46 (a) to (b): Kaolin+5% and 10% (W/W) Fly Ash composite sintered at 1000°C.

Fig.47 (a) to (d): Kaolin+α-alumina (B95) Denka fibres sintered at 1000,1200 and 1300°C.

Fig.48 (a) to (d): Kaolin+Saffil fibre composites sintered at 1200 and 1300°C.

Fig.49 (a) to (b): Kaolin+9.7% vol. mullite (B80K) Denka fibres sintered at 1000 and 1200°C.

Fig.50 (a) to (f): Kaolin+Graphite (Grafil-XAS) fibres sintered at 1000, 1200 and 1300°C.

Optical microscopy micrographs from alpha alumina, Saffil, mullite and Grafil fibre-kaolin composites are shown in fig.51.

In order to establish the aspect ratio of fibres, two fibre discs were prepared (see 3.3.10) and a minimum of ten micrographs were taken from each disc. The micrographs were then placed on a light box and fibre dimensions measured using a graticuled eyepiece lens. Mean fibre aspect ratios were calculated from more than 300 fibres.

SEM micrographs from Denka α-Al_2O_3, mullite, graphite and δ-Al_2O_3 fibres in "as received" condition and after sintering at various temperatures are shown in Figs.52-54 respectively. RF Saffil fibres (fig.54), have an almost circular cross-section. Their diameters range from below 1 μm to above 10 μm with a mean diameter equal to 3.4 μm (distribution is shown in fig.54b). Their length ranged from

50 to 200 μm with a mean value of 120 μm and the calculated mean aspect ratio is about 400. In some cases for large diameter fibres, closer examination revealed that they consisted from two fibres fused together (fig.54c). Non fibrous material, (known as "shot"), having a diameter usually larger than 20 μm, was occasionally observed amongst the fibres (e.g fig. 52c). Graphite Grafil XAS fibres (fig.53) showed a very high uniformity in diameter distribution with a mean value 6.2 μm and a mean length of 3mm, which gives an aspect ratio of about 500. No attempt was made to give the diameter distribution of Denka α-Al_2O_3 B95 (fig.52a-d) and mullite B80K (fig.52e-f) fibres since they presented a high degree of non uniformity in diameter (e.g. from 2 to 30 μm) and shapes (shots, non-fibrous inclusions).

4.4 X-RAY DIFFRACTION

A large number of X-ray diffraction patterns (angle 2 theta versus relative intensity) from the examined ceramics, fibres and composite systems, in "as received condition" and after sintering at the examined temperatures, were taken during this work. The XRD results are presented in figures 55-61. In most of the examinations the scanning angle was from 10 to 70 degrees. The XRDs are divided in the following three categories:

a). XRD from ceramics

Figure 55 gives the diffraction patterns of pure Remblend kaolin in " as received " condition and after sintering at 1000,1100,1200 and 1300 and 1500°C , and also the diffraction patterns of pottery mixture and brick-clay in as received

condition and after sintering at 900,1000 and 1100°C. In order to study the effect of soaking time on the structure of the brick-clay, XRDs at 1, 3, 6 and 24 hours at sintering temperature of 900°C were taken and shown in fig.56. XRDs from kaolin and fly ash combinations sintered at 1000°C are shown in fig.57.

b). XRD from fibres

X-ray diffraction patterns from the oxide fibres, mullite (B-80K), alpha alumina (B-95) and delta alumina (Saffil) and graphite fibres used in the present work, in "as received" condition and after sintering at 1300°C are shown in fig.58.

c).XRD from composites

XRDs from composite systems can be divided in those based on kaolin with oxide fibres and those based on kaolin and graphite fibres.

Fig.59 shows the XRD peaks of kaolin composites in as received condition with: (a) 4.7, 9.2 and 14 % (v/v) α-alumina (B-95) fibres

(b) 4.5, 9.7 and 14.75% Saffil fibres

(c) 9.7% (v/v) mullite fibres

Comparison of XRDs from pure kaolin with those from a kaolin composite containing 14% (v/v) α-Al_2O_3 fibres, both after sintering at 1000°C is shown in fig.60.

Fig. 61 shows the XRD peaks of kaolin composites after sintering:
(a) at 1200°C the α-Al_2O_3 composites , (b) at 1200°C the δ-Al_2O_3 composites and,(c) at 1000 and 1200°C the mullite 9.7 % (v/v) composite.The effect of sintering temperature on a kaolin+9.2 % vol. α-Al_2O_3 composite is presented in fig. 62.

4.5 THERMAL ANALYSIS

Thermal analysis curves, TG and DTA, from kaolin, pottery mixture, brick clay, and Fly Ash are shown in figure 63. Using special computer programmes, the weight loss and reaction temperatures were estimated. The possible transformation reactions are also shown on the graphs.

4.6 ACOUSTIC EMISSION

Generally, the amplitude distribution can be displayed by [270] a histogram distribution plot (number of events versus range of amplitudes), a cumulative distribution plot (total number of events with amplitudes greater than a narrow range of amplitudes versus this narrow range of amplitudes) or a logarithmic cumulative distribution plot.

A number of studies [278-280] have shown that the number of detected events n_e with peak amplitudes larger then V_a may be fitted to an equation. Pollock, [280,340] proposed the function known as " the power law distribution function", the exponent of which characterizes the failure mechanism when a single failure mode dominates the fracture process. The form of this function is:

$$n_e = N_o \left(\frac{V_\alpha}{A_o} \right)^{-b} \qquad \textbf{(eq.97)}$$

where A_o, and N_o, are constants , and b, is also a constant representing the slope of the log-log plot between n_e and V_α. ($\log n_e = b.\log A - b.\log V_\alpha$).

Since, physically, there must be a minimum detectable value for the amplitude, Graham [341] proposed a function called "the extreme value function" of the form:

$$n_e=N_o.\left[1-\exp\left(\frac{V_\alpha}{A_o}\right)^{-b}\right] \qquad \textbf{(eq.98)}$$

where No, A_o and b are constants.

Both functions show quite good agreement with data from various experiments when one mechanism of fracture occurs. Kuksenko [342] in a similar equation connected the number of cracks in a ceramic body with the number of AE counts when the body is stressed. In log-log expression a straight line between number of cracks and AE amplitude indicates that between the number of cracks and acoustic emission there exists a simple linear relation.

Ono et al. [343] reported that when more mechanisms are involved this simplified function is no longer correct. They studied AE on HSLA steels from MnS inclusions and they suggested that AE amplitude distribution data would be expected to fit a Weibull distribution of the form:

$$n_e=N_o\, e^{-C_o V_\alpha^{\,b_o}} \qquad \textbf{(eq.99)}$$

where N_o, C_o and b_o are constants

Evans and Linzer [269],proposed a similar expression, connecting the cumulative probability function F(V) with peak amplitude:

$$F(V)=1-e^{-\left(\frac{V_c}{V_\alpha}\right)^{b_o}} \qquad \textbf{(eq.100)}$$

where V_c and b_o are constants and F(V) is equal to:

$$F(V)=\frac{\beta_d}{\beta_r+1} \qquad \textbf{(eq.101)}$$

where β_d is the number of events with amplitude larger than V_a and β_r is the total number of events with peak amplitudes V between zero and infinity.

Linear transformation of the above function gives the expression:

$$lnln\left[\frac{1}{1-F(V)}\right]=a-b_o lnV_a \qquad \textbf{(eq.102)}$$

$$where \quad a=b_o lnV_c$$

Results from Acoustic Emission measurements from a number of specimens from selected formulations and firing temperatures are given in figures 64-76. The cumulative events-load curve and the event distribution from the glass specimens are presented in fig 64. In order to avoid useless repetition of similar features, a selected number of amplitude distribution, load versus deflection, event rate versus deflection or load or time, cumulative events versus load, Kaiser effect shown in cumulative-load curves during loadings, from pure ceramic and fibre ceramic composites are presented as follows:

In figures 65-67 AE results from "pure" ceramics (kaolin, pottery and brick clays). AE results from Kaolin+Fly Ash composites are shown in fig. 68. AE results from kaolin-fibre composites sintered at the indicated temperatures are presented in figures 69-72 (α-AI_2O_3, Saffil, mullite and Grafil fibre composites).

The effect of cyclic loading (load versus time) on acoustic activity (event rate) of ceramics and fibre ceramic composites is presented in fig.73 (compare with 72c).

The change of event rate distribution versus load, during repeated loadings in a kaolin- Grafil fibre composite in presented in Fig. 74.

Probability curves of AE counts as cumulative probability F(V) versus peak voltage (V) distribution and event versus peak amplitude distribution for selected specimens are also presented in figures 75 and 76 respectively.

4.7 STATISTICAL ANALYSIS

The Weibull and Neville functions were used and compared in statistical analysis of the results in the present thesis. Evaluation of the Weibull modulus m can be done by a number of ways (see paragragh 2. 3 .9) but the most common is the linear regression analysis.

The Weibull modulus m was estimated using the linear plotting between lnln[1/1-Pf] and ln (x) (where x represents flexural strength MOR or toughness K_{IC} values) of the Weibull function (paragraph 2.3.9.1), in accordance to a two parameter Weibull function and assuming at the beginning that the threshold value of x_u is equal to zero. The resulting least square line was used to find the x_u value for 0.1% probability of failure. This value was used for a three parameter Weibull function estimation. The estimators $P_{(x)}=i/[N+1]$ (the most popular estimator in Weibull modulus estimations) and $P_{(x)} = [1-0.3]/[N+0.4]$ (used by Neville in his function) were used in the above plotting and the results were compared.

The effect of estimator type on Weibull Modulus was examined in several formulations and sintering temperatures and as an example the results on the K_{IC} values of kaolin notched specimens sintered at 1100°C and tested at 3-point bending, and are presented in Table 20. Graphical representation of the results are also shown

in fig. 77. The effect of sample size (population) was studied on, 29, 63, 94 and 144 brick-clay samples fired at 900oC for 24h and is presented in Table 21. The Weibull distribution curves for the different sample sizes are shown in fig 78.

The failure probability P_f of flexural strength (MOR) and toughness (K_{IC}) from about 30 or more specimens tested at 3-point bending samples were used to plot the Weibull distributions between lnln[1/(1-Pf)] and ln(MOR) or ln (K_{IC}) and Neville distributions between ln[Pf/1-Pf] and ln [S], where S is the sampling $(MOR)^4$ or (K_{IC}^4), for most of the examined systems.

Figures 79-84, show the two and three Weibull parameter distributions and Neville distribution curves for MOR and K_{IC} of the examined kaolin (figs 79-80), pottery mixture (figs. 81-82) and brick-clay (figs. 83-84) ceramics. In a similar way the Weibull and Neville distributions were used to test the results of a number of composites: 10% (w/w) FA-kaolin composite sintered at 1000°C (fig.85), 4.7% vol α-AI_2O_3 fibre composite sintered at 1200°C (fig. 86), 9.2 vol α-AI_2O_3 fibre composite sintered at 1000°C and 1300°C (figs 87).

Results from the comparison of the statistical functions as applied to kaolin, pottery mixture and brick clay values, to test their fitness, using correlation coefficients are shown in Tables 22-24. In the same way results of the comparison of functions as applied to FA-kaolin and fibre-composite values are shown in Table 25.

The effect of the third Weibull parameter (the threshold value x_u) on the fitness of results was also examined. As an example, this effect on K_{IC} values of Kaolin specimens sintered at 1100°C is shown in fig. 88.

Finally, for comparison the Log-Normal distributions for selected specimen groups (kaolin notched and un-notched specimens, notched pottery mixture and kaolin+4.7% α-AI_2O_3 composite sintered at 1200°C) are shown in figure 89.

CHAPTER 5 DISCUSSION

5.1 INTRODUCTION

The following methods and experimental techniques were used in the present thesis, to gain an insight into the mechanical characteristics of the examined ceramic systems:

1. Methods giving information about the chemical composition and structure of the ceramic systems: XRF chemical analysis, Thermal Analysis (TG and DTA), X-ray Diffraction Analysis, Optical microscopy, SEM examination.

2. Methods giving information about the mechanical properties and the processes which take place during fracture of ceramics: Mechanical Testing of notched and un-notched specimens for measurement of K_{IC}, MOR, W_f and E_b, Measurement of Dynamic Modulus of Elasticity, Frost Resistance Testing, Acoustic Emission Testing.

3.Statistical analysis and comparison of analysis functions of strength and toughness data.

During the present work over 40 combinations of ceramic systems and sintering temperatures were examined and more than 3000 specimens were produced and tested in order to give adequate data for average values and statistical analysis. In some of them mechanical and acoustic emission measurements were performed simultaneously. During electron-optical examination several hundreds of micro-photographs were taken but for practical reasons only a few were included here.

In order to facilitate the analysisof results the discussion is divided into the following sub-chapters:

5.2 Discussion of results from powder ceramics (kaolin, pottery mixture, brick clay and kaolin+Fly Ash)

5.3 Discussion of results from ceramic matrix fibre-composites (Kaolin+ α-Al_2O_3, Kaolin+δ-Al_2O_3, Kaolin+mullite and Kaolin+Grafil fibres)

5.4 Comparison and discussion of AE Results from powder ceramic and fibre ceramic composite specimens.

5.5 Comparison and discussion of statistical analysis results from Weibull and Neville functions.

5.6 General discussion of Results.

Results from cement and cement+fly ash specimens and glass specimens, which were used as reference systems, differing from the above ceramics with respect to composition and structure and in production processes, are given in the appendixes (1 and 2) and mentioned when appropriate in the discussion.

5.2 DISCUSSION OF RESULTS FROM CERAMIC POWDERS

In this part discussion of the results from the ceramic clay powders sintered at various temperatures will be presented. The main production method used was slip casting (see 3.2), except in some brick-clay specimens where hydroplastic extrusion was used.

5.2.1 XRF, XRD, TG AND DTA ANALYSIS

Mineralogical analysis was performed by XRD analysis of the powders in as received condition and also after sintering. Generally, sharpening of XRD peaks means that a better defined structure of crystals has been formed. On the other hand disappearing of a group of peaks indicates that a crystal compound has been decomposed or combined to form another compound.

TG and DTA analysis gave valuable information about changes occurring in powders during heating.

5.2.1.1 Kaolin

EDXRF spectrum from the "as received " kaolin is shown in fig.24. (from the height of the peaks, the high alumina content of kaolin and the low content of "impurities" is apparent. Quantitative XRF analysis using the QMS program [304] is shown in Table 9 (page 155). The analysis of kaolin is in agreement with data from ECC International [297]. Remblend china-clay contains high amounts of silica and alumina which is quite close to English china clay.

XRD analysis (fig.55a), shows the main diffraction peaks of the raw and sintered kaolin. In combination with its chemical analysis it is seen that Remblend clay in "as received" condition contains mainly three mineralogical phases: kaolinite

[$Al_2Si_2O_5(OH)_4$], potash mica [muscovite $KAl_3Si_3O_{10}(OH)_2$] and feldspar [Orthoclase, $KAlSi_3O_8$].

Rational mineralogical composition analysis [297] shows that it contains: 83% kaolinite, 13% mica 2% feldspar and 2% other minerals. Because of their composition, the Remblend china clay ceramics are referred throughout this thesis as kaolin ceramics.

Sintering at temperatures from 1000 to 1500°C produces a series of different structures. The series of reactions which take place are presented in Table I. As TG-DTA curves (fig.63a) indicate generally kaolinites lose their absorbed water at 100°C. This endothermic peak does not show in fig. 63a, since prior to examination the powder was heated at 105-110° for an hour. TG-DTA analysis (fig.63a) reveals a large endothermic peak in the region of 500-700°C (with peak temperature 575°C) as a result of dehydroxylation of silicate lattice and decomposition of the clay [47], followed by a significant weight loss (loss of combined water). The possible reaction involves transformation of kaolinite to meta-kaolinite. As was indicated [26], dehydroxylation continues at to 900°C. The total weight loss calculated from the TG curve was about 12%, close to the 14% of pure kaolinite. As the temperature was increased a second strong exothermic peak was formed with peak temperature 996°C, which is not followed by weight loss in the TG curve, due to crystallization of mullite and/or γ-alumina and spinels [19,20,27]. A lot of disagreement still exists about the cause of the exothermic peak at 980°C (996°C for the examined kaolinite) and the composition of the spinel phase (see paragraph 2.1.1.3). Chakraborty and Ghosh [22] and Chakraborty [30] proposed a $3Al_2O_3.2SiO_2$ composition for silicon spinel phase and X-ray diffraction showed a small amount of mullite formation during metakaolin

reaction (No2 in Table 1). It is also suggested [37] that the relative ratio of spinel to mullite depends on the kaolinite origin. Further discussion of this issue, although it has considerable interest, is not a subject of the present thesis.

XRD analysis of kaolin (fig. 55a) shows that at 1000°C the crystalline phases have decomposed. The size of the " glass hump " (the elevated background between 18-50° 2-theta, [5]) decreases substantially as the sintering temperature is increased from 1000°C to 1500°C. No mullite is present at 1000°C. The first XRD indication of mullite formation starts at 1100°C, in agreement with results of other workers [e.g. 36], although as will be discussed later the presence of mullite was not evident below 1200°C in SEM . XRD shows the presence of mullite peaks at d-spacings 3.39, 3.42, 2.20, 5.4 Å with relative intensities of 100, 85, 74, 30 respectively. There is also quartz (low) (d-spacings: 3.34, 4.25) and evidence of SiO_2 (trace), probably as of cristobalite.

At higher temperatures (up to 1500°C), mullite formation is well developed, the higher the temperature the more intense the mullite peaks. The main mullite d-spacings remain the same but the absolute intensities are much higher (under the same experimental conditions the main mullite peak at 3.39 A, has absolute intensities 380, 625, 780, and 1000 at temperatures 1100, 1200, 1300 and 1500°C respectively) which is a quantitative indication that the mullite reaction was extended (SEM examination gave more evidence for it). At temperatures 1100-1200°C there is also a peak at d=4.06-4.08A with relatively high relative intensity which is an indication of cristobalite formation. This phase has a very short life since the peak disappears at 1300°C and higher temperatures, probably indicating that cristobalite is taking part in glass formation. These findings are in agreement with Alderson's [134],

who studied a similar china-clay under similar temperature range.

Mullite was considered to be formed from at least 1100°C. A sharpening of the X-ray peaks shows that a weak crystal structure is transformed to a better defined structure of the crystals as temperature increases.

The theoretical percentage of mullite for a completed reaction of alumina with silica (calculated from mullitization reactions-see Table I, paragraph 2.1.1.3) for Remblend china clay is 58.8 %. In the structures produced during sintering of kaolin specimens differ significantly in mullite content (no mullite at 1000°C).

Ghote et al., [344] analysed a mixture of a-alumina and amorphous silica fired at 1200°C with X-rays and found the presence of mullite although a minimum of 1400°C and 24 hours needed for the complete reaction to take place.

Tomlinson and Archer [345] reported that examination of the phases formed in an alumina-aluminosilicate sol refractory fired at 1200-1600°C showed that mullite formation was completed after heating at more than 25h at 1500°C or higher temperatures. A transitional amorphous phase also was observed as a product of reaction of cristobalite with α-alumina at 1500°C [346]. The mullite content in the system was increased with the addition of Al_2O_3 until about 73%.

Formation of mullite from kaolin at temperatures lower than the predicted from the phase diagram (1547-1587°C) can be attributed to the presence of feldspathic substances (about 3.5% of fluxing oxides K_2O, Na_2O, CaO, MgO form 2% feldspars) which lowers the mullite formation temperature since the feldspar-silica phase diagram has a lower eutectic point. Fluxing agents in ceramic technology are substances which enable liquid (i.e. glass) formation at lower sintering temperatures. Effective fluxes are the alkali oxides (e.g. K_2O, Na_2O, MgO and CaO).

5.2.1.2. Pottery Mixture

EDXRF spectrum from the "as received" powder is shown in fig.24. and quantitative analysis is given in Table 9. Pottery mixture has high SiO_2 and relatively low Al_2O_3 content and also contains CaO, Fe_2O_3, TiO_2 and other oxides.

The XRD peaks (fig. 55b) of the "as received " powder shows that it is a mixture of kaolinite with considerable amounts of quartz and large amounts of feldspar and minor quantities of mica and illite. Rational mineralogical composition analysis shows that it contains about 39% kaolinite 14% quartz, 11% potash feldspar, 0.8% soda feldspar, 28.65% lime feldspar and 6.7% miscellaneous oxides (Fe_2O_3, TiO_2, MgO and organic matter). It is apparent that the pottery mixture has a lower alumina content and a higher silica and calcium content compared to kaolin.

Sintering of the pottery mixture at temperatures from 900 to 1300°C produces a series of structures that have as a main characteristic the formation of mullite and glass. XRDs (fig. 55b) show that sintering at 900°C decomposes the clay and the only crystalline compound present is quartz. The main diffraction peaks of the pottery mixture fired at 900°C correspond to quartz (low). No mullite formation was found. The same structure is shown to exist at 1000°C but probably with higher "glass" content (because of the higher temperature). At 1100°C all the main mullite peaks are present (at d=3.39, 3.43, 2.21 and 5.39 Å), which is an indication that mullite crystals started to form . As the temperature is increased the intensity of quartz peaks are lowered (e.g. the absolute intensity of the main peak at 3.342 Å is lowered from 2500 to 610 as the sintering temperature is increased from 1100 to 1300°C) probably as a result of initiation of mullite formation and/or glass formation.

The theoretical percentage of mullite (with respect to its chemical composition) in a complete reaction is 39.2 % for the pottery mixture (significantly less than that of kaolin). Formation of mullite at lower temperature than in the case of kaolin is probably due to the higher presence of impurities. Increase of the amount of oxide "impurities" (e.g. K_2O, Na_2O, CaO, MgO probably form feldspathic compounds) and other compounds (e.g. carbonates) acting as fluxing agents facilitate liquid phase formation during sintering at lower temperatures, [10]. As an example the binary eutectic between potash feldspar ($K_2O.Al_2O_3.6SiO_2$) and silica melts at 990°C and the tertiary eutectic with slight addition of mullite or metakaolin at 985°C [5,347].

TG-DTA curves (fig 63b) show a 10% weight loss of combined and absorbed water. The endothermic peak at 96°C is due to absorbed water. A second larger endothermic peak is shown at 553°C (range 420-600°C), indicating dehydroxylation and decomposition of the clay structure and a smaller third one at 985°C due possibly to mullite formation. The later peak is not accompanied by weight loss since is due to recrystallisation and is not so well defined as for kaolin as a result of the impurities (higher fluxing oxide content).

5.2.1.3 Brick-clay

EDXRF spectrum from the "as received" powder is shown in fig.24. An increase of iron oxides from kaolin to brick-clay is apparent. Quantitative XRF analysis of the "as received" powders using the QMS program [304] is shown in Table 9. Brick-clay powder has similar to kaolin silica content, low Al_2O_3 content (lower alumina content than the other two clays) and high other oxide content mainly

Fe_2O_3 (the highest iron oxide content compared to that of the other powders), CaO, MgO, K_2O.

XRD analysis shows that it has a completely different structure with complete absence of kaolinite. XRD diffraction peaks from "as received" brick-clay powder (fig.55c) showed that it is a mixture of illite, chlorites, quartz, feldspars and probably potash mica. Zooming in the region 23-40° 2θ of the spectrum and computer-aided analysis of the peaks revealed that the main feldspars present were: Albite and Anorthite (sodium,calcium aluminum silicates).

XRDs from the sintered brick-clay (fig.55c) at temperatures from 900°C to 1150°C for 24 hours show that sintering produces structures very similar to each other, which only differ in the formed "glass" content. During firing at 900°C almost all the clay peaks disappear and only the quartz and some feldspar and oxide peaks remain. The disappearing of the clay XRD peaks when brick-clays are heated to 900°C is an indication of complete dehydroxylation of the clay at this temperature. X-ray peaks from brick-clay fired at 1000°C and 1100°C indicate an enhancement of the features observed at the temperature of 900°C.

Similar structures are formed also during other sintering programmes (programmes P7, P8, P9 -see fig 17) with shorter sintering times (15 minutes at high temperature) and maximum temperatures close to the above (850,950 and 1050°C respectively). Any expected differences in mechanical properties should be attributed to differences in formed glass content.

Testing the effect of soaking time (at sintering temperature) from 1h to 24h, at 900°C sintering temperature on the intensity of XRD peaks from the brick-clay (fig. 56) showed almost the same intensity at all testing times, which indicates that

decomposition of the clay and sintering reactions are completed very quickly.

TG-DTA curves (fig.71) show a 10% weight loss during heating up to 1000°C and three endothermic peaks, the familiar endothermic peak at 100°C indicating removal of absorbed water and another two in the region of 600-800°C indicating decomposition of the brick-clay, followed by an 8% weight loss as indicated by theTG curve. Since illite gives endothermic peaks at this temperature range (most normal micas do not give peaks from 0°C to 1000°C) and in relation to XRF and XRD results brick-clay has an illitic mineralogical composition. No new crystal phases are formed with heating up to 1100°C. Heating in temperatures in the region of 1150°C showed starting of melting of the clay, as a result of the high impurities content.

5.2.1.4 Kaolin+ F.A

EDXRF analysis of Fly Ash (F.A)(fig.24) and quantitative analysis (Table 9), show that the main characteristic of this substance related to its chemical composition is its high (32.2%) content CaO almost equal to that of silica. It also contains 34.4% SiO_2 and 19.6% Al_2O_3. XRD analysis shows that the main crystalline constituents of FA where quartz, anhydride ($CaSO_4$) and iron oxides. No indication of mullite or tricalcium aluminate (C_3A) was found.

A kaolin mixture with 5% and 10% F.A produce kaolin with lower (33.4%) Al_2O_3 and relatively higher (about 1.6 and 3.2 % rsp.) content of CaO. XRDs from kaolin, kaolin+5% FA and kaolin+10% FA (fig.57) sintered at 1000°C show no difference since the amounts of F.A are small and its main peaks are covered by that of kaolin.

5.2.2 MACRO, MICRO, AND SEM EXAMINATION

5.2.2.1 General Remarks

Macro-examination of the sintered specimens reveals that the colour of the specimens changes to darker shades of red as the sintering temperature is increased, especially in specimens with high iron content (e.g. brick-clays-Table 9) due to haematite (α-Fe_2O_3) formation in oxidizing atmospheres. At temperatures above 1100°C, the colour darkens due to thermal dissociation of α-Fe_2O_3.

Kaolin specimens remain white or almost white taking some shade of very light grey at temperatures of 1500°C, a fact which was expected due to their very low content in "colouring" oxides. Pottery mixture specimens change from almost white to pale pink (at 1100°C) and grey-green at 1300°C, due iron ions liberation. Brick-clay specimens turn from red to brown as sintering temperature is increased from 900°C to 1100°C. This change is due to a number of factors such as: liberation of iron ions, change of state of oxidation (ferrous to ferric), the firing atmosphere and other variables (see 2.1.1.4). Other oxides (e.g. CaO or MgO) counteract this colour change and "stabilize" the white colour.

Macroexamination of the shape of ceramic specimens after sintering shows that shrinkage is more pronounced as temperature is increased and is greater in the case of kaolin, probably because of the lack of any filler addition or the lack of other constituents having the same influence as that of the fillers. Generally, increase of the sintering temperature increases shrinkage and density and lowers porosity. However,

with respect to density and porosity changes, it must be pointed out that this is the net result of mainly two counteracting reactions:

a. The gas generation (e.g from liberation of H_2O from clays,CO_2 from carbonates, SO_2 from sulphates and sulphides) which decreases density and increases porosity; and

b. The liquid phase formation (e.g. glass formation) which fills the pores and cavities of the ceramic body and increases density.

The formation of a large number of microcracks between matrix and quartz particles is the result of contraction mismatch in coarse clay ceramics.

Increase of sintering temperature produces ceramic shrinking (for the reasons explained above), and an increase in "glass" formation (vitrification). Vitrification is a result of solid state reactions where silica reacts with fluxes (mainly oxides, e.g. N_2O, K_2O etc.) and form a liquid phase which on cooling does not crystallize but solidifies forming as amorphous glass phase. The highest sintering temperature where vitrification ends is about 1100°C for low-refractory clay (e.g.common brick-clays) going up to about 1600°C for pure china-clay [348]. The viscous liquid formed decreases porosity and acting as a bond between particles, increases strength and hardness.

Glass formation was detected by comparing etched and un-etched surfaces of the same specimen and sintering temperature. In the non-etched specimens when glass formation was present a blurring image of the surface features is observed which clears after etching with HF solution (see paragraph 3.3.9). The presence of impurities (fluxing agents e.g. feldspars and micas) lowers the glass formation

temperature.

A general observation is that both Micro and SEM examination reveal the presence of pores and cavities in most of the prints. As the sintering temperature is increased, a continuous vitrified structure is produced and the pores coalesce and form elongated cavities. Further increase of sintering temperature could have an adverse effect on porosity, since in cases where gas formation might happen from substances like, e.g. feldspars, it is possible to observe bloating. Bloating is the formation of spherical pores from gases released from chemical reactions, usually in the range of 1100°C for low-refractory clays [348].

Macroexamination of the fractured ceramic specimens, also show differences in the shape of the fractured surfaces. Low strength specimens from low sintering temperatures give an almost flat fracture surface perpendicular to specimen's long axis. As the strength of the specimens is increased the fracture surfaces become rough and inclined with respect to specimen's long axis. This is probably an indication of increase of work of fracture with increase of sintering temperature, as the strength and integrity of the structure are increased.

The SEM micrographs are taken from K_{IC} specimens and are representative of the surfaces examined in the present work. The area of the fracture surface shown in the micrographs does not necessarily include the part of the specimen near the notch induced by the razor blade. Examination of the bottom of the notch reveals a rough texture. Careful macro and SEM examination of the fractured surfaces revealed that in most of the cases the fractured surfaces do not reveal the point or the area where the catastrophic fracture starts. In the few cases where there were indications of the fracture initiation site, this was found near the notch, or inside the specimen body.

The above observations indicate that there is not an obvious single initiation point and it is quite possible the fracture to start from several points, from many possible initiation sites.

General SEM examination of the fractured surfaces reveals the absence of plastic flow in the surfaces.

The following changes in structure are directly connected with the mechanical behaviour of the ceramic systems which will be discussed later.

5.2.2.2 Kaolin

The fracture surface of a kaolin specimen before sintering is shown in fig.43a. The body consists of plastic aggregates of irregular kaolinite flakes of 10-20 μm. In most of the cases large cavities between the aggregates are observed.

The following structures were observed as the sintering temperature was increased from 1000°C to 1500°C (figs 43b-h):

a. After sintering the kaolinite at 1000°C some coalescence of the flakes takes place (fig.43b). No glass formation is seen. The structure is dominated by the point-to-point contact of the kaolinite flakes.

b. Sintering at 1100°C shows a starting glass formation (fig.43c). The point-to point contact is increased and a more compact structure starts to form. It can be assumed that some diffusion and sintering at the points of contact of individual crystallites has occured during the changes from metakaolin to silicon spinel structure (Table 1). Careful etching with a solution of hydrofluoric acid dissolves glass and leaves crystalline phases un-attacked. No mullite was observed by SEM, although its

presence is indicated by the XRD analysis (poorly crystalline mullite). Glass formation at temperatures below 1547-1587°C [5-7] is probably due to the presence of feldsparic substances which act as fluxing agents.

c. SEM micrographs from sintered specimens at 1200°C (fig. 43d) show formation of isolated pores in a well connected glass structure and mullite precipitation as very fine crystals embedded randomly in the glass matrix. As was expected, glass formation which started at 1100°C is further increased as temperature is increased. Mullite formation at this temperature is also a result of the fluxing agents influence.

d. At 1300°C SEM micrographs (fig.43c) show a clear and sharp increase in crystal structure (mullite crystallites) and further vitrification. Some of pores are connected and form series of cavities and some are filled with glass and disappear. The net result of all the above processes is that the specimen shrinks acquiring a more dense structure consisting of mullite needles with diameters of the order of a few tenths of a micron in a ceramic-glass matrix. Bloating is not observed.

Fracture appears to travel through mullite crystals in cases where mullite crystals are in a position perpendicular to fracture path, and along their length or cleaving them in cases where mullite crystals are in parallel positions to fracture path. No differential thermal mismatch stress cracks are observed between mullite crystallites and glass matrix.

e. At 1400°C and 1500°C SEM micrographs show a further increase (cf. XRD analysis) in mullite crystallites as the grow in size from the liquid phase which is a mixture of alumina and silica. The mullite diameter increases to

0.3-1 μm. Although mullite needles have a high aspect ratio (about 10:1), mullite in

the glassy matrix does not seem to form a barrier to crack propagation. Limited bloating is also observed after sintering at 1500°C.

5.2.2.3 Pottery Mixture

SEM examination of the fracture surface of a pottery mixture specimen before sintering shows a similar structure to that of kaolin. The surface shows aggregated irregular flakes to form a plastic mass and in some cases cavities formed during production of the specimen.

The following structures were observed as the sintering temperature was increased:

a. SEM examination of specimens sintered at 900°C (fig. 44a) show a structure similar to that of kaolin sintered at 1000°C. The structure has a flake appearance and some the flakes combine in a point to point manner. Examination of etched and non-etched specimens gave very weak evidence (if any) of glass formation.

b. At 1000°C (fig.44b) vitrification has started. The structure starts to become dense and the pores become more rounded and smaller and probably offering more resistance to fracture. Similar appearance is observed at 1050°C (fig.44c).

Alderson [134] reported a 10% remaining porosity in triaxial whiteware bodies at sintering temperatures up to 1550°C. Lundin [349], studying similar ceramics, reported a 5% remaining porosity even when a high sintering temperature was used to produce an impermeable vitreous material.

c. SEM examination of sintered specimens at 1100°C (fig.44d) shows formation of mullite and further vitrification as expected. The etched micrographs

show a dense mat of small mullite crystallites (smaller than those of kaolin specimens at 1200°C). Some of the mullite needles are shown to be in a horizontal position with respect to fracture path, while others to have been cut by cleavage. Formation of mullite at 1100°C is a result of the fluxing influence of the "impurities " (compare with kaolin which has lower impurities content and starts to form mullite at 1200°C) [28].

d. SEM examination at 1150°C shows a dense structure and massive mullite formation. Further increase in temperature (1300°C) results in bloating, i.e. gas formation inside the ceramic body, usually attributed to feldspathic content of the mixture and especially in the iron oxide reduction (e.g.[18,350,351]).

5.2.2.4 Brick-clay

The structure of brick-clay specimens before sintering is similar to that of kaolinite and pottery mixture with respect to glass formation but different with respect to complete absence of mullite and the presence of sand particles. A series of SEM micrographs (fig.45a to 45f) show that glass formation is the dominating change during sintering in these ceramics.

SEM micrographs after sintering at 900°C (fig. 45a) show that brick-clay fractured specimens have a structure similar to that of pottery mixture at the same temperature, except of the presence of sand particles. Increase of the sintering temperature to 1000°C (fig. 45b) produces a point-to-point connected structure, while at higher temperatures (1150°C) with increase of glass formation the structure becomes dense and well connected. At temperatures above 1150°C starts to bloat and

at even higher temperatures (1300°C) it starts to melt.

As the temperature is increased the glass formation is increased and development of coarse spherical pores with interconnections with adjacent pores are observed.

The sintered brick-clay specimens do not show any presence of mullite and they present a number of embedded sand particles in their structure (e.g. fig. 45e).

SEM examination of fractured brick-clay specimens after sintering at the sintering programmes P7, P8, P9 (see 3.2) (fig.45 g-j) show similar structures to that of brick-clay sintered at 900-1000°C. However, the limited soaking time (about 15 minutes) at which the specimens remain at the maximum temperature results in limited glass formation and less well connected structure.

5.2.2.5 Kaolin and Fly Ash

Specimens consisting of kaolin mixed with 5% and 10% fly ash sintered at 1000°C in order to examine the effect of F.A which increases the $CaSO_4$ content and incorporates graphite and silica particles. The SEM examination of the structures is given in fig. 46a-b. The presence of F.A is probably responsible for the formation of a crack network in the specimen structure. Increase of the calcium content probably results in vitrification at lower temperatures. Tite and Maniatis [352], using SEM, observed reduction of vitrification temperatures in clays with increase of $CaCO_3$ and production of a more porous structure. The other features of the structure are similar to those of pure kaolin sintered at 1000°c.

5.2.3 MECHANICAL TESTING RESULTS AND RELATION TO STRUCTURE AND SINTERING TEMPERATURE

5.2.3.1 General remarks

A scatter of mechanical testing results from identical specimens as high as 100% was not uncommon in our experiments. This is a usual phenomenon in ceramics and generally in brittle materials, while in ductile materials the strength variability is not more than 4-8 % [116].

The main reason for this is that in real materials there are flaws (cracks, inclusions, segregations, pores, cavities, etc.) of variable sizes, shapes and orientations and that the strength of ceramics is a statistical quantity depending on the volume and stress state.

Mechanical properties values, except the statistical analysis which will be discussed later, are presented in the conventional way of average (AVG), standard deviation (STD) and coefficient of variation (C_v) values, assuming that the measured values fall into some form of Normal Distribution curve. The average value gives a measure of the central tendency, the standard deviation gives an indication of the dispersion of data, while the coefficient of variation is a measure of the relative dispersion, since the significance of STD depends on the arithmetic mean.

The main methods of flexure testing of ceramics are performed in three-point and four-point bending rigs. The main difference between these methods is the area under testing which affects the types of possible flaws (intrinsic or manufacturing) which could influence fracture behaviour. In three-point bending the applied stress is

maximum only on the surface opposite the single central support (fig.11) and so there is a high probability that strength is influenced only by intrinsic flaws, while in four point bending the applied stress is constant over the volume between the two inner supports and so both intrinsic and manufacturing flaws can influence fracture. In order to avoid the influence of manufacturing flaws and examine only the effect of intrinsic flaws on strength, the three point bending test was chosen for the present work. A general observation made during flexure testing is that a certain amount of settling at the supports took place in most cases. Rejection of a number of tests was made when macroscopic examination of the fracture surfaces showed that a manufacturing flaw was in the fracture path and when calculated MOR or K_{IC} values were more than two standard deviations away from the mean value.

Fracture toughness is a LEFM parameter and can be defined as a resistance to crack propagation. K_{IC} is the critical value of the stress intensity factor at a crack tip necessary to produce catastrophic failure. The Modulus of Elasticity was calculated by the conventional method from bending tests and also by the dynamic testing method (see 3.3.5).

Mechanical testing results can be related to microstructure as revealed by XRD and DTA examinations and the observable features of the fracture surfaces in SEM examination. Furthermore these results can be related to determine the equivalent elastic crack length and assess any physical significance for it.

The main reactions which take place during sintering of the clay-based materials used in the present work are:

a. Mullite formation, if there is the proper chemical composition and the sintering temperature is high enough to allow a reaction of this kind (see phase

diagram fig.2 and Table 1).

b. Glass formation, since the mixture of oxides (SiO_2, Al_2O_3, CaO, K_2O, Fe_2O_3) and the high temperature facilitate glass formation.

c. Gas evolution, when gas forming substances like water, carbonates, sulphates, oxides, and appropriate high temperature, are present.

Generally mullite formation would be considered as beneficial to fracture stress of clay ceramics by altering the fracture path. Since the strength of hot-pressed mullite is about 172 MPa at density of 95% of the theoretical value (3.16 $g.cm^{-3)}$ rising to about 240 MPa at theoretical density [353] and that of glasses is about 50-55 MPa at density 2.3-2.4 $g.cm^{-3}$ [136] it is evident that mullite is stronger than glass and the reinforcing effect of mullite could be explained through the strong interface which exists between mullite and glass when mullite needles are formed and grown in a glass matrix. SEM examination, as discussed previously (5.2.2.2), showed the lack of cracking between mullite and matrix, a fact which suggests that, indeed, there is a strong interface between them with actually no thermal mismatch stresses and it is reasonable to suggest that fracture may prefer the easiest path, avoiding the area where there are random groups of mullite needles, instead of crossing them. The mullite needles in the glassy mixture could act as reinforcing agents in the same way as ceramic fibres reinforce ceramic composites by forcing the crack to travel around mullite it (as schematically is presented in fig.4). However examination of micrographs showing mullite areas (e.g. fig.43d-h), does not give evidence of such a reinforcing mechanism. If the crack path was going around, a considerable number of needles should be standing out of the surface (as will be seen in paragraph 5.3 in the case of fibre-composites), which is not the case here. The above indications rather

suggest that mullite does not play a major reinforcing role, a view given by Alderson [134]. A series of experiments with kaolinite and alumina, where no glass phase was formed, showed lower MOR and K_{IC} values from mixtures in which the glassy phase was formed.

Cooke [289] also indicated that in brittle ceramic materials differences in morphology of phases does not increase the resistance to crack propagation, e.g. the mullite needles in the glassy matrix do not act as reinforcing agents of the system. Lundin, [349] reported that whatever the various views regarding the reinforcing role of mullite, the major role is played by the glassy phase.

The formed glass at the sintering temperature is a viscous liquid which fills up the pores of the clay body increasing the density and upon cooling a decrease (shrinkage) of the overall volume occurs. On the other hand generated gases such as water liberated from clays, carbon dioxide from carbonates, sulphur oxides from sulphides and sulphates and oxygen from ferrous to ferric oxidations increase porosity and decrease density.

Glass formation acts to connect the structure making it more compact through liquid phase densification. The driving force for densification in the lowering of surface free energy by elimination of interfaces. Generally, the examined ceramics with respect structure and sintering temperatures range from those having a point bonded structure (bottom firing end) to those having a well defined dense glass-ceramic structure (top firing end).

The improvement of mechanical properties of brick-clays with sintering temperature where the only substance which is produced during sintering is glass, suggests that glass formation is beneficial to structure. However, above a certain

sintering temperature depending on the chemical composition of the original clay, a decrease of strength is observed probably as a result of structure breakdown from excessive gas formation (bloating) or microcracking, after excessive formation of the vitreous phase, as a result of mismatch stresses which are developed during cooling below T_g (glass transition temperature). The presence of impurities lowers the maximum sintering temperature because of their fluxing properties and the presence of sand particles lowers the flexural strength because of thermal mismatch stresses. Davidge [354], in a study of the effect of microstructure on the properties of ceramics, pointed out that in multiphase materials the addition of quartz particles of considerable size tends to produce cracking in the interface with matrix during cooling.

Since density values were needed for dynamic modulus E_d calculation and also for an evaluation of the porosity of the structures, the bulk densities of the ceramic materials were calculated by weighing the specimen and computing its volume by measuring its dimensions.

Generally the ratio of Young's modulus to average flexural strength of the examined materials was found to be of the order of 10^3 in agreement with most ceramic materials [116-118].

With respect to strain at which a brittle material fractures (critical strain, ϵ_C), Astbury [117] indicated that although brittle materials have a quite wide range of stresses at fracture, they show a very narrow range of critical strain. This critical strain, expressed as millistrain (1000 X ϵ_C), is usually 0.5-2 millistrains irrespective of the kind of the brittle material. Critical strain values for the examined materials are given in Table 26. It shows that ϵ_C values range between 0.84 and 2.93. Values

over 2.0 are given by structures poorly bonded. Comparison of ϵ_C values, shows that for the similar ceramics like kaolin and pottery, the values are quite similar and that there are no significant differences when sintering temperature increases above those giving point bonded structures. The brick-clay has also relatively constant values of ϵ_C with sintering temperature, but higher than the other systems. It seems that ϵ_C is affected by both composition and structure.

Material	Sintering Temperature °C	Millistrain
Kaolin	1000	2.93
	1100	1.61
	1200	1.12
	1300	0.95
	1400	1.23
	1500	0.88
Pottery Mixture	900	2.15
	1000	1.02
	1050	1.32
	1100	1.27
	1150	1.57
	1300	0.84
Brick-clay	900	1.97
	1000	1.57
	1050	1.86
	1100	1.28
	1150	1.67

Table 26. Millistrain values of examined ceramics sintered at various sintering temperatures

Analysis of mechanical testing results from ceramics in relation with their structure and sintering temperature shows the following characteristics.

5.2.3.2 Kaolin

Increase of sintering temperature from 1000°C to 1100°C increases (Table 11, fig.25 a-b) substantially the flexural strength (MOR), (about 3 times). However from 1200°C to 1300°C the increase is very small, probably because a steady state structure develops in this temperature region. A second steep increase, almost doubling the strength, takes place when the sintering temperature
increases to 1400°C, followed by an equally abrupt decrease as the temperature is further increased to 1500°C. This indicates that 1400°C is the optimum sintering temperature as far as strength is concerned. Decrease of strength at higher temperatures could be attributed to increasing porosity which produces surface flaws or cracks which lower MOR. Also mullite formation which continues up to higher temperatures, as was shown by XRD analysis, could lower strength since it "consumes" silica and decreases glass formation. All experimental observations support the hypothesis that the improvement of mechanical properties in kaolins is due to glass formation and is little affected by mullite formation and that above 1400°C it has an adverse effect. These results agree with Cooke's [156], who indicated that the increase in formation of a more crystalline (mullite), but less well bonded structure, results in inferior strength.

The fracture toughness, K_{IC}, shows a steady increase from 1000°C up to the optimum temperature of 1400°C. Above this temperature with the glassy phase completely formed the K_{IC} value levels out. The increase in porosity does not seem to affect toughness. Comparison of strength-toughness data show that probably different mechanisms exist in strength and toughness development. The low values of strength and K_{IC} in the kaolin sintered at 1000°C could be attributed in the absence or very limited formation of glassy phase, as it was found from SEM examination, which resulted in a " weak " point-bonded structure. As sintering temperature is increased, pore shapes become more rounded and sizes change becoming smaller, making the stress intensity field less severe and therefore affecting positively the K_{IC} values. Increase of mullite needles seems to have a very limited effect on toughness.

A similar effect of sintering temperature on density and modulus of elasticity from bend (E_b) and dynamic (E_d) testing seems to exist as is shown in Table 11 and fig.25a. There is a significant increase of E_b from only 2.28 GPa to 52.25 GPa, as the sintering temperature is increased from 1000°C to 1500°C. Generally, E_b is improved in a similar way to strength and toughness as sintering temperature is increased, probably as a result of structure development through glass formation and reduction of flaws. Point bonded structures (kaolin sintered at 1000°C) have low E values and as the "glassy" structure is developed the values of E are increased. E_b and E_d values show an almost parallel change up to the optimum temperature of 1400°C and a factor of 2 could be used for rough estimation of E_b from E_d values.

In the examined temperature range the work of fracture (Wf) shows a steady increase up to 1400°C. Above this temperature it levels out. It seems that toughness and work of fracture show similar behaviour. The temperature of 1400°C seems to

be the optimum sintering temperature as far all the mechanical properties are concerned. Density and porosity are influenced positively by sintering temperature up to 1400°C. The viscous "glass" formed at sintering temperatures reduces and changes the shape of the cavities inside the ceramic, reduces porosity and formes a glassy structure with higher strength. As explained above feldspathic or micaceous substances act as fluxing agents, lower "glass" formation temperature, and also reduce the sintering temperature range since at higher temperatures they cause bloating and melting. The calculated porosity after sintering at 1400°C is about 14% near that reported by Alderson [134] for triaxial whiteware. The calculated decrease of density at 1500°C could be attributed to increase of porosity as a result of bloating as evidenced by SEM examination. The sudden drop of strength at this temperature is a further consequence of porosity increase.

5.2.3.3 Pottery Mixture

The pottery mixture specimens sintered in the range from 900 to 1300°C and tested at 3-point bending present similar mechanical behaviour to that of kaolin. The results are presented in table 12 and fig. 26. Increase of sintering temperature from 900 to 1150°C increases strength by a factor of about 6.

The 900°C structure is a point-bonded structure (there is not enough glass formation shown by SEM). As the sintering temperature is increased the glass formation in increased producing a dense structure and strength of specimens sintered at 1100°C is almost equal to that of kaolin specimens sintered at 1300°C. In a similar way the strength of specimens sintered at 1150°C is almost equal to that of kaolin

sintered at 1400°C. This behaviour is probably the result of the fluxing agents (impurities) which lower "glass" formation temperature.

The above results are in agreement with the SEM observations, with respect to glass formation. The difference in the size of mullite crystallites (e.g. compare fig.43f with fig. 44d) does not have any significant effect on strength, an observation which agrees with the hypothesis that mullite does not play an important role in strength development of kaolin ceramics. At higher temperatures (1300°C) strength drops to about half of that of 1150°C, probably as a result of bloating and further formation of mullite in expense of glass (as already discussed in 5.2.3.2).

The fracture toughness increases with sintering temperature up to 1150°C and above that (at 1300°C) it drops to about the same value as that of specimens sintered at 1100 in a similar manner to that of kaolin. Both strength and toughness can be directly connected to structure. Glass formation and development are the main processes influencing strength. Excess sintering temperature has adverse effects as was discussed in the case of kaolin (vitrification ends at 1150°C while in kaolin it ends at 1400°C) in agreement with literature [348]. At complete vitrification temperatures kaolin and pottery mixture have similar strength, toughness and other mechanical characteristics.

The Modulus of elasticity values (Table 12, fig. 26a) from bending and dynamic tests show again behaviour a similar to kaolin. E_b values increase from about 5 to about 40 GPa as the sintering temperature increases from 900 to 1150°C.

The work of fracture is increased as the sintering temperature is increased and becomes about double when compared specimens sintered at 900 and 1150°C, in a similar manner to kaolin.

Density and porosity change adversely as the temperature is increased up to 1150°C for the same reasons analysed in 5.2.3.2. Considering that after sintering for 24h at 1150°C (which is the optimum sintering temperature with the best mechanical characteristics and the highest density) the theoretical amount of mullite (39.2%) is reached (with a density of 3.16g/cm^3) and that the rest (60.8%) is silica glass (with density 2.35 g/cm^3), the calculated porosity is 14.5% similar to that of kaolin.

5.2.3.4 Brick-clay

The main characteristic which makes this ceramic differ from the previous two is the presence of sand particles and the absence of mullite even after sintering at high temperatures. Since, as previously discussed, mullite seems to have little effect on the structure behaviour more attention will be drawn to sand particles.

Examination of testing results from brick-clays (Table 13, fig. 27a-b) shows that the useful range of sintering temperatures is between 900 and 1150°C. At lower than 900°C sintering temperatures their strength is low (less than about 10 MPa) since structure is only weakly bonded, while, at higher than 1150°C, they melt. Generally as in the other clay ceramics, increase of sintering temperature up to 1150°C, results in increase of MOR, K_{IC}, W_f, E and D.

SEM examination shows that sand particles (fig 45c and 45e) are cleaved by the fracture crack path and poorly connected with the rest of the structure, probably as a result of different contraction characteristics. This behaviour results in lower strength values as was indicated above, in agreement with literature [e.g. 5]. Furthermore sand particles are large enough to act as initiating sites of catastrophic

fracture without preceding substantial crack growth.

As previously shown in the case of the pottery mixture the 900°C structure is quite weak, with limited, if any, glass formation shown by SEM examination (fig.45a). Comparing this structure and mechanical characteristics with the pottery mixture sintered at the same temperature of 900°C it follows that they have similar structures (compare figs 44a-45a), and similar low values of E_b, E_d, K_{IC}, and MOR. It seems that the presence of sand particles at this sintering temperature has only slight effect and does not play an important role in fracture process, since point bonding is the limiting factor.

The E, K_{IC} and MOR values in brick-clay compared to that of the pottery mixture for specimens sintered at 1000°C and 1100°C are lower, probably because of the well developed "glassy phase" in which there are sand particles which now act as large flaws and also relieving cracks result from thermal mismatch stresses. Large particles or major flaws can initiate catastrophic failure giving low values of flexure strength. Comparison of MOR and K_{IC} values (Tables 12, 13) of the same sintering temperature between pottery mixture and brick-clay indicates that sand particles weaken microstructure and give low strength and toughness values.

The presence of impurities enhances glass formation at lower temperatures but also reduce the sintering temperature range (up to a maximum usable temperature of 1150°C) since they cause bloating and finally melting of the structure at higher temperatures. Experiments with the brick-clay showed that sintering above 1150°C resulted in partial melting of the specimens.

Density and porosity change in the same way as in kaolin and the pottery mixture. Brick clay specimens sintered at 1100°C have lower density than those of

pottery mixture at the same temperature, probably because they do not contain mullite (which has higher density than glass) and, as SEM indicates, they have higher porosity. The calculated porosity of brick-clay sintered at 1100°C is about 17.4%, slightly higher than that of pottery mixture and kaolin under complete vitrification conditions.

In order to examine the effect of soaking time in the firing temperature, three series of 20 specimens each were heated at 900°C for 1h, 3h, 6h and 24h. Comparison of the XRD peaks (fig.56) and of their fracture stress values show a high degree of similarity, which suggests that the examined brick clay even at 900°C acquires its structure very quickly , a fact which is economically very important for brick-clay industry.

Mechanical testing results from specimens of larger dimensions (Table 13), produced by hydroplastic extrusion and sintered at three different sintering programmes, show the effect of these variables on properties. Hydroplastic extrusion produces specimens with higher densities (e.g. compare Tables 12,13), as a result of reduced porosity since the plastic dough is pressed before and during extrusion. On the other hand the strength of the specimens is reduced as the volume of the specimens is increased, probably as a result of increased probability of occurrence of more fabrication and intrinsic flaws.

Testing of specimens in frost resistance (fig.27c) shows that even after only five cycles a decrease of strength is evident. The main cause of failure from frost formation is the 9% volume increase in the water as it transforms to ice. As a result high compressive stresses are developed in internal cavities (pores), with a magnitude mainly depending on the size of the pores, the amount of water filling the pores and the rate of freezing.

5.2.3.5 Kaolin + Fly Ash

The effect of fly ash addition to kaolin ceramics is shown in Table 15. As was shown by SEM examination the formation of cracks makes properties deteriorate. Addition of 5% (w/w) fly ash causes about 25% reduction of strength, while a 10% addition produces a overall reduction of about 28%.

The effects of fly ash addition to other properties are similar. As an example, for 5% addition, K_{IC} is lowered by 27%, and E_b by a factor of 3 at a sintering temperature of 1000°C. As was expected, addition of fly ash which has a lower density than brick-clay results in lower densities (compare densities in Tables 11 and 15).

This behaviour is probably the result of mixing of a non " compatible" ceramics. The fly ash which was used in this work contains high amounts of calcium sulphate, which makes the structure deteriorate. On the other hand, addition of fly ash in cement (APPENDIX 1) has beneficial effects, improving strength characteristics, probably as a result of compatibility between them and of pozollanic reaction. However, the addition of low calcium F.As which contain mullite (e.g. [56,60]) probably could have beneficial effects.

5.2.3.6 Equivalent elastic crack length

The equivalent elastic crack length concept was introduced in paragraph 2.2.13, as the hypothetical crack length which in accordance to Griffith theory could initiate fracture at the measured applied stress. Transformation of eq.41 gives the following relation between equivalent elastic crack length c_E, K_{IC} and MOR:

$$c_E = 0.27\left(\frac{K_{IC}}{MOR}\right)^2 \qquad \textbf{(eq.103)}$$

Using the strength and stress intensity values from Tables 11-13 the c_E values can be estimated. Table 27 shows that generally kaolin and pottery mixture structures have similar equivalent elastic crack lengths (comparing kaolin and pottery characteristics sintered at temperatures differing by about 200°C), while brick-clay is more coarse. It is also quite clear that the increase in sintering temperature which produces more dense well-connected structures gives lower equivalent crack lengths.

In the first two ceramics the dominating feature of the structure after sintering above 1100°C is mullite in a glass matrix while for the brick-clay structure it is the sand particles in a glass matrix. The particle size distribution for kaolin [297], shows that the maximum size in less than about 50μm, 40% is less than 2 μm and 20% more than 10 μm. The pottery mixture is essentially a ball clay with very fine particles the majority of which is less than 5 μm. Similarly the brick clay is very fine except sand particles which, as estimated from the SEM micrographs, are in the range of a few tenths of microns.

Ceramic Material	Sinter. Temp. °C	K_{IC} MPa.m$^{1/2}$	MOR MPa	c_E μm
KAOLIN	1000	0.18	6.68	196
	1100	0.386	16.44	149
	1200	0.73	34.22	123
	1300	0.88	37.2	151
	1400	1.15	60.11	99
	1500	1.19	46.21	179
POTTERY MIXTURE	900	0.31	11.09	211
	1000	0.67	21.73	257
	1050	0.76	31.27	159
	1100	0.83	36.02	143
	1150	1.22	63.36	100
	1300	0.85	33.2	177
BRICK-CLAY	900	0.34	9.7	332
	1000	0.33	10.47	268
	1050	0.42	12.76	292
	1100	0.69	25.01	205

Table 27. Equivalent crack length

The values of c_E for kaolin show to decrease as sintering temperature is increased from 196 μm at 1000°C down to a minimum which is around 100 μm at 1400°C (which is the optimum sintering temperature) and then to increase again to 179 μm. This behaviour seems to follow the flexural strength changes with sintering temperatures. The optimum sintering temperature for strength gives the smallest c_E value. On the other hand, toughness seems to improve when kaolin is sintered at 1500°C, where the c_E value is large again and near that of kaolin sintered at 1000°C. From the above, and taking into account the structural changes during sintering, it follows that if c_E has any meaning for these ceramics, it indicates that strength is a property related to particle or grain sizes, while K_{IC} is probably related to number, size and shape of pores.

Similar characteristics and comments could be made for the pottery mixture structures, except the toughness behaviour. The trend of values of c_E of pottery mixture is comparable with values of kaolin sintered at temperature about 200°C above that of pottery mixture. The lowest value of c_E for pottery mixture is 100 μm, again at the optimum sintering temperature of 1150°C where the best strength is attained. This value is equal to that of kaolin at optimum sintering temperature.

SEM examination shows that pottery mixture has smaller mullite grains and relatively less voids, cracks or pores. This structure could explain the toughness changes which, in contrast to what happens to kaolin, seems to follow the strength behaviour (toughness sensitivity on flaws is reduced resulting in parallel strength-toughness values). However, in both kaolin and pottery mixture structures there are no features near the computed values of c_E and extensive flaw linking must be assumed.

The brick-clay c_E values are higher but follow the same trend as kaolin and the pottery mixture, decreasing from 332 μm to 205 μm as sintering temperature is increased from 900°C to 1100°C. The higher c_E values could be explained by the presence of sand particles. Examination of all the fractured surfaces shows that the bonding of the sand grains into the material as a whole is improved as the sintering temperature is increased and more glass is formed and reduction of the c_E value is expected, as actually happens. However, the size of the sand grains and the computed values of c_E, are very different (by a factor of, say, 10).

From the above, it is clear that in none of the above formulations and structures there are any individual flaws near the estimated c_E sizes, which could be considered as sites for fracture initiation, except if extensive flaw linking is assumed.

In point bonded structures like those of kaolin, pottery and brick-clay fired at the lowest temperatures (900 or 1000°C), which are weak, equivalent elastic crack length has high values (about 200 μm for the first two and 330 μm for the brick-clay). Alderson [134] found similar values of c_E for other point-bonded structures (e.g. kaolin+alumina or kaolin+feldspar sintered at 1050 and 1150°C resp.). Again, there is no indication of any individual feature having this value and it may be suggested that before material failure extensive flaw linking must happen in order a crack equivalent to c_E to be developed.

5.3 DISCUSSION OF RESULTS FROM CERAMIC MATRIX FIBRE COMPOSITES

5.3.1 XRD ANALYSIS

X-Ray Diffraction Analysis of fibres in "as received condition" (fig.58a) show that initially Denka B95 fibres have a α-Al_2O_3 structure, Denka B80 fibres have a mullite structure and Saffil fibres have a tetragonal δ-Al_2O_3 structure, while Grafil are carbon fibres with a graphite structure. Fibres sintered at 1300°C (fig.58b), show that, with respect to phase transformation, the above fibres remain unchanged, except Saffil fibres which are converted in the alpha alumina structure although the silica addition which they contain stabilizes delta alumina against transformation. This transformation happens after sintering above 1200°C and increases hardness, modulus of elasticity and density but decreases strength since the crystal size is increased **[77]**.

XRD results from all the examined composites, in "as received condition" show (fig.59), that peaks characterizing fibre's presence are visible even at very low volume fractions, for example 4.2-4.7%, a fact which reconfirms the sensitivity of XRD measurements. Furthermore comparison of XRDs from sintered pure and composite kaolin ceramics (e.g. fig.60, 61, 62), shows that fibres are more clearly visible after sintering as a result of clay structure decomposition, a fact which removes any hindering effects from clay peaks.

5.3.2 MACRO, MICRO AND SEM EXAMINATION

The microstructures of the composites were studied by optical microscopy (OM) of polished sections and by scanning electron microscopy. Fig.51 shows polished sections from kaolin+α-Al_2O_3, Saffil, mullite and Grafil composites. The fibre distribution is quite uniform. In the case of Denka fibres (figs 51a,c) a considerable amount of non fibrous material is evident. On the other hand Saffil and especially Grafil fibres show a high degree of uniformity.

5.3.2.1 SEM examination of pure fibres

SEM examination of the fibres used in the present work in "as received" condition and after sintering at various temperatures (fig. 52) shows that all fibres have an almost circular cross-section.

The α-Al_2O_3 B95 Denka fibres (fig.52a-b) have a wide range of diameters ranging from about 2 to 30 μm with the majority around 5 μm and also some irregular shaped "shots" (fig.52c-d) having diameters up to 70 μm. With respect to lengths there was also recorded a wide range of lengths ranging from 10 to 200 μm. Examination of the same fibres after sintering and fracture (fig.52b) shows that the fibres conserve their integrity. The fracture surface of the fibre after 3-point bending shows a pure brittle fracture.

Mullite fibres in "as received" condition and after sintering at 1200°C (fig.52e-f) show a wide range of diameters (2-30 μm) and "shots" having

a wide range of diameters (50-200 μm). Quantitatively, mullite fibres contain a higher percentage of "shots" than the α-Al_2O_3 fibres. As stated (see 4.3), no attempt was made to give mean values and distribution due to the high degree of non uniformity. After sintering at 1200°C the fibres remain unchanged.

SEM examination of the RF δ-Al_2O_3 Saffil fibres showed a range of lengths from 50 to 200 μm and a mean length of 120 μm and also a range of diameters (from 1 to 10 μm) and a mean diameter of 3.4 μm (fig.54b) which is consistent with the distribution reported in the Saffil data sheet [80]. The calculated aspect ratio of these fibres is of the order of 30. In a few cases dual fibres (fig.54c) (two fibres fused together) and non-fibrous material (having diameters in the range of 15-25 μm) were observed. The small content of non-fibrous material is in agreement with a weight fraction of less than 0.1% of fibre measured by Dinwoodie [79]. TEM studies [355] revealed that RF Saffil fibres consist of fine crystals with a diameter of 10-80 nm and EDS showed that they contained of the elements associated with alumina (aluminium and oxygen) as well as small amounts of silicon. The small amount of silicon found with EDS is added in order to inhibit crystal growth during sintering and mullite formation at the alumina grain boundaries.

The Grafil graphite fibres (fig. 53a-b) present the higher uniformity of lengths and diameters. They have a mean diameter of 6.2 μm and are quite long with a mean length of 3 mm. The comparatively longer length and moderate diameter of these fibres, explains the high mixing energy input needed to mix them with clay to form uniform composites. The sintering at high temperatures in an inert atmosphere (Argon) (fig.53b) allows these fibres to retain their integrity.

5.3.2.2 SEM examination of oxide fibre composites

SEM examination of the fibre-composite fracture surfaces shows that the fibre-composite systems examined in this work can be divided in those having a strong fibre-matrix interface (the oxide fibre ceramic composites) in which fracture occurs by fibre fracture and in those having a weak fibre-matrix interface (the graphite fibre-ceramic composite) in which failure take place by fibre pull out.

In the case of oxide fibre CMCs (the α-alumina, δ-alumina and mullite kaolin composites) the strong interface does not permit fibre debonding and pull out. Fig.47 a-d shows micrographs from kaolin α-Al_2O_3 composites after sintering at various temperatures and fibre contents. In all cases the fibres are shown to conserve their integrity and a strong interface between fibres and matrix seems to exist, which is attributed to chemical compatibility between matrix and fibres.

Although micro and macro examination show that the fibre dispersion of the fibres in the composite is quite uniform, in some cases porosity in the form of dispersed cavities of about 30 μm was observed. Comparative observation of fractured specimens from composites differing only in fibre volume content shows an increase in porosity as the fibre content is increased. This could be attributed to the increasing difficulty for matrix material to occupy voids between clusters of fibres as the number of fibres is increased. The mullite formation temperatures and the size of mullite crystallites, due to matrix transformation, do not differ from those observed in pure kaolin ceramics.

Examination of the fracture surfaces of these composites shows the fractured fibres protrude from the surface which indicates that the crack front prefers to go

around fibres, a fact which could imply a reinforcing role for the fibres in these composite systems. Most of the fractured fibres show ceramic matrix crystals adhering to the fibre surface (e.g. 47a) which indicate that granular disintegration of the matrix occurred in the region of fracture.

Examination of fractured surfaces from the Saffil fibre-composite (fig.48a-d) show similar features to that of α-Al_2O_3 composites. The porosity of these composites seems to be higher, since Saffil fibres are thinner having a mean diameter of 3.4 μm, and for the same volume fraction, a larger number of fibres is present, producing higher porosity for the same reasons.

Similar characteristics are also observed in mullite fibre-composites (fig.49a-b).

5.3.2.3 SEM examination of Grafil fibre composites

Grafil kaolin composites sintered at various temperatures are presented in fig.50a-f. A close up of the Grafil fibre-kaolin matrix interface (fig.50b), shows that only a weak-bond between fibres and matrix exists. The fractured surfaces show extensive fibre pull out (e.g. fig50a,d and f).

A close examination of the pull-out areas show that the surface features of the fibres were replicated in the matrix (fig. 50d) . Another observation is that the fibre pull out length is increased as the sintering temperature is decreased. An estimated length of 70 μm is measured in most cases of Grafil composites sintered at 1000°C, dropping to about 30 μm at 1200°C sintering temperature and further to about 10 μm when the sintering temperature is increased to 1300°C. This behaviour is probably due

to increase of matrix strength through the increased vitrification as the sintering temperature is increased. When the composite is cooled the contraction around the fibres is higher as the sintering temperature is increased, friction is increased, making the pull out of fibres more difficult and resulting in shorter pull out lengths.

5.3.3 MECHANICAL TESTING AND RELATION TO STRUCTURE

5.3.3.1 General remarks

The general comments made already in discussion of mechanical properties of pure ceramics (see 5.2.3.1) apply to CMCs and will not be repeated here. Some further comments will be made with regard to issues which characterize composites.

The load-deflection curves of kaolin-alumina or mullite fibre-composites and kaolin-carbon fibre-composites underline the different fracture mechanisms governed by the interface type. Schematic representations of the load-deflection curves of the examined systems (fig.90) indicate the existence of a strong interface in kaolin-oxide fibre-composites and a weak interface in kaolin-carbon composites. In the latter case specific points in the curve indicate the first matrix crack (A), the region of load transfer to fibres (B) and the region of fibre pull-out (C) [67]. The behaviour of the fibre-composite load-deflection curve agrees quite well with idealized curves of CMCs (e.g.[338]) and clearly indicates these regions.

The theoretical analysis and evaluation of the strength of short fibre-composites as compared to that of continuous fibre composites is a complicated procedure and has been applied mainly to polymer matrix composites [381]. The reason for this is the fact that in short fibre-composites the fibres are randomly orientated in a three dimensional manner, so that a model analogous to that developed on aligned continuous fibre-composites is not possible.

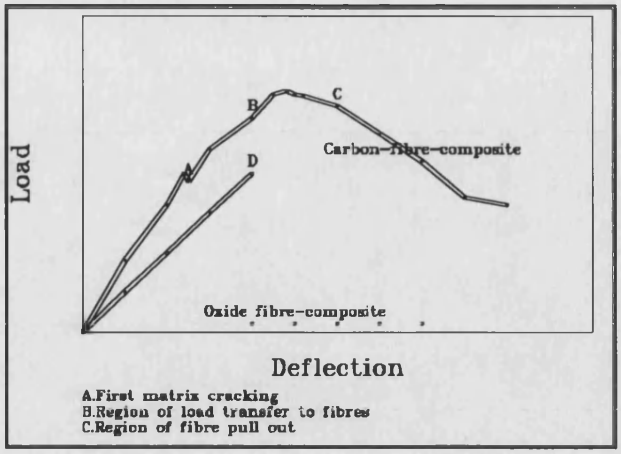

Fig.90 Schematic representation of load-deflection curves of fibre-composite ceramics A: First matrix cracking, B: Region of load transfer to fibres, C: Region of fibre pull out

The critical strain (ϵ_C) values of the composite systems examined in this work are given in Table 28. Comparison of these values shows that systems having a point bonded structure, e.g. kaolin+9.2% α-Al_2O_3 and kaolin+14% α-Al_2O_3, have high ϵ_C values and composites sintered at temperatures 1200-1300°C have lower and similar ϵ_C values. Generally there are not significant differences when sintering temperatures increase above those giving point bonded structures. These values could indicate a connection between critical strain and structure. Analysis of mechanical testing results from CMCs in relation to their structure (as was determined by XRD and SEM examination) and sintering temperature is presented in the following discussion. In all cases the kaolin matrix analysis remain the same as was presented in 5.2.3.2 .

Increased work of fracture was obtained in all composite systems. Crack

deflection by weak interfaces and fibre pull-out, in which the fibre-matrix shear strength is maintained during pull out, are the main mechanisms responsible for increase of work of fracture.

CMC	Sintering Temperature, °C	ϵ_c Millistrain
Kaolin+ 4.7%α-Al_2O_3	1200 1300	3.23 2.18
Kaolin+ 9.2% α-Al_2O_3	1000 1200 1300	5.87 1.36 1.39
Kaolin+ 14% α-Al_2O_3	1000 1200 1300	6.84 2.64 2.88
Kaolin+ 4.5 % Saffil	1200 1300	2.60 1.71
Kaolin+ 9.7 % Saffil	1200 1300	2.72 2.69
Kaolin+ 14.75 % Saffil	1200 1300	2.81 2.06
Kaolin+ 9.7% mullite	1000 1200	3.28 1.83
Kaolin+ 8.55% Grafil	1000 1200 1300	3.21 2.38 2,00
Kaolin+ 16.6% Grafil	1200 1300	4.26 3.62

Table 28. Critical strain values of CMCs sintered at various temperatures

With respect to relation between the modulus of elasticity values calculated from dynamic or bending tests, it seems that when a dense structure has been

developed (sintering temperatures at least 1200°C), E_b values multiplied by a factor between 2 and 3 give the corresponding E_d value.

5.3.3.2 Effect of thermal expansion coefficients

Before any attempt to explain the mechanical properties of composites the effect of thermal expansion coefficients must be discussed. This effect arises from the fact that the composites are first sintered at high temperatures and then are left to cool. As the temperature passes through a lower certain critical temperature T_c, stress-relaxation processes in the matrix are obstructed and stresses are built up between fibres and matrix due to thermal mismatch. This critical temperature for a glass-ceramic matrix (as in this study) is in the region of 1000°C (Table 4).

In order to investigate the stresses the thermal mismatch parameters Φ_α and Φ_r must be considered in accordance to eq.1 (see 2.1.2.2.3) page 26. Since this parameter is a function of $\Delta\alpha$, it can have positive values when the $\Delta\alpha$ values (α_m - α_f) are positive and negative values when Δ_α is negative.

In the kaolin matrix composites examined in the present work sintered above 1200°C, the matrix is approximately 50% mullite-50% glass with a computed thermal expansion coefficient of about $3x10^{-6}\,C^{-1}$ (50% mullite with $\alpha=5.3x10^{-6}\,C^{-1}$ and 50% silica glass with $\alpha=0.5x10^{-6}\,C^{-1}$) [84,137].

Taking into account that alumina fibres have thermal expansion coefficients above $8x10^{-6}\,C^{-1}$ (α-Al_2O_3 fibres have a coefficient of $8.5x10^{-6}\,C^{-1}$ [137]) and mullite a coefficient of $5.3x10^{-6}\,C^{-1}$, it is apparent that $\Delta\alpha$ between matrix and oxide fibres will always be negative and consequently the thermal expansion mismatch parameters Φ will always be negative in both axial and radial direction, since oxide fibres have

similar coefficients in both directions. This negative value indicates that there is a strong interface which also shown by SEM examination.

Similarly, the Grafil fibre composites considering a T_c value of about 500°C and σ_m=34 MPa, E_m=30 GPa (from Table 11) and α_{fa}=0 and α_{fr}=8x10^{-6} C^{-1} for the graphite fibres in axial and radial direction , the computed values of thermal expansion mismatch parameters are Φ_α=1.32 and Φ_r =-2.2. The positive value of Φ_α suggests that the matrix is in tension in the axial direction and the negative Φ_r indicates that the fibres shrink away from the matrix in the radial direction in agreement with SEM examination results which show that there is no bonding between fibres and matrix. Microcracking will take place if the local stresses are greater than the matrix tensile strength σ_m, that is when thermal expansion mismatch parameters take positive values of Φ_α and the cracking network will be perpendicular to fibre axis. Due to low value of Φ_α no cracking network was found in Grafil-composites.

5.3.3.3 Kaolin+α-Al_2O_3 fibre composites

Denka B-95 α-Al_2O_3 short fibres are high strength fibres with characteristics shown in Table 10. The variation of mechanical characteristics (D, E_b, E_d, MOR and K_{IC}) with sintering temperature and fibre content of this composite are shown in Table 16 and figs 29-31 and fig.40.

Generally, for the same fibre content, increase of sintering temperature results in strengthening of matrix and improvement of mechanical characteristics for the reasons discussed in 5.2.3.2.

Graphical representation of the effect of fibres on properties at various sintering temperatures is shown in fig.40. Addition of 4.7% Denka α-Al_2O_3 fibres in kaolin sintered at 1200°C influence a number of mechanical properties of the composites. The modulus of elasticity is reduced to about 1/3 of that of pure kaolin sintered at the same temperature. Application of the Voigt or Reuss models (considering E_b values similar to that of mullite) gives values of 36.81 and 35.5 GPa respectively which are far away from the experimental 11.09 GPa and shows the non-applicability of these models in short-random fibre-composites. The increase of density to (1.82 g/cm^3) as compared to that of kaolin (1.78 g/cm^3) sintered at the same temperature compared with the theoretical value of 1.86 g/cm^3, expected in accordance to rule of mixtures, shows that the difference is probably due to additional porosity which is introduced by incorporation of fibres. In a similar way with respect to strength, this addition of fibres gives a slight increase in strength (35.9 MPa MOR) compared to that of kaolin (34.22 MPa). Applying the above models (Voigt and Reuss), 111.1 MPa and 35.87 MOR values are computed for strength respectively. It apparent that the Reuss series model gives almost identical value of strength with that experimentally estimated. The above values indicate that the addition of 4.7% α-Al_2O_3 fibres is beneficial to composite properties with respect to strength but reduces elastic modulus and introduces extra porosity in the composite as was evidenced by SEM examination. Increase of sintering temperature to 1300°C does not change the above situation.

Increase the fibre content to 9.2% vol. and comparison to pure kaolin and to the composite with 4.7% vol. fibres sintered at 1200-1300°C shows that the increase of fibre content reduces strength and density and increases elastic modulus. The

reduction of density, although fibres have a higher density than matrix (3.3 compared to 1.78-1.95 g/cm^3 of the matrix after sintering at 1200°C or 1300°C) could be explained with the increase of porosity as is shown in SEM examination. However, in the weak point to point structure of a composite sintered at 1000°C, the addition of 9.2% fibres reduces density and modulus of elasticity but increases strength due probably to load transfer to high strength fibres in a weak matrix.

With respect to fracture toughness it is apparent that the addition of fibres increases toughness although this positive effect is offset by increasing porosity. For a 9.2% α-Al_2O_3 fibre composite at 1000°C sintering temperature, K_{IC} is doubled, from 0.18 to 0.365, while at 1200°C it becomes 0.78 MPa.m$^{1/2}$ (compared to 0.73 of pure kaolin) and finally is reduced to 0.74 (compared to 0.88 of pure kaolin) after sintering at 1300°C. Further increase of fibre content to 14% vol. does not change the above observations.

5.3.3.4 Kaolin+Saffil fibre composites

Saffil fibres, due to their fine structure, have high strength (2000 MPa) but relatively low Young's modulus of 300 GPa (Table 10). The mechanical characteristics of δ-Al_2O_3 Saffil kaolin composites are shown in Table 17 and figs 32-34 and 41. The values of E follows the values of MOR indicating that material properties significant for MOR determination are also important for E.

The effect of fibre addition in these composites shows an optimum volume fraction of fibres. As an example, with respect to strength and using as reference material the pure kaolin ceramic sintered at 1200°C sintering temperature, addition

of 4.5% fibres gives almost the same MOR value (34.1 MPa), increase of fibres to 9.7% increase MOR to 39.3 MPa, but further increase of fibre content to 14.75% reduces MOR drastically to 25.3 MPa. The behaviour of these composites at 1300°C sintering temperature is similar. Graphical representation of the variation of the measured characteristics at 1200 and 1300°C is given in fig.41. This behaviour, which is not uncommon in short random oriented fibre composites (e.g. [98-100]), could be explained by the formation at higher fibre volumes of a 3-dimensional fibre network where agglomeration is unavoidable resulting in reduction of density, increase of porosity and decrease of strength.

Comparison of values between 4.5% vol. Saffil and 4.7% vol. α-Al_2O_3 fibre-composites sintered at the same temperature (e.g. 1200°C) shows that Saffil composites have inferior properties. Taking into account that Saffil fibres have higher mechanical characteristics than Denka fibres this could probably attributed to higher porosity production since Saffil fibres are thinner and form clusters more easily which do not permit entrance of matrix material. The lower density and SEM examination confirms for this explanation.

5.3.3.5 Kaolin+ Mullite fibre composites

Mullite fibres have a similar effect to the other oxide fibres. Initially at low sintering temperatures strength is increased but at higher sintering temperatures the strength is decreased. The same effect is found for modulus of elasticity. Again an increased porosity is probably responsible for this behaviour.

5.3.3.6 Kaolin+Grafil fibre-composites

Grafil XAS fibres are high strength (4480 MPa) moderate elastic modulus (227 GPa) graphite fibres having a mean diameter of 6.2 μm (Table 10).

Assuming the absence of internal stresses, the simplified rule of mixtures (as applied to continuous fibre composites) indicates that the 8.55% and 16.5% Grafil composites sintered at 1200°C should have σ_c strengths equal to 414 MPa and 779.2 MPa respectively, values which are well away from the experimentally observed 23 MPa or 25.58 MPa respectively (Table 19).

Graphical representation of variation of mechanical properties with fibre content (fig.42) shows that increase of fibre content decreases density, modulus of elasticity and flexural strength at 1200 and 1300°C. On the other hand, for the same fibre content (8.55 and 16.5%), increase of sintering temperature increases the above characteristics through the development of a dense glass-ceramic structure.

Addition of 8.55% vol. fibres to kaolin matrix and sintering at 1000°C increases strength (MOR) from 6.68 to 9.53 MPa, but sintering at 1200°C and 1300°C results in strength decrease (Table 19). The elastic modulus follows a similar behaviour. These results probably are due to increased porosity of the composite. In the case of weak structures (sintering at 1000°C) the incorporation of high strength fibres gives a higher strength composite, but after sintering at higher temperatures the determining factor is porosity. The addition of graphite fibres which have a density of 1.79 g/cm^3, to a kaolin matrix of density 1.54 g/cm^3 in accordance to rule of mixtures should produce a composite with density of 1.56 g/cm^3. The measured density of 1.41 g/cm^3 indicates that an extra porosity was introduced in the composite

with the addition of fibres. It must be underlined that the inert argon atmosphere throughout sintering does not permit fibre oxidation of the carbon fibres, confirmed by SEM examination. Further increase of fibre content (Table 19) reduces the density more and increases porosity apparent from SEM examination.

SEM examination of the carbon fibre-kaolin composites reveals that there is no significant change to the matrix fracture surface compared to that of kaolin sintered at the same temperature, a fact which suggests that fibre pull out (which is observed in all fractured surfaces) is the main mechanism of work of fracture increase.

5.3.3.7 Equivalent elastic crack length in composites

The equivalent elastic crack length c_E has already discussed for pure ceramics of various compositions and sintering temperatures in 5.2.3.6. Using eq.103 the c_E values of the composites (where K_{IC} and MOR data are available) are computed and presented in Table 29. This table shows that there is a trend for the values of equivalent crack length in fibre-composites to decrease as the sintering temperature is increased. Furthermore it seems that at the same sintering temperature c_E values, no matter what percentage of fibres was used and irrespective of the kind of fibres, are in the region of 300-400 μm.

The matrix material in all cases is sintered kaolin and has been discussed in 5.2.3.6. The dominating feature at sintering temperatures of 1000°C is the point bonded structure, which has higher toughness due to the presence of fibres as compared to that of pure kaolin. At 1200°C and 1300°C, glass and mullite formation

produce more compact structures.

KAOLIN COMPOSITE	SINT. TEMP. °C	K_{IC} MPa.$m^{1/2}$	MOR MPa	c_E μm
9.2% α-Al_2O_3	1000	0.365	10.99	297.8
	1200	0.78	32.38	156.7
	1300	0.74	34.7	122.8
14% α-Al_2O_3	1000	0.36	9.3	404.6
9.7% mullite	1000	0.424	10.5	440.2
	1200	0.68	33.8	109.3

Table 29. Equivalent crack length in composites

SEM examination of all fractured surfaces show no features having the dimensions of c_E which could be considered as sites for fracture initiation as LEFM suggests and extensive flaw linking must be assumed.

5.4 COMPARISON OF ACOUSTIC EMISSION RESULTS FROM ALL SPECIMENS

5.4.1 GENERAL REMARKS

The monitoring of A.E. events from ceramic specimens which are stressed can be divided in two stages. In the first stage the damage (any active discontinuity) inside the specimen produces an acoustic event (the emission of acoustic energy) which propagates through the material and arrives at a transducer. In the second stage, the event is converted into an equivalent electronic signal and finally to an A.E. count. It is generally assumed [151] that in coarse structured polyphase ceramics where there are mismatch stresses between grains, the minimum stress at which acoustic activity starts coincides with the onset of grain size fracture. The minimum acoustic stress wave, in order to be detectable with the AE equipment used in this thesis, must give a signal of at least 10 μV (see 3.3.8). The interpretation of the AE counts is very complicated because the conversion ratios differ in different materials.

For comparison reasons the first samples which were acoustically analysed were specimens from glass plates having a thickness of 6mm (this thickness is similar to the thickness of the ceramic specimens) with other dimensions similar and testing conditions identical to that of all the other specimens. Glass is characterized as a completely brittle material quite "unique" in the sense that it has no crystalline structure and it produces a smooth surface during fracture. No Kaiser effect, as was expected, was observed in the glass specimens. The results presented in fig. 64 show a very quiet material where only a few (twenty) AE counts were recorded. In

agreement with others (e.g. [180]) it can be assumed that the absence of recordable AE events shows that glass fractures without sub-critical activity.

Another category of acoustically rather quiet material is cement and cement+fly ash composites (fig. A.3). Their AE analysis shows a low cumulative events number (of the order of 300 counts) and very low event rate of a few counts per second, increasing just before fracture.

All the reported AE results were taken from almost identical specimens during testing in three point bending under the same conditions (span length, speed of loading, temperature, atmosphere etc.). In all cases of AE testing, the simultaneous recording of AE events and load permits the development of load-deflection curves and load-events curves which give valuable information about acoustic activity.

Between the possible AE analysis techniques (described in 2.4.5) the amplitude analysis technique is the most popular and was used in the present work. The complexity of the signal-generation process, the influence of the propagation medium on the signals and sensing limitations are some of the difficulties which still exist in AE examination.

5.4.2 CLAY CERAMICS

Kaolin, in the as received condition (green specimens without sintering), is acoustically quiet material of low strength. Specimens break with almost nil acoustic emission (fig.65a). This is probably due to the absence of any connecting phase since it is composed of kaolin aggregates.

When kaolin specimens are sintered, they are acoustically active even at very

low stresses, with increasing activity as sintering temperature is increased (fig.65). This behaviour is probably a result of structure development. As was discussed previously (see 5.2.2 and 5.2.3), kaolin changes from the weak point-bonded structure to a well formed glass-mullite structure as sintering temperature is increased. The later structures are stronger and produce more AE events during testing since more sub-critical activity (micro-cracking) occurs before fracture.

The AE activity starts at very low stresses, virtually from the very beginning of load application. In most of the examined specimens application of a load of a few Newtons (2-3% of the ultimate fracture load) was enough for constant acoustic emission.

The tested kaolin specimens (fig. 65a-f) show an increase in cumulative AE as the sintering temperature is increased from 1000°C (only a few hundred) to 1300°C (around two thousand). In a similar way the event rate is increased from a few counts per second (at 1000°C) to a few hundred counts per second (at higher temperatures).

Generally, the event rate is low in the beginning and increases suddenly before fracture (fig.65e). No single critical event was observed to indicate the final failure. In particular, the event rate (count/sec) is extremely low (less than 5) during loading of specimens sintered at 1000°C and is increased to around 10 at fracture, while it is around 60 in specimens sintered at 1300°C and is increased to around 300 near fracture.

The amplitude analysis shows a distribution of counts in channels symmetrically descending towards the larger channel number (fig. 65b). The type of distribution of events per channel is the same, independent of sintering temperature

and differs only in the number of events in each channel. Similarly, examination of the amplitude analysis figures from the composite systems does not reveal different mechanisms with respect to non-reinforced ceramics.

The recording of load-deflection and load-event curves during AE testing (e.g figs 65f,65c) shows that kaolin is clearly elastic and the load-deflection curve is a line showing a deflection of a few tenths of a millimetre. The deflection is decreased as the sintering temperature in increased from 1000°C to 1300°C. This can be explain by the increase in stiffness of the structure (development of the glass-mullite structure) as the temperature is increased. The load-cumulative events curve is also an almost straight line, which shows that load application increases the AE activity linearly.

The Kaiser effect was observed in all kaolin specimens during recording of cumulative events versus load in repeated loadings (e.g fig.65d) and is especially clear in those ceramics with high AE activity. The first loading is sufficient to cause all the subcritical damage in the specimen up to that load. Further damage does not happen until the first load is exceeded. There is absolute lack of any AE activity during the second loading till the same load level, after which acoustic activity started again till fracture.

Although it is not absolutely correct to allocate to each AE event a subcritical event, since the number of AE events collected through the transducer is influenced by many factors, e.g. coupling of the transducer to the specimen, multiple reflection, ringing down etc., it is reasonable to accept that high AE counts indicates numerous subcritical events. As was indicated by Alderson [134], fracture may commence from anyone of several equivalent fracture sites formed by flaw linking during loading.

Pottery mixture specimens generally present the same behaviour as kaolin specimens (fig.66a-e). Structure and strength development increases the sub-critical sites for AE activity which are "activated" during mechanical testing. Pottery mixture specimens sintered at 900°C present the same kind of AE cumulative events, rate, distribution and linear relation between load and deflection as the kaolin specimens sintered at 1000°C. As the sintering temperature increases from 900 to 1300°C, AE activity becomes more intense in a similar manner to that of kaolin. Pottery mixture specimens show the Kaiser effect in a similar manner to that of kaolin (fig.66d).

Brick-clay specimens sintered at the same temperatures as pottery mixture, generally show the same behaviour and the Kaiser effect, but are more acoustically active (present higher cumulative events) and have a higher event rate (fig.67a-d). As an example, comparison of AE activity between pottery and brick-clay sintered at 1100°C (figs 66a-67a) shows almost four times higher cumulative AE events in the case of brick-clay specimen. This could be the result of the presence of sand particles in a glassy matrix. In agreement with this, Noone and Mehan [146], found that the presence of a second phase gives rise in acoustic activity and also suggested a relation of AE and grain size. During cooling of the sintered brick-clay radial tensile stresses are produced forming cracks due to difference in contraction between sand particles and glassy matrix. The application of external stresses produces an increase of the total stress field (enlargement of the process zone) with result of additional cracking and consequently additional AE events. In a similar way, Evans and Linzer [149], examining porcelain, found an increase in AE activity due to quartz particles and that the emission rate was a function of K_{IC}.

The effect of specimen volume and sintering programme on AE activity was

also examined in brick-clays. Increase in specimen volume increases the number sites in which AE events are produced (sub-critical crack growth) and higher activity is recorded. Increase of sintering temperature has also a positive effect on AE activity since it increases strength through the development of structure (increased glass formation).

With respect to event rate, in most of the cases brick-clays show some high rate peaks at about 50% of the fracture load instead of the gradual increase of rate common in clay ceramics. This behaviour could also be attributed to the presence of sand particles.

The effect of Fly Ash addition to acoustic behaviour of kaolin sintered at 1000°C is presented in fig. 68a-d. AE examination during mechanical testing of the powder composites with 5 and 10% (w/w) fly ash sintered at 1000°C shows low AE activity. This is lower than that of pure kaolin, since fly ash is a fine grain constituent (most has a grain size less than 45 μm) which when added in kaolin produces a cracked structure, reduces strength and fracture toughness and makes the structure weaker and looser.

5.4.3 FIBRE CERAMIC MATRIX COMPOSITES

The AE behaviour of kaolin matrix composites with oxide (alpha-alumina, delta alumina and mullite) and graphite fibres is presented in figs 69-72 in order to study the effects of sintering temperature, fibre chemical composition and volume fraction on AE behaviour.

General observations indicate that composites present higher AE activity

since, as well as matrix sub-critical events, fracture of the fibres, fibre-debonding or fibre pull out from the matrix may produce a comparatively large amount of AE events. Increase of sintering temperature produces composites with higher AE activity for similar reasons to that of powder ceramics.

Increase of the volume fraction of fibres in the kaolin matrix increases the AE activity. The results from specimens sintered at the same temperature and differing only in the volume fraction of the fibres are compared. So comparison of AE results taken from kaolin and 4.7% vol. α-Al_2O_3 kaolin matrix composite specimens, sintered at 1300°C shows almost the same number of events, since the small amount of fibres is not enough to change drastically the number of events. However the event rates are different. In pure kaolin a low event rate increases just before fracture (fig.65e), which is a general characteristic of clay ceramic materials (except brick-clays) studied in this thesis. In composite ceramics (and also in brick-clays) while the event rate is low at the beginning, later there is a comparatively high event rate at loading at about half of the fracture load which eventually drops before fracture. This behaviour could be attributed to the presence of fibres, the breakage of which produces a high event rate before final fracture.

Increase of fibre volume fraction produces a high increase of AE activity. As an example, comparison of results under identical conditions from pure kaolin and composite kaolin with 9.2% B-95 α-Al_2O_3 fibres, shows an increase of about 8000 events, which means that about 80% of the activity is due to fibres and only 20% to matrix sub-critical activity. Further increase of α-Al_2O_3 fibre content to 14% gives an increase to 26000 AE events, showing that about 90% of the AE activity is due to fibre content.

SEM examination show that the main fracture path is through matrix and fibre with no indication of fibre pull out or fibre-debonding. It could be assumed that with further increase in fibre content, there will a further increase in the number of AE events as a result of numerous sub-critical events due to fibre fracture during bending.

In almost all the cases, the way that events are distributed in channels is similar to that of kaolin specimens. Another general observation is that the event rate in composites under the testing conditions used in this work is about 1000 events/sec, and is almost constant irrespective of sintering temperature, fibre content and chemical composition of fibres.

Finally, the Kaiser effect was observed in all composite ceramics irrespective of the kind of the fibres (e.g. fig.69d, 71c, 72c). No acoustic activity was observed during unloading (e.g.72f), a fact which indicates that the sub-critical activity during loading is not a reversible process. Another observation was the difference of event rates between the first and second loadings (e.g. fig 69b, 72c). While during the first loading a high event rate (up to 800 counts/sec) was recorded in all cases with sudden peaks of high activity, during the second loading the event rate curve is smooth with a rate of almost nil up to the load of the first loading. Furthermore, repeated reloading and recording of load-time-rate curves in powder and especially in Grafil composite ceramics (fig.74) show not only change in the type of event rate curve but also a gradual decrease of maximum event rate although the loading cycles were constant (e.g. fig 73a-d). This is probably due to gradual non-reversible damage to the fibres of the composites after the first loading. It seems that fibre fracture and fibre pull out produces high energy burst events while matrix fracture produces

continuous AE events. This behaviour must be compared to the glass behaviour where there is only a very limited emission of AE events with a sudden increase just before fracture.

Based on the above observations, ceramic materials could be divided to two classes: class I (clay based ceramics and composites) and class II (glass). Cooke [288] reported a similar behaviour of a wide range of ceramics, (refractory high alumina firebrick, sand/NaCI model system kaolin/silica, feldspar etc.) in class I and recrystallized alumina, Refel silicon carbide, etc., in class II.

The first reloading stress at which AE started again (Felicity Ratio) R_f (eq.79) gave a wide range of values. The Felicity ratio observed in composite materials is in fact a quantification of the Kaiser effect. When $R=1$ the examined system has pure Kaiser behaviour, while for $R=0$ there exists non-Kaiser behaviour.

The load-deflection-AE event rate curves of oxide fibre and graphite composites show clear differences and similarities, which may be connected to interfaces and fracture mechanism of composites. The oxide fibre composites (e.g. 70b, 71b) have a load-deflection curve similar to that of powder ceramics with an almost linear increase of load with deflection up to fracture, since there is a the strong interface between matrix and fibres and fracture proceeds through matrix and fibres. The graphite composites (e.g. 72a) have a curve similar to that of unidirectional composites, where a first matrix cracking region, a load transfer to fibres region and a fibre pull out region and finally a fracture region can be detected, probably as a result of weak fibre-matrix interface giving fibre pull out.

Comparison of results from Saffil and B-95 Denka α-Al_2O_3 fibre-composites, sintered at temperatures above 1200°C, shows the effect of fibres having the same

chemical composition but different fibre diameter on AE activity. It must be noted that the Saffil fibres before sintering have a delta structure which is transformed to α-Al_2O_3 after sintering above 1200°C and the main difference which remains after sintering is the shape and fibre-diameter of the fibres (Saffil fibres have a diameter of 3.4 μm, while α-alumina B95 Denka fibres have a wide range of diameters and shapes (as revealed by SEM examination). Comparison of AE from a 9.2% vol. α-Al_2O_3-kaolin specimen with a kaolin+9.7% Saffil fibre-composite specimen, both sintered at 1300°C shows about the same event rate and also that Denka fibre-composites produce a little more cumulative events and higher event rate, a fact which justifies the hypothesis that fibre content is directly connected to AE events produced during 3-point bend testing. The difference in fibre diameters (which probably results in different number of fibres) also affects the AE behaviour of the composites. Due to higher range of lengths and diameters the number of Denka-alumina fibres is higher compared to that of Saffil composites with the same fibre content and so the number of AE events is higher.

AE activity from similar specimens sintered at the same sintering temperature, having about the same fibre content shows the effect of fibres having different chemical composition and dimension characteristics on AE behaviour. Comparison of AE activity from specimens sintered at 1200°C and having 9.2% content of Denka α-Al_2O_3, 9.7% content of Saffil fibres (delta fibres transformed to α-Al_2O_3 fibres at 1200°C), and 9.7% Denka mullite fibres shows that Denka alumina fibre-composites give higher numbers of AE cumulative events followed by Saffil fibre-composites and finally Denka mullite fibre-composites. The difference in AE events between the first two is rather small with Denka fibre-composites being a little more noisy. However,

comparison with the third (the Denka-mullite fibre-composite) shows a very high difference since it has only about 5% of the AE activity of the first two. This AE behaviour of the three composites has probably connected with the fibre diameters and shapes. The comparatively very low AE activity of the mullite composite (which was observed at other sintering temperatures as well) is probably due to Denka-mullite fibres having a high content of non-fibrous materials (appearing as large "shots" in the composite structure) which cannot produce as much AE events as the equivalent amount of fibres, confirmed by SEM.

The kaolin-graphite composites with Grafil fibres belong to a totally different class of ceramic composites with a different fracture mechanism. SEM examination shows there is a weak fibre-matrix interface and the fracture occurs after matrix cracking and fibre pull out, which indicates that any acoustic activity during loading may be due matrix cracking and fibre pull out. This fracture mechanism implies a high number of AE events since every matrix fibre pull out could give at least one AE event. However it must be noted that the graphite fibres have an almost constant diameter of 6.8 μm which is about double of that of Saffil fibres. This means that Saffil-kaolin composites will contain about twice as much fibres as the Grafil-kaolin composites for the same volume content and consequently it could be proposed that Grafil-composites with double fibre volume fraction could have about the same AE activity to that of Saffil-kaolin composites with half fibre volume fraction content. Comparison of AE activity from a 9.7% vol Saffil kaolin composite and a 16.5 % Grafil-kaolin composite (which have roughly the same number of fibres), both sintered at 1300°C, show roughly the same number of events, which means that the above hypothesis could be considered valid.

In accordance with an analysis made by Evans and Linzer [269], the cumulative probability function F(V) is connected to peak amplitude with a function similar to that of the Weibull distribution (see 4.6). The relation of lnln[1/1-F(V)] or $\ln(n_e)$ (cumulative number of detected events) versus ln(Peak Amplitude) in a number of AE results (figs.75,76) shows that a linear behaviour and a type III asymptotic extreme value distribution, characterize the acoustic behaviour of both powder and fibre composites. This is in agreement with Pollock's [280] proposal that a simple relation characterizes the failure mechanism in cases where a single failure mode dominates the fracture process.

5.5 STATISTICS

Fracture data can be analysed by applying statistical theories as well as LEFM fracture theory, Brittle fracture originates at a Griffith flaw or a number of flaws which may be intrinsic or formed during manufacture. The size and position of such flaws may vary from piece to piece, irrespective of the quality of specimen preparation. As a result a statistical variation of measured values is expected.

A number of factors such as inhomogeneity, lack of plastic deformation at crack tips, lower fracture toughness and sub-critical crack growth under static or dynamic stresses make the fracture behaviour of ceramics differ considerably from that of metals. The observed wide scatter in ceramic strength, resulting in low reliability and high inconsistency of design strength data, is due mainly to inherent micro and macrostructural chemical inhomogeneity and the presence of microcracks with various orientations, a large range of flaw sizes and the residual stresses arising from anisotropic contraction during cooling. These characteristics makes the use of statistical analysis functions in order to get meaningful results vital.

Among the statistical functions applied to brittle fracture is the well known Weibull empirical function [196,197] based on the " Weak Link Theory, WLT " (see 2.3.2) and a number of assumptions such as that materials fracture under large stresses and never fail in absence of tensile stresses and that a very large number of flaws are present in brittle materials.

According to WLT, as stress is applied stress intensity at the most severe flaw increases till a critical value of K_{IC} is attained and fracture occurs. A result of WLT is that measured values are influenced by the sample size and the method of testing.

It is apparent that a larger specimen is more likely to contain a large flaw and to have a lower strength. In a similar way, for example testing in four point bending, where a larger area is under stress compared to three point bending, lower values of fracture stresses are expected. For the same reason both bending tests give higher strength results compared with that of tensile testing.

The Weibull function is a Fisher-Tipper Type III distribution function of the cumulative probability of fracture P_f for linear isotropic brittle materials under uniaxial stress field. As Evans and Linzer [149] indicated, when a single flaw population is involved, the Weibull distribution, based on extreme value statistics, can be used in order to define the strength distribution of quartz particles. A multimodal Weibull function has been used in cases where the unimodal function gave poor fitting. With higher number of parameters, related if possible to defect sub-populations, it is logical for the fitting to improve.

Theoretically any distribution of points in a graph can match a function if an unlimited number of parameters is allowed. On the other hand, the physical meaning of the parameters decreases with their number and the scatter is increased [117].

The first criticism of the Weibull approach to brittle fracture is the lack of any physical consideration and the question of how well a purely statistical method, where strength or other mechanical characteristics are considered simply as variates, can be used to characterize brittle fracture. The weakness of this approach becomes obvious when it fails to give valid data in cases of extrapolation to larger sizes or in cases of more complex stress states. The use of probabilistic fracture mechanics might give more realistic results.

Another statistical function based in WLT theory where initiation of the failure

takes place in the weakest part of the failure-prone volume is an extreme value function recently developed by Neville [220-223], who tried to give a physical meaning to his function by considering the stress and strain near the crack tip (see 2.3.4).

Statistical analysis in the present work will be based on these two functions in order to investigate the validity of them in analysing fracture strength and toughness data.

Before any attempt at statistical analysis two parameters must be specified. The first one is what estimator should be used for estimation of the failure probability P_f and the second one is the minimum number of specimens which should be used for statistical analysis.

The first parameter which influences more or less analysis is the probability of failure P_f, a variable which goes straight into the statistical equation.
The most appropriate estimator from those used most often (see 2.3.10), was selected from examination of K_{IC} results from notched kaolin specimens sintered at 1100°C and fractured at 3-point bending (Table 20, fig 77).

Graphical representation shows that the slope of the linearly transformed function increases in the order : (i-0.5/n) , (i-3/8)/(n+1/4), (i-0.3)/(n+0.4), i/(n+1). However, no matter what the estimator type, its effect is small on the shape of the curve. Complete examination of the effect of the two estimators (i-0.5/n and i-0.3/n+0.4) on correlation coefficients shows that the **r** values do not change their relative order.

These results coincide with the results of other workers (e.g [235,236]) and show that the well known $P_f=i/(n+1)$ estimator gives the more biased m values and

is good for engineering predictions, since it gives the more conservative value (the lowest m value). The $P_f=(i-0.5)/n$ estimator gives the least bias to the m Weibull modulus, and the $P_f=(i-0.3)/(n+0.4)$ estimator was very close to the average value of the four examined estimators. This was chosen for use, together with the first estimator (i/n+1) in statistical analysis. The estimator (i-0.3/n+0.4) was also chosen for the reason that it was chosen by Neville in his analysis [220-224], since one of the aims of this thesis is to compare the statistical analysis results from Weibull and Neville functions.

The second parameter, concerning the effect of specimen population size on statistics, was estimated by analysing MOR data from un-notched brick-clay samples sintered at 900°C for 24 hours (Table 21, fig.78). It seems that the Weibull modulus remains nearly the same for a range of specimen numbers starting from 29 and going up to 144. The variation of the characteristic values of MOR and Weibull Modulus m is quite acceptable (about 0.5 STD of AVG values, and about 5% Coefficient of Variation). The number of about 30 specimens for statistics was considered suitable for this analysis, in agreement with the published literature [e.g.203,218].

The most common way of treating strength data of ceramics is first to collect experimental results and then to try to fit them in a model. The common set of parameters are the strength (σ or MOR), toughness (K_{IC}) and the cumulative probability of failure P_f.

Fitting the experimental distribution to the model can be done by linear plotting, using least squares method or the maximum likelihood method (see 2.3.9). For its relative simplicity the least square method was preferred in this work. Linear transformation of Weibull's function, assuming that x_u is zero and Neville's equation

give the following equations:

$$lnln\left[\frac{1}{1-P_f}\right] = m\ln x - mlnx_o \ (Weibull)$$

$$\ln\left[\frac{P_f}{1-P_f}\right] = D_p \ln[S] - D_p lnB_p \ (Neville) \qquad \textbf{(eq.104)}$$

where m and x_o are the Weibull shape and scale parameters and D_p and B_p are the shape and scale Neville parameters respectively.

It is clear that in the linear form the variates are:

$X=\ln x$ where x is MOR or K_{IC} and $Y= \ln\ln(1/1-P_f)$ for the Weibull function and $X=\ln S$ where S is MOR^4 or K_{IC}^4 and $Y=\ln(P_f/1-P_f)$ for the Neville function.

The above equations show that the shape parameter m can be found from the slope of the Weibull straight line and scale parameter x_o can be estimated from the value of x at $P_f=0.63$ since when $x=x_o$ $\ln\ln 1/[1-P_f]=0$. When the Weibull modulus tends to zero, fracture is probable at all values of stress while as m goes to infinity, fracture becomes deterministic and theoretically all samples fail at the same value of stress. In the same way the value of D_p can be estimated from the slope of the Neville straight line and B_p can be estimated from the value of S at $P_f=0.5$, since at $S=B_p$ $\ln[P_f/1-P_f]=0$.

However, although linear fitting is expected after linear transformation in the above equations, in many cases an S type curvature is formed connecting the points

of the above coordinates as shown schematically in fig.91. This curvature is mainly shown at medium and high strength data.

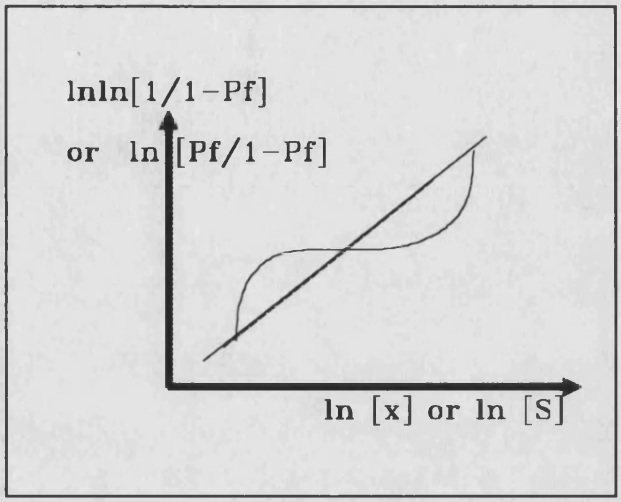

Fig.91 S type curve of data in accordance to Weibull or Neville functions

The usual 3-parameter Weibull function (P_f, m, x_u) in most of the cases in the literature is reduced to a 2-parameter function by taking σ_u or x_u as zero. The x_u value (which can be σ_u, MOR_u, K_{ICu} etc.) is the threshold value of variable x under which the probability of failure P_f is zero. In the 3-parameter function used in this work as x_u value was taken the one corresponding to P_f equal to 0.01.

Although it is argued [205] that for $x_u=0$ the safety factors are higher than those for other values of it, in reality the change of value of this factor does not influence significantly the measured variable at a given failure probability and the main reason for taking $\sigma_u=0$ is the simplicity of the calculations (but not for fibres where a real value of x_u is necessary).

The values from statistical analysis of pure ceramic and composite ceramic notched and un-notched specimens tested at 3-point bending, using 2 and 3 parameter Weibull and Neville functions are shown in Tables 22-25 and graphically represented in figures 79-87. As explained above in the two parameter Weibull function the σ_u value was considered as equal to zero.

The 2-parameter and 3-parameter Weibull functions and the Neville function were compared for best fitting of results by optical examination of the curves and by using correlation coefficients (see 2.3.7). The z_W and z_N values were not calculated using Fisher's transformation [181] since the relatively low number of specimens used for statistical analysis does not give a clue for a definite likelihood. Testing the effect of size population on correlation coefficients (Table 21) shows that increase of the number of samples does not influence r values much.

The effect of the third Weibull parameter x_u on the fitness of statistical results is shown in fig.88. The given values of x_u (1 to 5) are for Pf 0.1 , 0.01, 0.001, 0.0001 and 0.00001. As P_f goes to zero, the x_u value goes to a threshold limiting value (which is not equal to zero).

Results from MOR results from kaolin sintered in the range of 1100°C to 1300°C show that Weibull modulus remains almost constant with a mean value of 4.56 and standard deviation value of 0.29 irrespectively of sintering temperature. However when the notched specimens were tested the mean m value is 4.79 for temperatures 1100 and 1200°C, but at 1300°C sintering temperature it becomes about double this value. This shape parameter value is usual in ceramics where m values between 5 and 20 are recorded.

Transformation of Weibull equation to the form shown in eq.77 (2.3.11) shows that the Weibull Modulus m is a function only of the number of specimens and the ratio of maximum to minimum strength, which means that in Griffith materials m does not change with toughness. The change of m with toughness in these results could probably show that these ceramics do not follow the Griffith equation.

According to Jayatilaka and Trustrum [195], m is a material constant, expressing the brittleness but with no real connection to features in micro or macrostructure. However, if m is connected to flaw size distribution *f(c)*, the above deviation of K_{IC} values at 1300°C, could indicate a different flaw size and shape distribution showing that toughness is flaw size and shape dependent.

The appropriatness of Weibull's or Neville's functions is made apparent by comparing the correlation coefficients (Table 22). For the MOR values at 1100°C the 3-parameter Weibull function gives the best fitting, for 1200°C the 2-parameter function, but for the other four cases the Neville function gives better results than both 2 and 3 parameter Weibull functions. Optical examination of relative curves (fig.79, 80) shows that despite the high r values in all cases quite a lot of values in the upper and lower bound are off line and show the S type curve (e.g. 79a {K11}, 80c {K11}).

Results from the pottery mixture specimens (Table 23) show that in these ceramics the spread of MOR and K_{IC} values are less than those in kaolin, since a mean value of m=7.78 with a deviation of 1.32 is recorded for un-notched specimens (the higher the m value the less spread the experimental values). Measurements in notched specimens, show even higher values of Weibull modulus (mean value of m equal to 12.95 with deviation of 1.4).

Best fitting analysis (Table 23), shows that in this case the correlation coefficients give best fit using the Weibull 2-parameter function for MOR specimens sintered at 1000°C, using the 3-parameter function for MOR specimens sintered at 1100°C, for K_{IC} specimens sintered at 900 and 1100°C and using the Neville function for MOR specimens sintered at 900°C and K_{IC} specimens sintered at 1000°C. Optical examination of fitting (figs 81,82) confirms the above analysis and shows again the usual S type curve in some cases (e.g. fig.81a, P9).

Similar results were taken from brick-clay specimens. The un-notched specimens have similar values (mean value of m=9.23 with deviation of 0.86) irrespective of sintering temperature to those of kaolin and pottery mixture. The notched specimens show even higher values (m around 13) but the results from brick-clays sintered at 1000°C give a Weibull modulus quite low, near that of kaolin.

Best fitting results of brick-clay (Table 24), shows that in this case the correlation coefficients give best fit using the Weibull 3-parameter function for all MOR specimens and notched specimens sintered at 900°C, and using the 2-parameter function for notched specimens sintered at 1000°C. Finally the K_{IC} specimens sintered at 1100°C give best fit using the Neville function. Optical examination of fitting (figs 83,84) confirm the above analysis.

Comparison of the above results shows that in strength measurements Weibull modulus is dependent on the type of ceramic material but remains relatively constant irrespective of sintering temperature. On the other hand in toughness measurements it seems to change both with type of material and sintering temperature.

Although Weibull theory and generally statistical theories for strength evaluation do not apply to composites, since there is a changing flaw population with

load application (see 2.3.11) probably as a result of extensive subcritical activity [104], statistical analysis was performed on a number of composites. The Weibull moduli and correlation coefficients of a number of un-notched composite specimens with various fibre contents are given in Table 25 and graphically presented in figures 85-87. The relevant values from glass specimens are also given for comparison purposes. The kaolin based composites seem to have m with a mean value of 6.44 (deviation=1.58). This value is higher compared with that of pure kaolin and could indicate that the presence of fibres increases Weibull modulus and reduces the scatter of results in agreement with Kendall et al. [125]. The function which gives the better fit again shows a mixed picture. In most cases the Weibull function should be preferred. Examination of the graphs (figs 85-87) shows that in most cases, although the r values are high, most of the measurements are outside the least square line (e.g. fig.86a,b).

Analysis of glass specimens (Table 25) gives a Weibull modulus of 6.34 and ironically a better fit by Neville function. It must be underlined that glass was the material which Griffith used to develop this fracture theory.

In almost all the above cases both Weibull and Neville functions give correlation coefficients that have extremely high values, near the ideal, which is unity indicating complete fitting. However, other combinations of variables, could give equally good or even better fits. As an example, fig 89 shows a number of log-normal distributions between P_f and ln (x) from measurements in kaolin notched and un-notched, pottery mixture notched and kaolin composite specimens. In these cases the correlation coefficients show similar or better fitting of least square lines from both Weibull and Neville functions. This observation could indicate that both the above

functions cannot apply to the whole range of brittle materials and further research is needed in order a universal function to be developed. However, it is questionable if such a function exists, since any attempt to develop a statistical theory involves a number of assumptions related to flaw behaviour which may be different from one material to the other or be influenced by any other variables such as fabrication, thermal treatment etc.

5.6 GENERAL DISCUSSION OF RESULTS

5.6.1 RELATION OF MECHANICAL PROPERTIES TO STRUCTURE

It must be underlined before everything else that all the examined ceramic systems were not monolithic and homogenous but polycrystalline polyphase ceramics and composites that were heterogenous in nature and coarse in structure. Materials are characterized as polyphase when they are composed of different phases and generally when there are variations from grain to grain.

In early research on brittle fracture stress intensity factor (K_{IC}) and modulus of elasticity (E) were considered as material parameters, and fracture stress σ_f as a random, flaw dependent function. However, as Evans pointed out [299], the different methods of measuring fracture toughness often give different incomparible results, a fact which minimizes the utility of fracture toughness as material parameter. Additionally the large specimens needed for valid K_{IC} values can not always be fabricated.

Later [134,177], with increasing evidence that prior to fracture a critical crack length is necessary, σ_f was also considered as material parameter. It seems that in the case of fine grained ceramics where grains and pores are smaller than surface defects, strength is determined by random surface flaws but by the internal structure in the case of coarse grained ceramics. In polycrystalline ceramics there are several different types of flaws which can produce fracture at nearly the same stress. In such materials surface flaws could be removed by lapping and polishing but improvement in strength

is rather small because catastrophic fracture originates from other (internal) flaws and strength is a material property related to the structure. Generally flaws in ceramics are small (from a few tens up to hundreds of micrometers) and give a statistical character to strength, since in accordance to WLT the largest effective flaw dominates fracture.

In the present work it has been shown that ceramic and CMC properties can be influenced by a large number of structural defects introduced during fabrication and sintering (pores, cracks etc.) which can be classified into those characterising the surface and in those characterizing the internal ceramic structure. Both types of defects act as stress intensifiers and result in material failures well below the theoretical strength of ceramics. Sintering in the examined ceramics and composites produces heterogeneous structures depending on the sintering temperature and formulation. Increase of sintering temperature (in the region of 1100-1600°C depending on the chemical composition of the clay) results in:

a. Vitreous glass formation and could produce a better matrix bonding ceramic shrinking, decrease of porosity and increase of density; or

b. Above a certain temperature depending on also on chemical composition, bloating and porosity.

The process (a), increases matrix strength and hardness, while (b), results in decrease of mechanical properties.

The dominating mechanism in sintering of the examined kaolin-based ceramics, as was showed by SEM examination, is vitrification and flow of the liquid glass phase into the pores and transformation of a point-connected structure to glass-connected structure. The liquid glass phase must be sufficient and must have enough

fluidity to fill up the structure cavities. Both of these characteristics are controlled by the sintering temperature. Low sintering temperatures produce point bonded structures in all cases. Higher temperatures produce glass matrix with mullite crystallites (kaolin and pottery mixture). SEM examination shows that the common feature of all specimens are the internal pores and cavities which change in shape and size (being reduced as the sintering temperature is increased) and a continuous vitrified structure is produced as the sintering temperature is increased. No mullite is formed in ball-clays which contain also sand particles. Addition of fluxing agents reduces the fluxing temperature but also reduces the sintering range of ceramic. Generally kaolin structures are equivalent to pottery mixture structures sintered at about 200°C lower sintering temperature. The added fibres do not show any change with sintering temperature, except the transformation of structure (from δ to α-Al_2O_3) of Saffil fibres.

SEM examination and mechanical testing performed on the same specimens show that both MOR and K_{IC} were possibly related to structural features. Also the values of E could usually be related to visible features in the structure of ceramics. It was found to be affected by major cracks or flaws and this paralleled σ_f more than K_{IC}. Generally both fracture toughness and flexural strength show change in the same manner in relation to microstructure as well as distribution of flaws. Differences in phases in clay ceramics (e.g. mullite in glassy matrix) do not increase the resistance to crack motion.

Comparison of strength and toughness results in the ceramics and composites, examined in the present work, (figs 38,39), show that fibre composites have better characteristics in point bonded structures (low sintering temperature) but, as the

sintering temperature increases, porosity is the determining factor and, except for composites with very low additions of fibres, kaolin without fibres has the lower porosity and the best mechanical characteristics. Comparing the results from ceramics and composites with respect to modulus of elasticity, it is apparent that in ceramics point bonded structures have similar low values of E (2-5 GPa), while well bonded structures where glass phase is well developed have relatively higher values of E (40-50 GPa). Materials like the brick clays which can develop a glass phase but contain also large particles (e.g. sand) the E values are halved (around 20 GPa), since these particles can act as major flaws. Addition of substances which cause extensive crack formation (as FA) produce a further decrease of E values. The effect of short random oriented fibre addition, since it induces porosity, results in reduction of E. Generally conditions giving low E values, give low MOR and K_{IC} values.

Critical strain, ϵ_C, connecting fracture stress (MOR) and modulus of elasticity (E) according to Hooke's law, seems to be affected by structure and formulation. Ceramic point bonded structures have similar high values of ϵ_C above 2. Well bonded structures have lower ϵ_C values. Addition of fibres increases critical strain both in point-bonded and well bonded structures. Comparison of ϵ_C values in well bonded kaolin structures (e.g. sintered at 1200-1300°C), with and without fibres, shows them to double when fibres are added, probably as a result of increased flexibility since it expresses the elongation as load is applied. The large values of ϵ_C in relation to those found by other workers for polycrystalline single oxides, probably explains the insensitivity of σ_f (as confirmed in this work) to random surface flaws.

The equivalent elastic crack length c_E, is decreased as the sintering temperature is increased in all cases. Comparison of c_E in kaolin and kaolin fibre

ceramics shows that it generally increases with fibre addition probably as a result of increased porosity. However, in all cases there are no visible features in the structure which could be considered as sites for fracture initiation as LEFM suggests with the dimensions of c_E and extensive flaw linking must be assumed. If c_E has any meaning for the examined systems it indicates that strength is a property related to particle or grain size while K_{IC} is probably related to number, size and shape of flaws.

Comparison of the stress-deflection curves of the ceramic systems, kaolin, kaolin+fly ash, pottery and brick-clays and kaolin based carbon and oxide fibre-composites, shows that in all cases except carbon -fibre composites, stress increases almost linearly with deflection till the maximum strength, where unstable fracture occurs, and then decreases immediately. Fracture strength and deflection generally increase, for the same formulations, with increase of sintering temperature. On the other hand the load-deflection curves of carbon-fibre ceramics show the points of matrix cracking and the regions of unstable and stable failure (fig.90).

AE examination of the ceramics and composites examined in the present work supports the view that in coarse grained ceramics and composites the large number of acoustic events indicates high subcritical crack activity prior to fracture. Acoustic emission during three point bending of the examined ceramics shows the onset stress for sub-critical events. The number of AE events increases in an analogous way to load application and sintering temperature. In a similar way the event rate increases. No single event was found to indicate the final failure and it could be suggested that fracture may commence from any of several almost equally possible paths formed by flaw linking. The examined ceramics compared with glass and cement specimens present a different behaviour. They present the Kaiser effect while the glass does not.

After sintering to a vitrified structure, they are more acoustically active than glass and cement. AE activity increases from kaolin, to pottery mixture and brick-clays as a result of the incorporation of a second phase [146,149], in the matrix (e.g. sand particles). Comparison of AE from ceramics and composites shows that composites present much higher number of AE events.

In accordance with the Inglis equation (eq.8), the stress at the tip of a narrow crack depends on the radius of curvature ρ at the crack tip. In the absence of a plastic zone at the crack tip to remove or smear out of machining or material irregularities, which is the case for brittle ceramic materials, failure stress would be expected to have rather random values. However, SEM and AE examination results in the present work show that both strength and toughness in ceramics can be related to structure, a fact which indicates that a process analogous to plastic zone formation,"smooth" the effect of irregularities [134]. It seems that the large number of acoustic activity denoting a large number of subcritical crack events and the large number of alternative paths for crack growth available, keep the strength variations low, although in the beginning there is a period of random crack growth. On the other hand, in cases where grain size and pores are smaller than defects on the surface as in the case of e.g. glasses, it is reasonable to expect the fracture stress to be determined by random surface flaws and toughness by material properties as Inglis indicated.

5.6.2 STRENGTH OF SHORT FIBRE CERAMIC COMPOSITES

Combination of materials to form composites has made possible the formation of new material systems, suitable for use in practice in conditions where conventional systems had failed.

In the examined ceramic systems, a number of interfaces (e.g interfaces within the matrix, interfaces between the matrix and the fibres etc), varying according to sintering temperatures, may exist and influence their mechanical behaviour due to their polycrystalline and polyphase nature. With respect to matrix-fibre interfaces, strong interfaces exist in the case of chemically compatible systems and weak interfaces in the case of non-chemically compatible composite systems. The interface type determines the type of the crack path.

SEM examination of all ceramic and composites shows a completely brittle fracture surface with no differences near or away from the notched area and it is impossible to identify particular features of the structure where fracture started or the particular sub-critical events leading to fracture.

SEM examination and mechanical testing results show that the interface properties control the fracture behaviour of composites. Generally three types of interfaces may exist in polycrystalline and polyphase composites: interfaces between fibres and matrix, interfaces between phases and/or crystals and interfaces inside the fibres. In order for fibres to strengthen ceramics in CMCs, load must be transferred to fibres. While this is not difficult in long fibre-composites, in short random oriented fibre composites load cannot be applied at the fibre ends and stress must be transferred by shear forces at the fibre-matrix interface [71]. In cases where there is

a strong interface between matrix and fibres (eg. oxide fibres glass- mullite matrix of kaolinitic origin), a crack propagating in the matrix passes through the matrix and around fibres increasing toughness and work of fracture by crack deflection and by increasing the fracture surface. In cases where there is a weak interface (eg. carbon fibre glass-mullite matrix), debonding at the matrix-fibre interface, crack bridging and friction are the determining mechanisms. Frictional effects characterize the strength of the system. In this case load transfer from matrix to fibres take place and a tougher composite results.

As alumina and mullite fibres have higher K_{IC} values than the matrix material produced after sintering, it could be expected that composites will have higher K_{IC} values. However, the reinforcing efficiency of short fibres is less than that of long fibres, a fact which can be explained as follows. For short fibres to increase the strength in strong fibre-matrix interface composites, since the fibres cannot be loaded directly at their ends, stresses must be transferred into them from the matrix. This is effected by shear stresses near the fibre ends which produce an axial tensile stress in the fibres. When a load is applied to a composite containing a stiffer fibre a strain field is produced in which, away from the fibre ends, matrix and fibre strains are equal, but the fibre stress is greater since it has a higher Young's modulus. Near the fibre ends, the strains are not equal and hence there are shear stresses at the interface, which decreases towards the fibre centre (fig 9). The end regions of short fibres are not fully loaded and this is the main reason for having inferior properties and being less effective as a reinforcement when compared with continuous fibres. The less the fibre length the less the reinforcing effect (fig.10). As Harris [71] indicated there is a critical fibre length l_c in order fibres to carry the maximum stress.

Composites with weak fibre-matrix interfaces [69], like the Grafil fibre-kaolin composite examined in this thesis, have work of fracture increasing with V_f and fibre pull out length up to maximum (at $l=l_c$) and then decreasing since fibres break for $l>l_c$ and the amount of pull out decreases.

Comparison of results, from pure ceramics and fibre-composite ceramics, when a chemical compatibility exists between matrix and fibres, shows a different behaviour between second phases produced in situ (e.g. mullite crystallites growing in kaolin ceramics) and those added (e.g. mullite fibres added in composites). Addition of fibres usually increases the work of fracture and SEM examination shows a disturbed fracture path forced to go around fibres, while in mullite needles formed in a glass matrix there was no reinforcing effect. Similarly, Alderson [134], reported that mullite or zircon particles added directly to ceramics produce considerable reinforcement. This behaviour is probably due to characteristics of the interface which is formed. It is suggested that at the sintering temperature used the interface developed between fibres and matrix (even when chemical compatibility exists) does not approaches that of particles grown in situ, a fact which influences the moving crack front as it arrives at some discontinuity resulting in a disturbed fracture path.

Although continuous fibre-composites present higher mechanical characteristics than short fibre-composites, it is generally admitted [e.g 356] that the use of short fibre reinforced composites will reduce manufacturing costs, a fact which is necessary for mass market production and further research is necessary on aspects such as the critical fibre length for load transfer, the interface effect on load transfer and the role of short fibres as crack stoppers.

As expected the acoustic activity of composites is mainly due to fibres and is much higher than those of matrix ceramics e.g. in a 14% α-Al_2O_3 kaolin composite 90% of AE activity is due to fibre content. Activity increases with increase in fibre content and for similar fibre contents is higher with thinner fibres. They have also higher event rates and show the Kaiser effect. Repeated loading not only shows the Kaiser effect but also a change in the event rate and a gradual decrease in the maximum event rate. This behaviour is connected to the fact that no acoustic activity is observed during unloading (it is also not observed in ceramics), indicating that the sub-critical activity is not a reversible process. It also indicates that fibre fracture and fibre pull out produce high energy burst events while matrix fracture produces continuous AE events.

Dalgleish et al.[144], measured the fracture toughness and acoustic emission of sintered alumina and alumina-zirconia composites, using SENB and 3-point bending MOR specimens and interpreted their results in connection with microstructure. They indicated that good mechanical properties in single phase alumina were due to small grain size, high density and rounded pores. AE activity was connected with sub-critical crack growth and was found to be higher with increased grain size porosity and impurity percentage. It is worth mentioning that they did not find acoustic emission resulting from the production of the critical flaw in the MOR test of aluminas and they concluded that the unit step in the linkage process during sub-critical growth in these tests is smaller compared to that during SENB tests and consequently energy release is below the detection noise level of the equipment.

They also found that all alumina-zirconia composites were more acoustically active compared with aluminas and that increase of zirconia to an optimum of 12%

volume, reduced K_{IC} values as a result of linking of the micro-cracks, as Claussen also indicated [364]. However in all composites K_{IC} values were higher than that in aluminas, a fact which was considered to be as a result of the higher energy absorbed in opening up micro-cracks in the process-zone and in crack-branching during loading as SEM examination revealed.

Considering the composite properties of the examined systems in the present work, it can be assumed that they depend mainly on:

a. The development of a chemical bond between matrix and fibres when chemical compatibility allows for this.

b. The development of a mechanical bond determined by differences in thermal expansion coefficients of the fibres and the matrix.

c. The interlocking or keying effect of the matrix with possible irregularities in the surface of the fibres.

d. The presence of cracking in the matrix, due probably to thermal mismatch between fibres and matrix could also affect the mechanical properties of the composite.

e. The presence of large voids (cavities) which results when a 3D network of agglomerated fibres is formed.

Improvement of strength can be related with (a),(b) and (c) and decrease with (d) and (e).

For reliable ceramic materials to be produced two main parameters must be controlled: flaw characteristics (size and density) and toughening. Flaw size and density can be controlled by careful fabrication and development of new fabrication techniques. Toughening can be achieved by incorporating fibres or a second phase or

changes in the microstructure in a way which will disturb crack propagation (fig.4).

The addition of fibres to kaolin matrix has a different effect from that of particles grown in situ (like mullite needles) during sintering. SEM examination shows that although mullite formation continues to higher temperatures, its formation does not improve strength and mullite crystals grown in situ do not divert the crack front and do not have a reinforcing effect. This supports the hypothesis that the improvement of mechanical properties in kaolins is due to glass formation and is little affected by mullite formation.

According to general fracture equation (eq.29), the strength of ceramics and fibre-ceramic composites can be improved by influencing toughness and flaw sizes. Low toughness and large defects result in low strength. As an example, alumina, a well investigated ceramic has a theoretical tensile strength value of about 46 GPa [361], but in practice no more than 0.5 GPa can be achieved by conventional powder processing as a result of large defects (50-100 μm) trapped during powder compaction. In a similar way addition of fibres in composite systems is expected to improve strength characteristics and can be explained also with the fracture equation. Decrease of flaw sizes, e.g. by improving processing, or increase of toughness by introduction of fibres or adding another phase improve strength. Crack deflection in fibres composites or additions (e.g. of transformable zirconia) improves toughness. Alford et al [169], produced high strength ceramics by colloidal control to remove defects,(commercial alumina powder improved from 0.37 to 1.04 GPa).

5.6.3 APPLICABILITY OF LEFM TO COARSE-GRAINED CERAMICS AND COMPOSITES

Brittle materials fail under stress with no yielding or plastic deformation and phenomenological analysis through LEFM is used to examine the fracture results.

The deterministic approach of brittle fracture is based on the Griffith's flaw theory and the principles of LEFM, which assumes the presence of cracks of specified sizes, shapes and orientations, and attribute fracture to propagation of the least favourably orientated crack. The fracture-determining "inherent flaws" have generally the character of cracks in an elastic body, but cannot generally be detected by conventional methods and can only be assumed from the variation in strength of nominally identical specimens and the "size effect", which is the decrease of average strength as the size of geometrically similar specimens is increased. However this deterministic approach cannot describe sufficiently the size effect observed in smooth bar tests and stress concentrations in rounded notches [238].

In accordance with LEFM fracture surface energy increases with grain size and strength is generally assumed to be proportional to the square root of fracture energy. This suggests higher strengths for polycrystalline materials than for single crystals, which is not the case in practice where single crystals are stronger than polycrystals for which strength increases with decreasing grain size.

In the present work, the work of fracture (W_f) of kaolin, pottery mixture and brick clay show a steady increase with structure development, leveling out at higher temperatures where the structure has been almost completely developed. Comparison of the powder ceramics shows that the finer pottery mixture ceramics give higher

fracture energies. The absence of slip or twinning in ceramics near room temperature when they are stressed makes them more dependent on grain boundary fracture mechanisms and the effects of local inhomogeneity and anisotropy than metals where multiple slip is the primary mechanism for stress relief and energy absorption. The high fracture energy in polycrystalline ceramics must originate in the complexity of the local grain boundary network and in the tortuous path which a crack must follow.

In the case of kaolin fibre-composites studied in this work, fracture energies are higher compared to that of kaolin ceramics sintered at the same temperature, due probably to crack deflection by interfaces and fibre pull out in which the fibre-matrix shear strength is maintained during pull out. In some cases (e.g. 4.7% α-Al_2O_3 kaolin composite sintered at 1300°C or 4.5% Saffil fibre composite sintered at 1300°C) four times higher fracture energies have been measured.

As Evans and Tappin indicated [139], in many cases fracture occurs by flaw linking and not by extension by an isolated flaw, which makes questionable the use of fracture mechanics . They also underlined that the use of semi-empirical strength relationships often leads to misleading conclusions.

Maji and Shah [363], examining concrete specimens in tension indicated that when the fracture process zone is significant a straightforward application of classical linear elastic fracture mechanics (LEFM) may not be applicable and modification must be used.

Buresch [142], examining the influence of microstructure and geometrical factors on the stress state and the fracture toughness of ceramics, indicated that the fracture toughness is controlled by micromechanical features which occur by microcracking in the process zone (of size for most ceramics in the range of 0.1-

1mm) during stress redistribution.

With respect to the Griffith elastic crack length c_E, it is clear that in the polyphase polycrystalline coarse grained ceramics examined in this work, there are no observable features that can be related to it. The c_E values were always much larger and extensive flaw linking for crack extension must take place before fracture. In the case of brick-clay, the presence of sand particles are considered responsible for the higher c_E values.

In uniformly grained materials c_E has been successfully correlated with the grain size [134]. For example examination on alumina and silicon nitride [114], showed that with the presence of large crystals there was reasonable agreement between the calculated value of c_E and the crystal size.

In the polyphase clay ceramics examined in this work, c_E values were much greater than any observable feature of the structure which suggests that c_E has a meaning only if extensive flaw linking is assumed. However, c_E values should follow structure changes and be influenced by the presence of sand particles.

The above observations are in agreement with Alderson's [134] research on fine grained clay ceramics where c_E was several times larger than any observable fracture surface feature (he found a c_E of about 100 μm which was larger than any observable feature), suggesting that extensive connection between adjacent flaws or linking together of pores must take place before fracture.

The value of c_E as calculated from σ_f and K_{IC} tests, could be considered as the minimum crack length to result in catastrophic fracture. Unfortunately the size of the equivalent elastic crack length is only a few hundred microns and it is not possible to detect it by the usual inspection methods. In reality, there is no evidence that a

crack with this length (c_E) ever existed prior to fracture. Similarly, Harris et al [105], underlined that research in carbon fibre reinforced epoxy or polyester composites showed that for all composites c_E had the rather unlikely value of 1mm. They concluded that the presence of fibres and interfaces introduce heterogeneity and anisotropy which makes the application of LEFM to composites unsuitable.

The fundamental energy relations of fracture mechanics are based on linear elastic behaviour of homogeneous and isotropic materials having a continuum structure. Theoretically, brittle materials are considered as brittle elastic continuums and their fracture is treated by using Inglis equations (2.2.5), or approached on energy grounds and treated by Griffith equations (2.2.6.1). Griffith, the father of LEFM, proposed an equation relating strength, modulus of elasticity and surface energy and made independent measurements in glass specimens and estimating the value of elastic crack length. While these relations and principles appear to apply in materials like glass and fine-grained polycrystalline ceramics where typical flaws have dimensions much greater than ceramic microstructure, inconsistencies arise when they apply to coarser polycrystalline ceramics, where the size of the strength controlling flaws is probably similar to that of the grains themselves. As an example, in coarse grained ceramics grain boundaries will give rise to larger flaws and lower values of γ. Griffith probably succeeded with his equation because he worked with glass, a non-porous amorphous material which is probably the nearest approach to a continuum available in real materials, and fractures with a very smooth surface (virtually without AE sub-critical activity) allowing estimation of the formed surface area and where thermodynamic surface energy is equal to the total energy released during fracture. However, even in this case, work of fracture measurements on glass

show different values from that of Griffith's (Table 8).

LEFM applies in cases of fracture where there is a well defined defect and empirical statistical functions can apply to particular sets of data. Both the above considerations do not take into account the effect of microstructural features (sub-critical activity) on fracture mechanism. SEM examination in the present work shows that brittle ceramic materials do not fail by developing a zone of plastic flow (like metals) but they fracture by flaw linking in a series of discrete steps as the stress is increased till a critical value.

Davidge [135] indicated that although LEFM is used for a wide range of materials, the complexity of fracture processes probably changes in different brittle materials like glass, ceramics, cement etc. and in practice surface energy or K_{IC} is rarely a material constant dependent on specimen geometry. Evans and Tappin [139] indicated that catastrophic failure occurs with linking of existing flaws a fact which makes the application of LEFM to alumina ceramics insufficient. According to Cooke [143], toughness is controlled by the statistical distribution of microcracks in the process zone in front of the crack tips.

Dalgleish et al [144] indicated that AE from MOR specimens is due to linkage of flaws, while AE from K_{IC} specimens is due to sub-critical crack growth of pre-existing cracks.

Cooke [154] showed that fine grained materials (1 μm particle size) fail as result of a single flaw propagation, while coarse grained ceramics show significant sub-critical activity before they fail. In heterogeneous materials the non-linearity of the transfer of load to crack tip (non-uniform elastic field) adds further difficulties in the application of LEFM. Furthermore for critical strain of about 1 millistrain

[117], the difference in critical flaw size gives a scaling factor of the homogeneity of the microstructures.

The presence of a number of structural features like pores, second phase particles, large grains etc probably restrict application of LEFM to coarse structured ceramics.

Unfortunately, direct measurements of tensile strength, work of fracture and E, are not possible for most of the cases of ceramics and composites and indirect methods for γ calculation must be used. The coarse non uniform structures of polyphase clay ceramics and composites used in this work, do not permit experimental justification of Griffith's relation by the direct approach and the different concequences achieved from different formulations would require separate justification each time. The value of γ in ceramics is usually determined using the expression $\gamma=K^2_{IC}/2E$. Davidge [176] indicated that the most usual approach is to examine fracture origins for K_{IC} and σ_f specimens and, if no differences are apparent, the stress situation were considered similar and the above formula is valid. Examination of the SEM micrographs for the fracture origins in MOR and K_{IC} specimens did not show any difference so the above formula can be used.

It is suggested that fracture in both types of specimens starts with a period of random crack growth but variations of ultimate fracture stress results because of many alternative growth paths.

5.6.4 STATISTICS

In addition brittle fracture can be analysed statistically. This method uses, the empirical (in nature) Weibull function which is based on the weakest link theory (WLT) where the fracture is attributed to the weakest flaw when the local stress reaches the critical fracture value.

The high sub-critical activity of coarse-grained ceramics and composites indicated by AE events counting, implies that their strength could be predicted by examining flaw development and then evaluating their failure probability. Indeed, statistical analysis of AE events, happening in an array of adjacent grains able to form a crack or to extend an internal flaw subcritically, shows that they follow an almost ideal Weibull function which indicates that activity from microstructurally dependent flaws in the process zone [142,143] may control strength. Furthermore Cooke [156] indicated that in order to predict the mechanical behaviour of coarse polyphase ceramics a distinction must be made between the microscopic fracture events that occur subcritically and those that occur during macroscopic crack propagation during the failure process.

The present work has shown that simple estimators and a minimum number of thirty specimens are needed for statistical analysis. The so-called Weibull modulus (the shape parameter of Weibull function), no matter what it expresses, since there is no real connection to features in the structure, seems to be relatively constant in a ceramic irrespectively of sintering temperature. Similar comments could be made also for shape parameter in the Neville function.

Comparison of results from Weibull and Neville functions which are both based on WTL theory, using correlation coefficients shows that neither can be applied with absolute success, since best fit can be achieved from either in different cases. Moreover testing with the simple log-normal function shows that this function (and possibly many others) can be used.

The Weibull approach has some important limitations that restrict its ability to predict the failure of large components with complex geometries and subjected to multiaxial stress. The main criticism is the lack of incorporation of a physical description of the fracture initiating flaws. The Neville function, taking into account the stress and strain conditions near the crack tip , has a physical basis but needs further development. Application of these functions to composites where change and interaction of flaws is highly probable and where extensive subcritical activity is recorded is questionable. Analysis of the behaviour of both ceramics and composites with the two functions (showing similar trends) and the comparison of correlation coefficients from ceramic and composites (showing similar values) is another indication that probably neither are solutions to the statistical problem of brittle fracture.

Since ceramics are brittle by their nature, the influence of internal or surface flaws (in the form of pores, cracks or microcracks) on their mechanical characteristics is very important. Microcracks can have negative of positive influence on stress intensity at the tip of the macrocrack depending upon their position. Although density and porosity play an important role on ceramic strength and toughness, the alteration of fracture path by influencing the stress field is more important. An inhibition of the critical crack growth could result from different orientations of grains to the load

direction. If some orientations can carry more load, the stress distribution ahead of the crack tip will be significantly altered. Furthermore, initiation of grain boundary microcracks ahead of the primary crack can easily occur because of anomalies of the stress field. The final result could be a more complicated crack path because of secondary cracking and high apparent fracture energy.

The density of microcracks in most cases is high and microcrack interaction in notched macrocracked specimens may influence the process zone or generally the fracture path in the case of fracture of un-notched specimens. However in most of the published work on statistical analysis of fracture this interaction has been ignored (e.g. 186,207) or has been analysed in a rather complex way (e.g. 358, 359,360), where other assumptions may still lead to erroneous results.

An interesting alternative to WLT was proposed by Glucklich [164], who hypothesized that so many possible crack paths exist, that offset the random nature of the original initiation, so that WLT statistics apply only for crack initiation and not for the whole fracture. He suggested that WLT is a limiting case and applies when initiation and final fracture coincide. Alderson [134], analysing his results from coarse clay mixtures, indicated that Glucklich's theory applies when a three point bending rig is used which reduces the area under stress.

Any probabilistic approach will have certain limitations, the most important of which are the following:

a. When more than one flaw population exists, the use of statistics based in one flaw population may be erroneous.

b. The flaw population in a structure may be modified during use (during application of stress).

c. In practice the stress state may be multiaxial, while most of the testing conditions deal with uniaxial stress conditions.

d. In some cases the number of tests is not adequate for safe determination of the Weibull modulus or any other parameter of other functions.

e. The use of Weibull's, Neville's or other functions may not characterise the fracture statistics of a certain ceramic structure.

The real effort must be to develop a theoretically based function with as few parameters as possible, because the use of many parameters may give better fits only because of the number of the parameters, even when there is no theoretical justification.

CHAPTER 6. CONCLUSIONS AND SUGGESTIONS FOR FURTHER WORK

A number of conclusions can be made considering all the results of the research:

a. Sintering in clay ceramics and fibre-composites changes the microstructure from point-bonded with low mechanical properties to a glass-ceramic dense microstructure whose composition depends on the original composition of the clay and that of fibres with higher mechanical properties. As an example point-bonded structures, where there is no glass formation (e.g. kaolin sintered at 1000°C, pottery mixture at 900°C and brick-clay sintered at 900°C and 1000°C), have low values of E (around 2-5 GPa) MOR (around 7-10 MPa) and K_{IC} (around 0.2-0.35 MPa.$m^{1/2}$).

Structures where glass formation started but was not enough to produce a strong network (e.g. kaolin sintered at 1100 °C pottery mixture sintered at 1000°C) and well developed glass-bonded structures with large flaws like sand particles present (e.g. brick-clays sintered at 1100°C) which act as sites of fracture initiation, have medium values of E (around 10-20 GPa), MOR (around 15-20 MPa) and K_{IC} (0.4-0.7 MPa.$m^{1/2}$). Well-developed glass-bonded structures without major flaws (e.g. kaolin sintered at 1200°C and 1300°C or pottery mixture sintered at 1100°C) have relatively high E (around 30-40 GPa), MOR (35-40 MPa) and K_{IC} (0.7-0.9 MPa.$m^{1/2}$) values. Kaolin structures sintered at 1400°C reach their maximum properties, while pottery mixture specimens attain their optimum properties after sintering at 1150°C. Generally, kaolin and pottery mixture have similar structures after sintering at temperatures differing by about 200°C. The brick-clays show an increase up to

1150°C but any further temperature increase results in melting. Kaolin and pottery specimens sintered at temperatures higher than the optima show reduced properties as a result of increased porosity and bloating.

The addition of fibres to ceramic results in the formation of a CMC, the properties of which depend on the matrix and fibre structure and relative volumes, the fibre-matrix interface and the length of the fibres. Oxide fibres form a strong interface with kaolin matrix since there is a chemical compatibility between fibres and matrix which increases strength by crack deflection, while graphite fibres a weak interface which increases the strength by fibre debonding and bridging. The fibre length should be greater than a critical value in order to carry the full applied load.

b. A major problem in short fibre CMCs is the increase of porosity. Relative increase of strength and toughness with incorporation of fibres is achieved with limited additions of fibres and mainly in weak point bonded structures. The short random oriented fibres form in all cases three dimensional agglomerated clusters of fibres which induce porosity and decrease density of composites. The overall result in most cases is the decrease in strength of composites. Generally the thinner the fibres the higher porosity. Development of production methods which reduce porosity probably will result in increase of strength.

c. Development of reliable ceramics and composites can be achieved by flaw size and density reduction controlled by development of new fabrication methods and toughening by incorporation of fibres or second phases.

d. Large particles (e.g. sand particles) or major flaws (e.g porosity) can initiate catastrophic failure giving rise to low strength values. These flaws do not

necessarily influence microstructure as a whole since K_{IC} remains relatively high. Strength (MOR), toughness (K_{IC}), modulus of elasticity (E) and work of fracture (W_f) are material properties in coarse polyphase heterogeneous ceramics and composites, where there are large grains and internal flaws. In most cases strength and toughness change in a parallel way. Sand particles in brick-clay ceramics influence strength more than toughness.

e. The fundamental energy relations of fracture mechanics are based on linear elastic behaviour of homogeneous and isotropic materials.

Inconsistencies arise when these relations are applied to polycrystalline ceramics and CMCs. Application of LEFM to the examined ceramics and composites shows that the calculated equivalent elastic crack length c_E, is many times more than any observable feature in the fractured surfaces. This indicates that before catastrophic failure flaw linking takes place until a critical value is reached. On the other hand evaluation of the LEFM parameters K_{IC} and W_f depend on the specimen size giving usually incompatible results, a fact which minimizes the utility of fracture toughness as material parameter. Additionally the large specimens needed for valid K_{IC} values cannot always be fabricated. Although fracture mechanics is a recognized tool for characterising toughness of homogeneous materials, its application to the examined ceramics and CMCs, where heterogeneity and anisotropy is added and where non-uniform elastic fields exist, add further difficulties in application of LEFM and probably preclude the practical application of it or at least the neccessity of modification.

f. The statistical approaches to brittle fracture (Weibull or Neville) have cerain limitations although they give values of modulus which may be used as a reference.

Weibull analysis is a pure statistical method having no physical meaning and relation to microstructure, while Neville's function, although having a physical basis, needs further development. However, it is questionable if there is a universal statistical function and the best treatment may not be to treat all ceramics in the same way, since there is such a wide range of ceramic materials (e.g. glasses which are the nearest elastic continuums in real materials and where flaws are mainly of the surface, cements which have different thermal history in producing a dense structure, heterogeneous ceramics which have internal flaws larger or equivalent to structure grains and composites which have a changing flaw population and flaw interaction etc.).

g. Acoustic emission testing in ceramics shows that acoustic activity increases with strength and with fibre addition so that for the same matrix microstructure fibres produce about 90% of the AE activity. Since brittle materials do not fail by developing a plastic zone but by flaw linking in a series of steps the measured acoustic activity could be attributed to flaw linking. AE testing is a valuable tool, which can distinguish matrix cracking from fibre cracking and could further be used in research on prediction of mechanical behaviour of ceramics and CMCs. AE counts seem to follow a statistical distribution. Further development of the AE technique could distinguish the microscopic subcritically occurring AE events from those occurring during the macroscopic crack propagation.

Further research should be addressed to investigation of other fine-grained and coarse grained ceramics and fibre composites with aims similar to the present thesis. The development of ceramics and composites following different production methods (e.g. isostatic pressing, sol-gel methods etc.) with a controllable flaw size and

density of flaws and also a minimum porosity and a controlled directionality will probably result in improved ceramics and short-fibre CMCs. Improvement of AE techniques will also assist further research in brittle fracture and also research on the relation of AE events to fabrication methods.

Structural ceramics could also be used as starting materials for production and investigation of the so called advanced ceramics through reduction-oxidation reactions.

As was mentioned in the literature review on CMCs and fibres (2.1.2.1), the majority of information concerned aligned long fibres and that much of it was found in the form of patents or proprietary methods and thus is not referenced in the usual sources. More research is necessary for theoretical development of strength distribution is short random oriented CMCs.

Finally the use of other testing techniques, such as indentation toughness and comparison between methods could probably aid research on the mechanical properties of ceramics and CMCs.

Research on statistics of mechanical properties of ceramics and CMCs could be done after their division in groups having similar characteristics. The statistical analysis of AE could probably indicate the existence or not of different flaw populations and their effect on structure.

REFERENCES

1. Worrall W.E,(1982),"Ceramic Raw Materials", 2nd ed.,Pergamon Press,Oxford.
2. Higgins I. and Hendry A., (1986), Br.Ceram.Proc.,37,pp.163-178.
3. Higgins I. and Hendry A., (1986), Br.Ceram.Trans.J.,85,pp 161-166.
4. Pask J.A. and Tomsia A.P., (1991), J.Am.Ceram.Soc., 4,10, pp.2367-2373.
5. Kingery W.D., Bowen H.K., and Uhlman D.R.,(1975). "Introduction to Ceramics", p.77, J.Wiley & Sons, N.York.
6. Majumbar A.J, Welch J.H.,(1963), Trans.Brit. Cer.Soc., 62,p. 603.
7. Aksay I.A., Pask J.A.,(1974),Science,183,p.69.
8. Ghate B.B., Haselman P.D.H. & Spriggs R.M.,(1973), Bull. Am.Ceram.Soc., 52,p 670.
9. Nurishi Y., Pask J.A.,(1982), Ceram.Int.,8,p 57.
10. Khalil A.A.A., El-Korashy S.A.,(1989), Ceram.Inter.,15, pp 297-303.
11. Peters T. and Iberg R., (1978), Amer.Ceram.Soc.Bull, 57, p. 503.
12. Hamano K., Lee E.S.,(1972), Bull.Tokyo Inst.Tech., 108, p95.
13. MacKenzie K.J.D., Brown I.W.M, Meinhold R.H.& Bowden M.E.,(1985), J.Am.ceram.Soc., 68,6, pp.293-97.
14. Brown I.W.M., MacKenzie K.J.D., Bowden W.E.& Meinhold R.H., (1985), J.Am.Ceram.Soc.,68,6,pp.298-301.
15. Chakravorty A.K., Ghosh D.K.& Kundu P.,(1986) J.Am.Ceram.Soc., 69, 8, C-pp200-201.
16. Mazumdar S., Mukherjee B.,(1986), J.Am.Ceram.Soc,69,8,C-p.201.
17. Chakravorty A.K., Ghosh D.K.,(1986),J.Am.Ceram.Soc.,69,8,C-pp202-203.

18. Komarneni S., Roy R.,(1986), J. Am. Ceram.Soc., 69,[8],C-p204.

19. Brindley G.W, Nakahira M.,(1959)J.Am.Ceram.Soc.,42[7], pp.319-24.

20. Leonard A.J.,(1977), J.Am.Ceram.Soc.,[60],(1-2),p. 37.

21. Defrancesco F.,Tomasi A., Soraru G.D., J.Mat.Sci,(1987),22,pp. 2493-2496.

22. Chakraborty A.K.,Ghosh D.K., (1978), J.Am.Ceram.Soc.,61,3-4, pp.170-173.

23. Brown I.W.M.,Mackenzie K.J.D.,Bowden M.E. & Meinhold R.H., (1985) , J.Am.Ceram.Soc.,68,6,pp.298-301.

24. Okada K.,(1987),J.Am.Ceram.Soc.,70 [9] C-p223-C-p224.

25. Chakraborty A.K., Ghosh D.K.,(1989) J.Am.Ceram.Soc.,72,[8], pp.1569-70.

26. Bain J.A, Morgan D.J.,(1969), Clay Miner.,[8]2,p.175.

27. Richardson H.M, Wilde F.G.,(1952),,Trans.Br.Cer.Soc., 51,p.387.

28. Sequit E.K.& Anderson C.A.,(1971),Am.Cer.Soc.Bull,50,5,p.480-83.

29. Percival H.J.& Duncan J.F.,(1974), J.Am.Cer.Soc., 57, 2, p.57.

30. Chakraborty A.K.,(1979),J.Am.Ceram.Soc.,62[3-4], pp.120-24.

31. Glass H.D.,(1954), Am.Mineralogist,39,p. 193.

32. Roy R., Roy D.M.,Francis E.E,(1955), J.Am.Cer.Soc.,38,6, p.198.

33. Comer J.J.,(1960), J.Am.Cer.Soc.,43,7, p.378.

34. Comer J.J.,(1961), J.Am.Cer.Soc.,44,1,p. 20.

35. Rue J.W. and Ott W.R.,(1974), J.Thermal Anal.,6,p. 513-519.

36. Lach V., (1974), Interceram.,1, p 27.

37. Bulens M, Leonard A.J., and Delmon B., (1978), J.Am. Ceram. Soc, 61[1-2],pp.81-84.

38. Hoffman D.W.,Roy R.and Komorneni S.,(1984) J.Am. Ceram. Soc.,67[7], pp. 468-71.

39. MacKenzie K.J.D., Brown I.W.M.,(1987),J.Am.Ceram.Soc., 70 [9] C-p222-C-p223.

40. Okada K.,Otsuka N.& Ossaka J.,(1986),J.Am Ceram.Soc. 69 [10] C-p251-C-p.253.

41. Okada K.,Otsuka N.,(1986), J.Am.Ceram.Soc.,69[9],pp. 652-56.

42. Sonuparlak B.,Sarikaya M.& Aksay I.A.(1987) J.Am. Ceram.Soc.,70 [11],p.837-42.

43. Sanz J., Madani A.& Serratosa J.M.,(1988), J.Am.Ceram.Soc, 71[10], C-p418-C-p421.

44. Chakraborty A.K.and Ghosh D.K.,(1988), J.Am. Ceram.Soc., 71,[11], pp.978-87.

45. Serrano J.,Bastida J.,Amigo J.M.,Sanz A. and Caballero A.,(1993), 3rd Euro-Ceramics,1, pp. 161-168.

46. Mackenzie R.C,(editor),(1972),"Differential thermal analysis" Vol.2, Academic Press,London.

47. Smykatz-Kloss,W.,(1974),"Differential Thermal Analysis" Applications and results in mineralogy, Minerals and Rocks, Springer-Verlag,Berlin,N.York .

48. MacKenzie,R.C,(1957),"The Differential Thermal Investigation of Clays ", Mineralogical Soc., London.

49. Garn P.D.,(1965),"Thermoanalytical Methods of Investigation", Academic press, N.York.

50. Wendlandt,W.W,(1974),"Thermal methods of analysis", J.Wiley & Sons, N.York.

51. Earnest C.M.(1988)"Compositional Analysis by Thermogravimetry, ASTM 997,p.273.

52. Chmielecki W., Monko B.& Szymanski A.,(1974),Proc.4th ICTA, Budapest, Thermal Analysis,Vol 3,p.679.

53. Evans A.G.,(1970), Proc.Br.Cor.Cer.Soc.,15,10,p.113.

54. Diamont S.,(1984), Cem.Concr.Res.,14, p.459.

55. Manz O.E.,(1984), Cem.Concr.Res.,14,pp. 513-520.

56. Mehta,P.K.,(1985), Cem.Concr.Res.,15, pp.669-674.

57. Matthews Y.E.& Nathan Y.,(1988),Cem.Concr.Res.,18, pp.503-512.

58. Diamond S.,(1986), Cem.Concr.Res.,16,pp 569-579.

59. Valenti G.L. and Cioffi R.,(1988), Cem.Concr.Res.,18,pp.91-102.

60. Gibergues A.C. and Aitcin P.C.,(1986), Mat.Res.Soc.Symp. Proc.,vol 65, p.161, Materials Research Society.

61. Turner C.W.,(1984), Cem.Concr.Res.,14,pp. 513-20.

62. Snel A., " Fly Ash utilization in the Netherlands, EPRI,2,1981.

63. Housing Sci. & Its Appl.,3,pp 431-463,1971.

64. Manz,O.E.,Cem.Concr.Res.,14,pp.513-520,1984

65. Day R.L.,Jochi R.C.,Slota R.J.,Langan B.W., Mat. Res. Soc.Proc., Vol 65, p.47,The Materials Res. Society, 1986.

66. Johnson D.D & Sowman H.G.,(1988), "Engineered Materials Handbook, Vol1 Composites, Ceramic fibers, p.60,ASM,Ohio, USA.

67. Warren R.,(ed),(1992),"Ceramic Matrix Composites",Blackie,Glasgow and London.

68. Watt W., Harris B., and Ham A.,(eds),(1980),("New Fibres and their Composites), Royal Society,London.

69. Hull D., (1982), " An Introduction to composite Materials", Cahn R.W, Thompson M.W. and Ward I.M.(Eds) , Cambridge Uni.Press.

70. Kelly A. and Rabotinov Y.N. (ser.erds), (1985),"Handbook of composites, Vol.1-Strong Fibres (Vol.ed. Watt W. and Perov B.V.), p.117 North-Holland, Amsterdam.

71. Harris B.,(1986)," Engineering Composite Materials",The Institute of Metals, A.P.C., USA.

72. Schioler L.J. and Stiglich J.J.Jr.,(1986),Cer.Bull,65,2, pp. 289-292.

73. Evans A.G. and Marshall B.D.,(1990),"Fiber Reinforced Ceramic Composites", Mazdiyasni K.S. (ed), Noyes Pub.,N.Jersey.

74. Khorami J.,Lemieux A.,Dunnigan J. and Nadeau D.,(1987) Thermochimica Acta, 120, p.1-7.

75. Young J.,Rea M.S. and Briggs G., (1989), Br.Ceram.Trans.J.,88, pp.58-62

76. Bunsell A.R.(ed.), (1988), "Composite Materials Series Vol. 2"-Fibre Reinforcement for composite Materials", p.429 ,Elvevier.

77. Dinwoodie J., Moore E., Langman C.A.J. and Symes .R.,(1985), Proc. 5th Int. Conf.Composites,ICCM, pp. 671- 685, AIME , N.Y.

78. Clyne T.W.,Bader M.G.,Cappleman G.R.& Hubert P.A. (1985), J.Mat.Sci.,20, pp.85-96.

79. Dinwoodie J.,(1987),SAE Tech.Paper series 870437, Int.Congress and Expo., Detroit,Mich.USA.

80. Datasheet on RF Saffil,(1982)ICI Mond Division,Runcorn, Cheshire, U.K.

81. Kelly A.(ed),(1989),"Concise Encyclodedia of Composite Materials", Pergamon Press,Oxford.

82. Phillips D.C.,(1983),"Handbook of Composites, Vol.4,Fabrication of Composites, Chap.VII:Fibre Reinforced Ceramics",pp.373-428,Kelly A.& Mileiko S.T.(eds), Elsevier Sci.Pubs.

83. Aveston J.,(1971),Proc.Conf.Prop.Fibre Composites, IPC Sci.& Tech.Press Ltd., Guildford.

84. Donald I.W. & McMillan P.W.,(1976), J.Mat.Sci.,11,pp. 949-72.

85. Sambell R.A.J.,Bowen D.H.& Phillips D.C.,(1972), J.Mat.Sci,7, pp. 663-675.

86. Sambell R.A.J.,(1972),J.Mat.Sci.,7,p. 663-675.

87. Prewo K.M. and Brennan J.J.,(1982), J.Mat.Sci.,17,p. 1201.

88. Wei G.C. and Becher P.F.,(1985), Amer.Ceram.Soc.Bull.,64, p. 298.

89. Petrovic J.J., Milewski J.V., Rohr D.L.and Gac F.D. (1985), J.Mat.Sci., 20, pp. 1167-1177.

90. Phillips D.C.,Sambell R.A.J. and Bowen D.H.,(1972),J.Mater. Sci.,7, p.1454.

91. Sambell R.A., Phillips D.C. and Bowen D.H., Harwell Report AERE-R-7612, Feb. 1974.

92. Alexander H.& Haasen, (1972), Ann.Rev.Mat.Sci.,2, p. 291.

93. Hasselman D.P.H. & Fulrath R.M.,(1966), J.Am.Cer.Soc.,49, p.68.

94. Nivas Y. & Fulrath R.M.,(1970), J.Am.Cer.Soc.,53, p.188.

95. Flajsman F.,Cahn D.S. & Phillips J.C.,(1971), J.Am.Cer.Soc.,54,p.129.

96. Phillips D.C., (1975), J.Mat Sci, 7, pp. 1175-1191.

97. Rice R.W. & Freiman S.W.,(1976),Proc.6th Inter.Mat.Sypm. on Ceramic Microstructures, J. Wiley and Sons.

98. Sheldon D.A.& Lewis D.,(1976), J.Am.Cer.Soc.,59,7-8,372-375.

99. Wang J., Piramoon M.R., Ponton C.B. and Marquis P.M.(1991), Br. Ceram. Trans. J.,90, pp. 195-110.

100. Maschio S. and Lucchini E., (1992) , Cer.Acta, 4, pp. 27-34.

101. Ruh R., Mazdiyasni K.S. & Mendiratta M.G.,(1988), J.Am. Ceram. SOc.,71,6, pp. 503-12.

102. Samanta S.C. and Musikant S., (1985), Proc.Ceram.Eng.Sci., 6, 7-8, pp. 663-672.

103. Mashima M., Mise T., and Okada K., (1982), Proc. 4th Int. Conf.Mat.,ICCM-IV, Japan Soc.Comp.Mat.,North-Holland,vol.2, p. 1203.

104. Pabst R.F.,(1986), "Brittle Matrix Composites 1" Brandt A.M. and Marshall I.H.,(eds),Elsevier, London. pp. 109-129.

105. Harris B.,Dorey S.E. & Cooke R.G.,(1988) Composites Science and Technology, 31,p121-141.

106. Habib F.A.,Cooke R.G. and Harris B., (1990),Br.Ceram.Trans.J.,89, pp.115-124.

107. Nemets I.I, Zlatkovskii V.B., Bel"maz N.S.& Trubitsyn N.A.,(1988), Steklo i Keramika,11,pp16-18,Translated I.A.Grishmanov BTISM, (1989), Plenum Pub. co.

108. Knott J.F.,"Fundamentals of Fracture Mechanics",(1973), Butterworths, London.

109. Broek D." Elementary Engineering Fracture mechanics ",(1986), 4th ed., Martinus Nijhoff, The Hague,The Netherlands.

110. Ewalds H.L. & Wanhill R.J.H.,(1986),"Fracture Mechanics",3rd ed.,E. Arnold Ltd, London.

111. Davidge R.W.,(1979),"Mechanical behaviour of ceramics" Cambridge Uni.Press, Oxford.

112. Orowan E., (1949),Rep.Prog.Phys.,12,p. 185.

113. Kirchner H.P.,(1979)," Strengthening of Ceramics", M.Dekker Inc, N.York.

114. Kirchener H.P.,Gruver R.M. and Sotter W.A.,(1976), Mat.Sci. and Eng.,22, p 147.

115. Romualdi J.P.,(1974),Mat.Sci.Engineering,15,p31.

116. Jayatilaka A.de S., (1979),"Fracture of Engineering Brittle Materials",Applied Sci.Pub.Ltd,London.

117. Astbury N.F.,(1963),"Advances in Materials Research in the Nato Countries", p.369 ,Pergamon Press , London .

118."Fibre reinforced cement composites",The Concrete Society, Tech.Rep. 51.067, July 1973.

119. Courthey T.H.," Mechanical Behaviour of Materials" (1990), McGraw Hill, N.York.

120. Inglis C.E.,(1913),Trans.Inst.Nav.Archit.,55,p219.

121. Tetelman A.S ,Evans A.G.,(1973), Symposium on Fracture Mechanics of Ceramics ,Uni. of Pennsylvania, Vol II, p.895-924 .

122. Tetelman A.S.,McEvily,(1967),"Fracture of Structural Materials, Wiley, N.York.

123. Griffith A.A.,(1921),Phil.Trans.R.Soc.Lond, A221,p163.

124. Sack R.A.,(1946),Proc.Phys.Soc.,58,p. 729.

125. Kendall K., Alford N.McN. and Birchall J.D., (1987)," Advanced Structural Ceramics", Becher P.F.,Swain M.V. and Somiya S. (eds), Mat.Res.So., vol.78, N.York, pp. 189-197.

126. Paris P.C. and Sih G.C.,(1965), ASTM Spec.Tech.Bul.,No381,pp. 30-31.

127. Griffith A.A., (1924),Proc.First Int.Congress on Applied Mechanics (ed.C.B.Biezeno & J.M.Burgers) p.55 J.Waltman, Delft.

128. Hasselman D.P.H., Krohn D.A.,R.C.Bradt R.C. and Coppola J.A., (1973), Symposium on Fracture Mechanics of Ceramics,Uni. of Penn., Vol.II,pp749-754.

129. Irwin G.R.,(1948), Fracture of Metals ,ASM, Cleveland.

130. Davidge R.W., Evans A.G.,(1979),Mat.Sci.Eng,6,p.281.

131. Gilman J.J.,(1962),J.Appl.Phys.,27,p.1262.

132. Friedal J.,(1959)"Fracture",Chapman & Hall,London.

133. Clarke F.J.P., Tattersall H.G.& Tappin G.,(1966), Proc.Brit.Ceram.Soc., 6, p.163.

134. Alderson J.P.,(1977),"The Influence of Structure on the Fracture of Brittle Certamic Materials ,Ph.D.Thesis,Uni.of Bath.

135. Davidge R.W., Phil.Trans.R.Soc.Lond.,(1983), A 310, pp.113-125.

136. Ashby M.F. and Jones D.R.,(1986),"Engineering Materials 2", Pergamon Press, Oxford.

137. Pampuch R.,(1991),"Constitution and Properties of Ceramic Materials", Mat.Sci.Monographs, Elsevier.

138. Bansal G.K.,(1976), J.Am.Ceram.Soc.,59,1-2, p.87.

139. Evans A.G.,Tappin G.,(1972), Proc.Br.Cer.Soc.,20,4, pp. 275-297.

140. Claussen N., Pabst R.& Lahmann C.P.,(1975),Proc. Brit.Cer.Soc.,25, p.139.

141. Davidge R.W. and Tappin G.,(1970), Proc. Brit. Ceram. Soc.,15, p.47.

142. Buresch F.E., (1981), Advances in Fracture Research, ICF5, pp.2293-2301.

143. Cooke R.G.,(1982),Proc.Brit.Cer.Soc.,32, pp.171-180.

144. Dalgleish B.J.,Fakhr A.,Pratt P.L and Rawlings R.D.,Advances in Fracture Research ,(1981), ICF5, pp. 2031-2038.

145. Kerper M.J. & Scuderi T.G.,(1964), Am.Cer.Bul., 43,9,p. 622.

146. Noone M.J., Mehan R.L.,(1973),Symposium on Fracture Mechanics of Ceramics, Uni. of Pennsylvania,Vol.1, pp201-229.

147. Rice R.W.,(1977), "Treatise on Materials Science and Technology",vol 11,R.K. MacCrone ed,Academic Press,N.York.

148. Rice R.W., Freiman S.M, Pohanka S.M., Mecholsky J.J.Jr.& Wu C. Cm., (1978)," Symposium on Fracture Mechanics of Ceramics", Bradt R.C.et al eds, Uni.of Penn.,Vol IV, Plenum Press, N.Y., p. 849-876.

149. Evans A.G.,Linzer M.,(1973),J.Amer.Cer.Soc.,56,[11], pp.575-581.

150. Evans A.G.,Linzer M.& Russell L.R.,(1974),Mat Sci.Eng.15,p.253.

151. Dunegan H.L.,Harris D.O & Tatro C.A.,(1968), Eng.Fract. Mech.,1,p105-122.

152. Lloyd D.J.and Tangri K., (1975), Br.Cer. Soc.,25, pp 169-178.

153. Okada T and Sines G, (1983), J.Am.Cer.Soc., 66.

154. Cooke R.G.,(1981),Proc.5th Int.Conf.Fracture (ICF5), France, "Advances in Fracture Research",Vol 2,D.Francois Ed,pp. 1083-1089.

155. Kennedy P., (1979), UKAEA,Reactor Fuels Lab. Data Sheet.

156. Cooke R.G.,(1981),Proc.of 11 Inter.Conf.on Science of Ceramics,Vol II, Karlson R. & Karlson S. eds, pp.405-412.

157. Rice R.W. and Lewis D.III, (1973), "Sypm. on Fracture Mechanics of Ceramics" ,Vol 5,Bradt R.C et al.,eds, Uni of Penn. USA,p.659

158. Rice R.W., (1974), " Fracture Mechanics of Ceramics", Vol 1, R.C.Bradt et al eds, pp. 323-345, Plenum Press, N.Y.

159. Rice R.W. and Pohanka R.C., (1979), J.Am.Ceram. Soc, 62,11-12,pp.559-63.

160. Lange.F.F,(1973),Symposium on Fracture Mechanics of Ceramics, Uni of Pennsylvania, Vol II, p599-609.

161. Binns D.B.,(1962) ,Science of Ceramics, Ed. G. H. Steward, Vol.1,Academic Press, pp 315-335.

162. Davidge R.W.,and Green T.J., (1968), J.Mat.Sci,3, p.629.

163. Gupta T.K.,(1974), J.Mat.Sci, 9. pp 1585-89.

164. Glucklich J, (1970), J.P.L.Tech.Per. 32- 1438 , N.A.S.A.

165. Glucklich J. and Cohen L.J., (1967), Int.J.Frac.Mech.,3, p. 278.

166. Glucklich J.,(1963),J.Eng.Mech.Proc.,ASCE,89, p. 127.

167. Lange F.F., (1973), J.Amer.Cer.Soc., 56[9], pp.445-450.

168. Cox.H.L.,(1952),Br.J.Appl.Phys.,3,72-79.

169. Alford N.McN,Birchall J.D. and Kendall K., (1987),Nature, 330, pp.51-53.

170. Ashby M.F.and Jones D.R.H.,"Engineering Materials 2: An Introduction to Microstructures,Processing and Design", 1986, Pergamon Press, Oxford.

171. Duckworth W.H.,(1951),J.Am.Cer.Soc.,34,1,pp 1-7.

172. Bell D.A.,(1988),Br.Ceram.Trans.J.,87,pp33-38.

173. Bansal G.K.& Duckworth W.H.,(1979), ASTM STP 678, p. 38.

174. Nakayama J., J.Amer.Ceram.Soc.,(1965),48, p.583.

175. Tattersall H.G.and Tappin G.,(1966),J.Mat.Sci.,1, p.296-301.

176. Davidge R.W., (1969), Contemp.Physics,10,2, p.105.

177. Meredith H. and Pratt P.L., (1974), Spec. Cer.,6, p.107 pub. Br.Cer.Res.Ass.(1975).

178. Davidge R.W., and Tappin G., (1968), J.Mater.Sci., 3, pp.165-173.

179. Brown W.F.,Srawley J.R.,(1965),ASTM STP 381 and (1966) ASTM STP 410.

180. Graham L.J., Alers G.A.,(1973),Symposium on Fracture Mechanics of Ceramics,Uni. of Penhsylvania, Vol.1, p.175-188.

181. Spiegel M.R.,(1991),"Theory and Problems of Statistics",2nd ed., McGraw-Hill inc ,USA.

182. Neville D.J. and Knott J.F.,(1986), J.Mech.Phys.Solids,34,p. 256.

183. Davies D.G.S.,(1973),Proc.Brit.Ceram.Soc.,22, pp. 429-452.

184. Batdorf S.B.,(1974),J.Am.Cer.Soc.,57,1,pp 44-45.

185. Mihashi H. and Wittmann F.H.,(1980), in Hu X.Z.,Cotterell B. and Mai Y.W., (1985), Proc.R.Soc.Lond.A 401, pp.251-265.

186. Hu X.Z.,Cotterell B. and Mai Y.W.,(1985) Proc.R.Soc.Lond.A ,401, pp. 251-265.

187. Wittman F.H.,(1983)," Fracture mechanics of concrete" Elsevier, N.York, p.43

188. Lamon J.,(1988),J.Am.Ceram.Soc.,71[2],p.106-12.

189. McClintock F.A.,(1973),Symposium on Fracture Mechanics of Ceramics,Uni.of Pennsylvania,Vol.1,p93.

190. Evans A.G.,(1978),J.Am.Ceram.Soc.,61[7-8],p308.

191. Batdorf S.B., Crose J.G.,(1974),J.Appl.Mech., 41 , p.459-65.

192. Batdorf S.B., Heinisch W.L.,Jr.,(1978), J.Am.Ceram.Soc 61,[7-8], pp355-58.

193. Freudenthal A.M.,"Statistical Approach to Brittle Fracture.Fracture: An Advanced Treatise Vol.2: Mathematical Fundamentals ",(1968), Liebowitz H. (ed), Academic Press, pp.591-619.

194. Daniels H.E, (1945), Proc.R.Soc.Lond.A 183, p 405.

195. Jayatilaka A.De S. & Trustrum K.,(1977),J.Mat.Sci.,12, pp.1426-1430.

196. Weibull W.,(1939),Proc.Roy.Swedish Inst.Eng.Res. No 153.

197. Weibull W., (1951),J.Applied Mech.,18,p293-297.

198. Bury K.V.,"Statistical Models in Applied Science," J.Wiley & Sons USA, 1975.

199. Kapur K.C. and Lamperson L.R.,"Reliability in Engineering Design", (1977), J.Wiley & Sons, USA.

200. Kittl P. and Diaz G.,(1990)Eng.Frac.Mech.,36,5, pp. 749-762.

201. Pankow D.H., Finnie I.,(1979),ICM 3,Cambridge,England, Vol.3,pp. 67-76.

202. Phani K.K., Maitra A.K.,(1987),Mat.Sci.& Eng.,93,L5.

203. Pai S.S. and Gyekenyesi J.P., (1988), NASA Tech.Memorantum 100890, USA.

204. Neville D.J.,(1987), Eng. Fracture Mech.,27[2],p143-155.

205. Trustrum K. and Jayatilaka A.De.S.,(1979), J.Mat.Sci.,14, pp. 1080-1084.

206. Petrovic J.J, Stout M.G,(1981), J.Am.Ceram.Soc., 64,11 pp.661-66.

207. Trustrum K. and Jayatilaka A.De S.,(1983), J.Mat.Sci.,18,pp.2765-2770.

208. Batdorf S.B.,(1973),Symposium on Fracture Mechanics of Ceramics Uni. of Pennsylvania,Vol.3,p1.

209. Lamon J., Evans A.G.,(1983), J.Am.Ceram.Soc.,66,3, p.177-182

210. Rickerby D.G.,(1980), J.Mat.Sci., 15, pp. 2466-2470.

211. Wallin K.,(1984),Eng.Fract.Mech.,19,6, pp. 1085-93.

212. Neville D.J.,(1989),Eng.Fract.Mech.,34,3,pp. 771-776.

213. Wu R. and Qiu C.,(1989),"Brittle matrix Composites 2",
A.M.Brandt and I.H. Marshall (Eds),Elsevier ,London.

214. Scott W.D. and Gaddipati A., Fracture Mechanics of Ceramics Vol.3,
R.C.Bradt et al (eds),1978, pp. 125-142.

215. Goda K. and Fukunaga H.,(1986), J.Mat.Sci, 21, pp. 4475-4480.

216. Asloun E.M.,Donnet J.B.,Guilpain G.,Nardin M.,and Schultz J., J.Mat.Sci.,
(1989),24,pp. 3504-3510.

217. Breder K., Andersson T. and Scholin K., (1990), J.Am.Ceram.Soc., 73,7,
pp. 2128-30.

218. Masson J.J. and Bourgain E., Int.J.Fract.,(1992),55,pp. 303-319

219. Kim A.S.,Bengtsson and Warren, (1993),Comp.Sci.Tech.,pp. 331-337.

220. Neville D.J.,(1987),Proc.R.Soc.Lond.A.410,p421-442.

221. Neville D.J.,(1987),Int.J. of Fracture,34,p309-315.

222. Neville D.J.,(1988),Int.J. of Fracture,36,p233-239.

223. Neville D.J.,(1990),Inter.J.Fracture,44,p79-96.

224. Neville D.J.,(1985),Phd Thesis,University of Cambridge.

225. Tradinik W.,G.Popp G. & R.F.Pabst R.F., (1982),Z.Werkstoff Tech.13,p.254.

226. A.C.I.Committee 214,J.of the Amer.Concrete Inst. (1955), 52,p41.

227. Pineau A & Mudry F.,(1987),Int,J.Fract.,34,pp 309-315.

228. Kies J.A.,(1958) NRL Report 5098, Naval Reseaerch Lab, Washington D.C.

229. Somerville P.N. and Bean S.J., J.Stat. Comp. Simul., (1982), 14,3-4,
pp. 229-239.

230. Langlois R.,(1991),J.Mat.Sci.Lett.,10,pp. 1049-1051.

231. Olshansky R. and Maurer R.D.,(1976),J.Appl.Phys., 47,10,pp 4497-4499.

232. Kalish D., Basant K.T and Pickwick R.O.,(1977), Am. Ceram. Soc. Bull.,56, 5,pp. 491-503

233. Snowdon W.E., Fract.Mechanics of Ceramics ,Vol.2 R.C.Bradt et al (eds), 1978, pp143-159.

234. Braiden P.M., Mat. in Engineering, (1980),2, pp 73-82.

235. Bergman B.,J.Mat.Sci.,(1984), 3,pp.689-692.

236. Kennedy J.B and Neville A.M.,(1986)," Basic Statistical Methods for Engineers and Scientists", 3rd ed., Harper and Row.

237. Davies J.J.R.,Preston R.F.,Lee R.J. and Walls K.N., (1990),Inst.Phys. Conf.Ser. No111, p.197.

238. Bourgain E. and Masson J.J.,(1992), Compo.Sci.Tech.,43, pp. 221-228.

239. Warren R.and Anderson C.H.,(1984), Composites, 15,pp. 16-24.

240. Lamon J and Guillaumat L.,(1992), "Developments in the Science and Technology of Composite Materials", ECCM5, Bordeaux,France, pp. 585-590.

241. Liptai R.G., Tatro C.A.,(1976),Metals Handbook,Vol11, 8th Ed., ASM, pp.234-243.

242. Forster F., Scheil E.,(1936), Zeitschrift fur Metallkunde, Vol. 29 No9, pp. 245-247.

243. Mason W., McSkimin H.J.and Shockley W.,(1948),Phyical Review Vol.73,No10, pp1213-1214.

244. Millard D.,(1950), Ph.D. University of Bristol.

245. Kaiser J.,(1950),Ph.D.,Tech.Hochshule Munchen.

246. Goldman R.,(1965),"Ultrasonic Technology", John Wiley & Sons,N.York.

247. Drouillard T.F.,(1979),"Acoustic Emission:A bibliography with Abstracts",ed. F.Laner, IFI/Plenum ,N.York.

248. Drouillard T.F. and Hamstad M.A., (1983) First Int.Sym. on AE from Reinforced Comp.,San Francisco,Cal., July 19-21.

249. Swinddlehurst W.,(1973),N.D.Testing,June,p.152-158.

250. Druillard T.F., (1988),Mat.Evaluation,46,p174.

251. Drouillard T.F.,(1975),ASTM STP 571,pp 241-284.

252. Tonolini F., Sala A.& Villa G.,(1987), Int.J.Pres. Ves. & Piping,28,pp179-201.

253. Lord A.E.Jr.,(1975),"Physical Acoustics", ed.W.P. Mason , R.N. Thurston,Vol XI,Academic Press.,N.York.

254. Beattie A.G., (1983),J.Acoustic Emission, p.95-128.

255. Hull B.,John V.,(1988),"Non Destructive Testing" Macmillan, London.

256. Liptai R.G., Harris D.O,(1972),ASTM STP 505,p.3.

257. Dunegan H.L & Green A.T.,Acous.Emission,ASTM STP 505,p.100.

258. Wheeler,B.D.,Symp. XRFA in Agrochemistry,Tzino Inst., Moscow, USSR, 1979 ,(Spectroscopy,vol 3,No3).

259. Kaiser J.,(1953),Arkiv fur das Eisenhuttenwesen, AREIA, Vol.24,1/2,pp.43-45.

260. Kerawalla J.N., (1965),Phd , in A.E.Lord ,Chap.6 "Acoustic Emission", in "Physical Acoustics ", W.P.Mason and R.N.Thurston, Vol XI,(1975),Academic Press, N.York.

261. Spanner J.C.,(1970), MSc , Washington State Uni., in A.E.Lord Chap.6 "Acoustic Emission", in Physical Acoustics ", W.P.Mason and R.N.Thurston, Vol XI,(1975),Academic Press,N.York.

262. Duke J.C.,(1982),ASTM STP 772,pp 97-112.

263. Funa M. et al ,(1974), Proc. Conference,NPL ,pp77-79.

264. M.G.Phillips M.G.& Harris B.,(1980),"Reinforced plastic constructed equipment in the chemical process industry Manchester Symp.,March 21.

265. Dieter G.E., (1986), "Mechanical Metalurgy", 3rd ed., McGraw-Hill N.York.

266. Orowan E.,"Internal Stresses and Fatigue of Metals",(1959), Elsevier Pub. Co. N.York.

267. Sankar N.G.,(1969),"Unload emission behavior of Materials and its relation to the Bauschinger effect ,Ph.D. thesis ,Uni of Michigan.

268. Frederic J.R.& D.K. Felbeck D.K.,(1971),ASTM,STP 505, p.138.

269. Evans A.G., Linzer M.,(1977),Ann.Rev.Mater.Sci.,7, p.179-208.

270. Phillips M.G. ,(1988),Amer.Soc. for NDT,Vol 5 2nd ed.

271. Brindley B.J., Holt J., Palmer I.G.,(1973) , N.D Testing, pp.299-306.

272. Curtis G.J.,(1974), AERE Tech Report R.7684.

273. Lorenzo L. and Hahn H.T.,(1983),Proc.First Int. Symp. Acoust. Emission from Reinnforced Composites,Session 2, 1-13, N.York, USA.

274. Fuwa M., Bunsell A.R.and Harris B.,(1975),J.Mat.Sci.,10,pp.2062-2070.

275. Guild F.J., Harris B., Willis A.J. (1982), J.Acoustic Emission,1,p.244-250.

276. Guild F.J., Ackerman F.J., Phillips M.G.and Harris B.(1983), Proc.Int.Sump. AE from Reinforced Composites , Session 5,1-7, N.York, USA.

277. Lorenzo L. and Hahn H.T, (1986), J. of AE ,Vol.5,1, pp.15- 24.

278. Evans A.G., Graham L.J.,(1975), Acta Metall, 23, p.1303.

279. Nakamura Y.,Veach C.L., McCauley B.O, (1972) ASTM STP 505, p.164.

280. Pollock A.A.,(1973),Acoustic and Vibration Progress 1, ed.R. W.B Stephens,H.G.Leventhall ,London,Chapman and Hall,p.51.

281. Clarke F.J.P.,(1964),Acta Met.,12,pp139-143.

282. Davidge R.W., Tappin G.,(1968), J.Mat.Sci., 3, pp 297-301.

283. Romrell D.M. and .R. Bunnell L.R.,(1970), Mat.Evaluatawn,28,[12], pp.267-270.

284. Gatti A.,Mehan R.L.,Noone M.J., (1971), Final Rep. N00019-71C-02126, Naval Air Systems Command, G.E. Lab. Penn., USA.

285. Wright R.E. ,(1972),J.Am.Ceram.Soc.,55[1],p.54.

286. Evans A.G.,(1972),Phil.Mag.,26[6],pp.1327-44.

287. Schuldies J.J.,(1973),Mat.Evaluation,3[10],pp209-213.

288. Cooke R.G.,(1979),Proc.10th Int.Conf.on Science of Ceramics, Hansner H. ed.,W.Germany,pp. 499-503.

289. Cooke R.G.,(1977), Proc.Inter.Conf.on Science of Ceramics,De Vries K.J. ed,The Netherlands,p.527-534.

290. Nadeau J.S.,(1977), Fracture, Vol 3, ICF4, Canada, pp. 979-983.

291. Nadeau J.S.,(1981),J.Amer.Cer.Soc.,Vol 64,10, pp. 585-590.

292. Becht J., Schwalbe H.J.,Eisenblaetter,(1976), Composites, 7, pp. 245-248.

293. Brecht et. al.,(1976), Composites, 7, p.245.

294. Couild F.J., Phillips M.G. and Harris B.,(1980), NDT Int., 13, p.209.

295. Berthelot J.M.,(1985), J. of A.E ,Vol4,2-3, pp. S178-181.

296. Caneva C.& Mazzola M.,(1987),Composites,No3 , Mai-Jun , pp. 95-98.

297. E.C.C.International,"China and Ball Clays for the Ceramic Industry, prospectus C90.

298. Sambell R.A.J.,(1970),Composites,Vol.1, 5, pp. 276-85.

299. Evans A.G.,(1990),J.Am.Ceram.Soc.,73,2,pp. 187-206.

300. Simpson L.A.,(1974),J.Amer.Ceram.Soc.57,p151.

301. Link Analytical,Application Note " Chemical Analysis of Portland Cement,Raw Mix and Related Raw Materials by EDXRF.

302. Wheeler,B., ASTM Report E-2SM10-34,ASTM, Phil.,1982.

303. Bye G.C.,(1983), Portland Cement , The Institute of Ceramics, Pergamon Press, Oxford .

304. QMS, Link Analytical Limited,High Wycombe, Bucks. U.K.

305. Reed S.J.B.,(1983),"Energy Dispersive X-ray Spectrometers" in "Quantitative Electron-probe Microanalysis", Scott V.D. and Love G., Ellis Horwood ltd, Chichester.

306. Goodhew P.J. and Humphreys F.J.,"Electron Microscopy and Analysis ", (1988), 2nd ed.,Taylor and Francis , London.

307. Larsen D.C. and Stuchly S.L.,(1990),"Fiber Reinforced Ceramic Composites", Mazdiyasni K.S. (ed), Noyes Pub.,N.Jersey, pp. 182-193.

308. Nicholls,(1976) "Composite Materilas Handbook" , Prentice- Hall Inc.,Englewood Cliffs, N.J.

309. Higgins R.A.,"Properties of engineering materials ", Hodder & Stoughton Educ. Ltd, U.K.

310. Filipczynski L.,Pawlowski Z., and Wehr J.," Ultrasonic Methods of Testing Materials",(1966), Butterworths, London.

311. Weiheim V.C.H., " Materials Science and Technology , A comprehensive Treatment", Vol 2A,Part 1, P.W.cahn, P.Haasen and E.J..Kramer Editors.

312. ASTM E-473,(1985)," Standard definitions of Terms relating to Thermal Analysis",

313. Webb T.L., "Thermal Analysis" ,ed.J.P. Redfern, MacMillan, London, p. 249, 1965.

314. Ramachandran V.S.,"Applications of Differential Thermal Analysis in Cement Chemistry", Chem.Pub.Cp., N.York,1969.

315. Webb T.L. and Krugger J.E.," Differential Thermal Analysis" ed. Mackenzie R.C.,Vol. II,P. 181 , Academic Press,London, 1972.

316. Ben-Dor L.,"Thermal Methods" in "Advances in Cement Technology" S.N. Ghosh, pp. 673-703, Pergamon Press Oxford , 1983.

317. Midgley H.G., Cem.Concr.Res.,9.1,pp 77-82, 1979.

318. Marsh B.K., Day R.L. and Bonner D.G.,Mag. Concr.Res., V 38, 134, pp. 23-29, 1986 .

319. Marsh B.K. and Day R.H.,Cem.Concr.Res.,18,pp. 301-310, 1988.

320. Papargyris A.D.,Botis A.I.,Spiliotis X., Kasidakis D., and Papapolymerou G., (1992), 8th SIMCER, Int. Symp. on Ceramics , Rimini,Italy .

321. Papargyris A.D.,Botis A.I.,Papapolymerou G.,Spiliotis X. and Kasidakis D.,(1993), Proc.3rd ECERS, Madrid, Spain .

322. Ouyang C.,Landis E. and Shah S.P.,(1991), Exper.Tech., pp 24-28.

323. Yang M.and Scott V.D.,J.Mat.Sci.,25,1991.

324. Russell-Floyd R.,(1991),"AE and Acousto-ultrasonics on Aromatic Composites,Ph.D. Thesis,Uni of Bath.

325. Russel-Floyd R.,(1990), Software for A.E. Collection and Analysis,Uni of Bath, School Mat.Science.

326. Modin H.,Modin S.,(1973)" Metallurgical Microscopy",trans. by G.G.Kinnane, Butterworths, London.

327. Smallman R.E. and Ashbee K.H.G.,(1966)," Modern Metallography", Pergamon Press, Oxford.

328. Majumdar A.J,(1972),Proc.Brit.Cer.Soc.,No20,1972, p43.

329. Freeman,I.L. and Rayment D.L.,(1968), Trans.Brit. Ceram.Soc., 67,p. 611.

330. Diamond S.,(1976), Proc. Confer.Uni.Sheffield, April 1976, pp.2-30.

331. Williamson R.B.,(1972),"Solidification of PC, Progress in Materials Science, 15:3,Pergamon Press, pp. 189-286.

332. Double,D.D.,(1983) Phil.Trans.R.Soc.Lond.,A310, pp. 53-66.

333. Grudemo Ake , (1979), Cem.Concr.Res.,, 9,pp. 19-34.

334. Cullity,(1978)," Elements of X-ray diffraction ", 2nd ed., Addison-Wesley Pub. Co, USA.

335. DENKA ALCEN-BULK-FIBRE Grades,(1989) Spec., DENKA-ALCEN & Nitivy Co Ltd, Japan.

336. Donnet J.B. & Bansal R.C., (1990),"Carbon Fibers" 2nd Ed.,Marcel Dekker Inc, N.York.

337. Timoshenko S.,(1955),"Strength of Materials ",Part I,3rd ed., Von Nostrand, N.York.

338. Richerson D.W.,(1982),"Modern Ceramic Engineering", M.Dekker Inc, N.York & Basel.

339. BS 1902:Section 4.1, 1984.

340. Pollock A.A.,(1981), Int. Advances in NDT ,7, pp.215-239.

341. Graham L.J.,(1977), Spec.Rep. ARPA-AFML Contract F33615-74-C-5180,Rockwell Int. Sci. Center,Ca, USA.

342. Kuksenko V.S.,(1977),Proc.Inter.Conf.Fracture Mechanics and Technology , Hong Kong , Sih G.C. & Chow C.C.(Eds),Vol 1, pp. 1039-1052.

343. Ono K.,Landy R. and Ouchi C., (1978), Proc. 4th AE Symp., Tokyo,VI, pp.35-45.

344. Ghote B.B., Hasselman ,Spriggs R.M.,(1973), Am.Cer.Soc.Bull ,53 [9], p.670.

345. Tomplinson W.J., Archer P.C.J., (1990), J.Mat.Sci.Lett.,9,p.125-126.

346. Staley W.G., Brindley, (1969), J.Amer.Ceram.Soc., 52, p.616.

347. Wyatt O.H. & Dew-Hughes D., (1974),"Metals,Ceramics and Polymers", Cambridge Uni.Press.

348. Maniatis Y.,(1976)," Examination of Ancient Pottery using the SEM", PhD Thesis,Uni of Essex, England.

349. Lundin S.T., (1959) ," Studies on Triaxial Whiteware Bodies", Pub. Almquist and Wiksell, Stockholm.

350. Maniatis Y. and Tite M.S.,Trans.Brit.Cer.Soc.,(1975), 74, pp 229-32.

351. Kromer H., Interceram, (1971), 20, p.41.

352. Tite M.S.& Maniatis Y.,Trans.Br.Ceram.Soc.,(1975), 74, pp.19-22.

353. Metcafe B.L. and Sant J.H., Trans.& J.Br. Cer. Soc.,(1975), 74,6, pp.193-201.

354. Davidge R.W.,(1973),Symposium on Fracture Mechanics of Ceramics Uni of Pensilvania,Vol 2,p.447.

355. Durrant G.,(1992),"The forging of Saffil Fibre Reinforced Aluminium", PhD Thesis , Uni of Bath, England.

356. Figueiredo J.L., Bernardo C.A., Baker R.T.K. and Huttinger K.J.,(eds), (1990)," Carbon Fibers- Filaments and Composites ", p. 367 , NATO ASI series.

357. Chou T.W,(1992),"Microstructural design of fiber composites", Cambridge Uni.Press, N.York.

358. Rubinstein A.A.,(1985),Int.J.Fract.,27,pp 113-19.

359. Gong S.X. & Horii H.,(1989), J.Mech.Phys.Solids, 37,pp.27-46.

360. Lam K-Y,Cotterell B. and Phuo S-P,(1991),J.Am.Ceram. Soc., 74, pp.352-57.

361. Kelly A and Mackmillan N.H.,(1986),"Strong Solids", Ch.1, Clarendon Oxford.

362. Buresch F.E.,(1979), ASTM STP 678 ,S.W. Freiman Ed,ASTM, pp. 151-165.

363. Maji A. & Shah S.P.,(1988), Exper.Mechanics, Vol 28,1, pp 27-33.

364. Claussen N, (1976), J.Am.Ceram.Soc.,59, pp 49-51.

TABLES
11-25

MECH. PROP.	SINT. TEMP.	1000 °C	1100 °C	1200 °C	1300 °C	1400 °C	1500 °C
E_b GPa	AVG	2.28	10.19	30.4	39.2	48.59	52.25
	STD	0.25	2.21	6.10	6.70	9.41	4.92
	C_v	10.9	18.1	20.0	17.0	19.4	9.4
E_d GPa	AVG	6.8	23.8	46.4	67.0	96.25	80.12
	STD	0.30	1.80	2.70	2.60	5.40	5.40
	C_v	4.4	7.5	5.8	3.9	5.3	6.8
MOR MPa	AVG	6.68	16.44	34.22	37.2	60.11	46.21
	STD	0.40	3.60	7.10	10.0	5.31	7.69
	C_v	6.0	22.4	20.7	26.8	8.84	16.6
K_{IC} $MPa.m^{1/2}$	AVG	0.18	0.38	0.73	0.88	1.15	1.19
	STD	0.014	0.09	0.10	0.11	0.10	0.25
	C_v	5.9	24.0	13.7	12.5	9.2	21.41
W_f J/m^2	AVG	7.12	7.32	9.02	10.13	13.74	13.61
D g/cm^3	AVG	1.54	1.57	1.78	1.95	2.37	2.19

Table 11. Mechanical characteristics of Kaolin samples sintered at various temperatures.

Abbreviations used in all Tables:

Mech.Prop. = Mechanical Properties
Sint.Temp. = Sintering Temperature
E_b = Modulus of Elasticity from 3-point bending tests
E_d = Modulus of Elasticity from Dynamic testing
MOR = Modulus of Rupture
K_{IC} = Fracture Toughness
W_f = Work of Fracture
D = Density

MECH. PROP.	SINT. TEMP.	900 °C	1000 °C	1050 °C	1100 °C	1150 °C	1300 °C
E_b GPa	AVG	5.15	21.20	23.6	28.2	40.31	38.5
	STD	0.69	2.14	3.2	2.7	7.9	5.2
	Cv	13.3	17.1	13.5	9.6	19.5	13.5
E_d GPa	AVG	10.76	23.55	32.29	43.4	58.58	
	STD	0.31	0.44	1.23	1.68	0.80	
	Cv	2.90	1.80	3.8	3.8	1.36	
MOR MPa	AVG	11.0	21.73	31.27	36.02	63.36	33.2
	STD	1.35	3.78	3.47	4.57	11.28	4.78
	Cv	12.20	17.4	11.11	12.6	17.8	14.4
K_{IC} $MPa.m^{1/2}$	AVG	0.31	0.67	0.76	0.83	1.22	0.85
	STD	0.02	0.05	0.04	0.07	0.113	0.17
	Cv	8.5	8.5	5.2	9.4	9.28	21
W_f J/m^2	AVG	9.66	10.52	12.46	12.39	18.50	9.32
D g/cm^3	AVG	1.81	1.95	1.99	2.02	2.12	

Table 12. Mechanical characteristics of Pottery Mixture samples sintered at various temperatures,

MECH. PROP.	SINT. TEMP.	900 °C	1000 °C	1050 °C	1100 °C	1150 °C
E_b GPa	AVG	4.90	6.64	6.85	19.45	20.46
	STD	0.62	0.77	0.52	3.2	4.2
	Cv	12.6	11.6	7.6	16.5	20.52
E_d GPa	AVG	11.6	12.4	16.0	33.13	
	STD	0.39	0.39	0.34	0.91	
	Cv	3.3	3.2	2.13	2.7	
MOR MPa	AVG	9.7	10.5	12.8	25.01	34.15
	STD	1.34	1.14	1.35	3.27	4.12
	Cv	13.8	10.9	10.6	13.0	12.08
K_{IC} $MPa.m^{1/2}$	AVG	0.34	0.33	0.42	0.69	
	STD	0.03	0.07	0.04	0.07	
	Cv	8.8	21.2	9.4	10.7	
W_f J/m^2	AVG	12.15	8.72	12.9	12.61	
D g/cm^3	AVG	1.54	1.58	1.64	1.94	

Table 13. Mechanical characteristics of Brick-clay samples sintered at various temperatures.

MECH. PROP.	SINTERING PROGRAMME	P7	P8	P9
E_b GPa	AVG	1.15	3.1	3.3
	STD	0.11	0.51	0.48
	Cv	9.5	16.4	14.5
E_d GPa	AVG	7.47	10.97	11.01
	STD	0.11	0.32	0.41
	Cv	1.5	2.91	3.7
MOR MPa	AVG	5.4	7.0	8.17
	STD	0.62	1.15	1.4
	Cv	11.4	16.4	17.1
D g/cm^3	AVG	1.57	1.607	1.610

Table 14 . Mechanical characteristics of Brick-clay large (25X50X70 mm) specimens produced by extrusion and sintered at three different sintering programmes,

MECH. PROPERTIES	COMPOSITE: KAOLIN +	5% (W/W) FLY ASH	10% (W/W) FLY ASH
	SINTERING TEMP.	1000°C	1000°C
E_b GPa	AVG STD Cv	0.67 0.08 11.94	0.63 0.06 9.5
E_d GPa	AVG STD Cv	5.2 0.27 5.3	5.2 0.3 5.7
MOR MPa	AVG STD Cv	5.04 0.49 9.7	4.82 0.61 12.6
K_{IC} $MPa.m^{1/2}$	AVG STD Cv	0.13 0.019 14.6	0.129 0.016 12.8
W_f J/m^2	AVG	12.7	13.4
D g/cm^3	AVG	1.37	1.35

Table 15. Mechanical characteristics of Kaolin+Fly Ash Composite samples sintered at 1000°C .

COMPOSITE:KAOLIN + 4.7vol.α-AI_2O_3 (B-95) FIBRES			
MECH. PROP.	SINT. TEMP.	1200 °C	1300 °C
E_b GPa	AVG STD Cv	11.09 2.2 19.8	20.15 3.0 14.9
E_d GPa	AVG STD Cv	39.7 2.9 7.3	57.4 1.0 1.7
MOR MPa	AVG STD Cv	35.9 7.1 19.7	44.0 8.0 18.2
D g/cm^3			

COMPOSITE:KAOLIN + 9.2 vol.α-AI_2O_3 (B-95) FIBRES				
MECH. PROP.	SINT. TEMP.	1000 °C	1200 °C	1300 °C
E_b GPa	AVG STD Cv	1.87 0.23 12.2	23.7 9.8 11.8	24.85 3.63 14.6
E_d GPa	AVG STD Cv	8.1 0.6 7.4	31.7 1.2 3.8	45.3 0.53 1.2
MOR MPa	AVG STD Cv	10.99 1.3 12.6	32.38 4.9 15.1	34.7 7.2 20.7
K_{IC} $MPa.m^{1/2}$	AVG STD Cv	0.365 0.027 10.4	0.78 0.066 8.4	0.74 0.05 7.16
W_f J/m^2	AVG	35.6	12.83	11.01
D g/cm^3	AVG	1.44	1.68	1.90

Table 16. Mechanical characteristics of α-AI_2O_3 (DENKA B-95) Fibre-composite samples sintered at various temperatures (continued)

COMPOSITE:KAOLIN + 14 vol.α-Al_2O_3 (B-95) FIBRES				
MECH. PROP.	SINT. TEMP.	1000 °C	1200 °C	1300 °C
E_b GPa	AVG STD Cv	1.36 0.18 13.20	12.0 1.1 9.1	12.42 1.31 10.5
E_d GPa	AVG STD Cv	9.2 0.8 9.4	29.4 2.0 6.8	40.95 2.4 5.9
MOR MPa	AVG STD Cv	9.3 1.6 17.2	31.7 4.5 14.2	35.8 5.65 15.8
K_{IC} MPa.$m^{1/2}$	AVG STD Cv	0.36 0.05 15.4		
W_f J/m^2	AVG	47.6		
D g/cm^3	AVG	1.55	1.68	1.87

Table 16. Mechanical characteristics of α-Al_2O_3 (DENKA B-95) Fibre-composite samples sintered at various temperatures

COMPOSITE:KAOLIN+4.5%vol.δ-Al_2O_3 (SAFFIL) FIBERS			
MECH.PROP.	SINT.TEMPER.	1200 °C	1300 °C
E_b GPa	AVG STD Cv	13.1 0.8 6.1	23.5 2.8 11.9
E_d GPa	AVG STD Cv	36.6 1.16 3.2	58.45 1.65 2.8
MOR MPa	AVG STD Cv	34.1 3.8 11.1	40.25 4.2 10.4
D g/cm^3	AVG	1.78	2.0

Table 17 . Mechanical characteristics of δ-Al_2O_3 Saffil fibre composite samples at various temperatures (continued)

COMPOSITE:KAOLIN+9.7%vol. δ- Al_2O_3 (SAFFIL) FIBERS			
MECH.PROP.	SINT.TEMP.	1200 °C	1300 °C
E_b GPa	AVG STD Cv	14.4 0.9 6.25	15.6 1.1 7.0
E_d GPa	AVG STD Cv	36.4 2.4 6.6	54.3 0.9 1.65
MOR MPa	AVG STD Cv	39.3 6.6 16.8	42.1 6.6 15.6
D g/cm^3	AVG	1.85	1.96

COMPOSITE:KAOLIN+14.75%vol.δ-Al_2O_3 (SAFFIL) FIBERS			
MECH.PROP.	SINTER. TEMP.	1200°C	1300°C
E_b GPa	AVG STD Cv	9.0 0.7 7.7	15.5 1.4 9.0
E_d GPa	AVG STD Cv	24.7 0.64 2.6	43.1 1.3 3.0
MOR MPa	AVG STD Cv	25.3 3.5 13.8	31.95 4.6 14.4
D g/cm^3	AVG	1.62	1.85

Table 17. Mechanical characteristics of δ- Al_2O_3 (SAFFIL) fibre-composite samples sintered at various temperatures

MECHANICAL PROPERTIES	SINTERING TEMPERATURE	1000 °C	1200 °C
E_b GPa	AVG STD Cv	3.2 0.4 12.5	18.45 4.2 22.7
E_d GPa	AVG STD Cv	8.4 0.4 4.8	31.6 0.9 2.8
MOR MPa	AVG STD Cv	10.5 1.0 9.5	33.8 4.2 12.4
K_{IC} $MPa.m^{1/2}$	AVG STD Cv	0.424 0.037 8.76	0.68 0.04 5.9
W_f J/m^2	AVG	28.09	12.53
D g/cm^3	AVG	1.45	1.73

Table 18. Mechanical characteristics of 9.7 % vol. Mullite (B80-K) Fiber Kaolin Composite samples sintered at 1000 and 1200°C .

COMPOSITE:KAOLIN +8.55% CARBON (GRAFIL) FIBRES				
MECHANICAL PROPERTIES	SINTERING TEMPERATURE	1000 °C	1200 °C	1300 °C
E_b GPa	AVG STD Cv	2.96 0.07 2.36	9.65 1.1 11.4	18.5 2.6 14.0
E_d GPa	AVG STD Cv	12.1 1.1 9.0	29.4 0.5 1.7	42.2 2.9 6.9
MOR MPa	AVG STD Cv	9.53 1.6 16.5	23.0 3.6 15.6	37.0 9.0 24.0
D g/cm^3	AVG	1.41	1.50	1.74

COMPOSITE:KAOLIN+16.6% vol. CARBON (GRAFIL) FIBRES			
MECHANICAL PROPERTIES	SINTERING TEMP.	1200 °C	1300 °C
E_b GPa	AVG STD Cv	6.0 1.3 21.6	8.0 1.0 12.5
E_d GPa	AVG STD Cv	25.67 1.0 3.9	31.76 2.5 7.8
MOR MPa	AVG STD Cv	25.58 4.3 16.8	28.96 7.4 25.5
D g/cm^3	AVG	1.35	1.49

Table 19. Mechanical properties of Carbon (Grafil) fibre-composite samples, sintered at various temperatures.

ESTIMATOR	WEIBULL MODULUS
$\frac{i}{(N+1)}$	4.77
$\frac{i-0.5}{N}$	5.20
$\frac{i-0.3}{N+0.4}$	5.01
$\frac{i-\frac{3}{8}}{N+\frac{1}{4}}$	5.08

Table 20. Effect of type of Estimator on Weibull Modulus of K_{IC} for Kaolin Notched specimens sintered at 1100°C and tested at 3-point bending.

i= ith (ranked) order of failure of specimen
N= total number of specimens

STATISTICAL CHARACTERISTICS OF BRICK-CLAY UN-NOTCHED SPECIMENS SINTERED AT 900°C						
N_s	MOR MPa.	m	r_o	r_1	r_N	MOR_{th} MPa
29	8.54 [1.16]	8.54	0.9882	0.9868	0.9765	5.31
63	8.69 [1.01]	9.66	0.9931	0.9899	0.9719	5.58
94	9.16 [1.13]	9.35	0.9908	0.9934	0.9829	5.92
144	9.7 [1.34]	8.52	0.9848	0.9958	0.9844	5.52

Table 21. Variation of statistical characteristics of Brick-clay un-notched specimens sintered at 900°C as a function of the number of tested specimens.

N_s = Number of tested specimens
m = Weibull modulus from 2-parameter Weibull function
r_o = Correlation coefficient in a 2-parameter Weibull function
r_1 = Correlation coefficient in a 3-parameter Weibull function
r_N = Correlation coefficient in a Neville function

MOR_{th} = Threshold value of MOR

STATISTICAL CHARACTERISTICS OF KAOLIN UN-NOTCHED SPECIMENS					
SINT. TEMP.	WEIBULL MODULUS m	CORR. COEFF. IN 2-PAR. WEIBULL FUNCT. r_o	CORR. COEFF. IN 3-PAR. WEIBULL FUNCT. r_1	NEVILLE CORREL. COEF. r_N	MOR_{th} MPa
1100 °C	4.74	0.9783	0.9878**	0.9798*	6.36
1200 °C	4.79	0.9899**	0.9755	0.9603	14.58
1300 °C	4.15	0.9729	0.9863	0.9869**	13.06

STATISTICAL CHARACTERISTICS OF KAOLIN NOTCHED SPECIMENS					
SINT. TEMP.	WEIBULL MODULUS m	CORR. COEFF. IN 2-PAR. WEIBULL FUNCT. r_o	CORR. COEFF. IN 3-PAR. WEIBULL FUNCT. r_1	NEVILLE CORREL. COEF. r_N	K_{ICth} $MPa.m^{1/2}$
1100 °C	4.77	0.9490	0.9660	0.9688**	0.169
1200 °C	4.82	0.9798	0.9906	0.9941**	0.406
1300 °C	8.31	0.9614	0.9861	0.9901**	0.532

Table 22. Comparison of Statistical Characteristics of Kaolin specimens resulting from Weibull and Neville functions,using Correlation Coefficients.

MOR_{th} = Threshold value of MOR in 3-parameter Weibull function
K_{ICth} = Threshold value of K_{IC} in 3-parameter Weibull function

** indicates the best correlation coefficient
* indicates the best correlation coefficient between 2-parameter Weibull and Neville functions.

STATISTICAL CHARACTERISTICS OF POTTERY MIXTURE UN-NOTCHED SPECIMENS					
SINT. TEM.	WEIBULL MODULUS m	CORR. COEFF. IN 2-PAR. WEIBULL FUNCT. r_o	CORRELAT. COEFF. IN 3-PAR. WEIBULL FUNCT. r_1	NEVILLE CORREL. COEF. r_N	MOR_{th} MPa
900 °C	8.93	0.9673	0.9858	0.9865**	6.88
1000 °C	5.93	0.9915**	0.9794	0.9696	10.48
1100 °C	8.48	0.9717	0.9870	0.9818*	22.19

STATISTICAL CHARACTERISTICS OF POTTERY MIXTURE NOTCHED SPECIMENS					
SINT. TEM.	WEIBULL MODULUS m	CORR. COEFF. IN 2-PAR. WEIBULL FUNCT. r_o	CORR. COEFF. IN 3-PAR. WEIBULL FUNCT. r_1	NEVILLE CORREL. COEF. r_N	K_{ICthh} MPa.$m^{1/2}$
900 °C	12.58	0.9654	0.9859**	0.9839*	0.223
1000 °C	14.83	0.9633	0.9829	0.9875**	0.496
1100 °C	11.46	0.9908	0.9915**	0.9892	0.565

Table 23. Comparison of Statistical Characteristics of Pottery Mixture specimens resulting from Weibull and Neville functions, using Correlation Coefficients.

MOR_{th} = Threshold value of MOR in 3-parameter Weibull function
K_{ICth} = Threshold value of K_{IC} in 3-parameter Weibull function

** indicates the best correlation coefficient
* indicates the best correlation coefficient between 2-parameter Weibull and Neville functions.

CHARACTERISTICS OF BRICK-CLAY UN-NOTCHED SPECIMENS					
SINT. TEM.	WEIBULL MODULUS m	CORR. COEFF. IN 2-PAR. WEIBULL FUNCT. r_o	CORR. COEFF. IN 3-PAR. WEIBULL FUNCT. r_1	NEVILLE CORREL. COEF. r_N	MOR_{th} MPa
900 °C	8.64	0.9822*	0.9945**	0.9765	5.52
1000 °C	10.46	0.9810	0.9950**	0.9875*	6.82
1100 °C	8.61	0.9859*	0.9813**	0.9813	15.02

STATISTICAL CHARACTERISTICS OF POTTERY MIXTURE NOTCHED SPECIMENS					
SINT. TEM.	WEIBULL MODULUS m	CORR. COEFF. IN 2-PAR. WEIBULL FUNCT. r_o	CORR. COEFF. IN 3-PAR. WEIBULL FUNCT. r_1	NEVILLE CORREL. COEF. r_N	K_{ICth} $MPa.m^{1/2}$
900 °C	12.96	0.9658 *	0.9862**	0.9631	0.246
1000 °C	4.83	0.9843**	0.9843	0.9806	0.135
1100 °C	13.07	0.9661	0.9900	0.9918**	0.496

Table 24. Comparison of Statistical Characteristics of Brick Clay specimens resulting from Weibull and Neville functions,using Correlation Coefficients.

MOR_{th} = Threshold value of MOR in 3-parameter Weibull function
K_{ICth} = Threshold value of K_{IC} in 3-parameter Weibull function

** indicates the best correlation coefficient
* indicates the best correlation coefficient between 2-parameter Weibull and Neville functions.

STATISTICAL CHARACTERISTICS OF COMPOSITE SPECIMENS					
TYPE OF MATERIAL	m	r_o	r_1	r_N	MOR_{th} MPa
KAOLIN BASED COMPOSITES					
4.7%vol α-AI_2O_3 sintered at 1200°C un-notched	5.44	0.9346	0.9574	0.9602**	16.77
9.2% vol α-AI_2O_3 sintered at 1000°C un-notched	8.64	0.9818	0.9902**	0.9865*	6.82
9.2% vol α-AI_2O_3 sintered at 1300°C un-notched	4.98	0.9890**	0.9651	0.9724	15.18
10% (w/w) Fly Ash sintered at 1000°C un-notched	8.80	0.9902	0.9911**	0.9855	3.09
GLASS	6.34	0.9741	0.9781	0.9839**	68

Table 25. Comparison of Statistical Characteristics of Composites resulting from Weibull and Neville functions,using Correlation Coefficients.

MOR_{th} = Threshold value of MOR in 3-parameter Weibull function

** indicates the best correlation coefficient

* indicates the best correlation coefficient between 2-parameter Weibull and Neville functions.

FIGURES
25-89

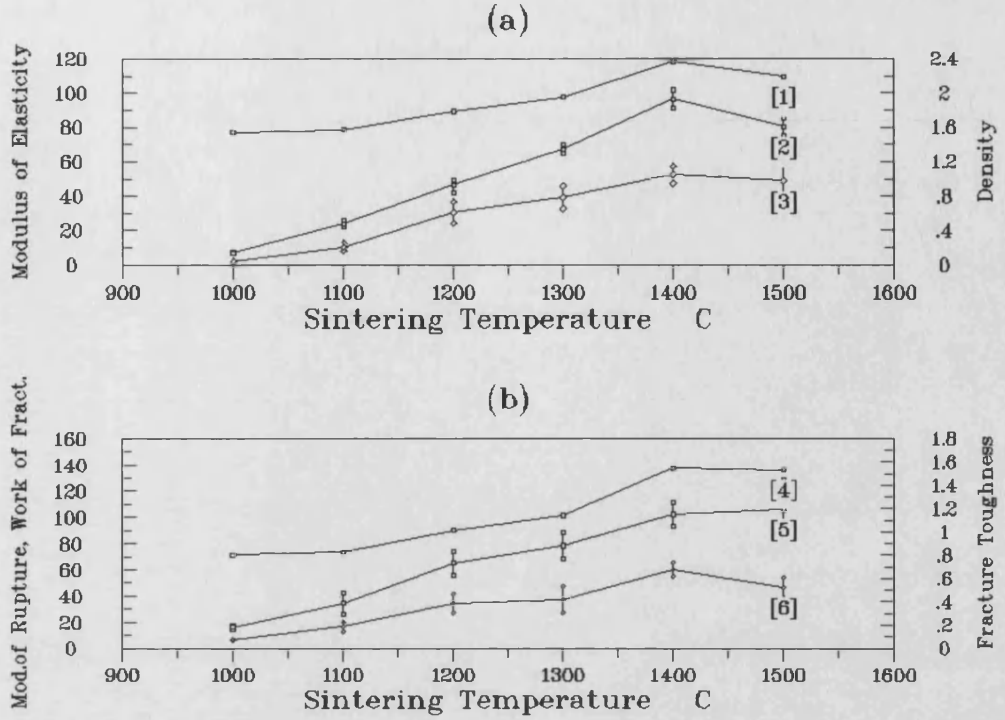

Fig.25 Variation of mechanical characteristics with sintering temperature in kaolin ceramics; **(a)** [1] Density g/cm^3, [2] Modulus of elasticity from dynamic testing E_d GPa, [3] Modulus of Elasticity from bending, E_b GPa, **(b)** [4] Work of Fracture,W_f , 10xJ/m^2 , [5] Fracture Toughness K_{IC} , MPa.m$^{1/2}$ [6] Modulus of Rupture, MOR, MPa.

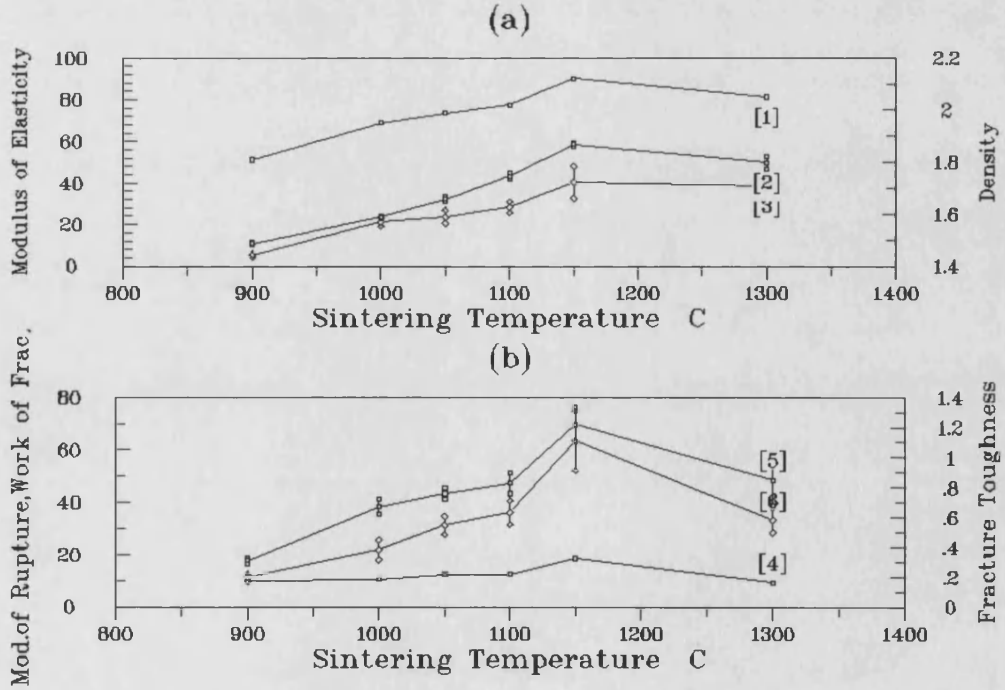

Fig.26 Variation of mechanical characteristics with sintering temperature in pottery mixture ceramics; **(a)** [1] Density g/cm^3, [2] Modulus of elasticity from dynamic testing E_d GPa, [3] Modulus of Elasticity from bending, E_b GPa **(b)** [4] Work of Fracture, W_f , J/m^2 , [5] Fracture Toughness K_{IC} , MPa.m$^{1/2}$ [6] Modulus of Rupture, MOR, MPa.

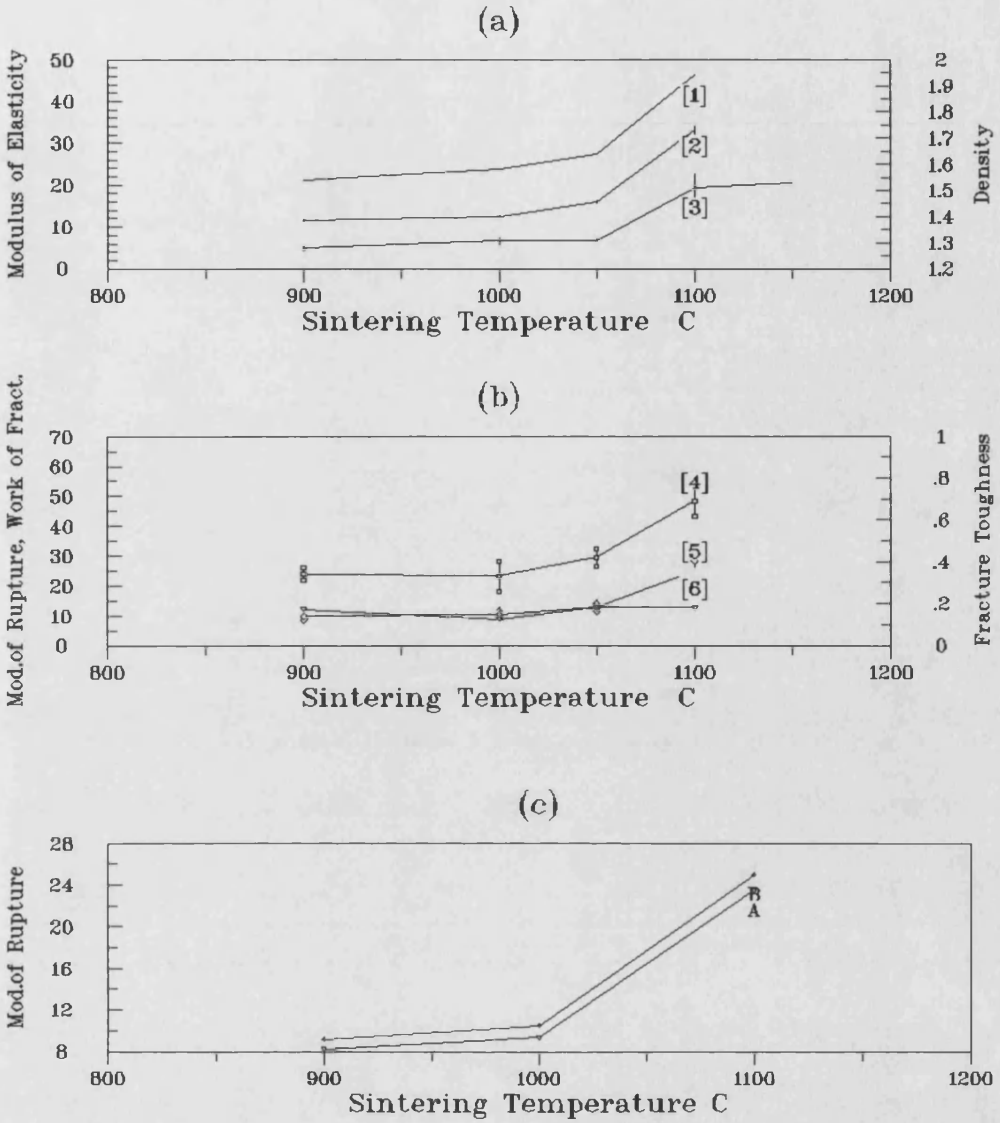

Fig.27 Variation of mechanical characteristics with sintering temperature in brick-clay ceramics; **(a)**: [1] Density (g/cm^3), [2] Modulus of elasticity from bending E_b (GPa) [3] Modulus of Elasticity from dynamic testing E_d (GPa), **(b)**: [4] Fracture Toughness K_{IC} (MPa.m$^{1/2}$), [5] Modulus of Rupture MOR (MPa), [6] Work of Fracture W_f (J/m^2), **(c)**: Effect of frost testing on MOR (MPa), Modulus of Rupture before (A) and after (B) frost testing.

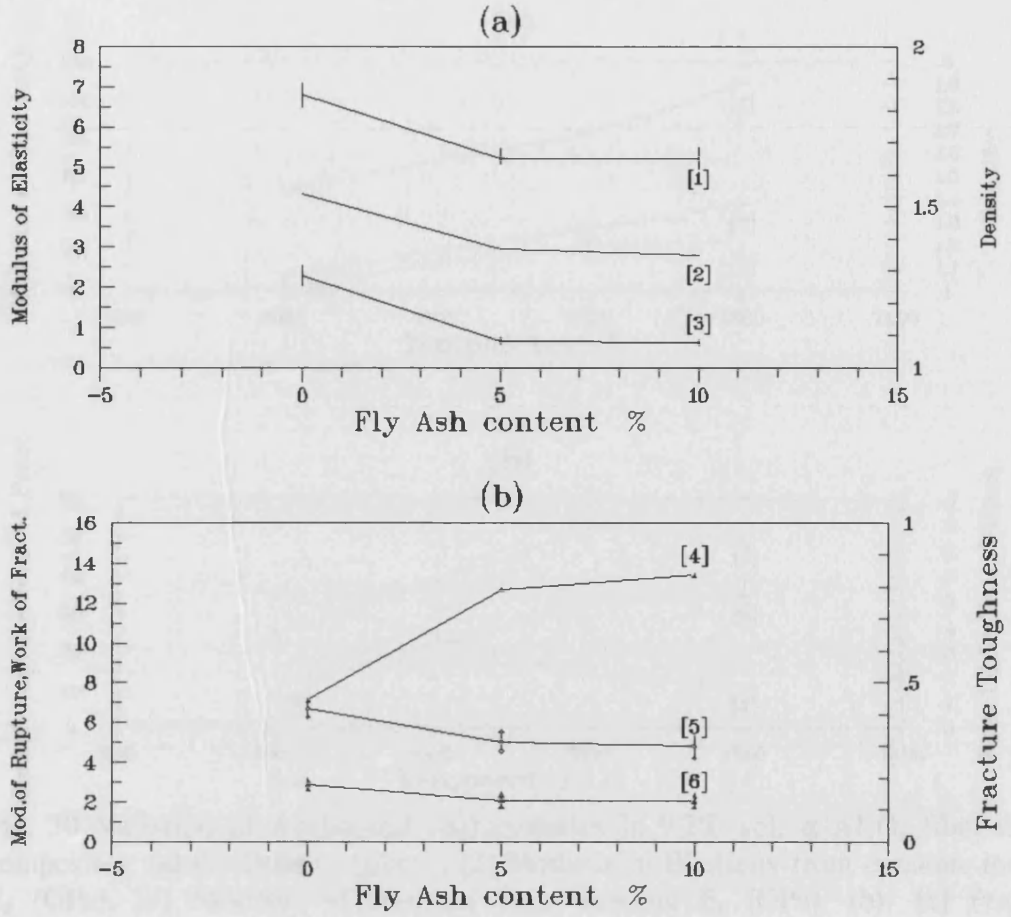

Fig.28 Variation of mechanical characteristics with Fly Ash content in Kaolin-Fly Ash composite ceramics; **(a)**:[1] Modulus of Elasticity from dynamic testing, E_d (GPa), [2] Density (g/cm^3), [3] Modulus of elasticity from bending E_b (GPa), **(b)**: [4] Work of Fracture W_f (J/m^2),[5] Modulus of Rupture MOR (MPa), [6] Fracture Toughness K_{IC} (MPa.m$^{1/2}$).

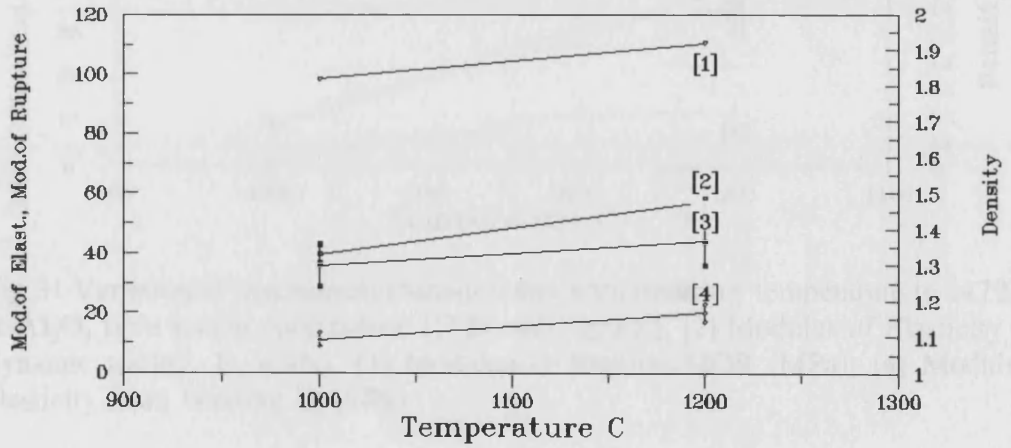

Fig.29 Variation of mechanical characteristics with sintering temperature in 4.7% vol. α-Al_2O_3 fibre kaolin composites: [1] Density (g/cm^3), [2] Modulus of Elasticity from dynamic testing, E_d (GPa), [3] Modulus of Rupture MOR (MPa), [4] Modulus of elasticity from bending E_b (GPa).

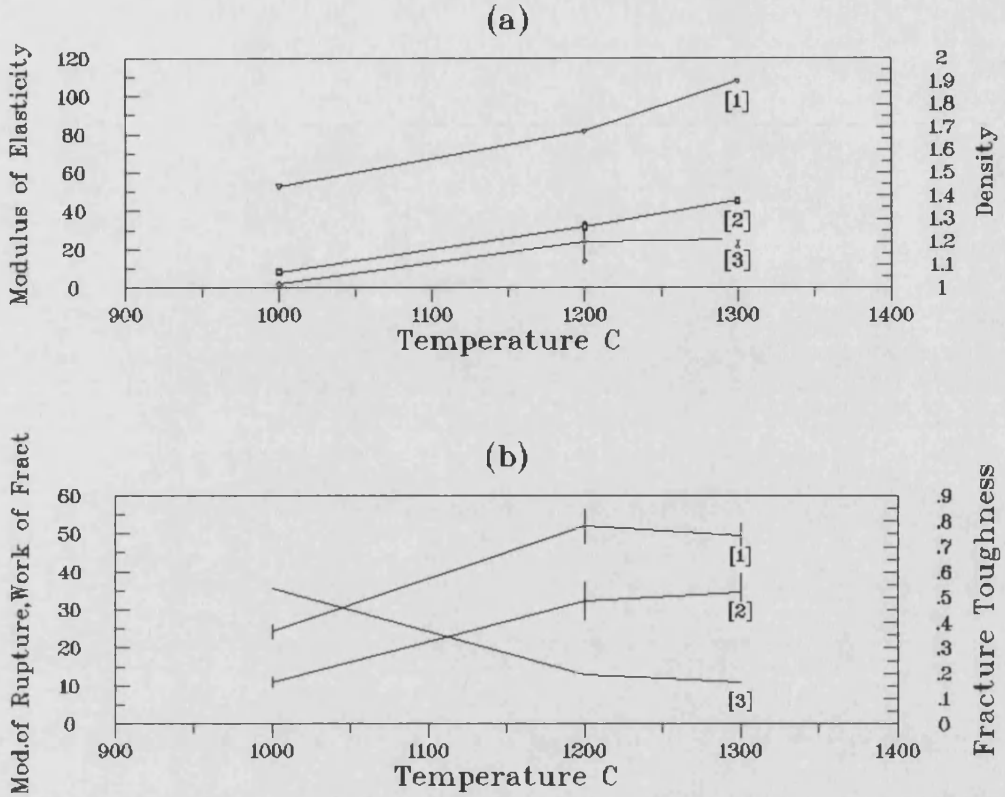

Fig. 30 Variation of mechanical characteristics in 9.2% vol. α-AI_2O_3 fibre kaolin composites: **(a)**:[1] Density (g/cm^3), [2] Modulus of Elasticity from dynamic testing, E_d (GPa), [3] Modulus of elasticity from bending E_b (GPa), **(b)**: [1] Fracture Toughness K_{IC} (MPa.m$^{1/2}$), [2] Modulus of Rupture MOR (MPa), [3] Work of Fracture W_f (J/m^2) .

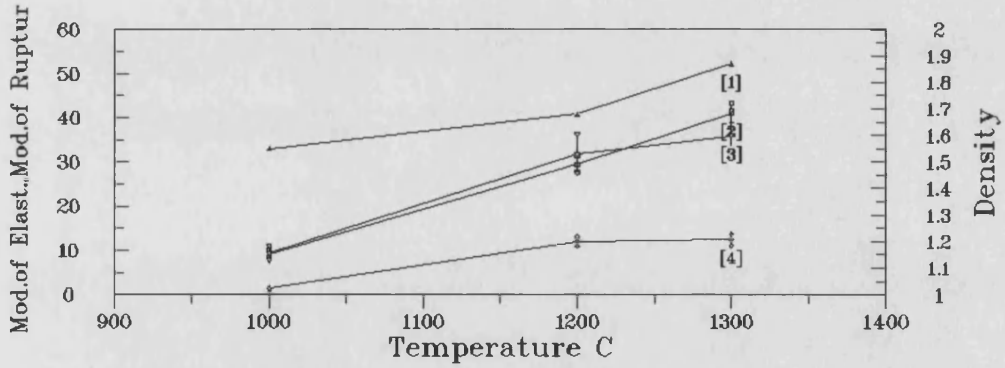

Fig.31 Variation of mechanical characteristics with sintering temperature in 14.7% vol. α-AI_2O_3 fibre kaolin composites: [1] Density (g/cm^3), [2] Modulus of Elasticity from dynamic testing, E_d (GPa), [3] Modulus of Rupture MOR (MPa), [4] Modulus of elasticity from bending E_b (GPa).

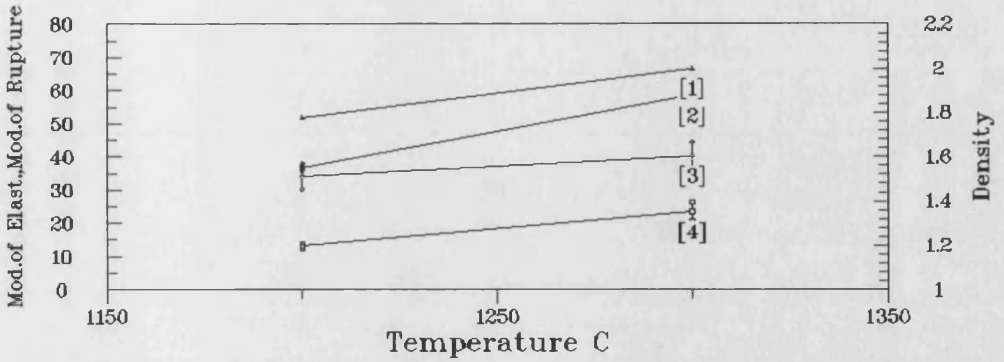

Fig.32 ariation of mechanical characteristics with sintering temperature in 4.5% vol. Saffil fibre kaolin composites: [1] Density (g/cm^3), [2] Modulus of Elasticity from dynamic testing, E_d (GPa), [3] Modulus of Rupture MOR (MPa), [4] Modulus of elasticity from bending E_b (GPa).

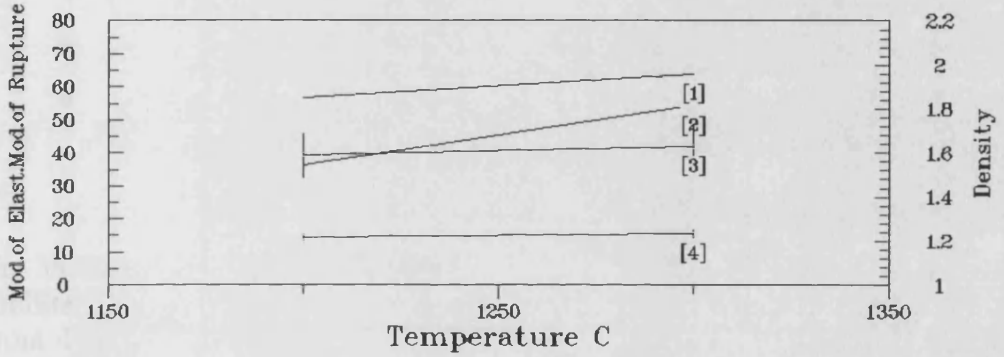

Fig.33 Variation of mechanical characteristics with sintering temperature in 9.7% vol. Saffil fibre kaolin composites: [1] Density (g/cm^3), [2] Modulus of Elasticity from dynamic testing, E_d (GPa), [3] Modulus of Rupture MOR (MPa), [4] Modulus of elasticity from bending E_b (GPa).

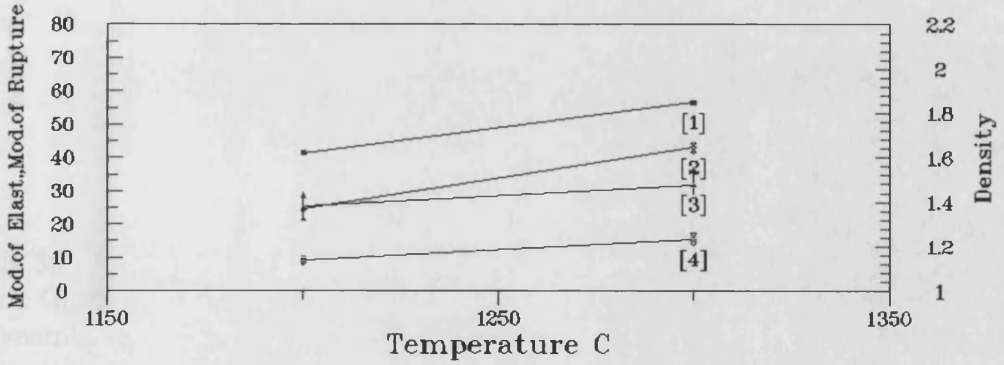

Fig.34 Variation of mechanical characteristics with sintering temperature in 9.7% vol. Saffil fibre kaolin composites: [1] Density (g/cm^3), [2] Modulus of Elasticity from dynamic testing, E_d (GPa), [3] Modulus of Rupture MOR (MPa), [4] Modulus of elasticity from bending E_b (GPa).

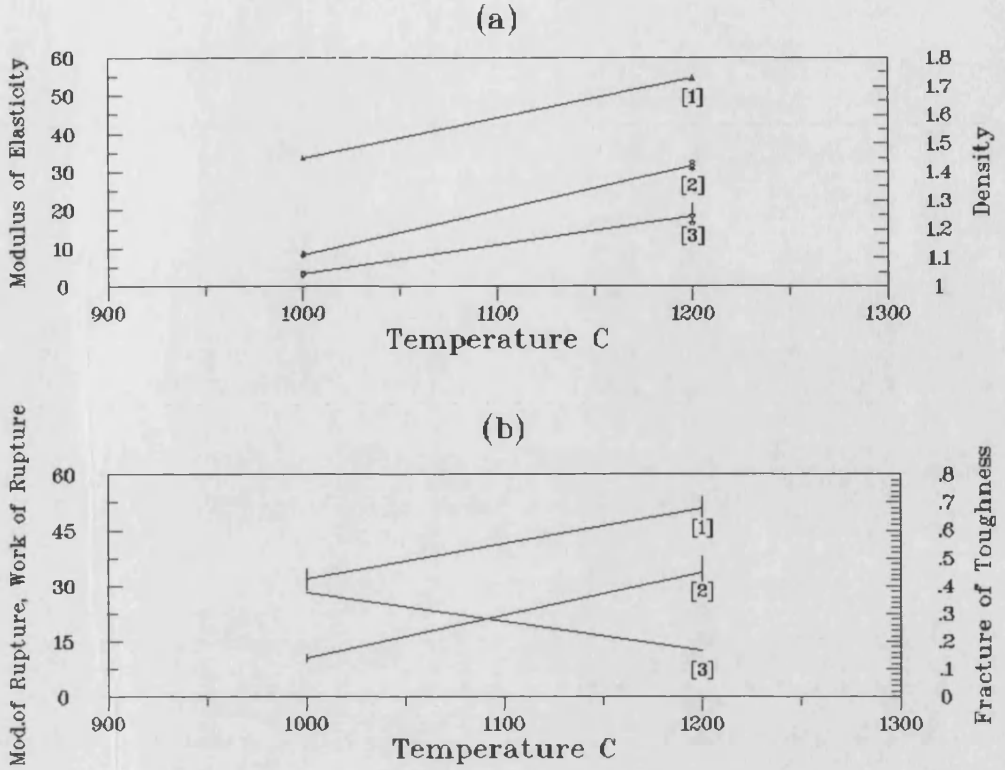

Fig.35 Variation of mechanical characteristics with sintering temperature in 9.7% vol. mullite fibre kaolin composites: **(a)**: [1] Density (g/cm^3), [2] Modulus of Elasticity from dynamic testing, E_d (GPa), [3] Modulus of elasticity from bending E_b (GPa). **(b):** [1] Fracture Toughness K_{IC} (MPa.m$^{1/2}$), [2] Modulus of Rupture MOR (MPa), [3] Work of Fracture W_f (J/m^2) .

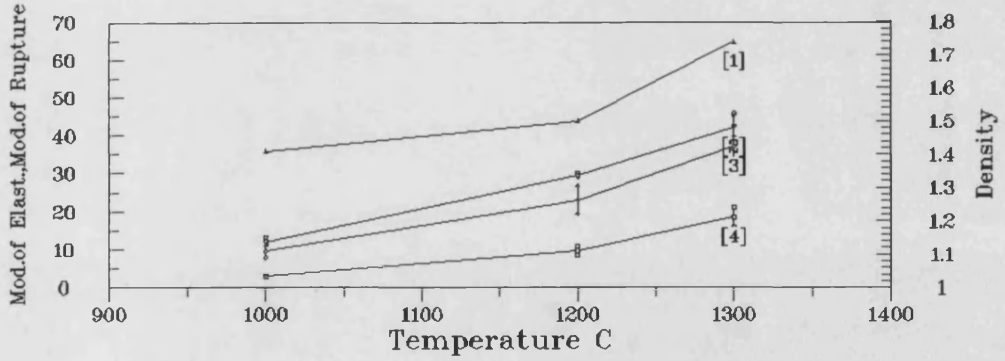

Fig.36 Variation of mechanical characteristics with sintering temperature in 8.5% vol. Grafil fibre kaolin composites: [1] Density (g/cm^3), [2] Modulus of Elasticity from dynamic testing, E_d (GPa), [3] Modulus of Rupture MOR (MPa), [4] Modulus of elasticity from bending E_b (GPa).

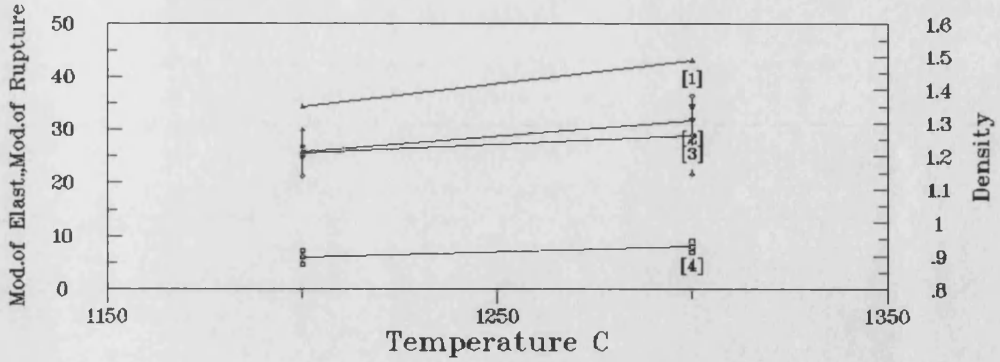

Fig.37 Variation of mechanical characteristics with sintering temperature in 16.5% vol. Grafil fibre kaolin composites: [1] Density (g/cm^3), [2] Modulus of Elasticity from dynamic testing, E_d (GPa), [3] Modulus of Rupture MOR (MPa), [4] Modulus of elasticity from bending E_b (GPa).

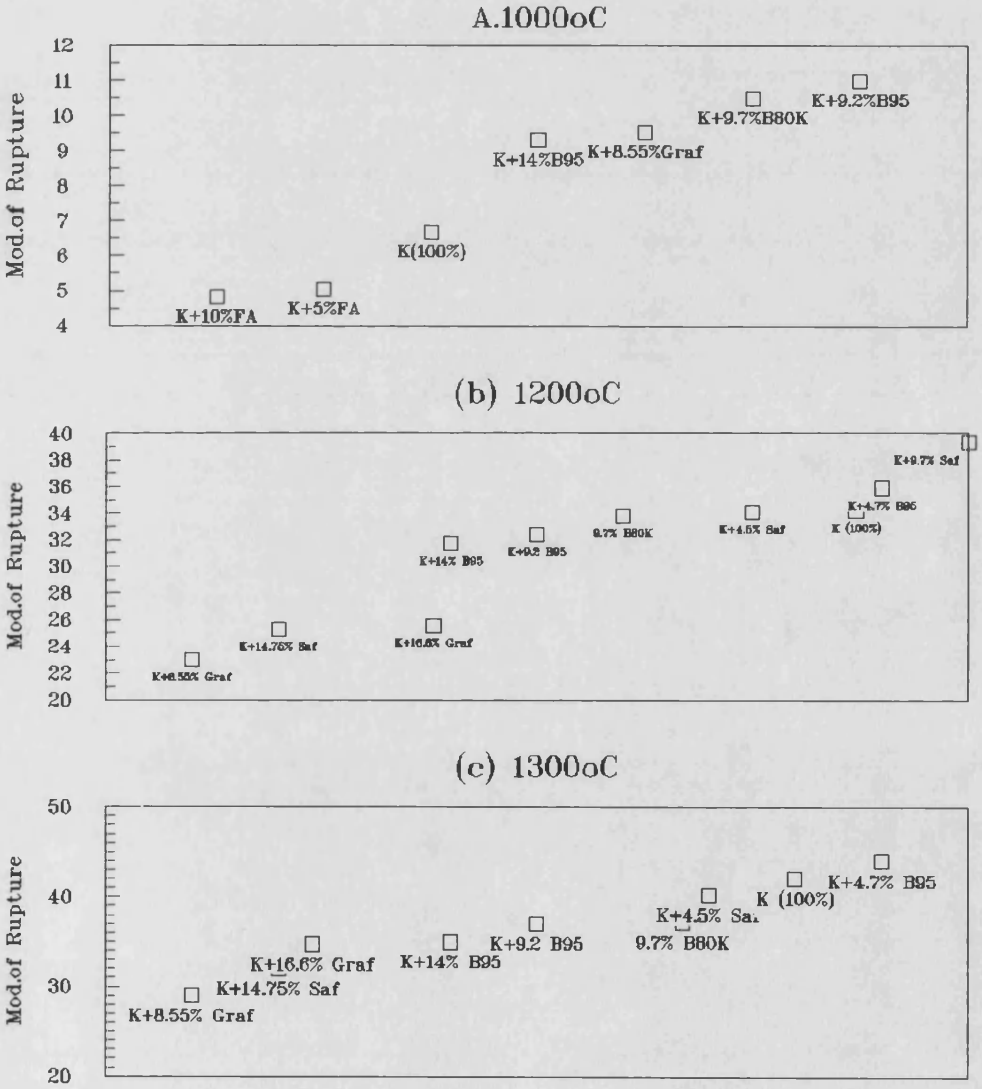

Fig.38 Graphic representation of flexural strength with sintering temperatures of various ceramics and composites with the same matrix (kaolin).

(K+Saf=Kaolin+Saffil Fibres, K+Graf=Kaolin+Grafil fibres, K+B95=Kaolin+α-Al_2O_3 B95 fibres, K+B80K=Kaolin+mullite B80K fibres, K+FA+Kaolin+Fly Ash)

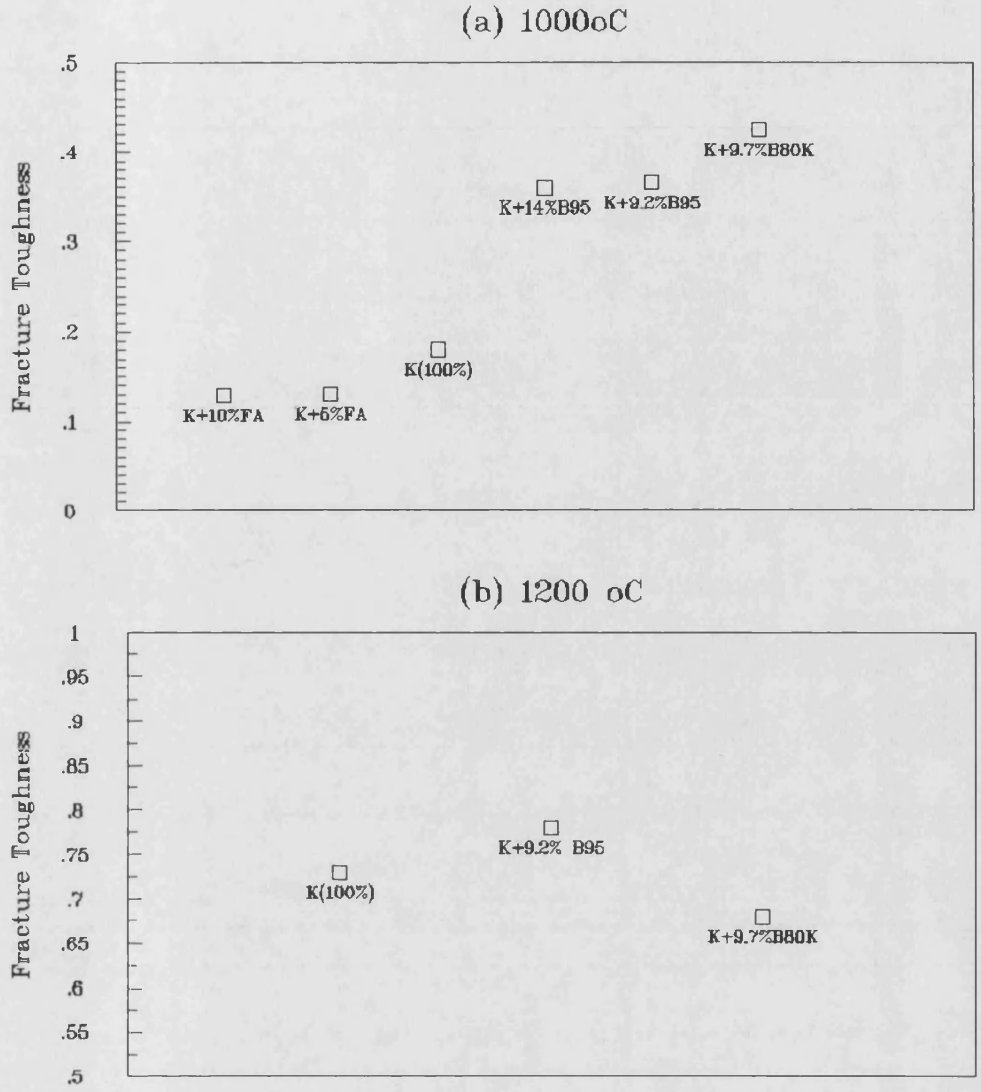

Fig.39 Graphic representation of fracture toughness (K_{IC}, $MPa.m^{1/2}$) with sintering temperatures of various ceramics and composites with the same matrix (kaolin).

(K(100%) = Kaolin , K+B95=Kaolin+α-Al_2O_3 B95 fibres, K+B80K=Kaolin+mullite B80K fibres, K+FA+Kaolin+Fly Ash)

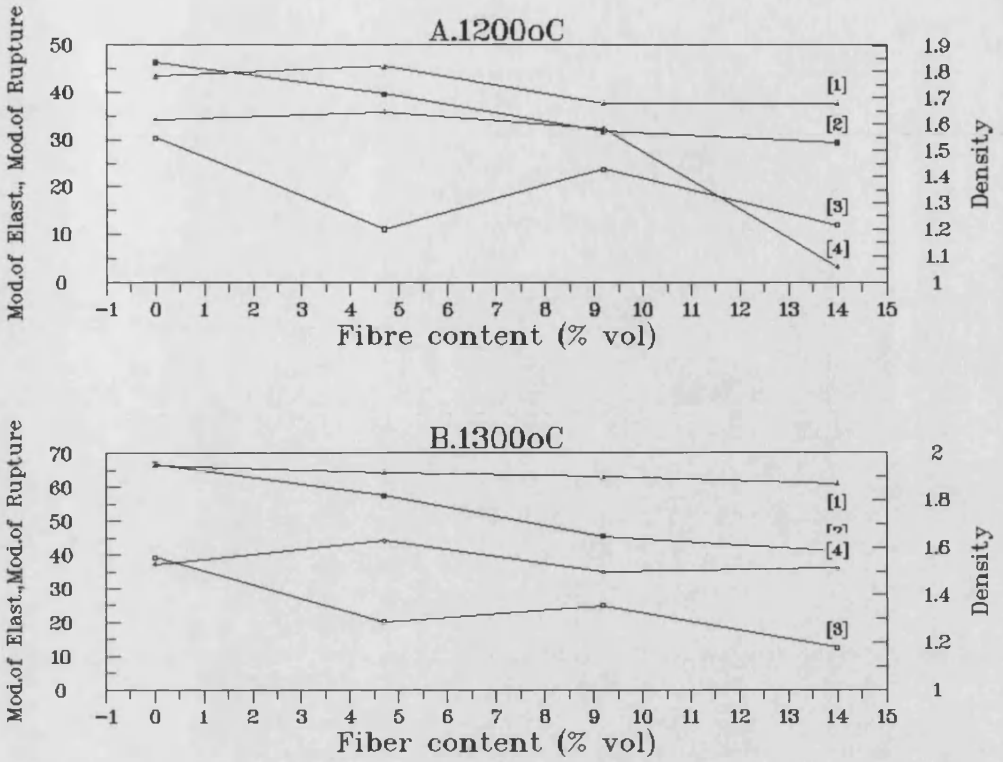

Fig.40 Graphic representation of the variation of mechanical properties with α-AI_2O_3 (B-95) fibre content at different sintering temperatures **(a) 1200°C**: [1] Density (g/cm^3), [2] Modulus of Elasticity from dynamic testing, E_d (GPa), [3] Modulus of elasticity from bending E_b (GPa), [4] Modulus of Rupture MOR (MPa) , **(b) 1300°C**: [1] Density (g/cm^3), [2] Modulus of Elasticity from dynamic testing, E_d (GPa), [3] Modulus of Rupture MOR (MPa) , [4] Modulus of elasticity from bending E_b (GPa)..

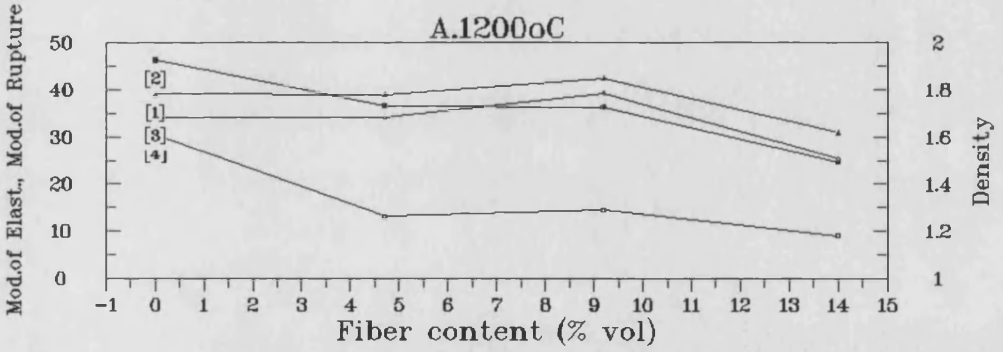

Fig.41 Graphic representation of the variation of mechanical properties with δ-AI_2O_3 (Saffil) fibre content at different sintering temperatures; (a)1200°C :[1] Density (g/cm^3), [2] Modulus of Elasticity from dynamic testing, E_d (GPa), [3] Modulus of Rupture MOR (MPa) , [4] Modulus of elasticity from bending E_b (GPa)..

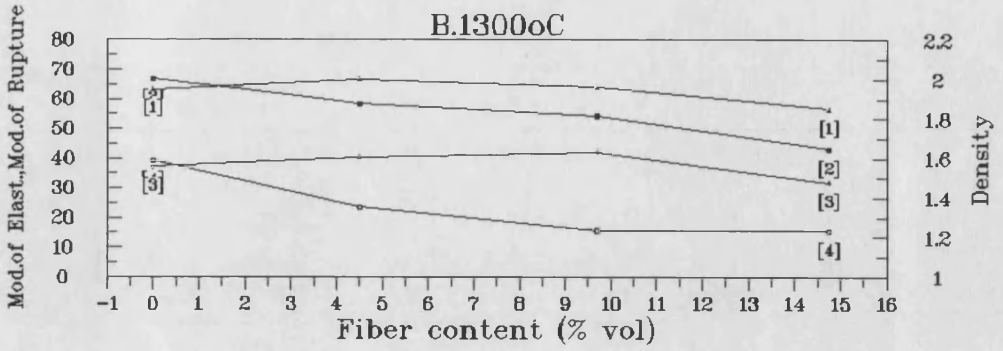

Fig.41 (cont.) (b) Graphic representation of the variation of mechanical properties with δ-AI_2O_3 (Saffil) fibre content at 1300°C:[1] Density (g/cm^3), [2] Modulus of Elasticity from dynamic testing, E_d (GPa), [3] Modulus of Rupture MOR (MPa) , [4] Modulus of elasticity from bending E_b (GPa).

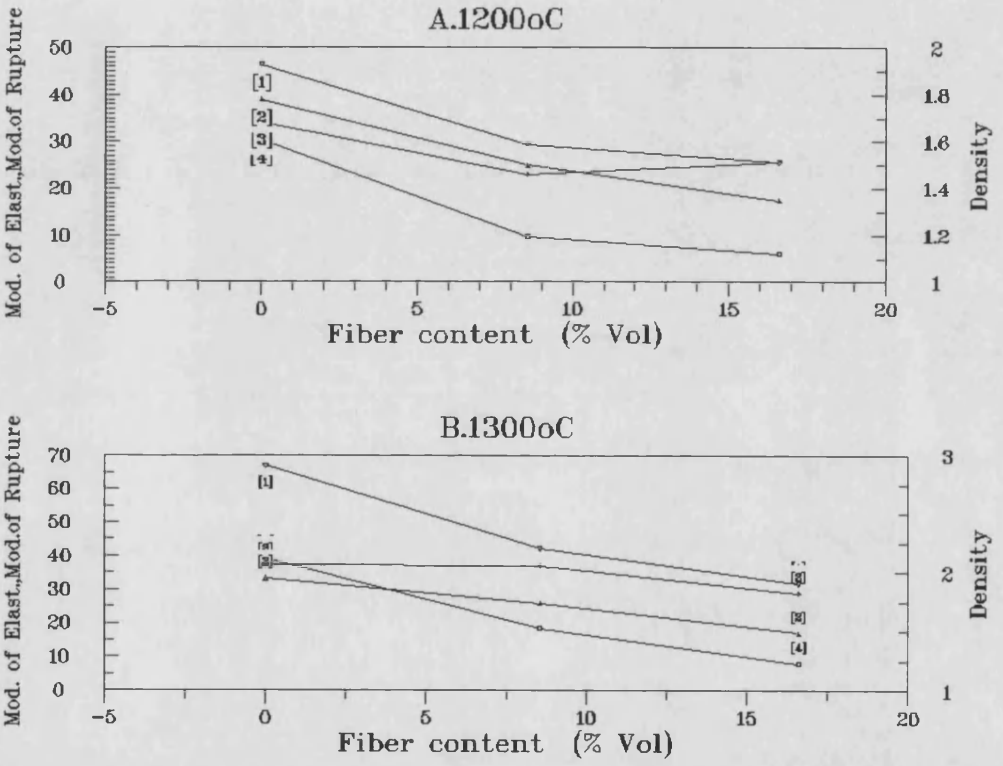

Fig.42 Graphic representation of the variation of mechanical properties with Grafil fibre content at different sintering temperatures; **(a)1200°C , (b) 1300°C** :
[1] Modulus of Elasticity from dynamic testing, E_d (GPa), [2] Density (g/cm^3), [3] Modulus of Rupture MOR (MPa) , [4] Modulus of elasticity from bending E_b (GPa).

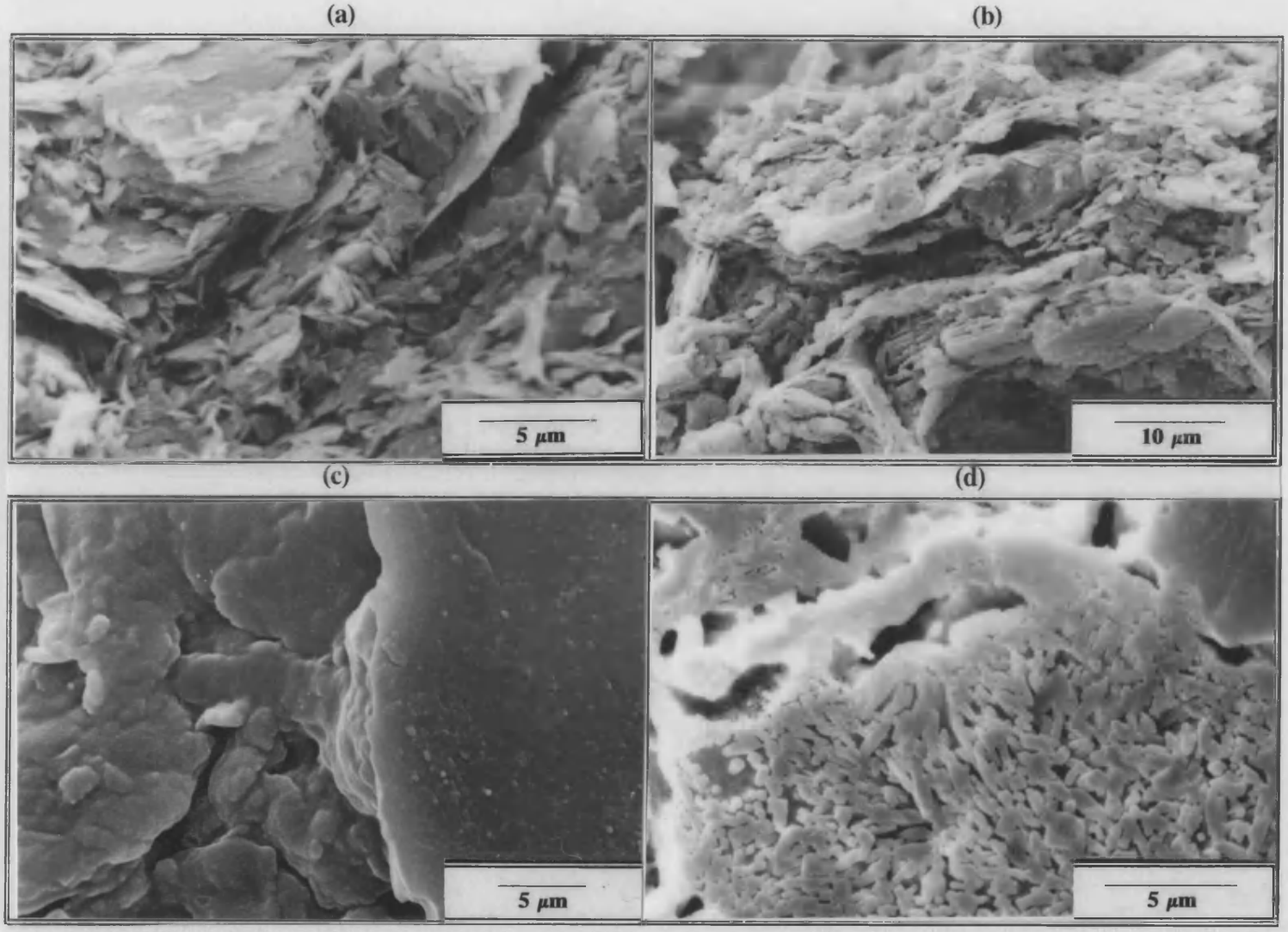

Fig.43 SEM micrographs from Kaolin (a) in "as received condition" and sintered at: (b) 1000°C, (c) 1100°C, and (d) 1200°C.

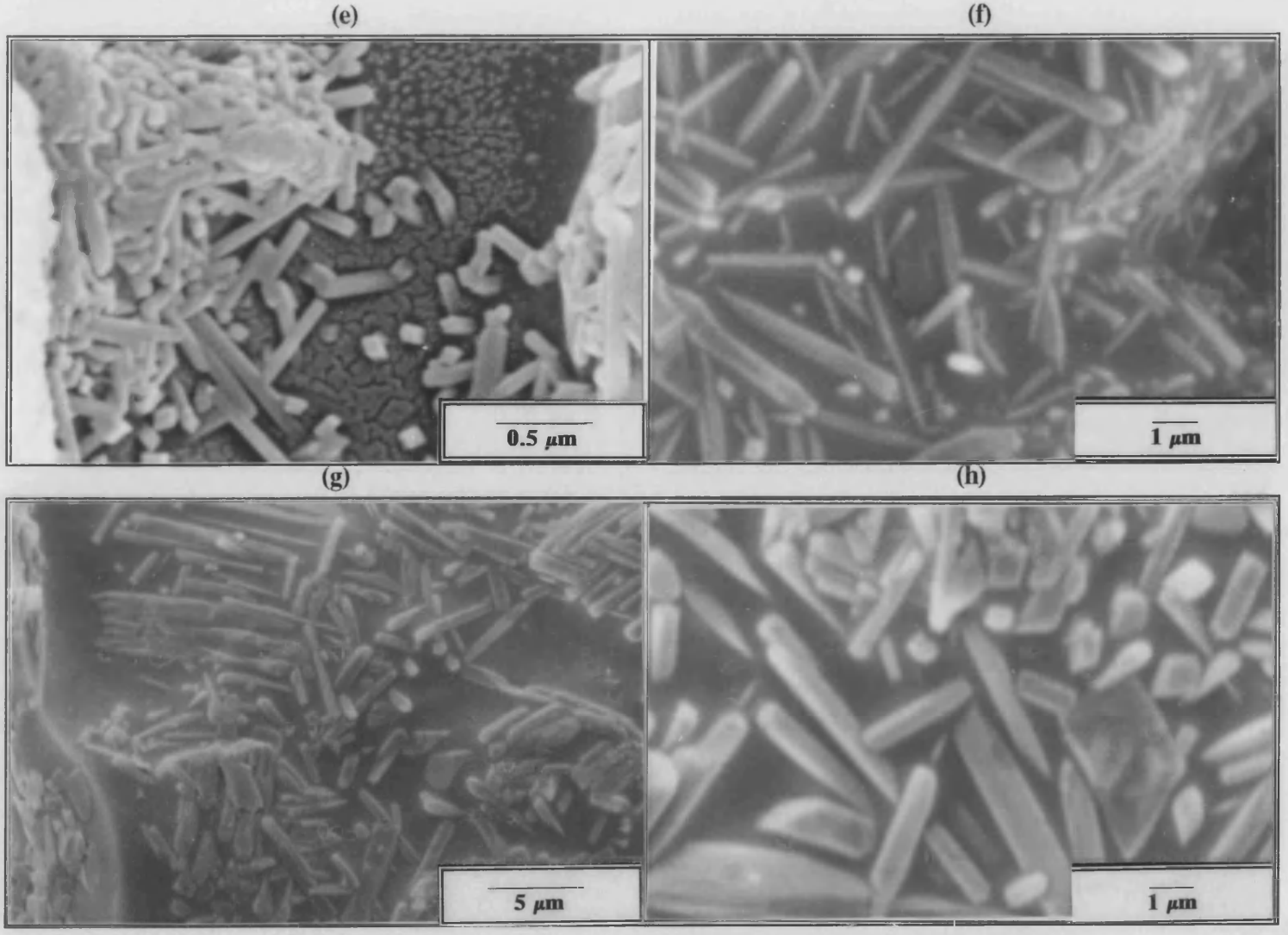

Fig.43 (cont.) SEM micrographs from Kaolin (e) 1300°C, (f) 1400°C (g) and (h)1500°C.

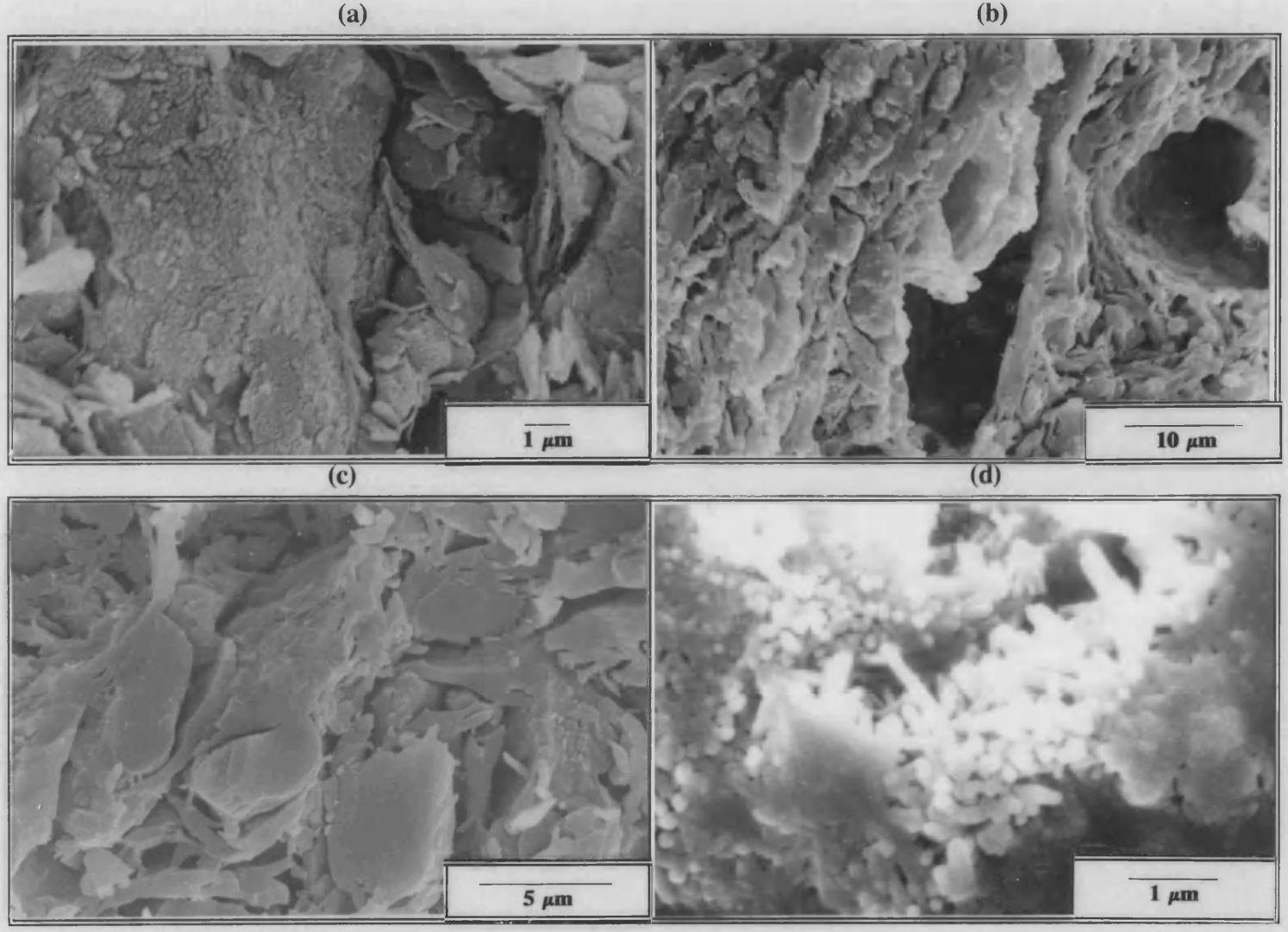

Fig.44 SEM micrographs from Pottery (a) 900°C, (b) 1000°C, (c) 1050°C, (d) 1100°C.

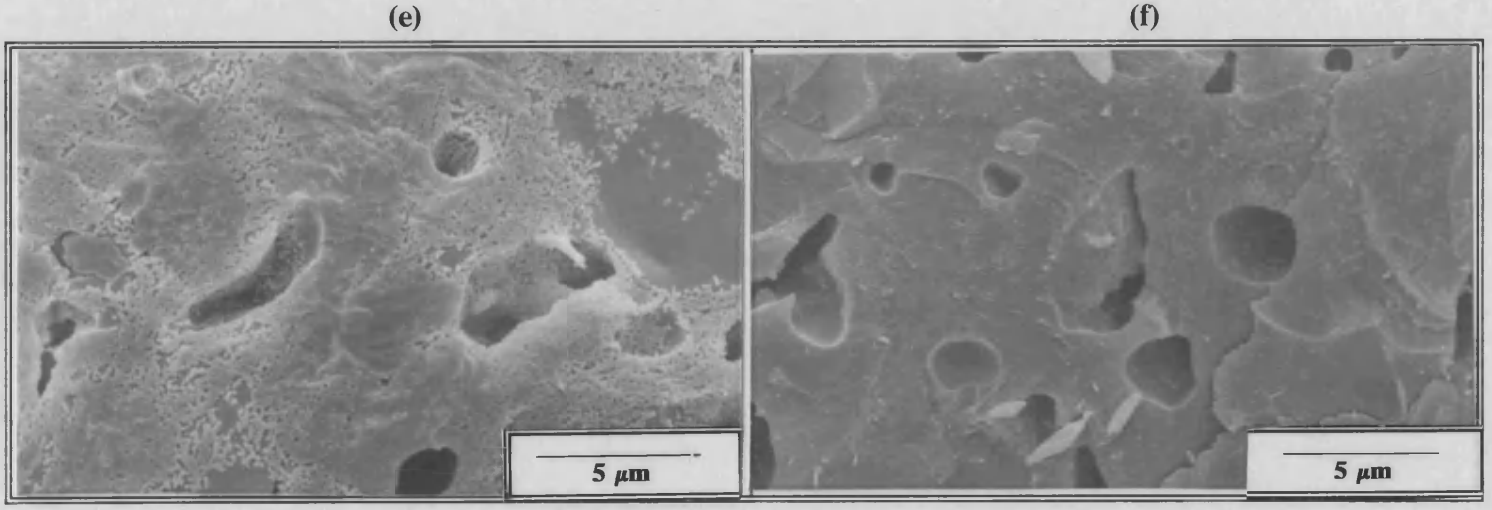

Fig.44 (cont.) SEM micrographs from Pottery Mixture sintered at: (e) and (f) 1150°C

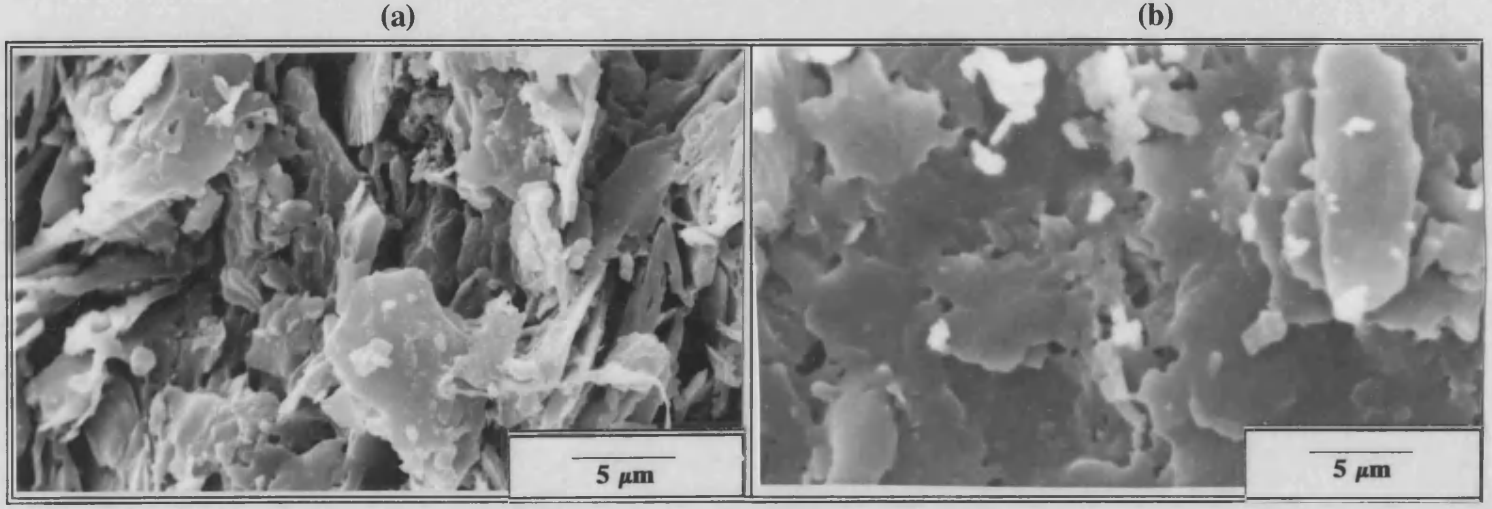

Fig.45 SEM micrographs from Brick-clay sintered at (a) 900°C, (b) 1000°C

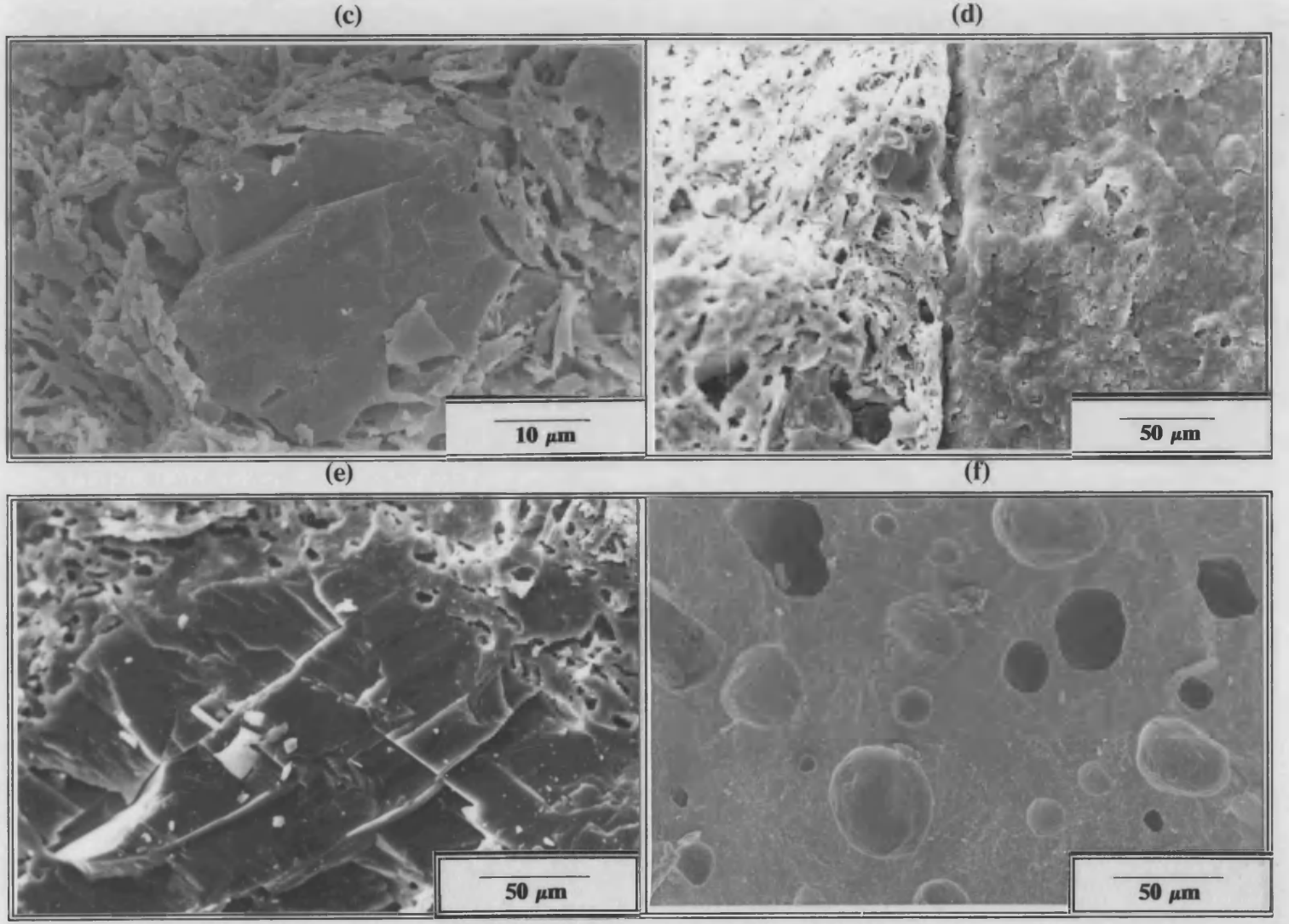

Fig.45(cont.) SEM micrographs from Brick-clay sintered at: (c) 1050°C, (d) 1100°C , (e) and (f) 1150°C,

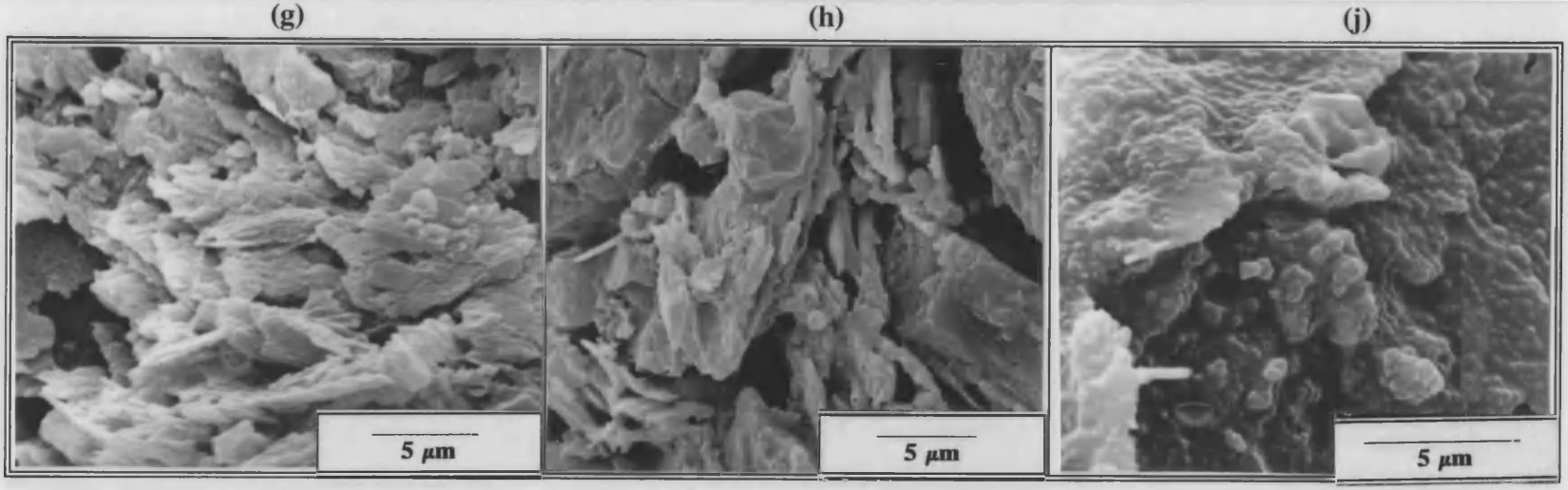

Fig.45 (cont) SEM micrographs from Brick-clay sintered at (g) P7, (h) P8, and (j) P9 sintering programmes

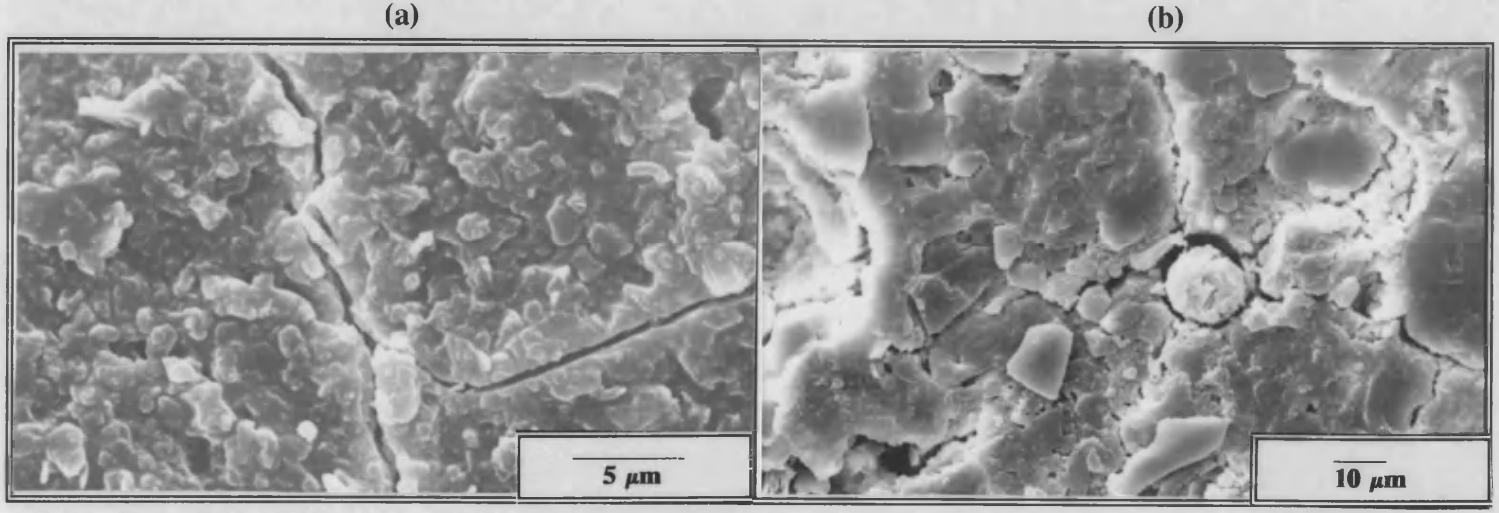

Fig.46 SEM micrographs from Kaolin+5% and 10% (W/W) Fly Ash composite sintered at 1000°C.

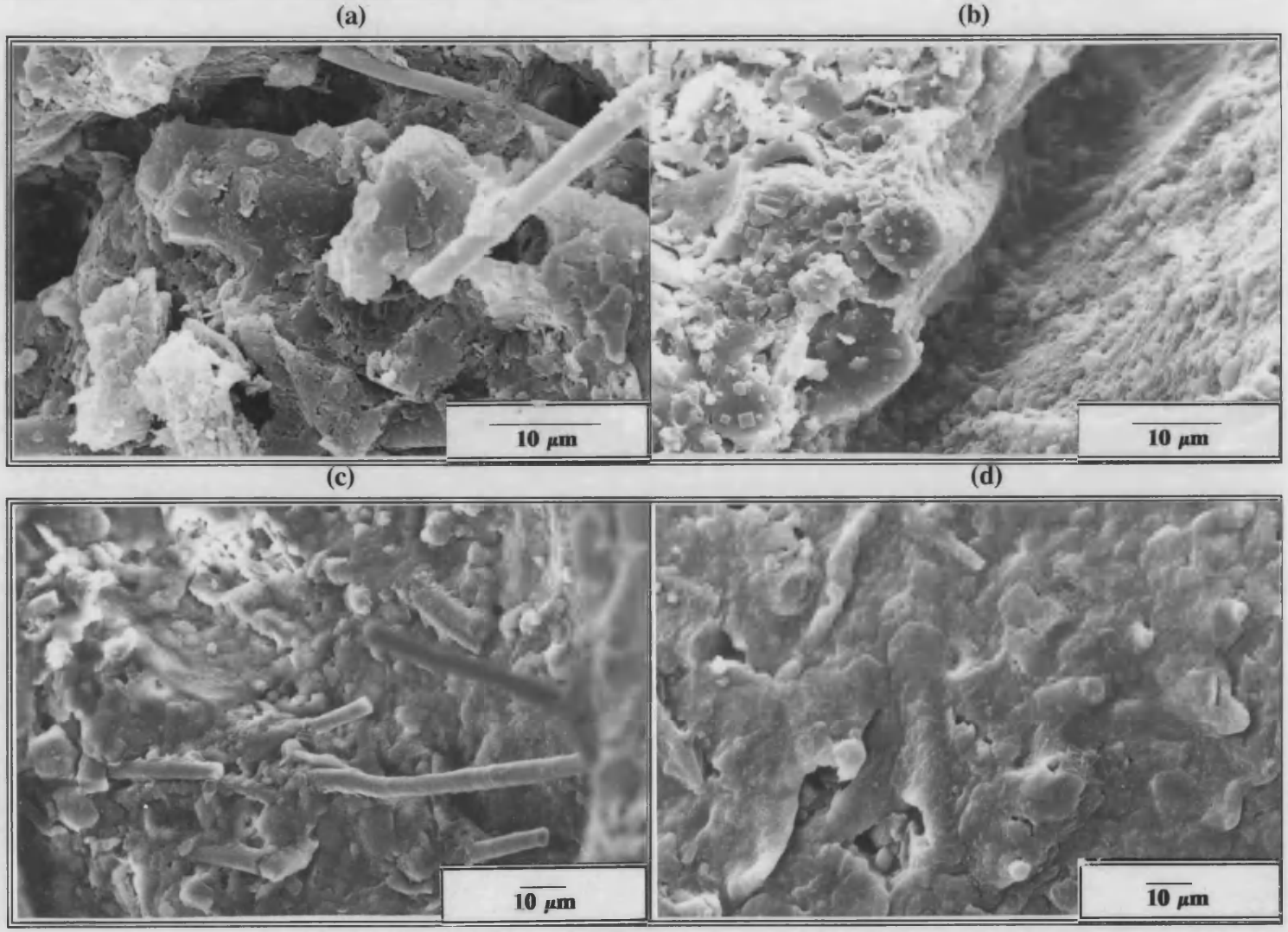

Fig.47 SEM micrographs from Kaolin+α-alumina (B95) Denka fibres sintered at 1000,1200 and 1300°C.
(a):9.2% fibres sint. at 1000°C, (b) 4.7% fibres sint. at 1200°C, (c) 14% fibres sint. at 1300°C, (d) 9.2% fibres sint. at 1300°C.

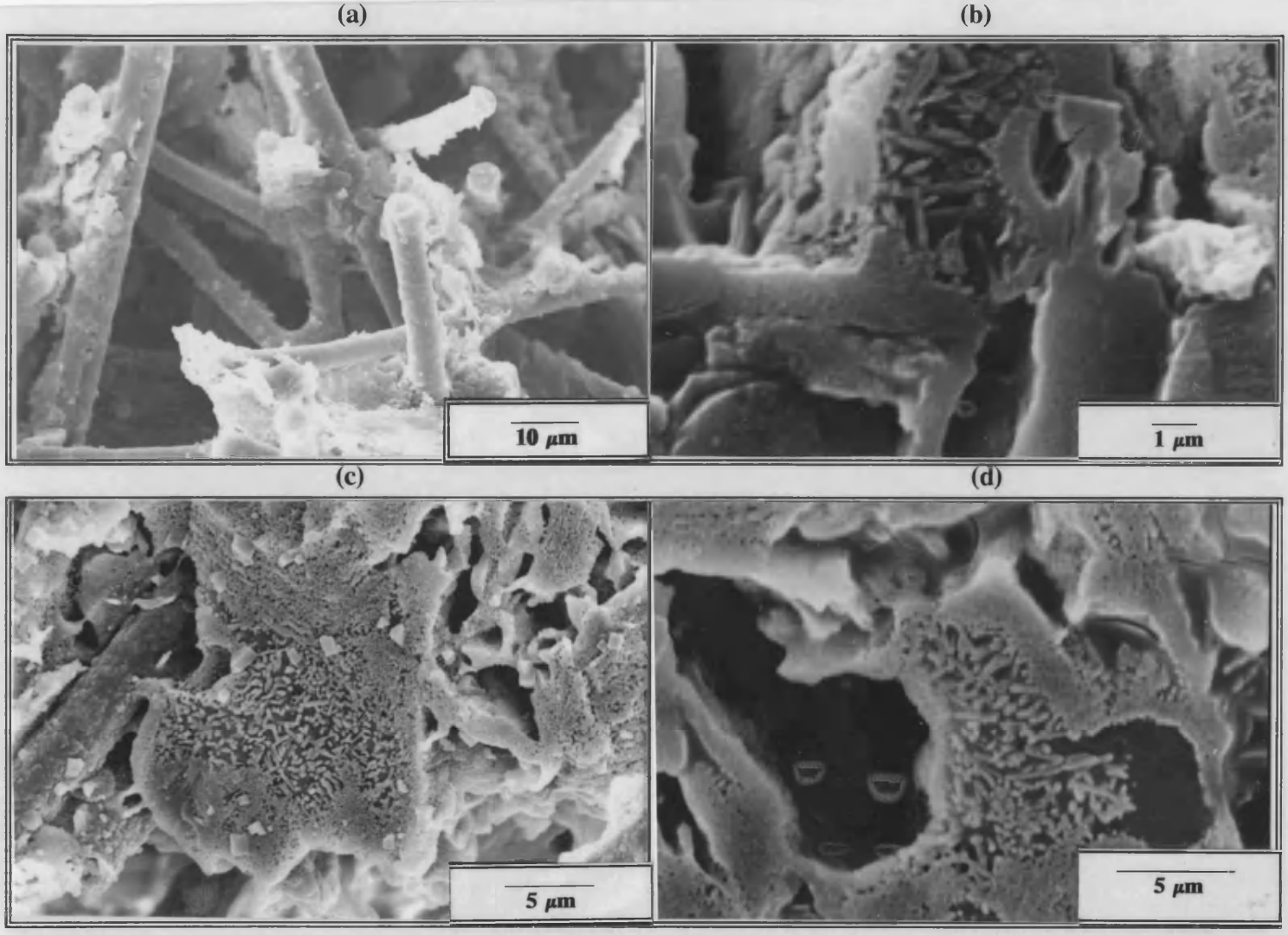

Fig.48 SEM micrographs from Kaolin+Saffil fibres sintered at 1200 and 1300°C, (a):9.7% fibres sint. at 1200°C, (b) 14.75% fibres sint. at 1200°C, (c) 4.5% fibres sint. at 1300°C, (d) 14.75% fibres sint. at 1300°C.

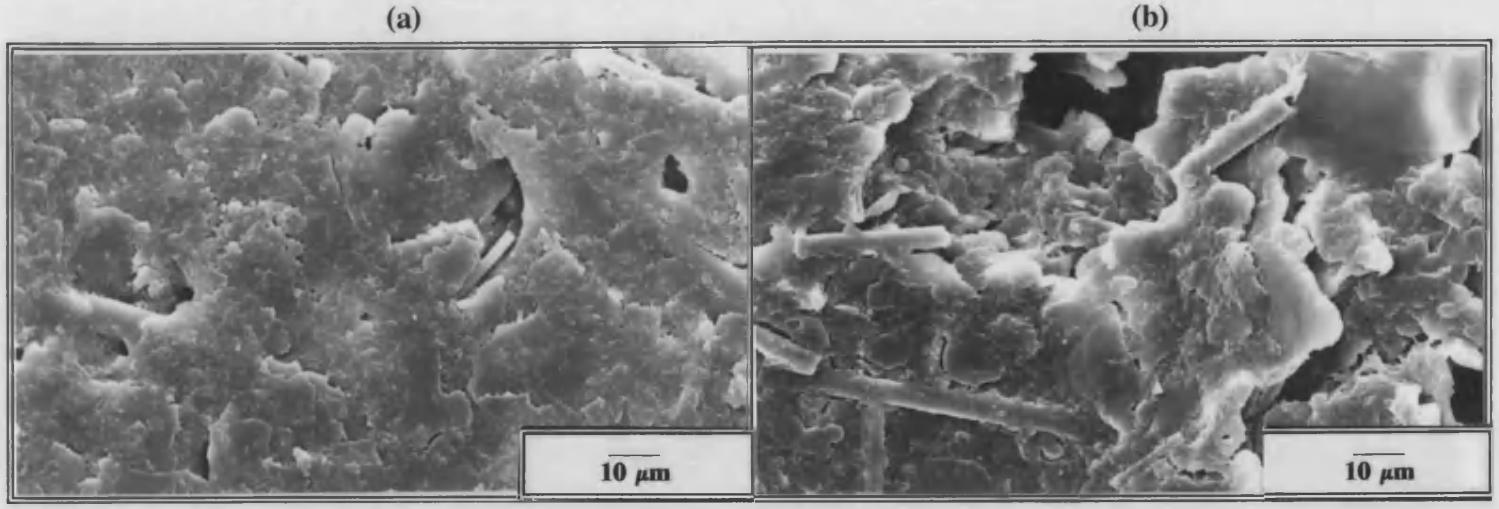

Fig.49 SEM micrographs from Kaolin+9.7% vol. mullite (B80K) Denka fibres sintered at: (a) 1000 and (b) 1200°C

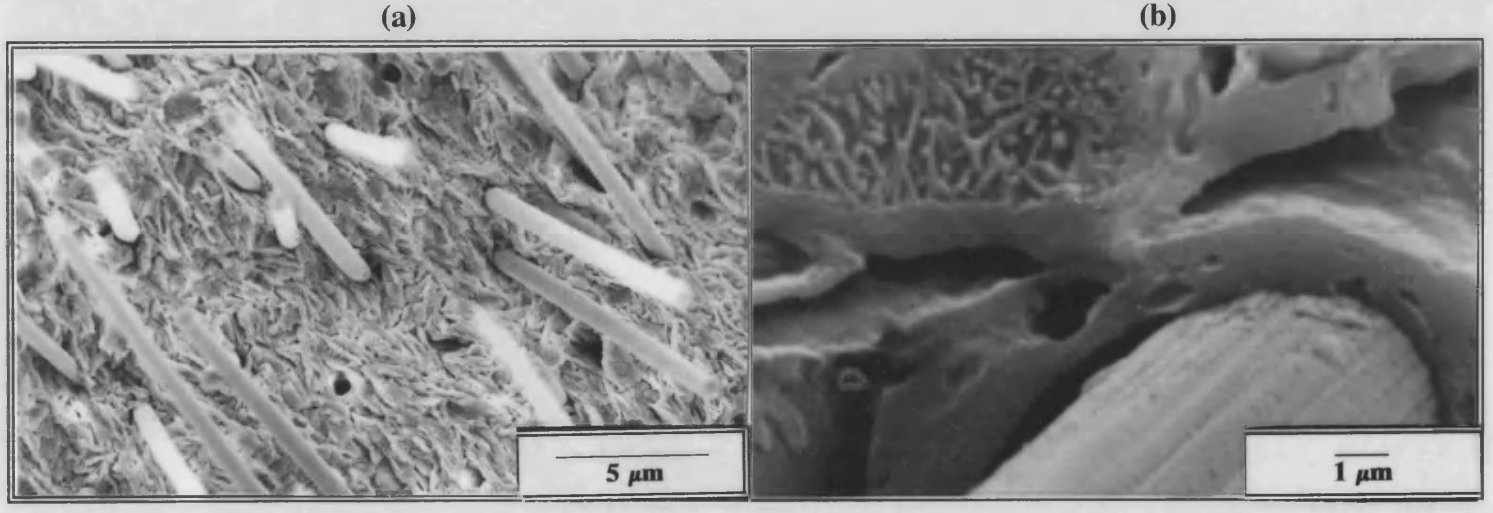

Fig.50 SEM micrographs from Kaolin+Grafil: (a) 8.55% fibres sint. at 1000°C, (b) 16.6% fibres sintered at 1200°C.

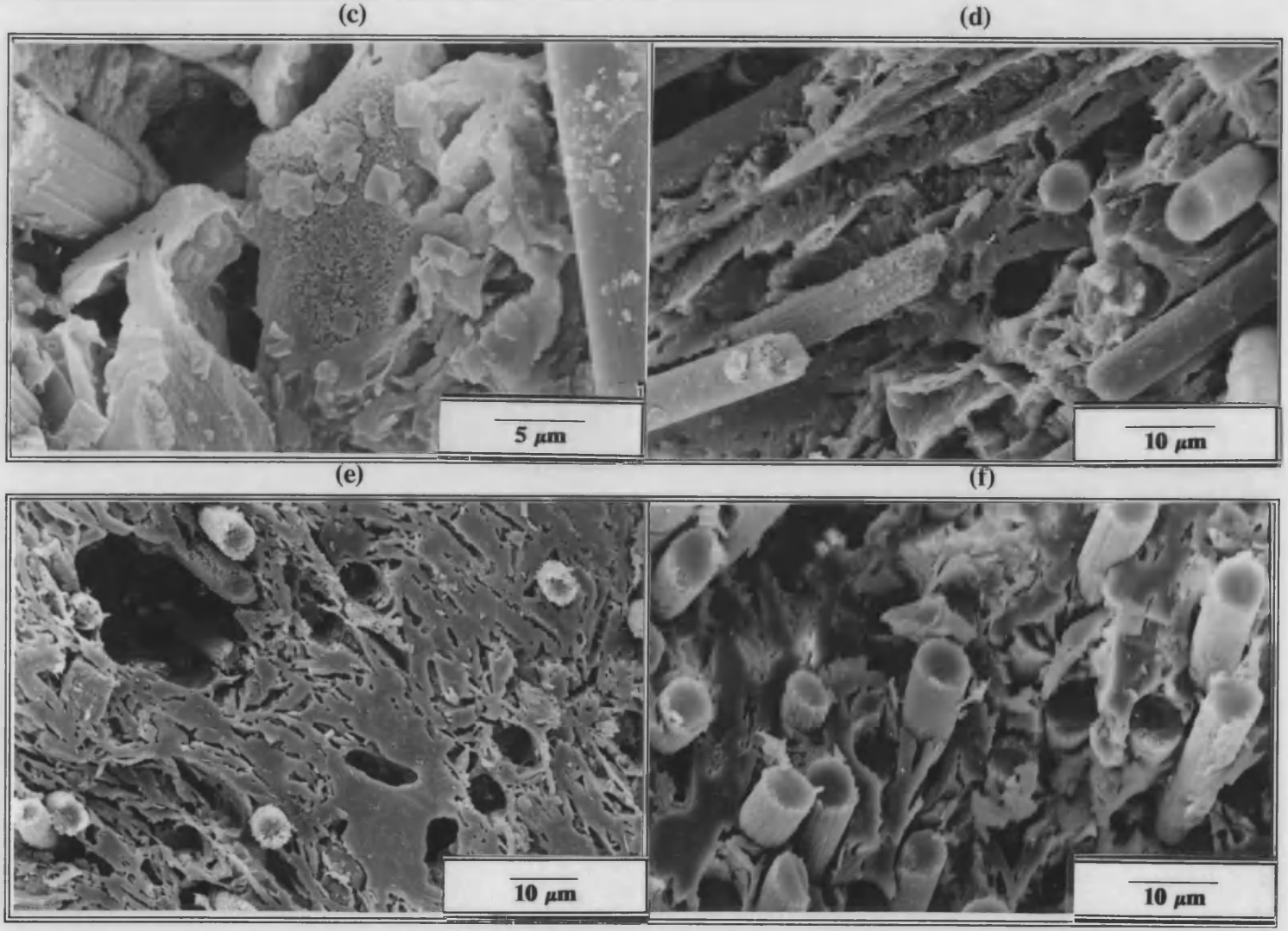

Fig.50 (cont.) SEM micrographs from Kaolin+Grafil fibres: (c) and (d) 16.6% fibres sintered at 1200°C, (e): 8.55% fibres sintered at 1300°C, (f) 16.6% fibres sintered at 1300°C.

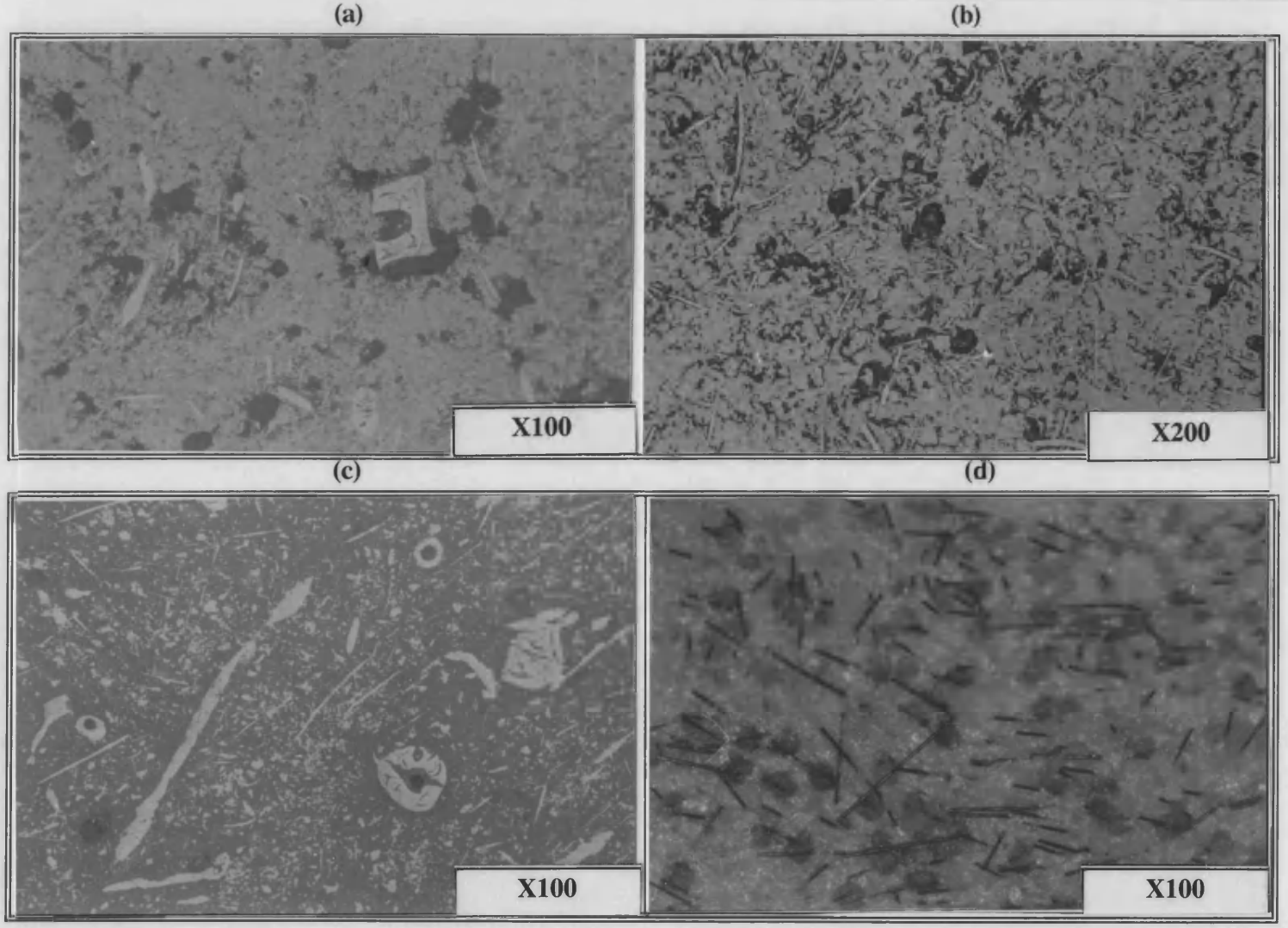

Fig.51 OM micrographs from fibre-kaolin composites: (a) 9.2% α-Al_2O_3 sint. at 1200°C, (b) 4.5% Saffil sint. at 1300°C, (c) 9/7% mullite sint. at 1200°C, (d) 8.55% Grafil sint. at 1000°C.

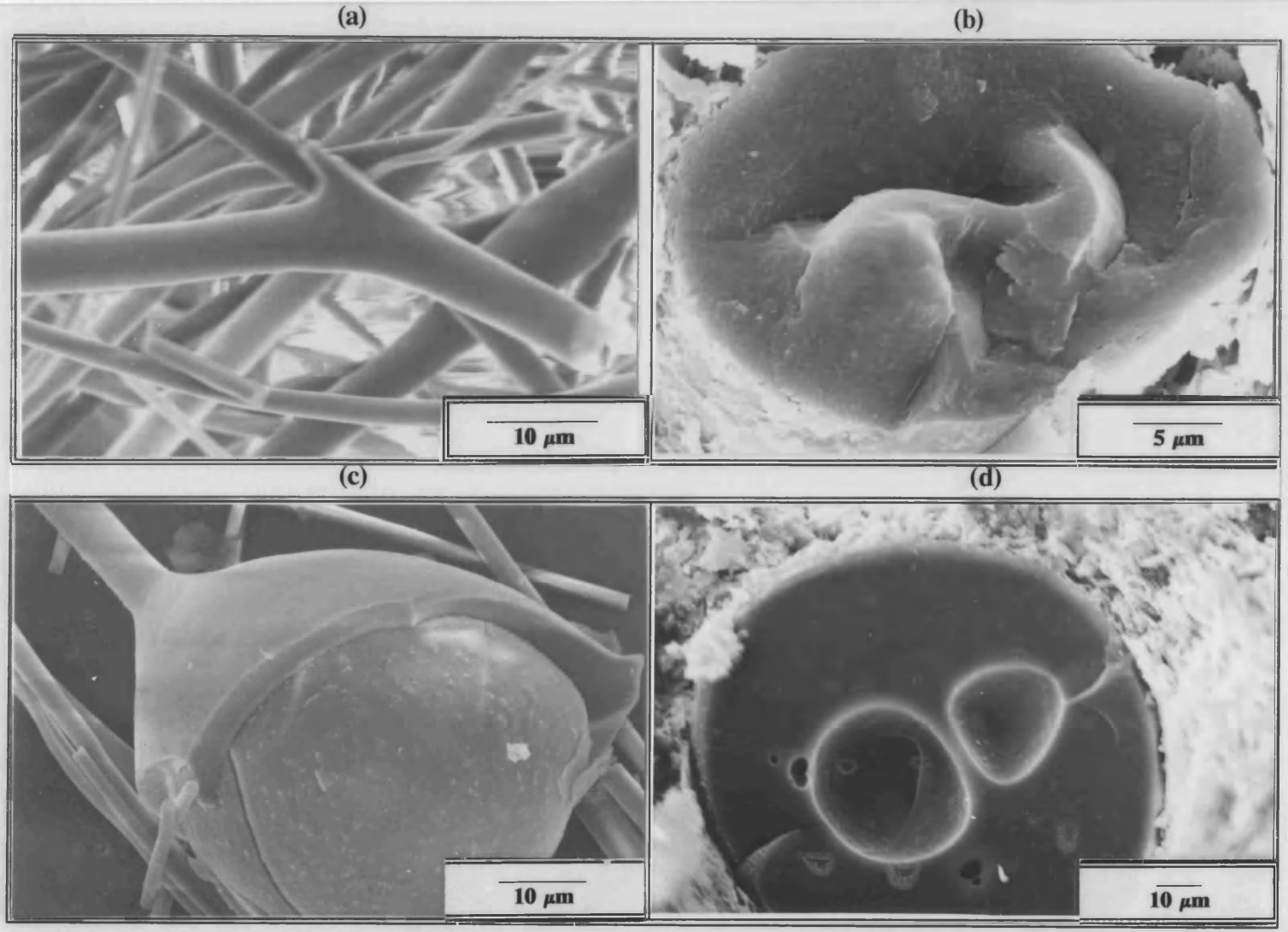

Fig.52 SEM micrographs from Denka fibres: (a) α-Al_2O_3 fibres in "as received condition", (b) fractured after sintering at 1200°C (c) and (d) non-fibrous material in "as received" condition and after sintering at fracture at 1000°C respectively.

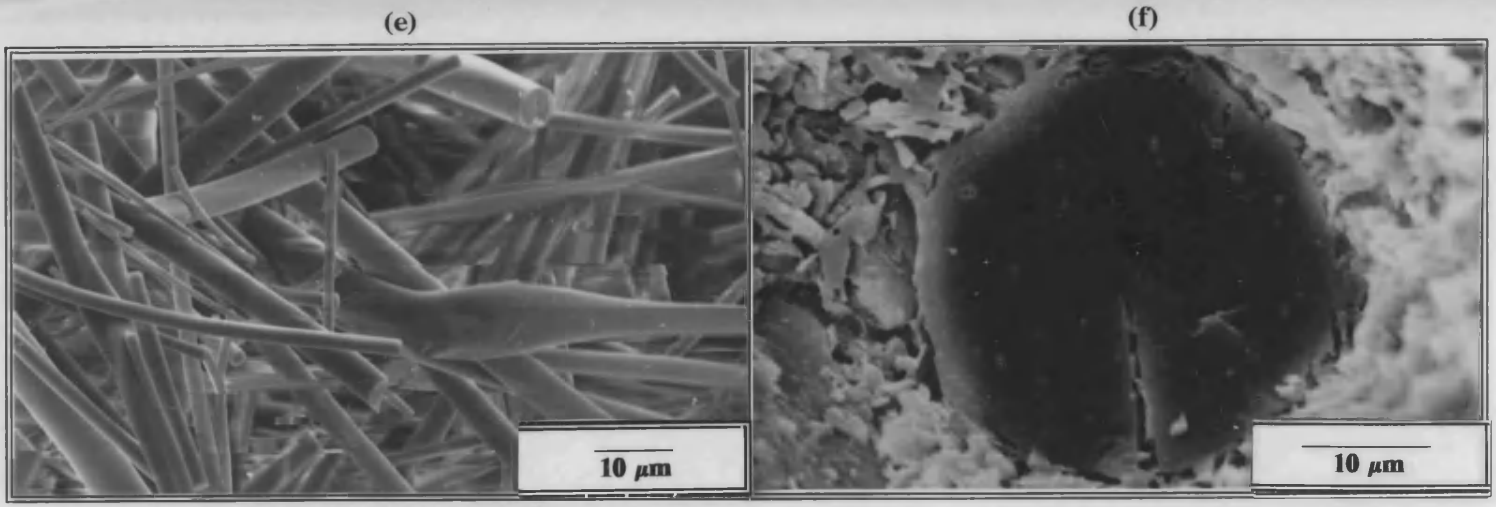

Fig.52 (cont.) (e) mullite fibres in "as received" condition, (f) fractured after sintering at 1200°C

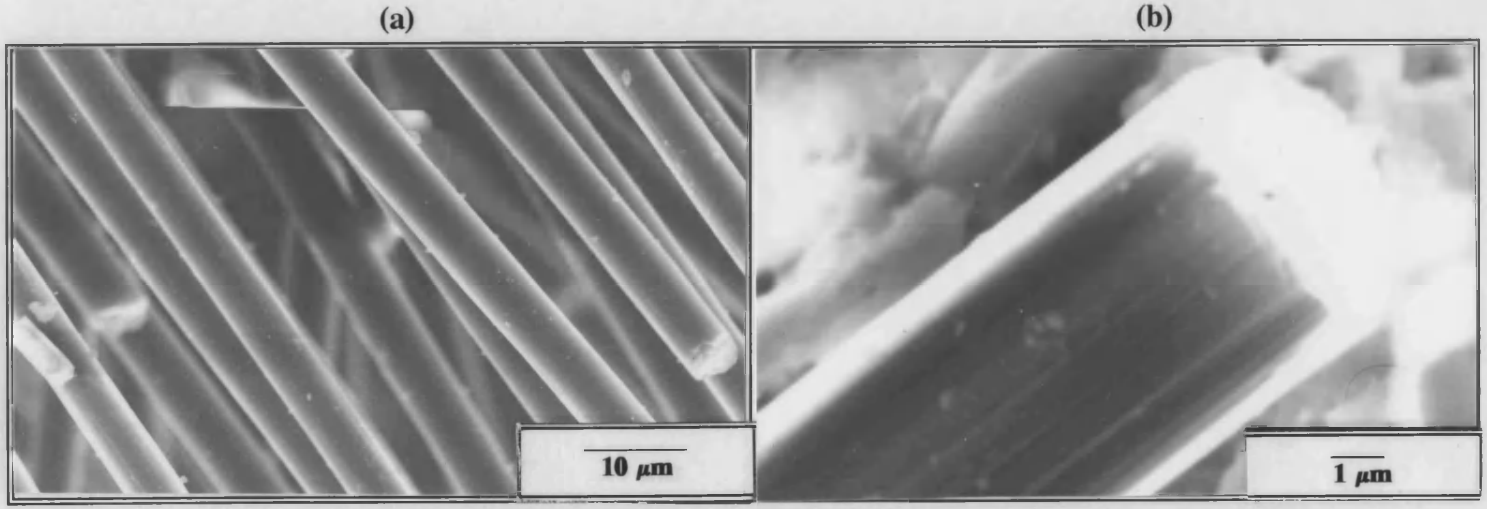

Fig.53 SEM micrographs from Grafil fibres: (a) in "as received condition, (b) fractured after sintering at 1200°C.

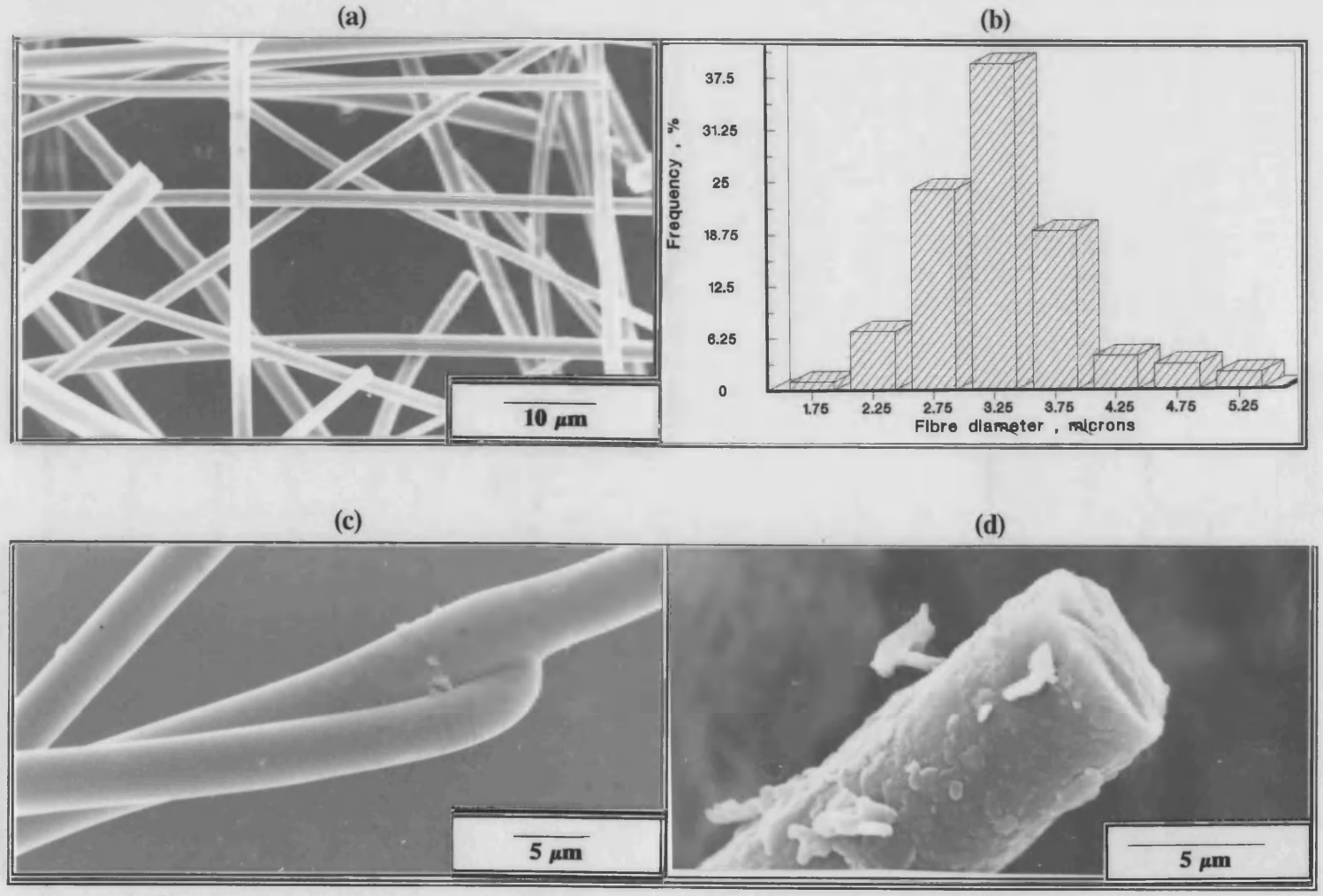

Fig.54 SEM micrographs from Saffil δ-Al_2O_3 fibres: (a) in "as received condition, (b) diameter distribution, (c) twin fibres in "as received condition" and (d) fractured fibre after sintering at 1200°C.

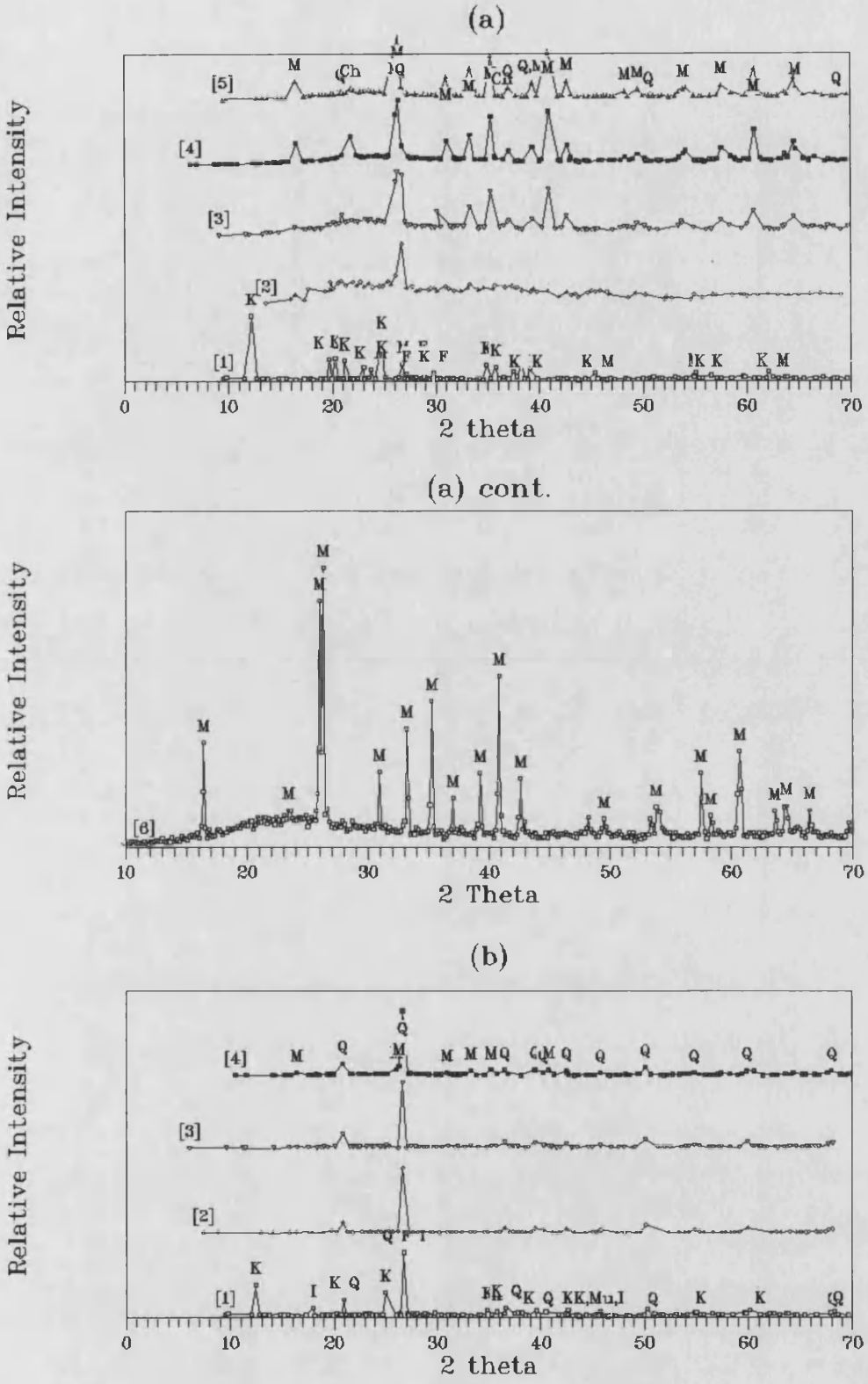

Fig.55 X-ray Diffraction patterns of pure ceramics; (a) Remblend kaolin: [1] "as received" condition and after sintering at [2] 1000, [3] 1100, [4] 1200 [5] 1300 and [6] 1500°C. (b) Pottery mixture: [1] in "as received condition" and after sintering at [2] 900, [3] 1000 and [4] 1100°C.
K=Kaolinite, Q=Quartz, Mu=Muscovite, I=Illite, F=Feldspar, M=Mullite

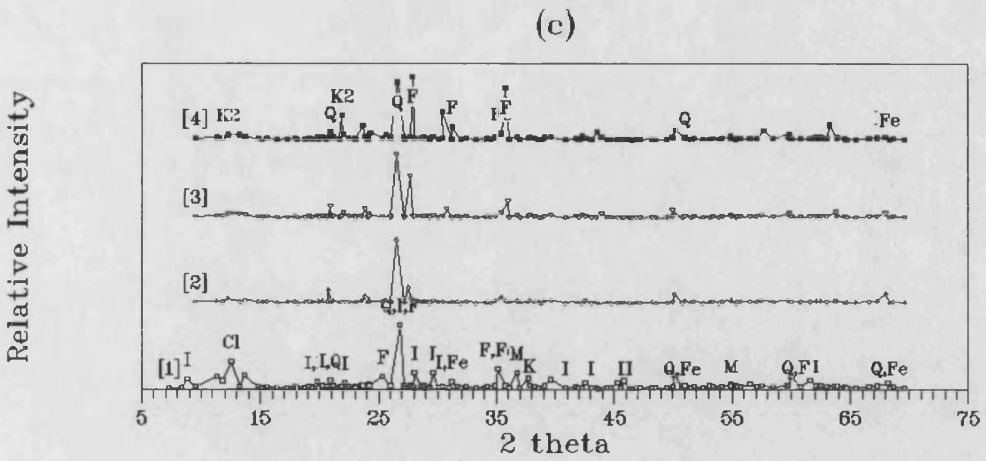

Fig.55(c) Brick-clay in [1] "as received condition" and after sintering at [2] 900, [3] 1000 and [4] 1100°C.

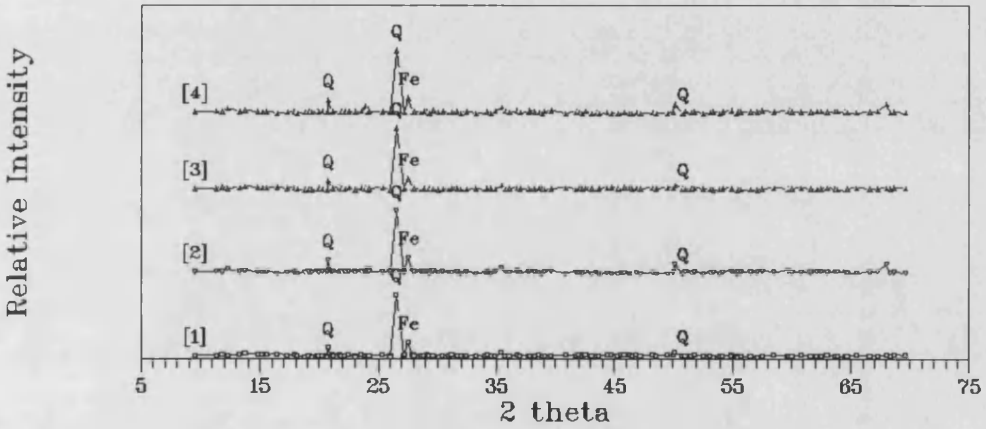

Fig.56 XRDs of Brick-clay sintered at 900°C at soaking time: [1] 1h, [2] 3h, [3] 6h, [4] 24h. Q=Quartz, I=Illite, F=Feldspar, Fe=Fe oxide, Cl=Chlorates, K_2=Potassium Oxide

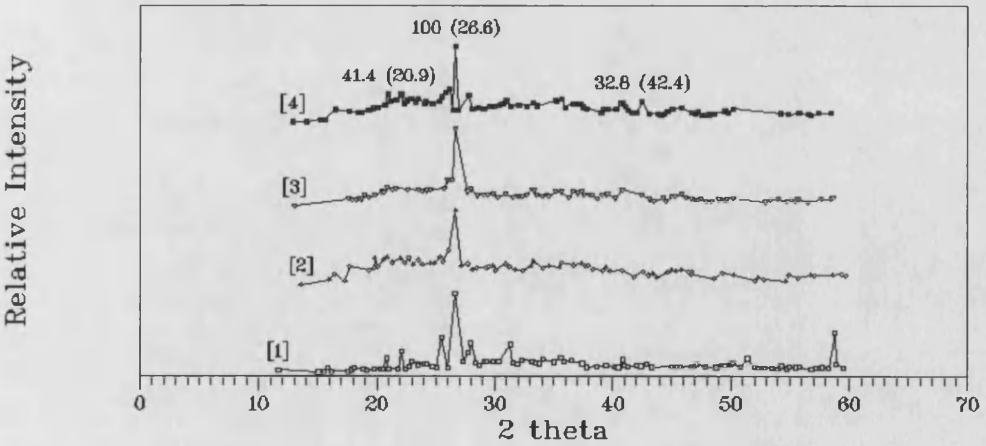

Fig.57 XRDs from Kaolin and Fly Ash combinations: [1] Kaolin, [2] Fly Ash, [3] kaolin+5% FA and [4] Kaolin+10% FA sintered at 1000°C.

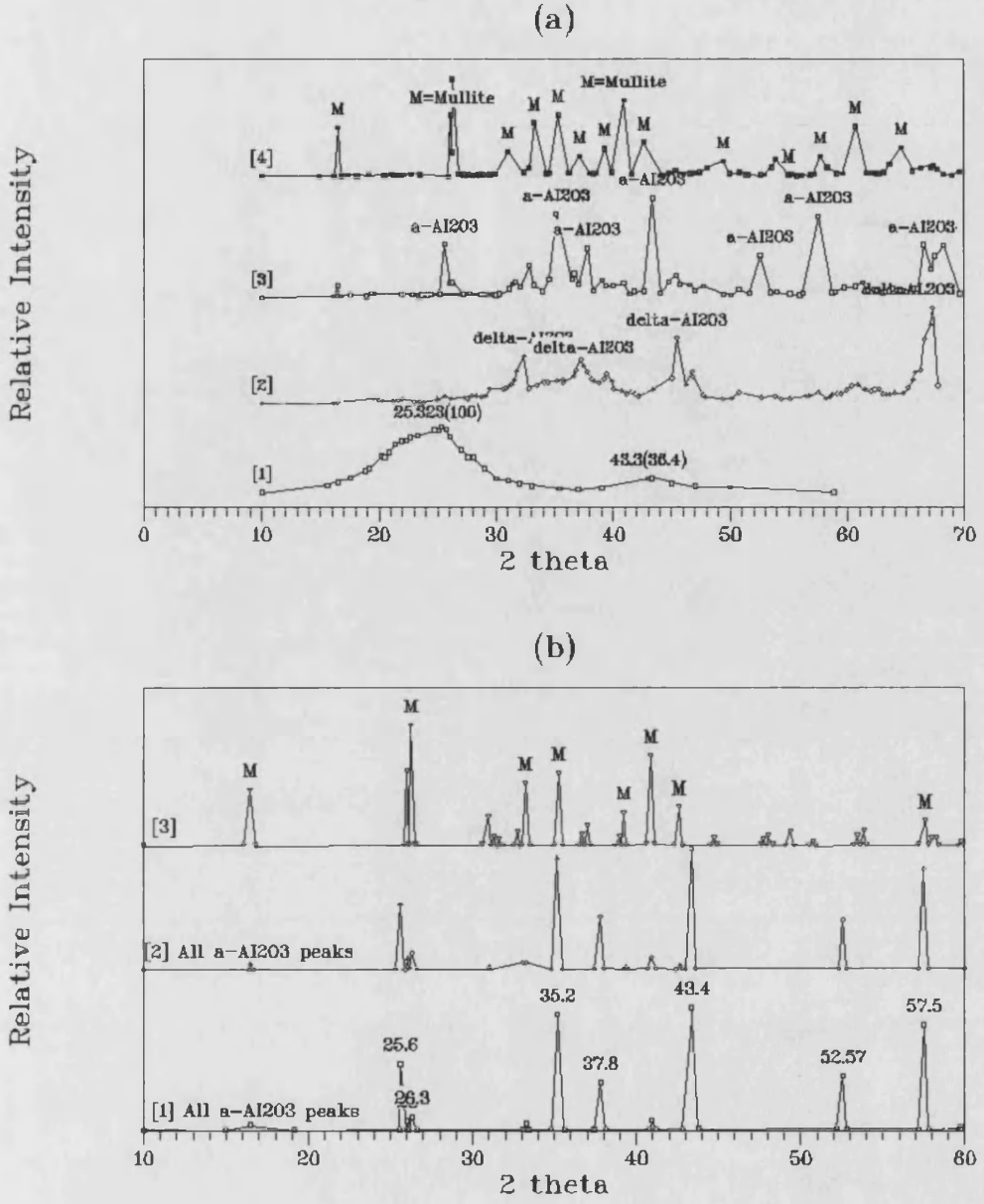

Fig.58 X-ray diffraction patterns from fibres:
(a) In as "received" condition: [1] Graphite Grafil fibres, [2] Saffil, [3] α-Al_2O_3 (B-95) and [4] mullite Denka B80K fibres .
(b) After sintering at 1300°C: [1] Saffil fibres, [2] α-Al_2O_3 B95 fibres
[3] mullite 80K fibres.

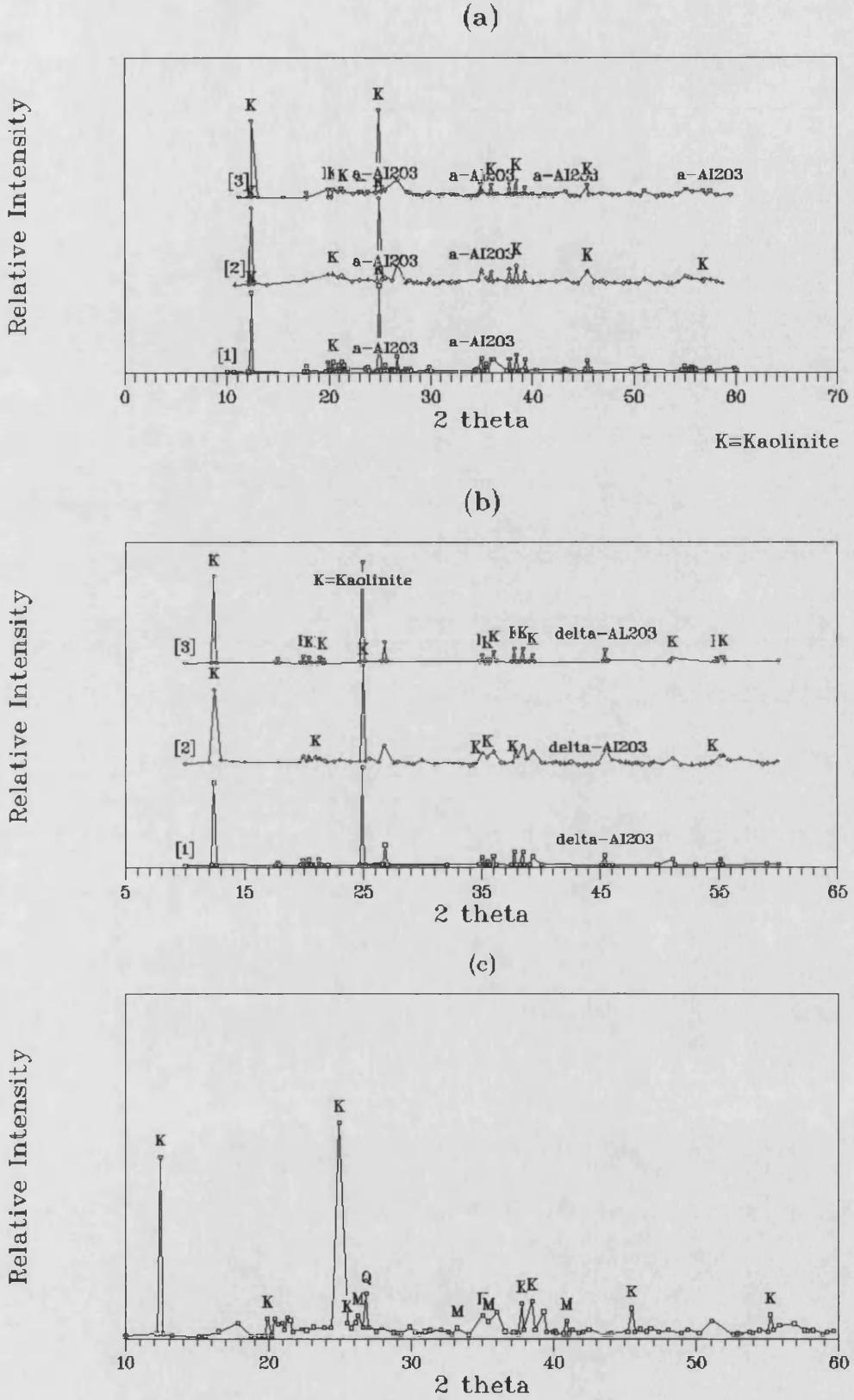

Fig.59 XRD peaks of Kaolin composites in as received condition with:
(a) [1] 4.7% , [2] 9.2 % and [3] 14 % (v/v) α-AI_2O_3 (B-95) fibres
(b) [1] 4.5% , [2] 9.7 % and [3] 14.75% Saffil fibres
(c) [1] 9.7% (v/v) mullite fibres.

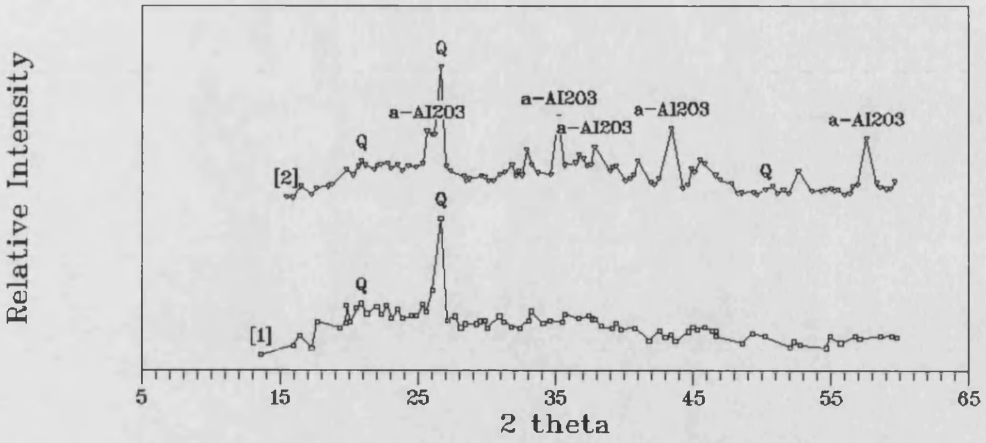

Fig.60 Comparison of XRDs from [1] pure kaolin with those from [2] kaolin composite containing 14% (v/v) α-AI_2O_3 fibres, both after sintering at 1000°C.

(a)

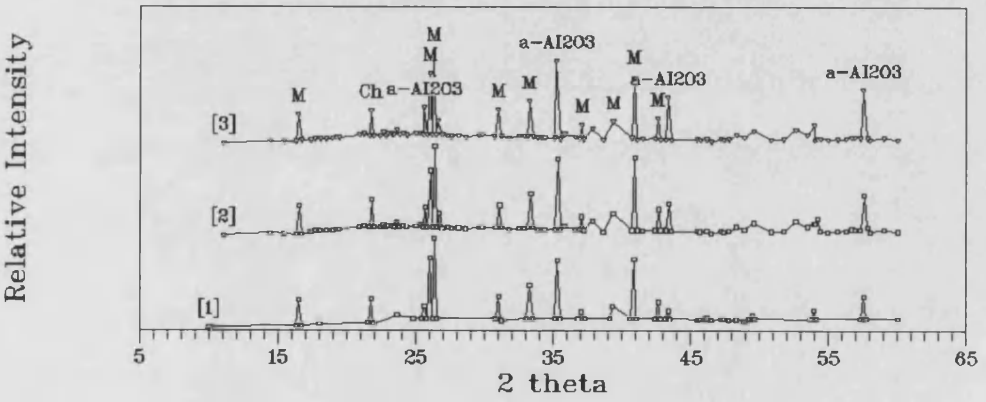

(b)

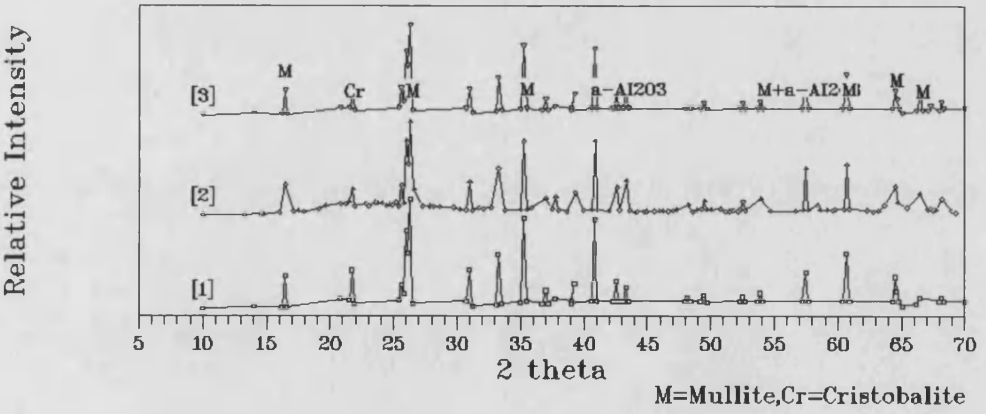

Fig.61 XRD peaks from kaolin composites after sintering at 1200°C:
(a) α-AI_2O_3 fibres: [1] 4.7% , [2] 9.2%, [3] 14% vol. fibres.
(b) δ-AI_2O_3 fibres: [1] 4.5% , [2] 9.7%, [3] 14.75 % vol. fibres.

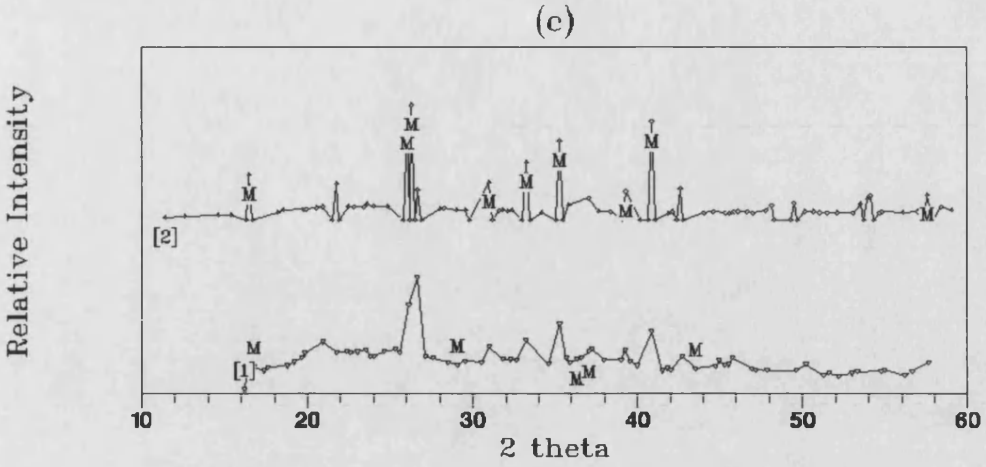

Fig.61(c) XRD peaks from kaolin+ mullite 9.7 % (v/v) composite at [1] 1000°C and [2] 1200°C.

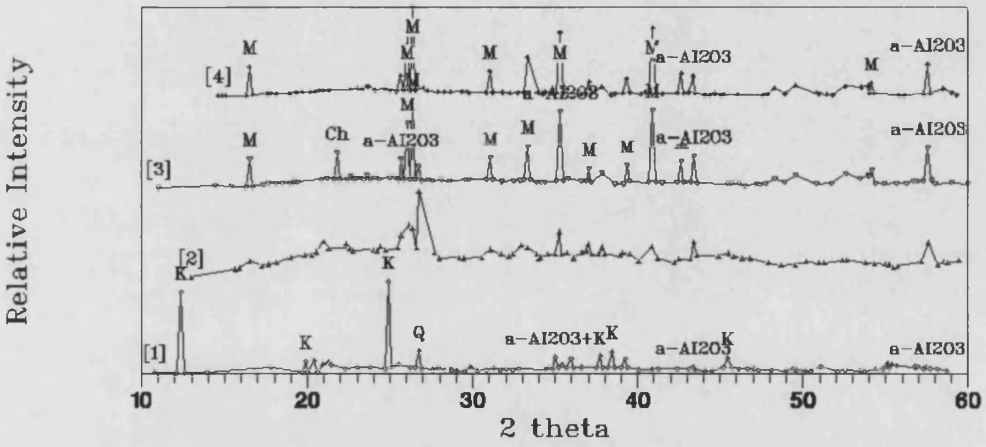

Fig.62 The effect of sintering temperature on a kaolin+9.2 % vol. α-AI_2O_3 composite: [1] "as received condition", [2] 1000°C, [3] 1200°C [4] 1300°C.

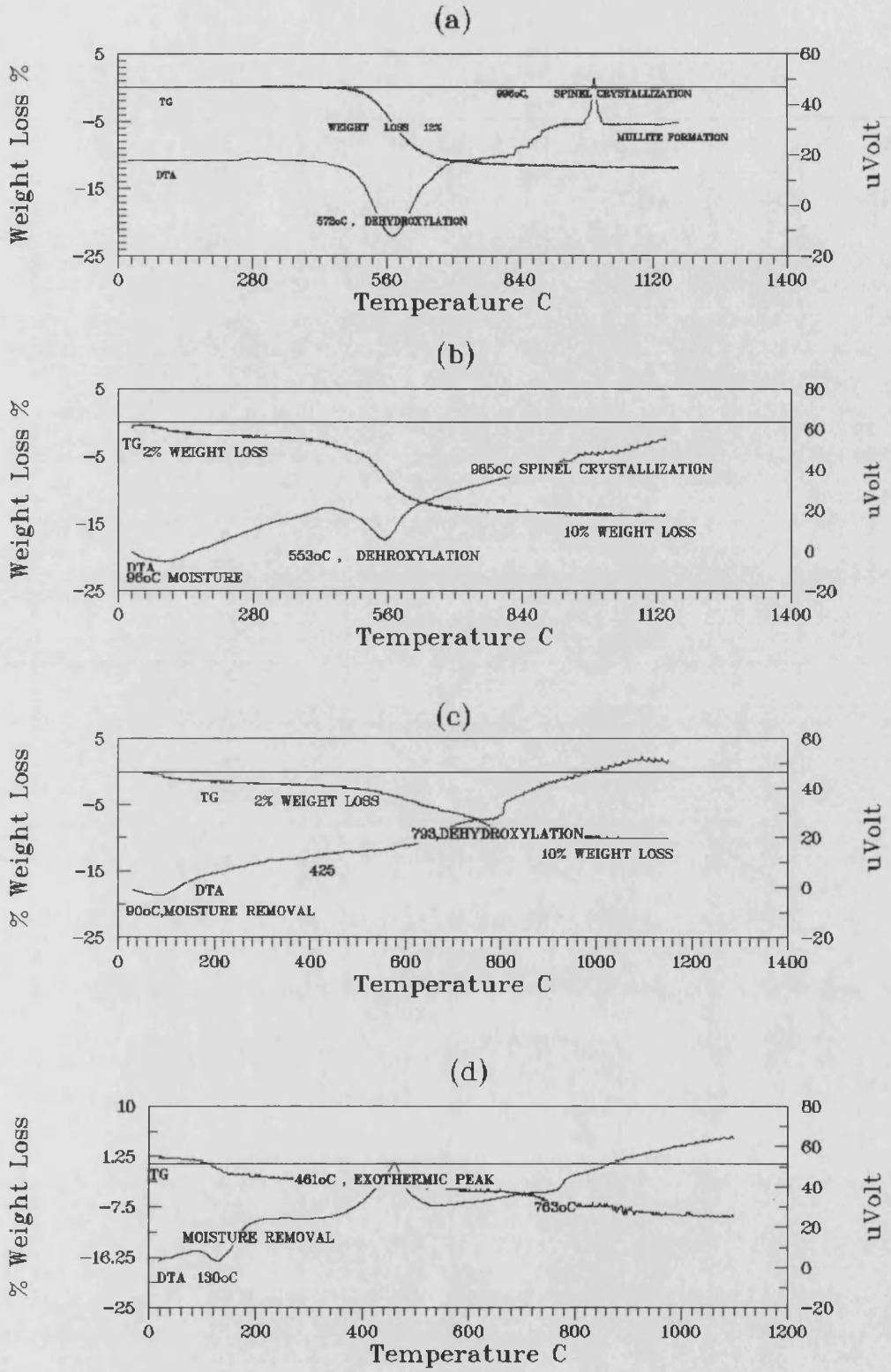

Fig.63 Tg-DTA curves of ceramic powders in as received condition;
(a) Kaolin ,(b) Pottery Mixture ,(c) Brick-clay , (d) Fly Ash

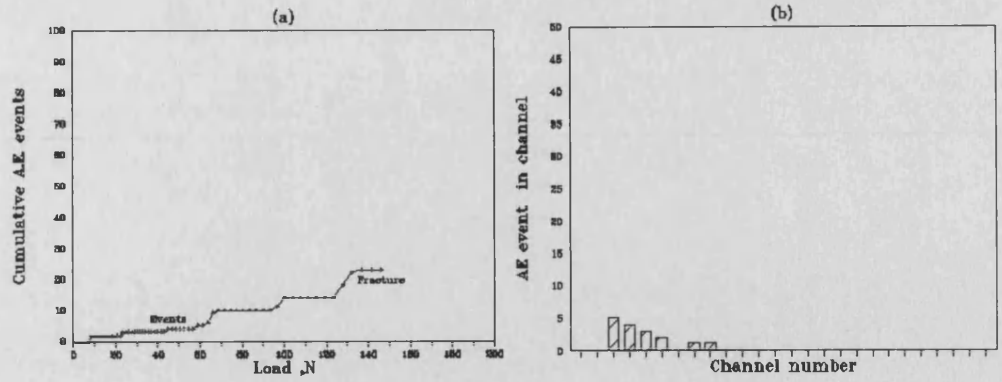

Fig.64 AE from glass specimens during 3-point bending : **(a)** The cumulative events-load curve and **(b)** Event distribution in channels .

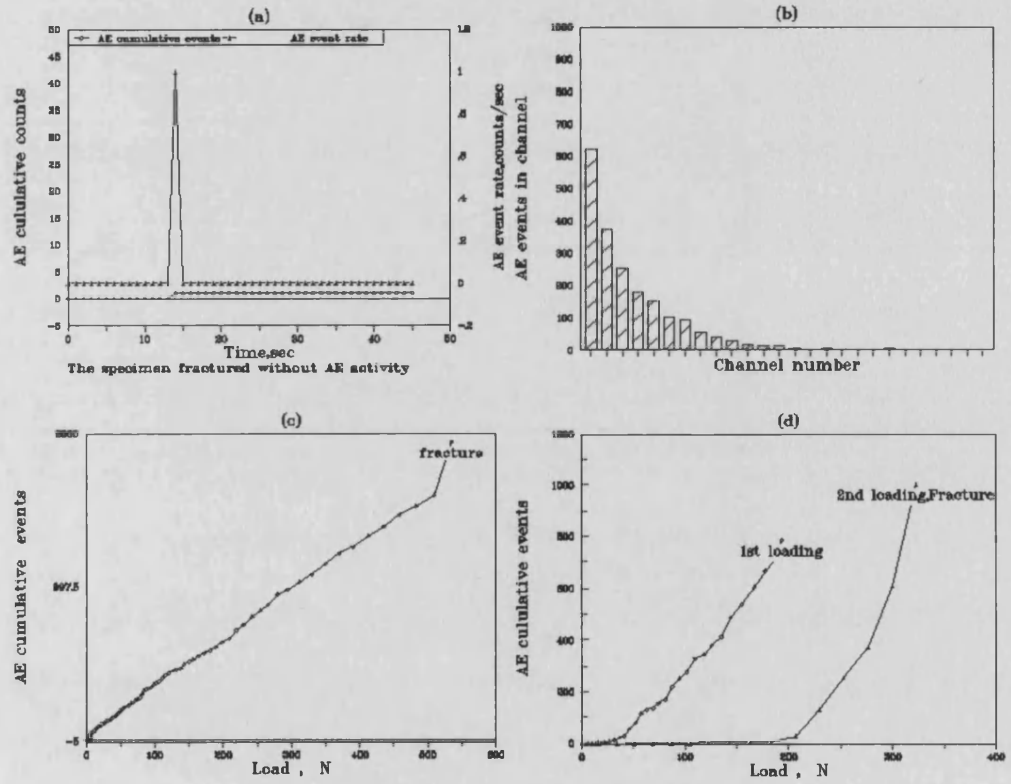

Fig.65 AE from kaolin specimens:during 3-point bending :
(a) AE cumulative events and rate as a function of time from kaolin in as "received" condition , (b) Typical AE amplitude distribution after sintering at 1300°C, (c) AE events as a function of load after sintering at 1300°C, (d) Kaiser effect after sintering at 1300°C.

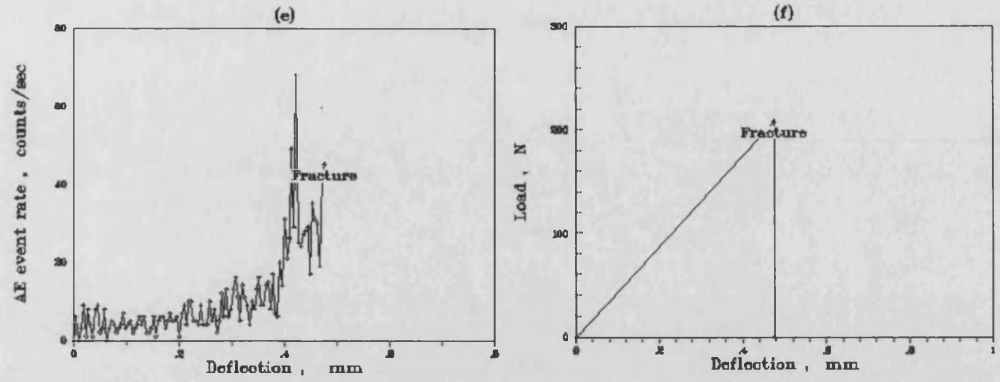

Fig.65 (cont.) (e)Event rate distribution as a function of deflection after sintering at 1100°C, (f) Typical load-deflection curve after sintering at 1100°C.

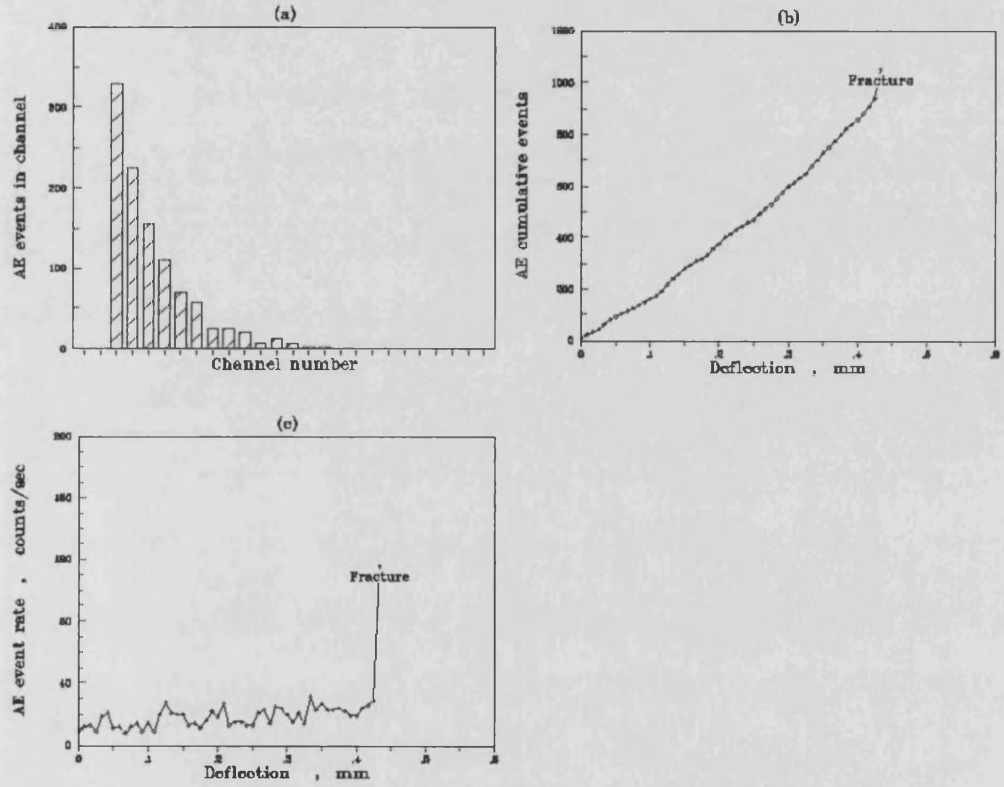

Fig.66 AE from pottery mixture specimens tested at 3-point bending: (a) Amplitude distribution after sintering at 1000°C, (b) AE events versus deflection after sintering at 1000°C, (c) AE event rate versus deflection after sintering at 1000°C.

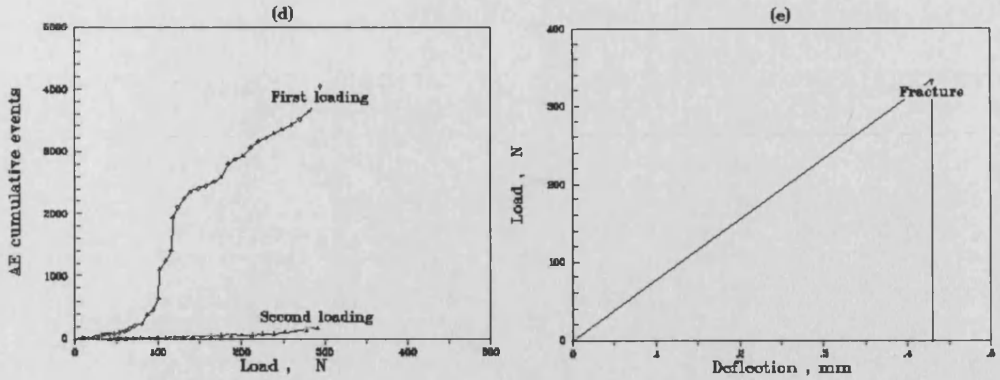

Fig.66 (cont.) Pottery Mixture (d) Kaiser effect after sintering at 1100°C, (e) load-deflection after sintering at 1000°C..

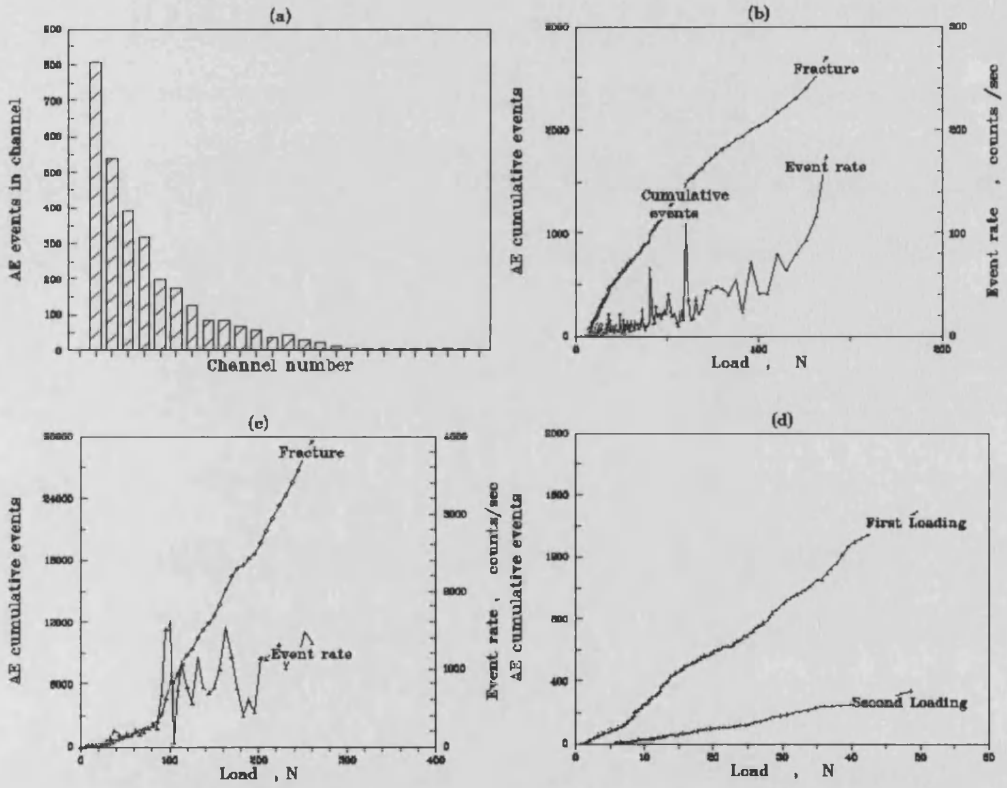

Fig.67 AE from Brick-clay specimens during 3-point bending: (a) Amplitude distribution after sintering at 1100°C, (b) Event-load distribution after sintering at 1100°C, (c) AE events and rate versus load after sintering at 950°C , (d) Kaiser effect after sintering at 1100°C.

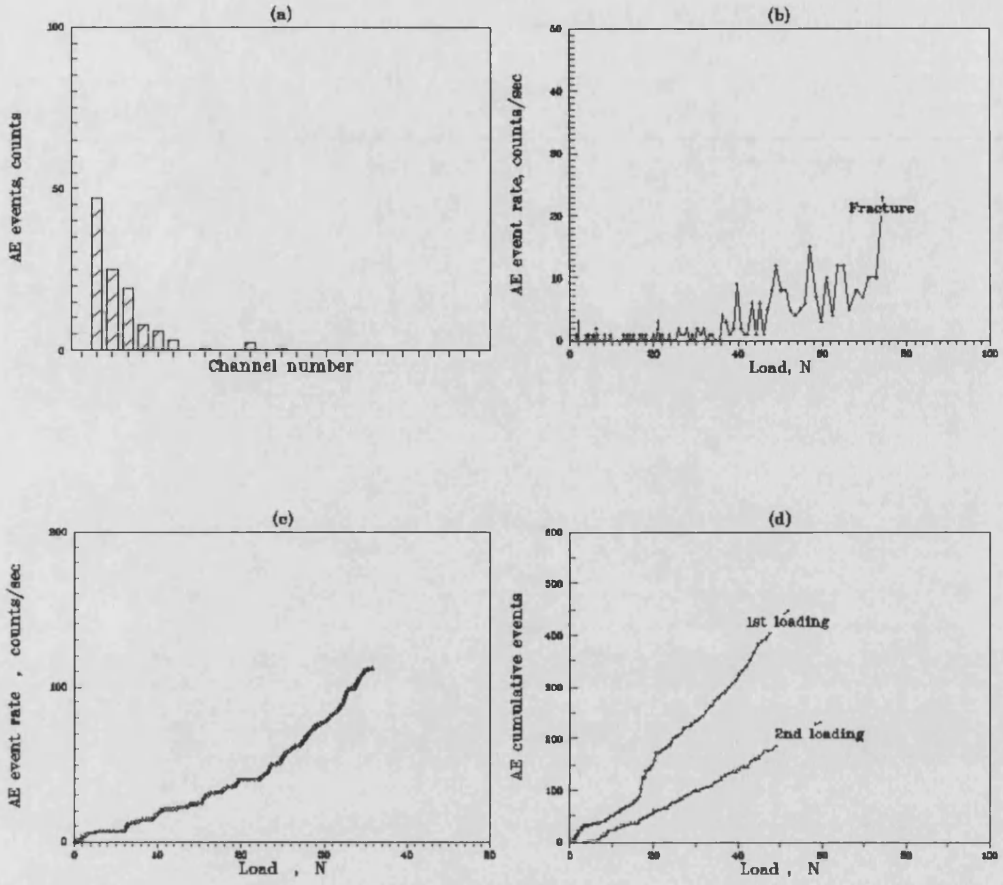

Fig.68 AE from Kaolin+Fly Ash composites: **(a)** Amplitude distribution from a 10% (w/w) mixture after sintering at 1000°C, **(b)** Event rate -load distribution from a 10% (w/w) mixture after sintering at 1000°C, **(c)** Event rate versus load from a 10% (w/w) mixture sintered at 1000°C, **(d)** Kaiser effect from a 5%(w/w) mixture sintered at 1000°C.

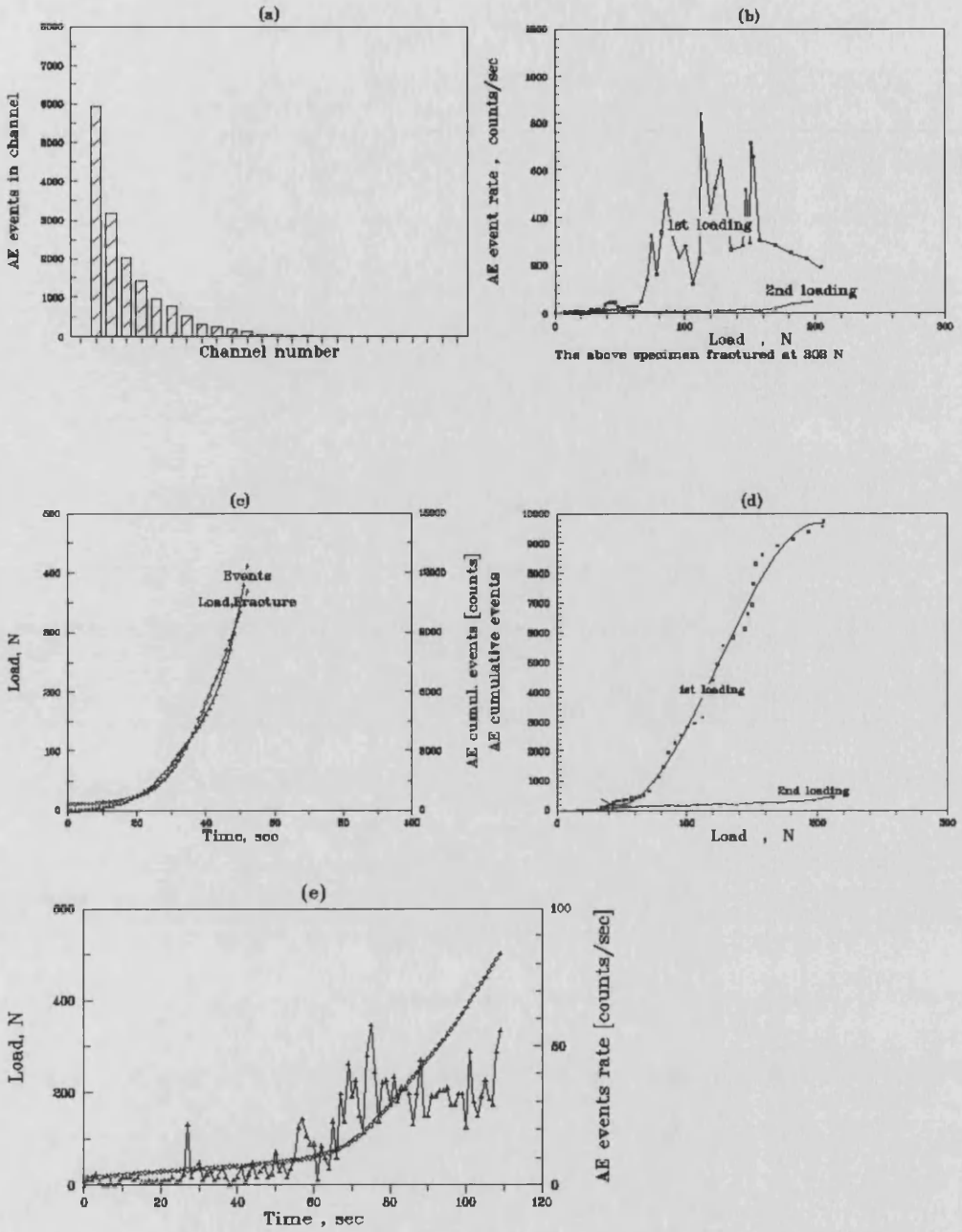

Fig.69 AE results from kaolin α-Al_2O_3 fibre composites during 3-point bending: (a) Amplitude distribution in a 9.2% vol mixture after sintering at 1200°C, (b) Event rate versus load in a 9.2% vol. mixture after sintering at 1000°C, (c) Load and cumulative events versus time in a 14% vol. mixture after sintering at 1300°C , (d) Kaiser effect in a 9.2% vol. mixture after sintering at 1300°C , (e) Load and event rate versus time in a 4.7% vol. mixture sintered at 1300°C .

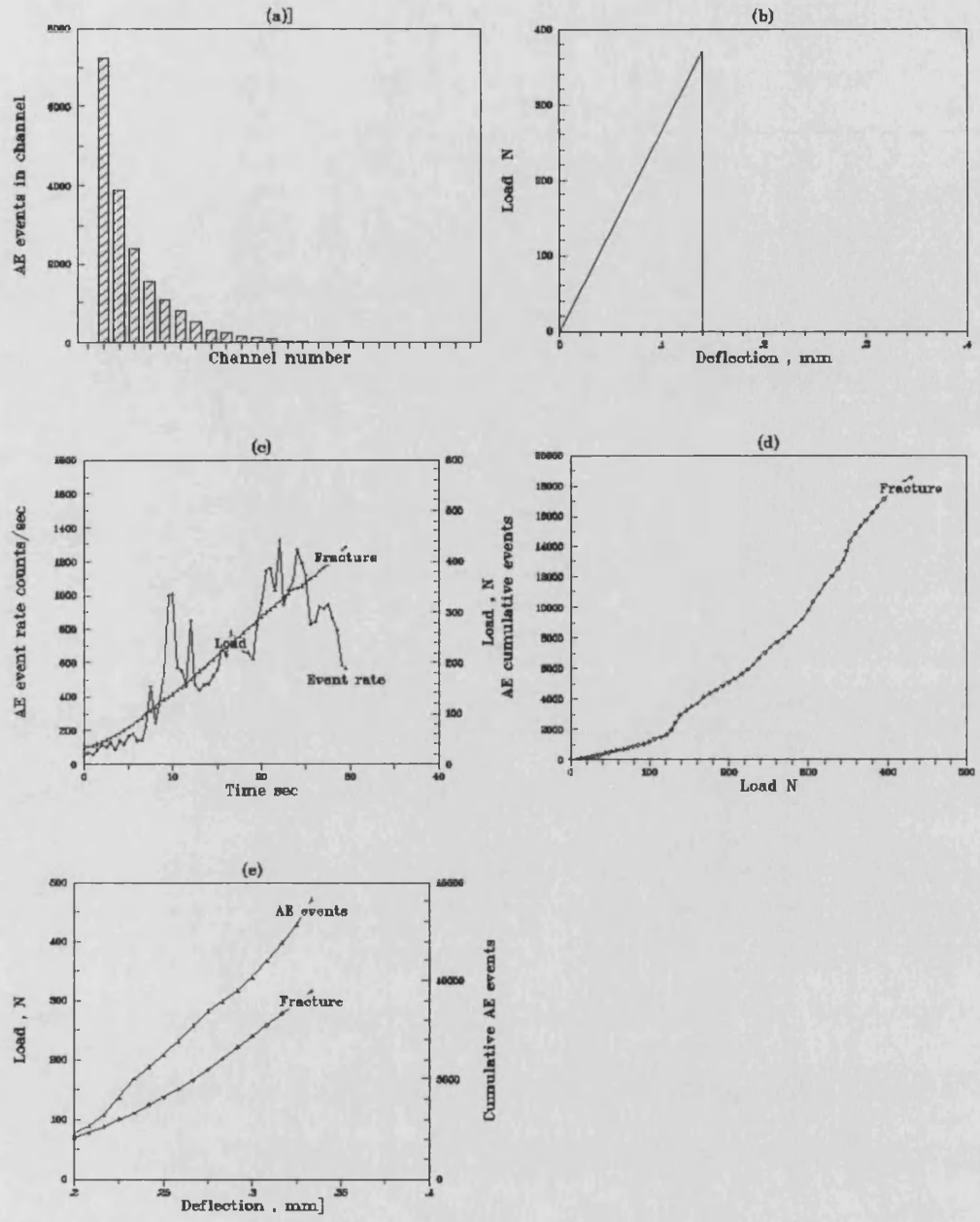

Fig.70 AE from Kaolin-Saffil fibre composites tested at 3-point bending . (a) Amplitude distribution in a 4.5% vol. mixture sintered at 1200°C, (b) Load-deflection distribution in a 14.75% vol. mixture after sintering at 1300°C, (c) Event rate and load versus time in a 4.5% vol. mixture sintered at 1200°C, (d) Cumulative AE events load distribution in a 4.5% vol. mixture sintered at 1200°C, (e) Load and cumulative events versus deflection in a 9.7% mixture sintered at 1200°C.

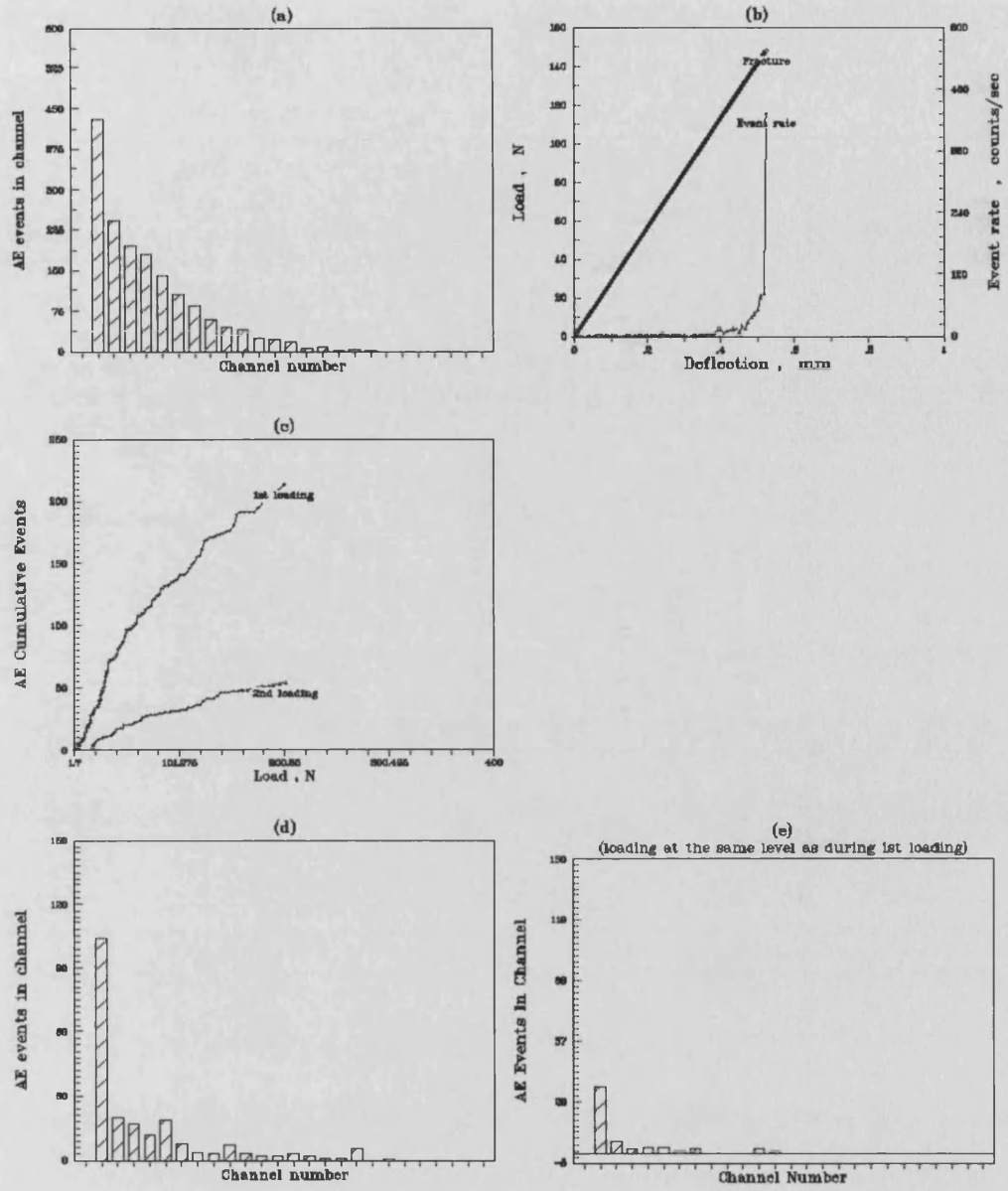

Fig.71 AE from Kaolin-mullite (B80-K) fibre composites tested at 3-point bending: (a) Amplitude distribution in a 9.7% vol. mixture sintered at 1000°C, (b) Load-event rate distribution versus deflection in a 9.7% vol. mixture after sintering at 1000°C, (c) Kaiser effect in a 9.7% vol. mixture sintered at 1200°C, (d) Amplitude distribution in a 9.7% vol. mixture during first loading, (e) Amplitude distribution during second loading of the specimen tested previously at (d).

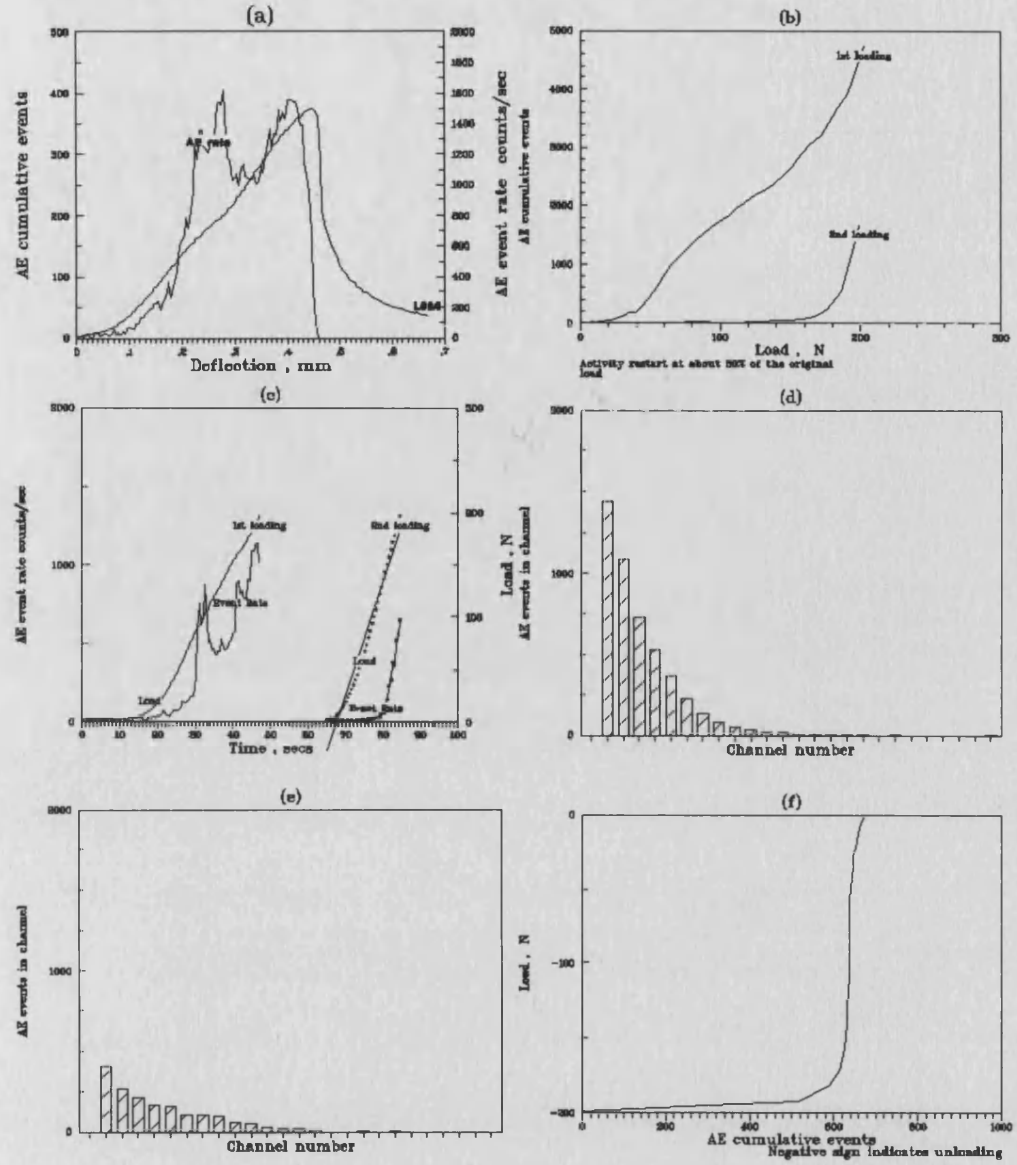

Fig.72 AE from Kaolin-Grafil fibre composites tested at 3-point bending: (a) AE events and rate versus deflection in a 16.6% vol. mixture sintered at 1200°C, (b) Kaiser effect in a 8.5% vol. mixture after sintering at 1300°C, (c) Event rate and load versus time in a 16.6% vol. mixture sintered at 1200°C, (d) Amplitude distribution in a 8.5% vol. mixture after sintering at 1300°C, (e) Amplitude distribution during second loading of the specimen tested previously at (d), (f) AE activity during un-loading in a 8.5% vol. mixture sintered at 1300°C.

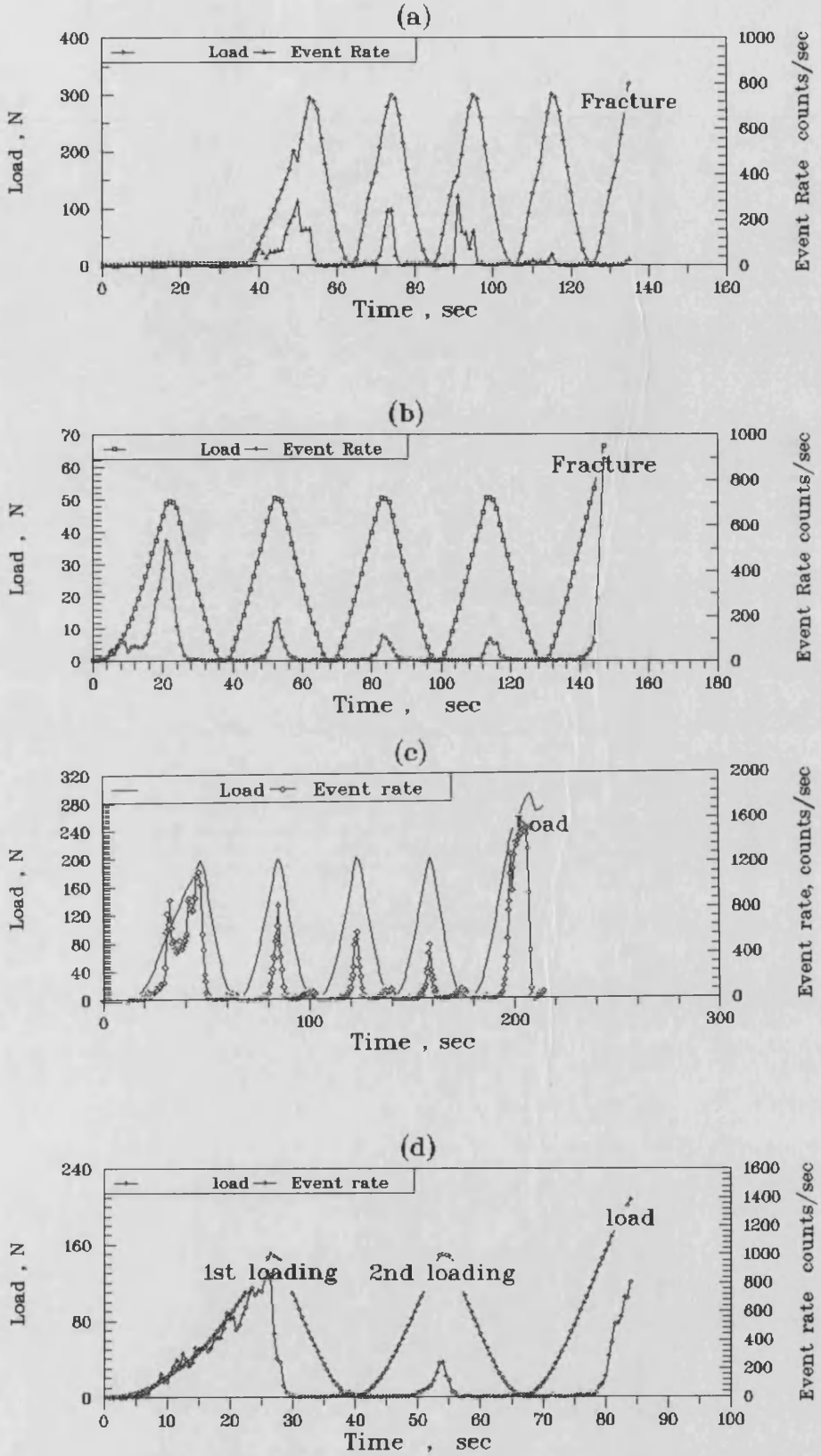

Fig.73 The effect of cyclic loading (load versus time) on acoustic activity (event rate) of ceramics and fibre ceramic composites. (a) Kaolin sintered at 1400°C (b) Pottery mixture sintered at 1150°C , (c) kaolin+16.6% Grafil composite sintered at 1200°C, (d) kaolin+16.6% Grafil composite sintered at 1300°C

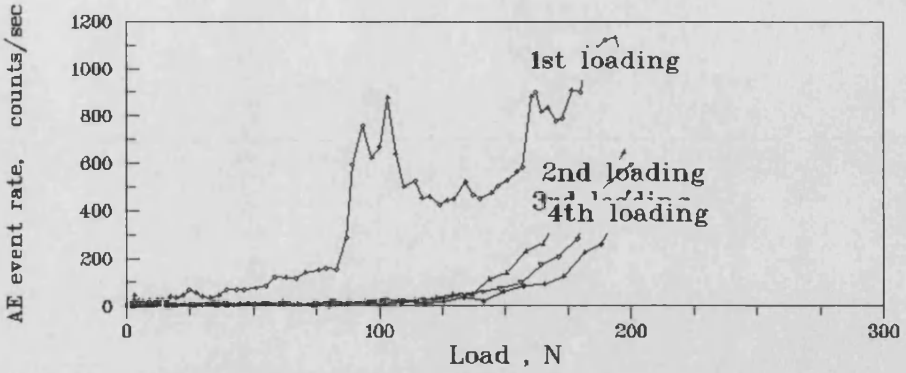

Fig.74 The change of event rate distribution versus load, during repeated loadings in a kaolin- 16.6 % vol.Grafil fibre composite sintered at 1200°C.

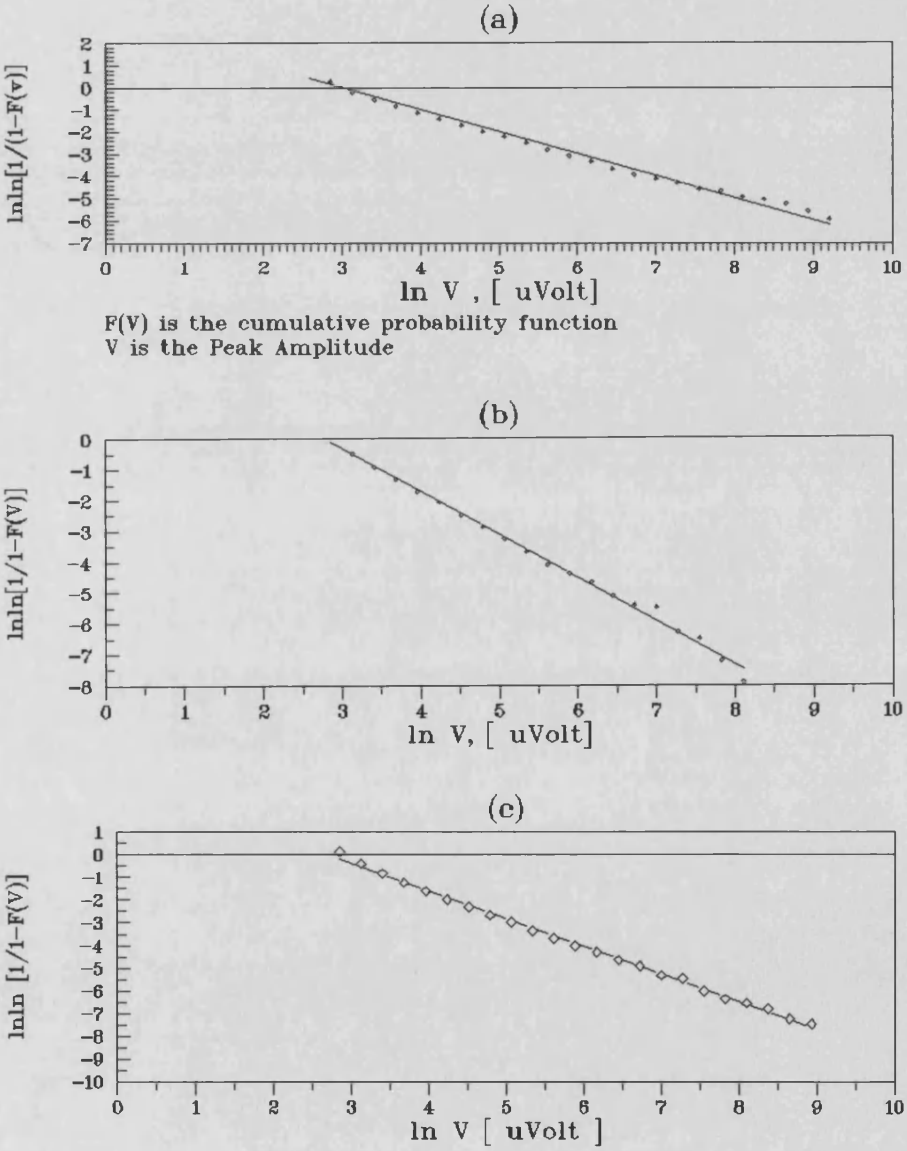

Fig.75 Weibull type probability curves from AE activity in ceramics :(a) kaolin sintered at 1300°C, (b) brick-clay sintered at 1100°C, (c) pottery mixture sintered at 1100°C. F(V) is the cumulative probabaility function and V is the peak amplitude.

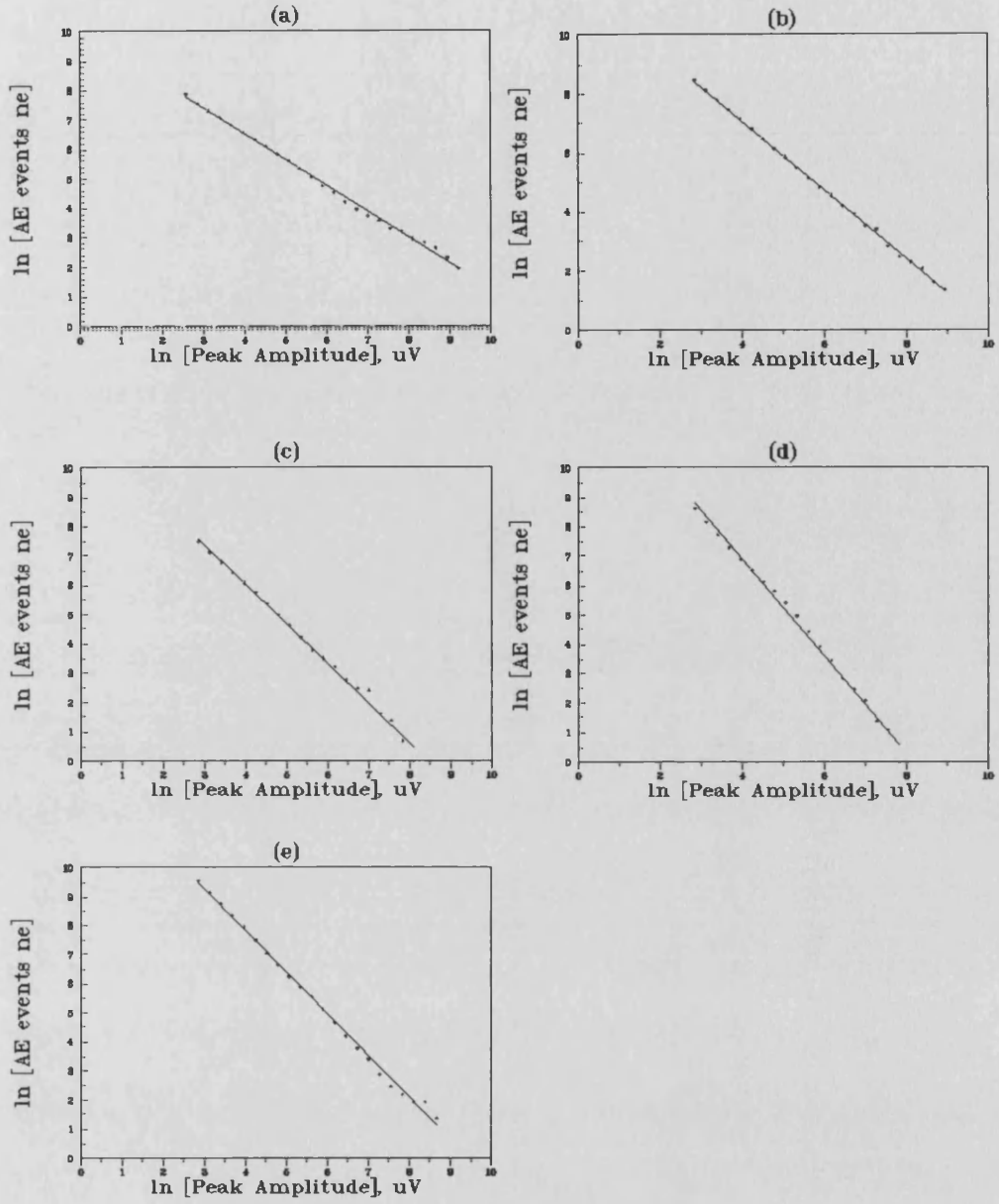

Fig.76 Event-Peak amplitude distribution (number of detected events ne with amplitude larger than V , versus peak amplitude) log-curves from ceramics and composites: (a) kaolin sintered at 1300°C, (b) pottery mixture sintered at 1100°C, (c) brick-clay sintered at 1100°C, (d) 14.75% vol. Saffil composite sintered at 1300°C, (e) 8.6% Grafil composite sintered at 1300°C.

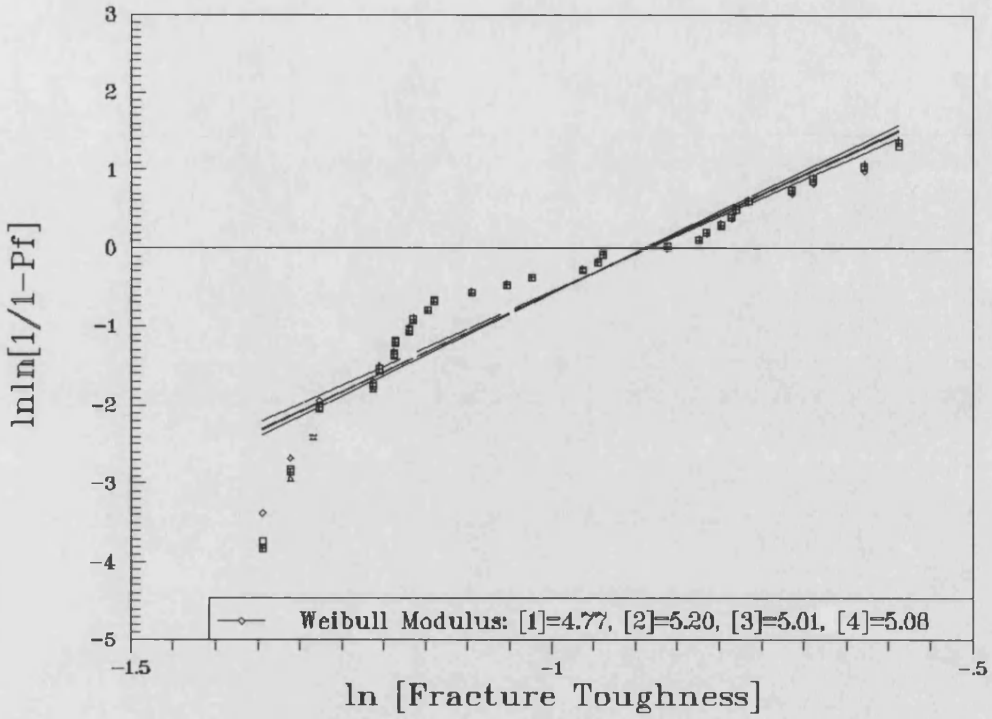

Fig.77 Graphic representation of the effect of estimator type on Weibull modulus of notched Kaolin specimens sintered at 1100°C and tested at 3-point bending: 1.i/(N+1), 2.(i-0.5)/N, 3.(i-0.3)/((N+0.4), 4.(i-3/8)/(i+1/4)
Pf=Prpbability of fracture, Fracture Toughness K_{IC} in MPa.$m^{1/2}$.

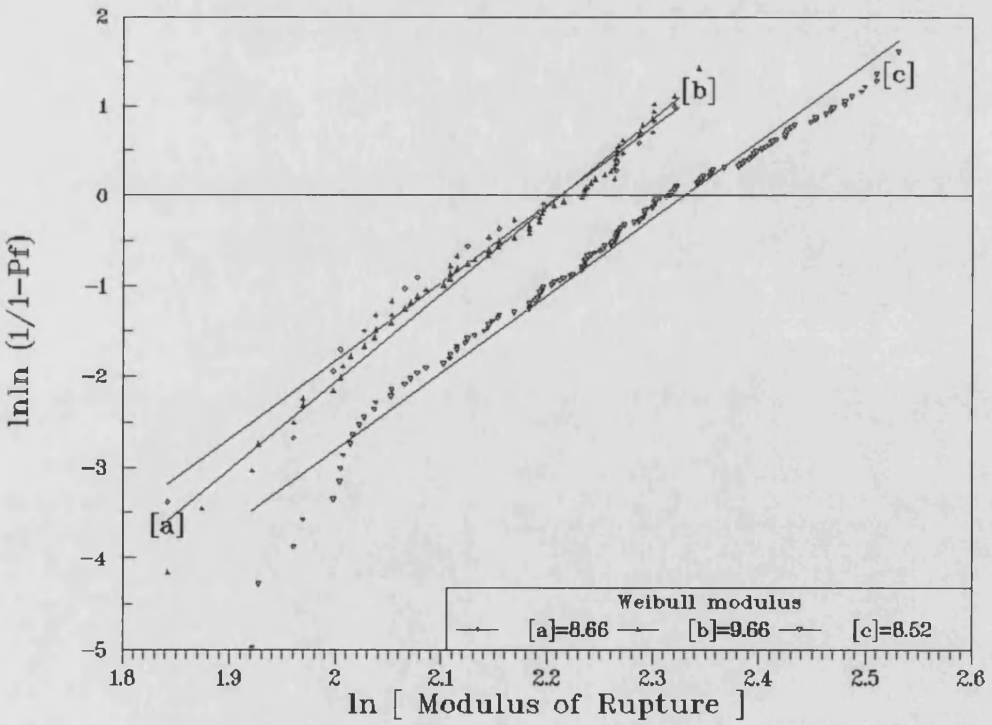

Fig.78 Graphic representation of the effect of specimen population on Weibull modulus of Brick-clays sintered at 900°C and tested at 3-point bending. Specimens: (a) 29, (b) 63, (c) 144. Modulus of Rupture MOR in MPa.

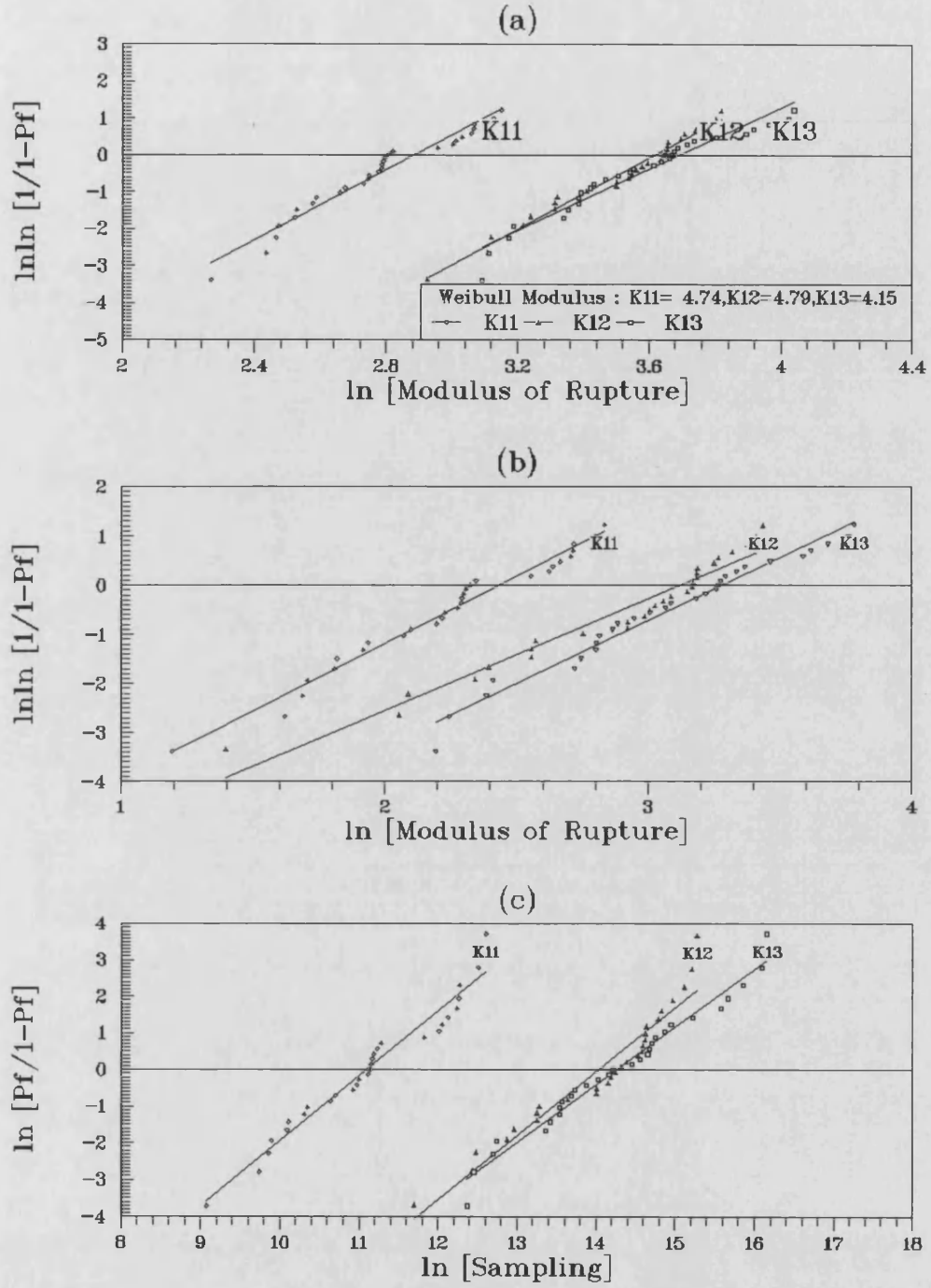

Fig.79 The two and three Weibull parameters distribution and Neville distribution curves for MOR values of un-notched kaolin specimens. K11=sintered at 1100°C, K12=sintered at 1200°C, K13= sintered at 1300°C.
(a) 2-parameter function, (b) 3-parameter Weibull function (at P_f=0.01 MOR_{th}=6.36, 14.58 and 13.06 MPa from specimens sintered at 1100, 1200, 1300°C rsp. (c) Neville function. Modulus of Rupture MOR in MPa, Sampling S= MOR^4.

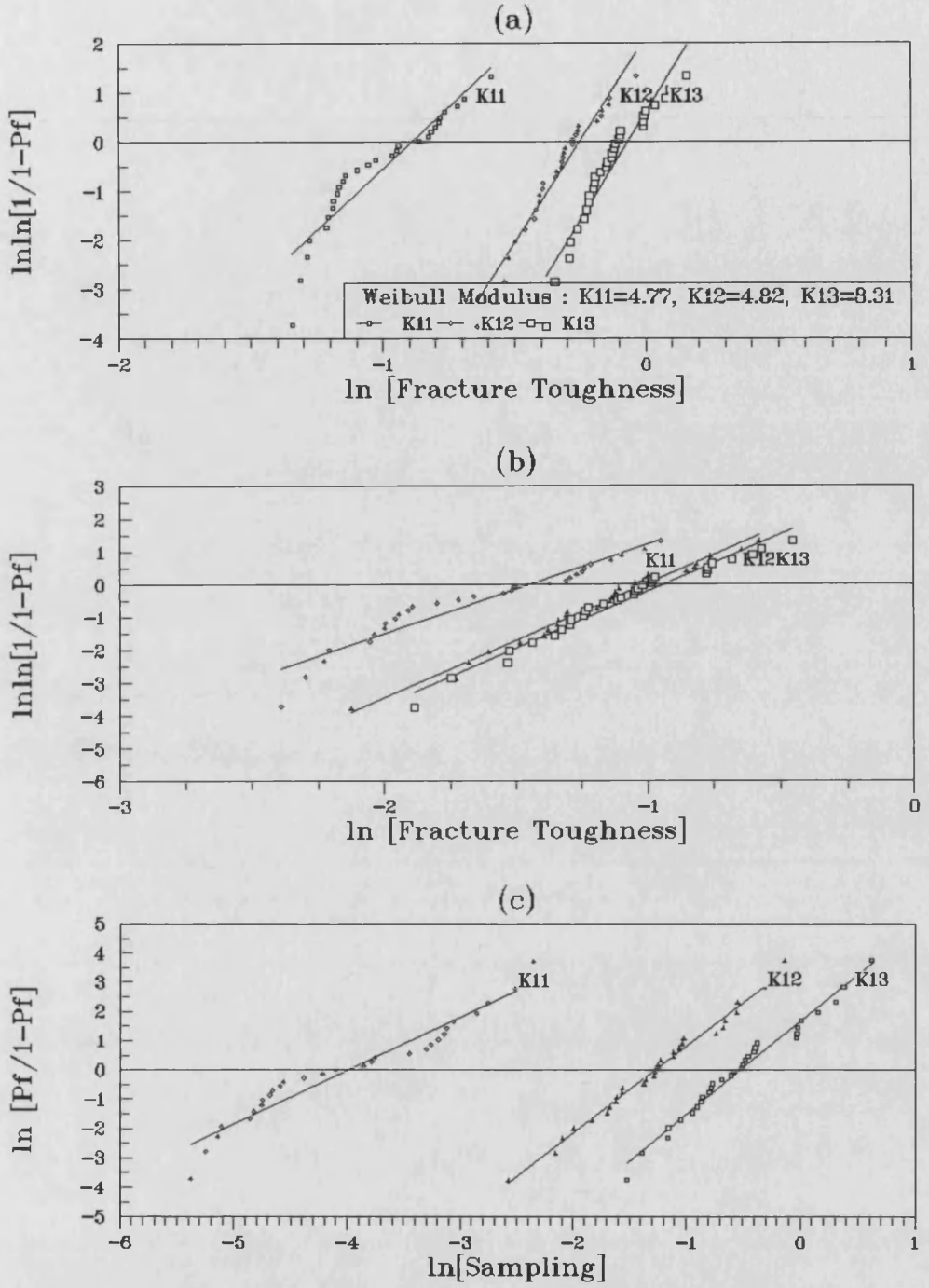

Fig.80 The two and three Weibull parameters distribution and Neville distribution curves for K_{IC} values of notched kaolin specimens.K11=sintered at 1100°C, K12=sintered at 1200°C, K13= sintered at 1300°C.
(a) 2-parameter function, (b) 3-parameter Weibull function (at P_f=0.01 K_{ICth}=0.165, 0.406 and 0.532 MPa.$m^{1/2}$ from specimens sintered at 1100, 1200, 1300°C rsp.
(c) Neville function. Fracture Toughness K_{IC} in MPa.$m^{1/2}$. Sampling S=K_{IC}^4

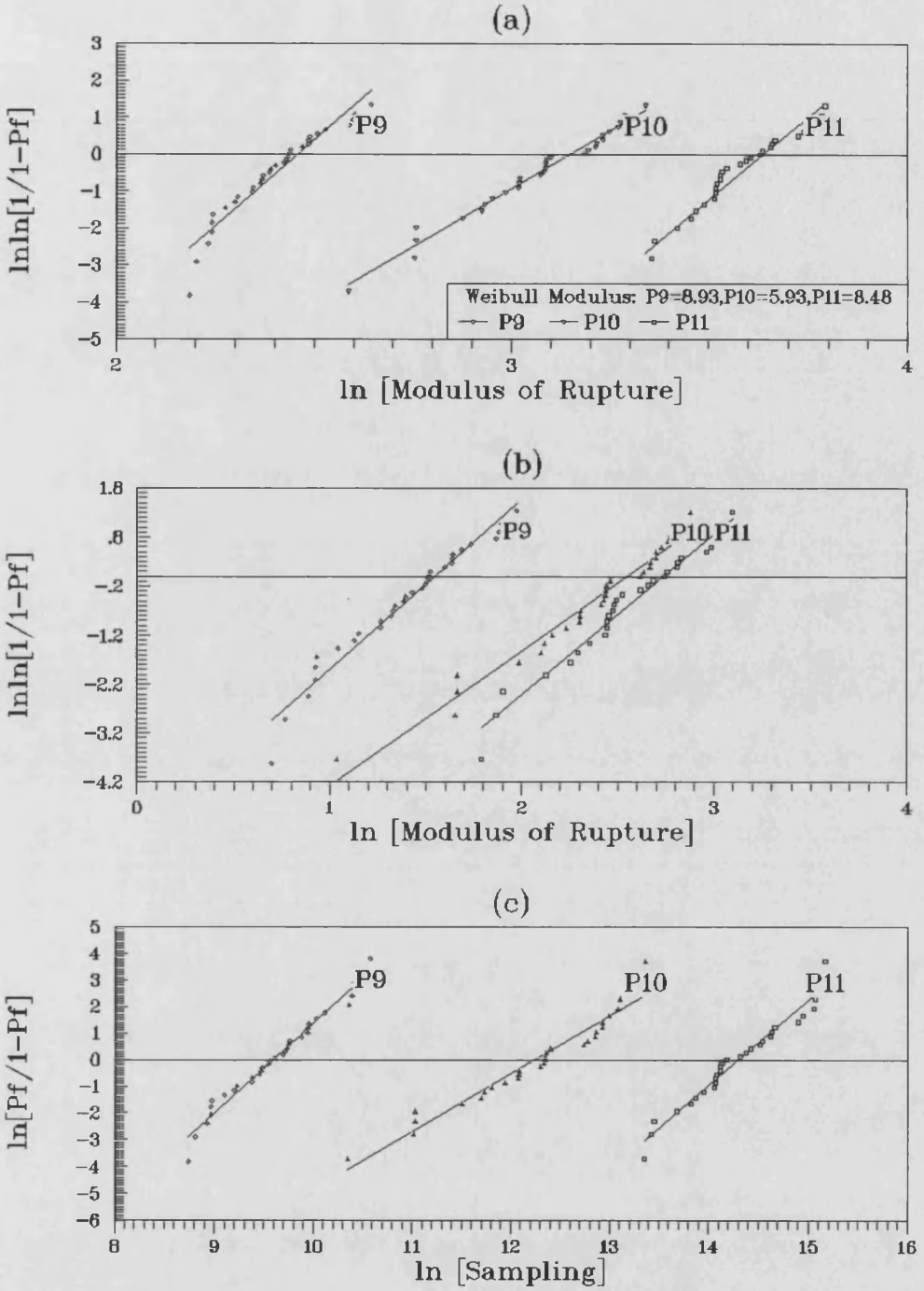

Fig.81 The two and three Weibull parameters distribution and Neville distribution curves for MOR values of un-notched pottery mixture specimens. P9=sintered at 900°C, P10=sintered at 1000°C, P11=sintered at 1100°C. (a) 2-parameter function, (b) 3-parameter Weibull function (at P_f=0.01 MOR_{th}=6.88, 10.48 and 22.19 MPa from specimens sintered at 900, 1000, 1100°C rsp. (c) Neville function. Modulus of Rupture MOR in MPa . Sampling $S=MOR^4$.

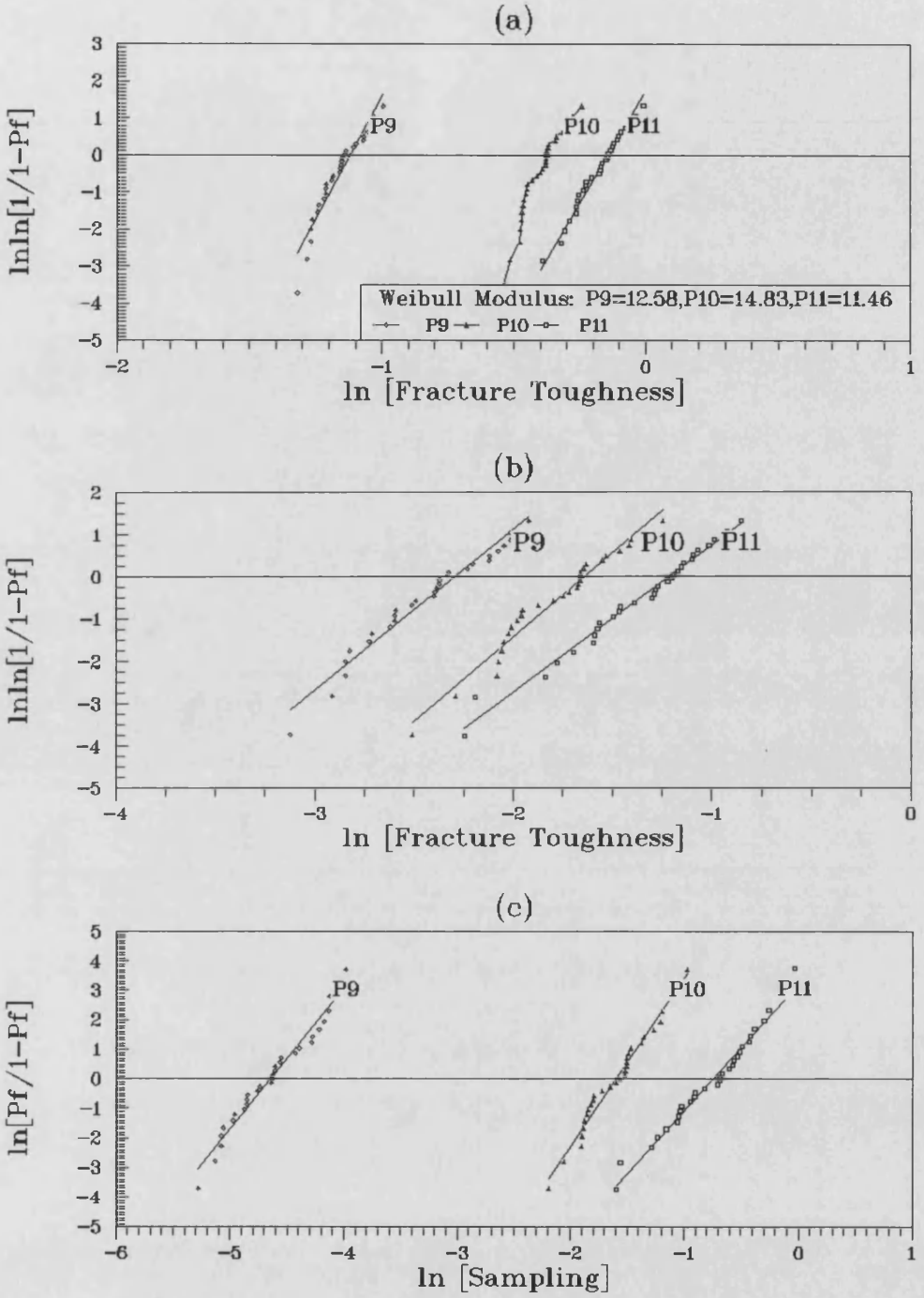

Fig.82 The two and three Weibull parameters distribution and Neville distribution curves for K_{IC} values of notched pottery mixture specimens.
P9=sintered at 900°C, P10=sintered at 1000°C, P11=sintered at 1100°C.
(a) 2-parameter function, (b) 3-parameter Weibull function (at P_f=0.01 K_{ICth}=0.223, 0.496 and 0.565 MPa.m$^{1/2}$ from specimens sintered at 900, 1000, 1100°C rsp. (c) Neville function. Fracture Toughness K_{IC} in MPa.m$^{1/2}$.
Sampling S = K_{IC}^4 .

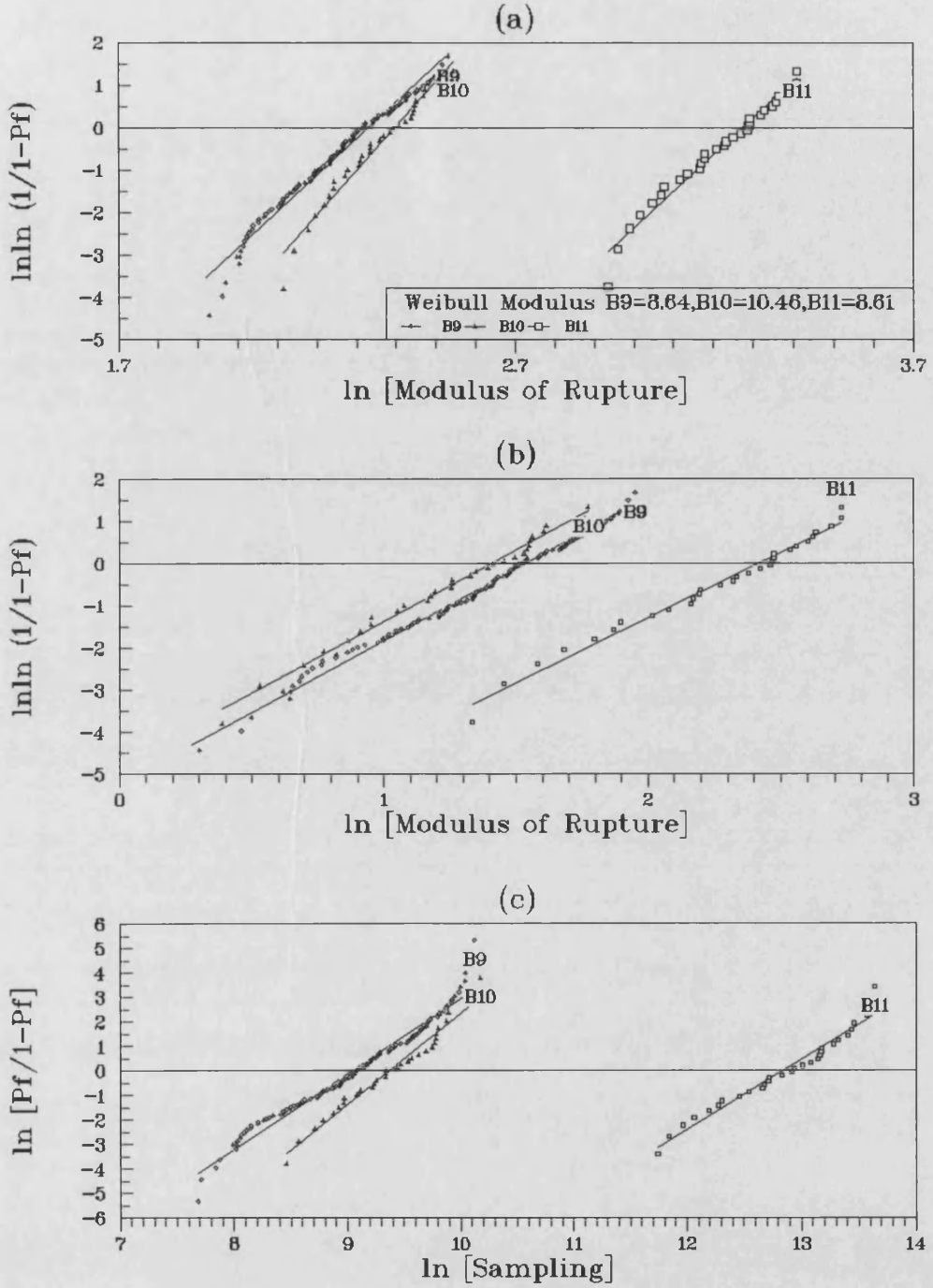

Fig.83 The two and three Weibull parameters distribution and Neville distribution curves for MOR values of un-notched brick-clay mixture specimens. B9=sintered at 900°C, B10=sintered at 1000°C, B11=sintered at 1100°C. (a) 2-parameter function, (b) 3-parameter Weibull function (at P_f=0.01 MOR_{th}=5.52, 6.82 and 15.02 MPa from specimens sintered at 900, 1000, 1100°C rsp. (c) Neville function. Modulus of rupture MOR in MPa. Sampling $S=MOR^4$.

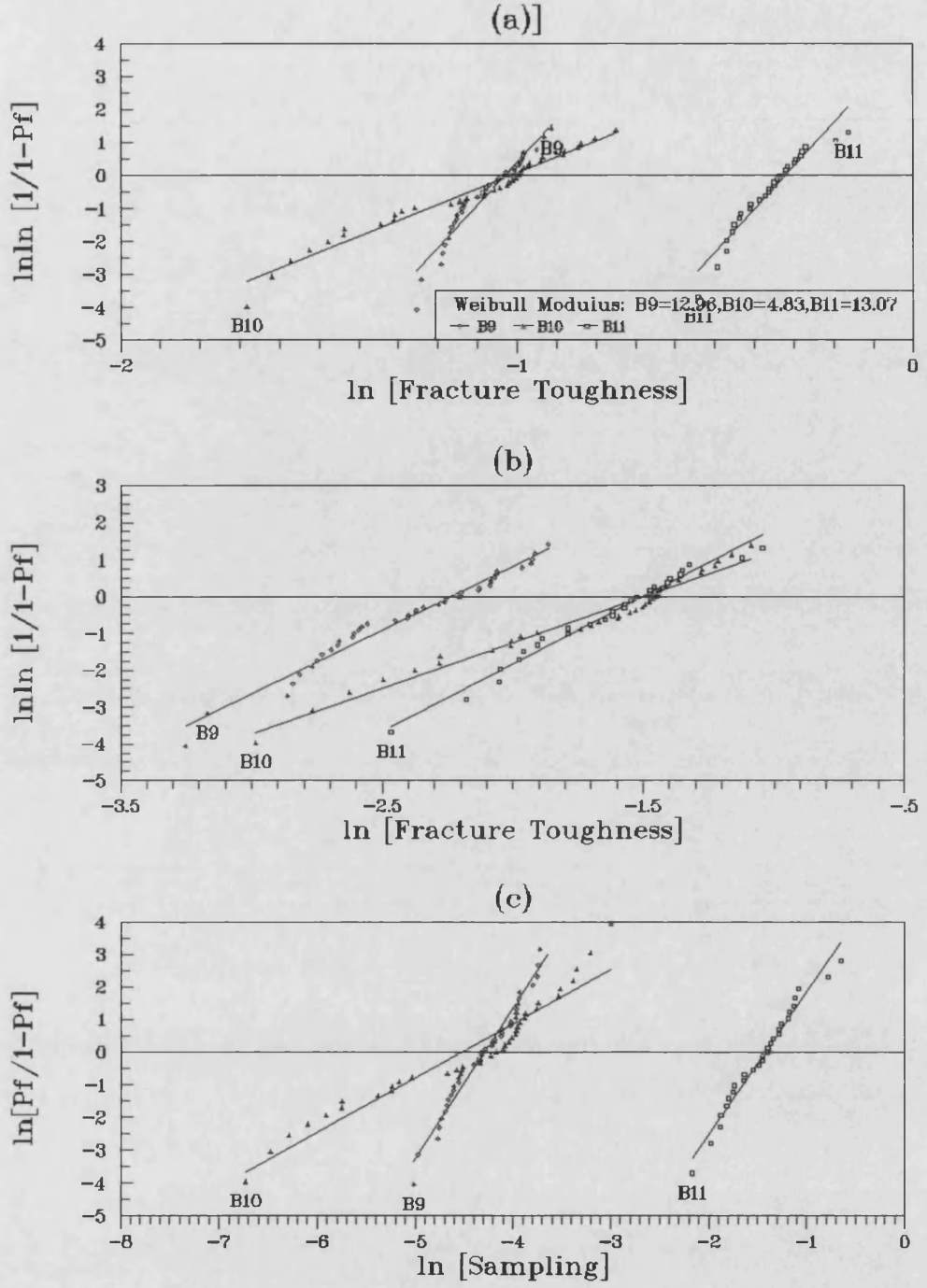

Fig.84 The two and three Weibull parameters distribution and Neville distribution curves for K_{IC} values of notched brick-clay specimens.
B9=sintered at 900°C, B10=sintered at 1000°C, B11=sintered at 1100°C.
(a) 2-parameter function, (b) 3-parameter Weibull function (at P_f=0.01 K_{ICth}=0.246, 0.135 and 0.496 MPa.m$^{1/2}$ from specimens sintered at 900, 1000, 1100°C rsp. (c) Neville function. Fracture Toughness K_{IC} in MPa.m$^{1/2}$.
Sampling $S=K_{IC}^4$

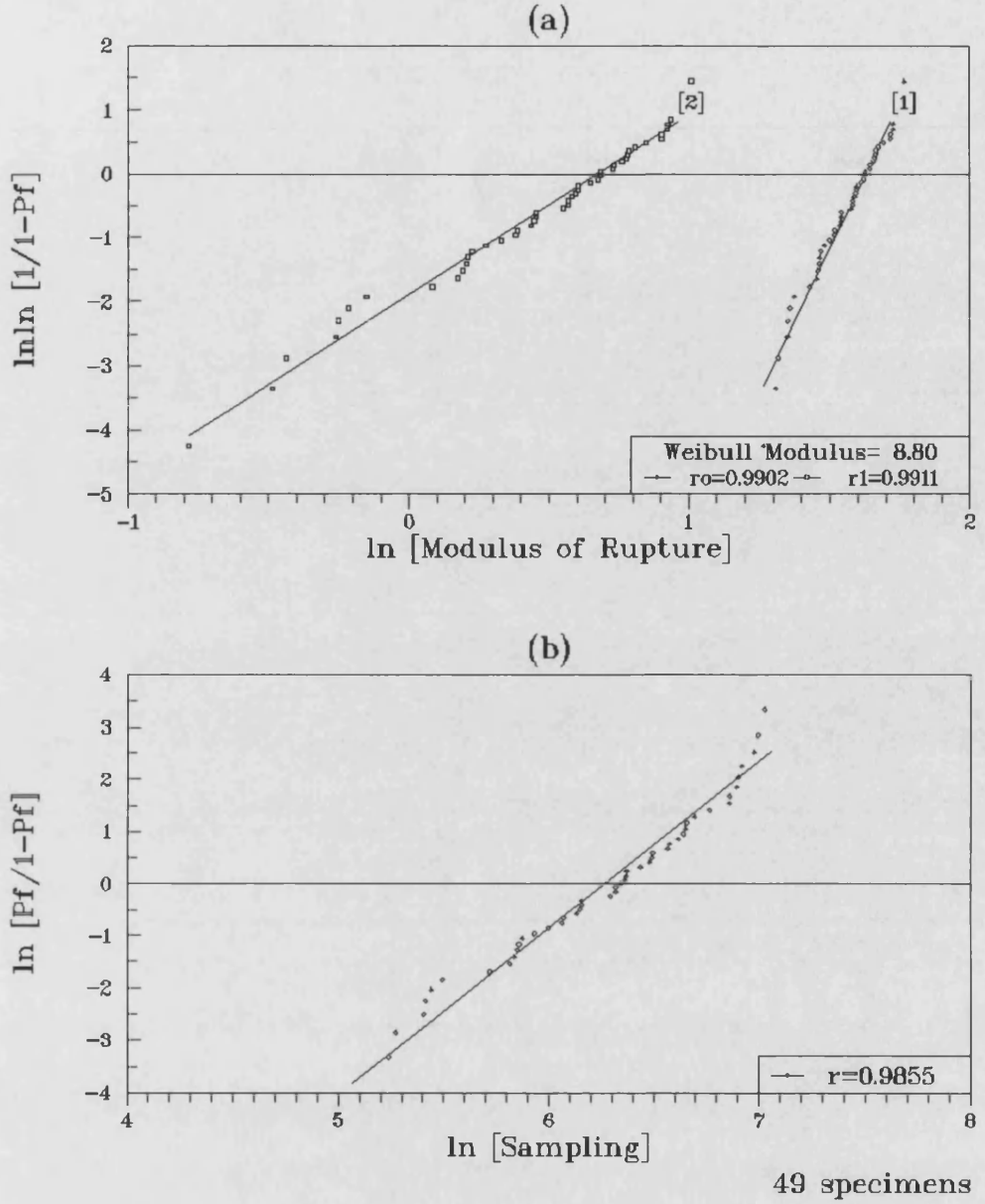

Fig.85 The two and three Weibull parameters distribution and Neville distribution curves for MOR values of un-notched 10% (w/w) FA-kaolin composite specimens sintered at 1000°C.
(a) [1] 2 parameter function , [2] 3-parameter function (at P_f=0.01 MOR_{th}=3.09 MPa , (b) Neville function. Modulus of Rupture MOR in MPa . Sampling $S=MOR^4$.

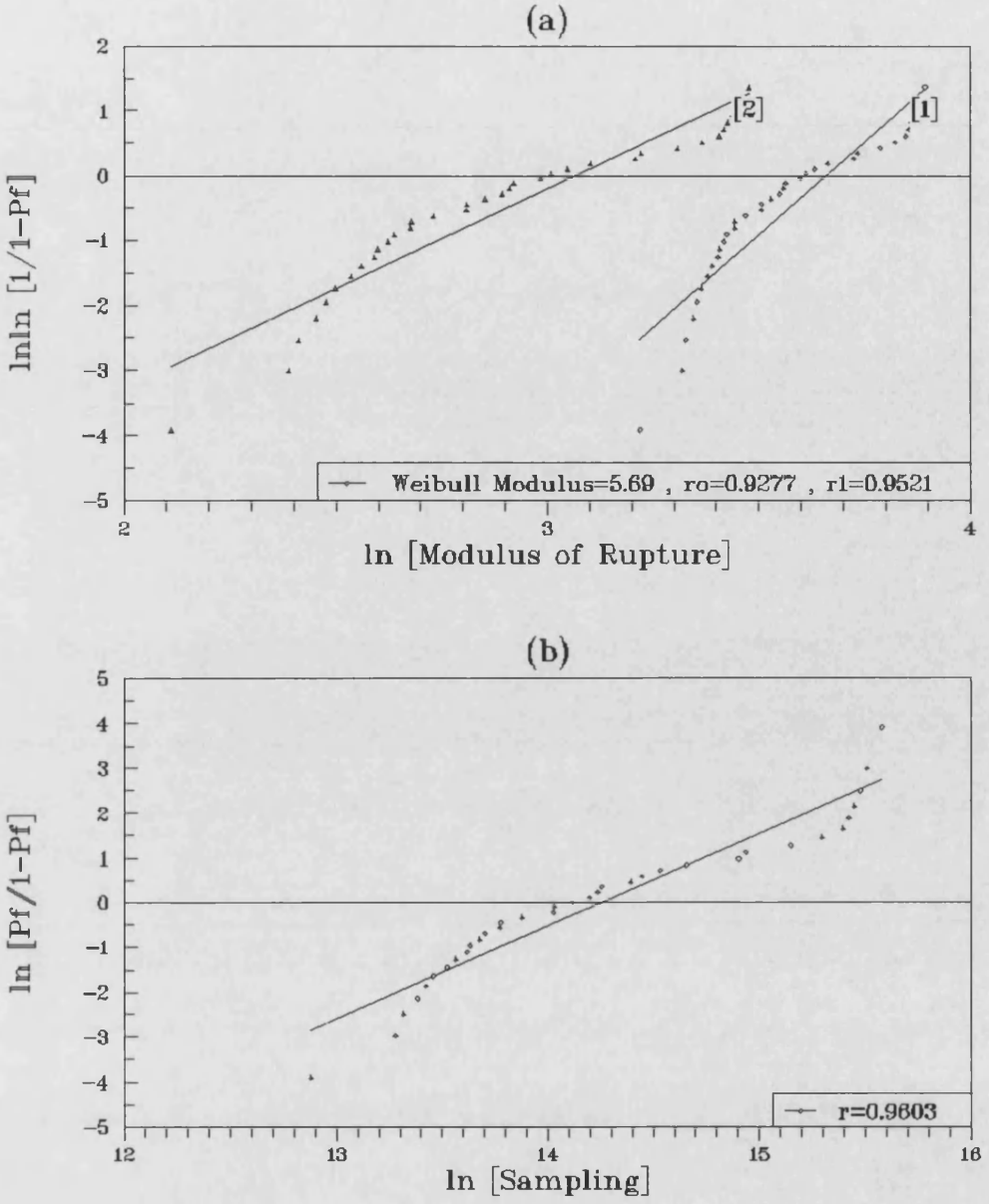

Fig.86 The two and three Weibull parameters distribution and Neville distribution curves for MOR values of un-notched 4.7% vol α-Al_2O_3 fibre composite specimens sintered at 1200°C.
(a) [1] 2 parameter function , [2] 3-parameter function (at P_f=0.01 MOR_{th}=16.77 MPa , (b) Neville function. Modulus of Rupture in MPa. Sampling $S=MOR^4$.

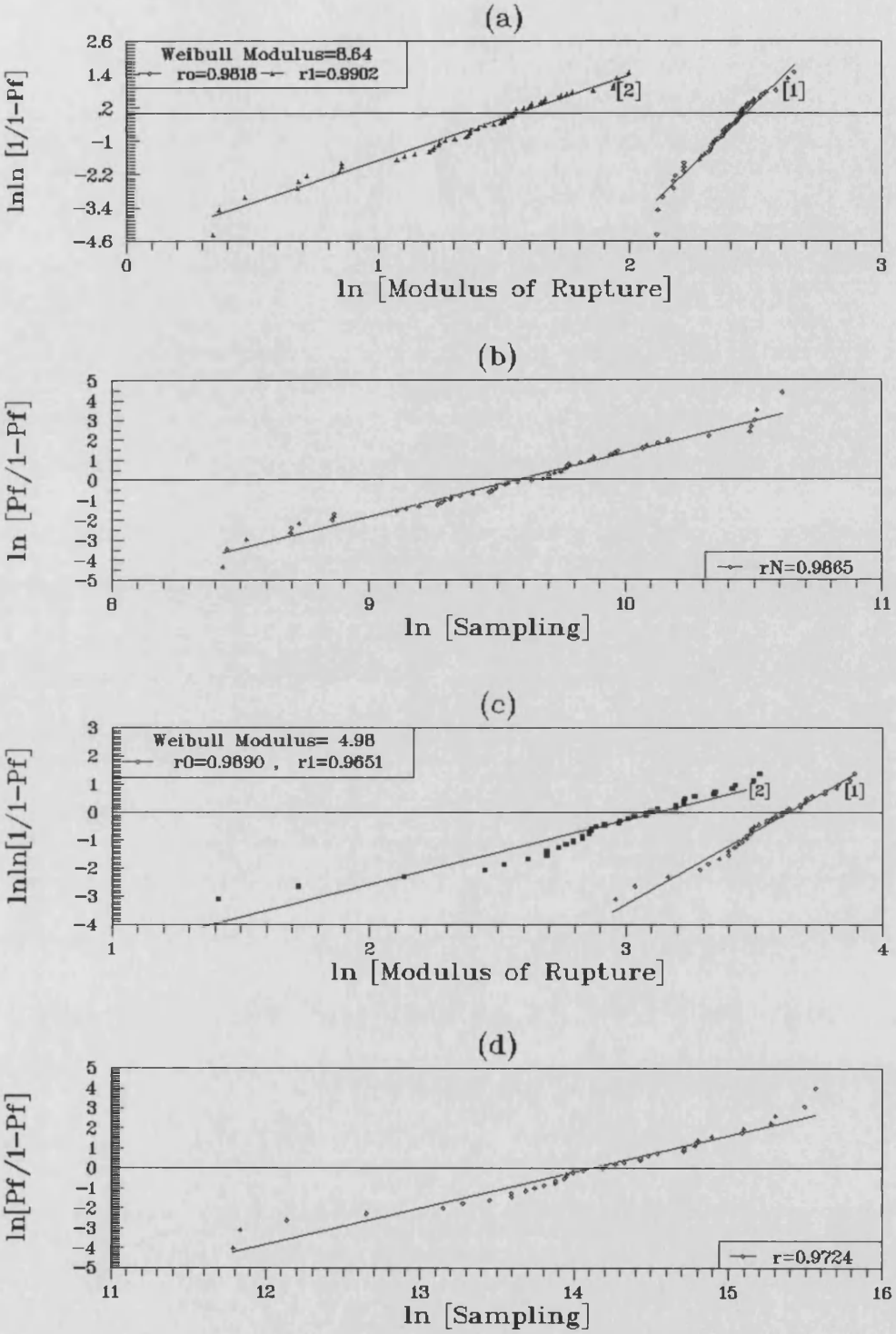

Fig.87 The two and three Weibull parameters distribution and Neville distribution curves for MOR values of un-notched 9.2 vol α-AI_2O_3 fibre composite specimens sintered at 1000°C and 1300°C.
(a)sintering temperature 1000°C: [1] 2-parameter function, [2] 3-parameter function (at P_f=0.01 MOR_{th}=6.82 MPa),(b) sintering temperature 1000°C:Neville function
(c) sintering temperature 1300°C : [1] 2-parameter function, [2] 3-parameter function (at P_f=0.01 MOR_{th}=15.18 MPa), (d) sintering temperature 1300°C : Neville function. Modulus of Rupture in MPa. Sampling $S=MOR^4$.

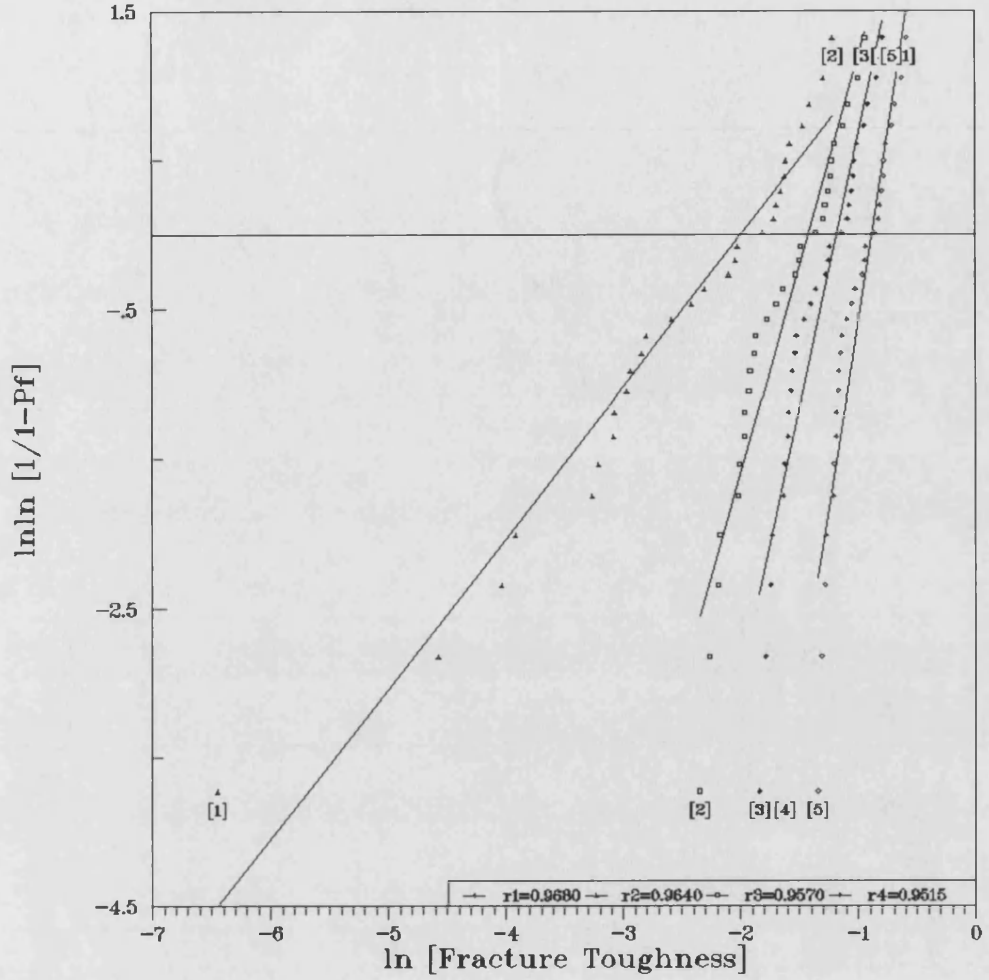

Fig.88 The effect of the third Weibull parameter x_u on the fitness of results of K_{IC} values of Kaolin specimens sintered at 1100°C. fracture Toughness K_{IC} in MPa.$m^{1/2}$

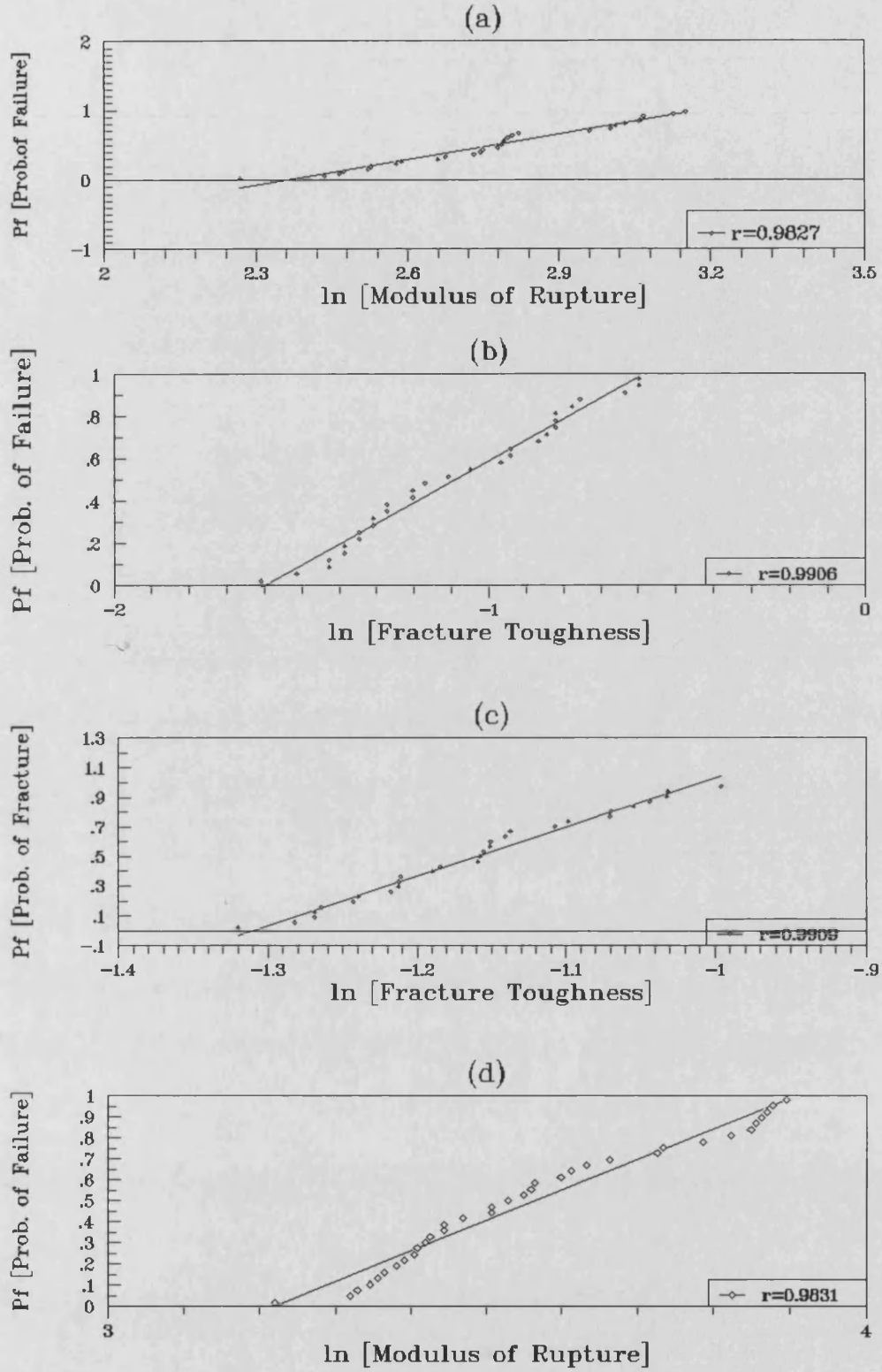

Fig.89 Log-Normal distributions for selected specimen groups; (a) Kaolin un-notched specimens sintered at 1100°C, (b) Kaolin notched specimens sintered at 1100°C, (c) Pottery notched specimens sintered at 900°C,(d) Kaolin+4.7% α-AI_2O_3 composite sintered at 1200°C .
Modulus of Rupture MOR in MPa. Fracture Toughness in $MPa.m^{1/2}$.

APPENDIX 1. CEMENT

A 1.1 COMPOSITION AND STRUCTURE

Cement, a very old material known to Egyptians and Greeks, is a mixture of different substances (Ordinary Portland Cement is based mainly on the ternary system of calcium, silicon and aluminum oxides and from mineralogical point of view, is a mixture of alite C_3S ($3CaO.SiO_2$) and belite C_2S ($2CaO.SiO_2$)) which develops rigidity and strength by hardening when is mixed with water and although appears to constitute a different class of material, it has some similarities to ceramics with respect to processing and chemical composition, and often is included in the class of ceramics. This was the main reason to choose, the most commonly used type of white Ordinary Portland Cement (OPC) pure and in mixtures with Fly Ash (FA), as a reference materials is this work.

A number of reviews [e.g A1-A5] and books [e.g A2,A6,A7] have attempted to refine the literature and clarify the chemistry, kinetics and microstructure of cement.

A 1.2 HYDRATION AND HARDENING AND STRENGTH OF OPC

All cements harden by reaction and not by drying and sintering as in the majority of ceramic materials. The main hardening reactions [A8], which start after about 3 hours of the initial mixing of OPC with water, are the hydration exothermic reactions of C_2S and C_3S, resulting in the formation of tobermorite gel (C_x-S-H_y)

which forms protuberances like thin rods, made of $C_3S_2H_3$ and radiating around the grains, [1], and occupies about 70% of the structure and crystalline calcium hydroxide (CH) known as portlandite. Water is necessary for the chemical reaction and the filling of gel pores. This reaction continue for long time and thus cement behaviour is very different when compared with other materials which remain static after mechanical and/or thermal treating.

The strength development of cement [A9] depends on mainly on its chemical composition and physical condition (e.g. fineness), the hydration temperature and the concentration of the gel formed during hydration (its concentration is dependent on the degree of hydration of the cement and the initial water/cement ratio) and especially on the ratio of the volume of hydrated cement to the sum of the volumes of the hydrated cement and capillary pores and finally the air content of the paste.

A 1.3 FLY ASH CEMENT

Fly Ash is a product of combustion of lignitic coal in electric power stations with pozollanic behaviour. Mills [A10], examining the reaction products of high lime FA in mixtures with Portland cement., using EDX and SEM, found beneficial effects of P.C. substitution with FA. From technological point of view energetic environmental and economic considerations make the use of such fly ash mixtures with P.C. an interesting alternative, since the addition of FA improves the workability, durability to chemical attack and lowers the heat of hydration [A11-A14]. However, the use of FA as a supplementary cementing material in the cement industry ,is low, due partially to lack of quality control and test methods able to

evaluate adequately the performance of FA. Systematic characterisation of FAs and further development of testing methods, as well as systematic research and discussion results could probably increase the use of FAs.

The cementitious properties of high calcium FA are attributed to the presence of C_3A, anhydride and some free CaO [A11]. Halse and Pratt, [A15], examined the development of microstructure and other properties in OPC- 30% FA systems with w/s ratio of 0.45-0.50. They found that the $Ca(OH)_2$ content initially increased, but after a maximum reached in 7-14 days decreased as a result of pozolanic reaction (formation of hydrated calcium silicates, C_xSH_y) and finally the compressive strength was increased.

A 1.4 FRACTURE OF CEMENT

Strength development in cement is very fast in the beginning and gradually decreases [A16]. After 3 days the values reach about 30% and after 7 days about 60% of the compressive strength of 28 days. Less steep is the change of flexural strength. After 3 days the values reach about 70% and after 7 days the values reach about 85% of the flexural strength of 28 days.

Grudemo [A17], reviewed the possible relationships between fracture strength, porosity, solid-phase composition and crack structure in cement paste and underlined that cement is a material of variable composition and water content , consisting of phases changing with time and simplified expressions of strength functions do not take into account the influence of a number of factors which are very important in the case of cement (i.e heterogeneous distribution of matter in the solid phase, stress

concentrations variations of stress intensity factors due to different pore shapes etc). Additionally the internal microstructure of the cement, that is, the arrangement of particles with different micro-phases having different size and shape, the strength of bonds (ionic in water molecules and Van Der Waals across phase boundaries and microcracks), are factors of great importance.

As a result of the above a more accurate analysis of the influence of microstructure on strength and fracture mechanism would require a more complicated expression. Although observation of details, such as microcrack initiation, in the range of micrometers, is resolution dependent, special illumination techniques used by Higgins and Bailey [A18], during examination of cement paste in tensile loading, indicated the formation of parallel microcracks in the crack zone.

Grudemo, [A17], hypothesized that under load the possible crack paths developed include lamellar cracks between CH blocks, radial cracks through the outer and inner envelopes spherical cracks around undydrated cement particles and ruptured contact zones between adjoining outer gel coats. He also expressed the view that since the crack length c for brittle materials is a few microns and vary from point to point , the significance of E, G_c and c for cement paste and concrete is rather enigmatic .

A 1.5 AE IN CEMENT-BASED MATERIALS

AE of concrete notched specimens, [A19], revealed that no significant activity of AE take place in the elastic part of the stress-strain curve. When the load is increased a sharp increase in the event rate take place.

Analysis of the AE activity showed that it is dependent on the notch ratio of the specimen. The deeper the notch the more intense the activity in the elastoplastic field and the higher the cumulative AE counts.

Maji and Shah [A20], studied the process of localization of cracks and the movement of the fracture process zone in concrete and mortar under uniaxial tension and under cyclic tests, using AE, and indicated that the fracture process zone (FPZ) can be significant, depending upon material's microstructure, grain size, rate of loading, type of specimen and other parameters and direct application of linear elastic fracture mechanics (LEFM) may not be applicable. They concluded that some AE events were produced in a region near the notch (process zone) was before fracture load was attained but events continue to occur far behind the crack tip near the notch tip. The AE event rate has sharply increased before fracture and the highest rate occurred after peak load was attained. The Kaiser effect found to be present in concrete up to about 80 % of the ultimate strength [A21,A22].

A 1.6 EXPERIMENTAL RESULTS

A number of cement specimens was prepared by mixing OPC powder with water (0.4 w/c). Curing of the moulds (25 X 25 mm ,in diameter and height) carried out at 2O° ± 1° C , in a high humidity sealed cabinet for the first 24 hours and after demoulding for 28 days.

Quantitative XRF analysis results and XRF spectrum from OPC in "as received" condition are shown in fig. A.1a and Table A.1 .

They are in agreement with OPC composition standards. OPC is a mixture, consisting

Compound	% Composition	Compound	% Composition
CaO	71.8	SiO_2	23.2
Al_2O_3	4.6	Fe_2O_3	0.2
MgO	0.1	Na_2O	0.1
K_2O	0.1	TiO_2	0.1

Table A.1 Quantitative XRF results of OPC composition.

mainly from lime, silica and alumina . TG-DTA analysis (fig. A.1b) show that cement is a quite stable material. XRD analysis of OPC, FA and mixtures OPC+5% FA and OPC+10% FA after ageing for 28 days are shown in fig.A.1c.

The main peaks which are shown, as it was expected belong to portlandate (at 18.08, 28.7,34.12,47.14, 50.8, 2 theta). Selected SEM micrographs revealing the morphology of fractured specimens under 3-point bending shown in fig A.2. Hydrated products are visible at compact and heterogeneous mass forms. In some cases the C-S-H gel structure is visible.

(a)

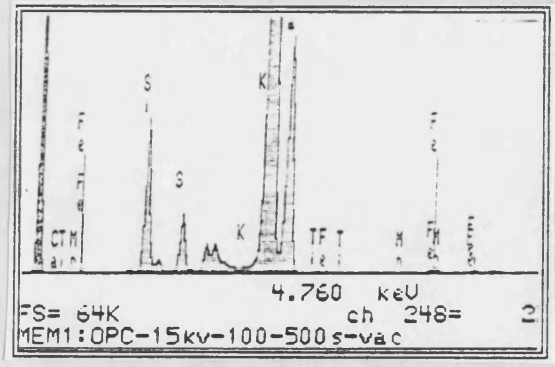

Fig A.1 (a) XRF spectrum of OPC,

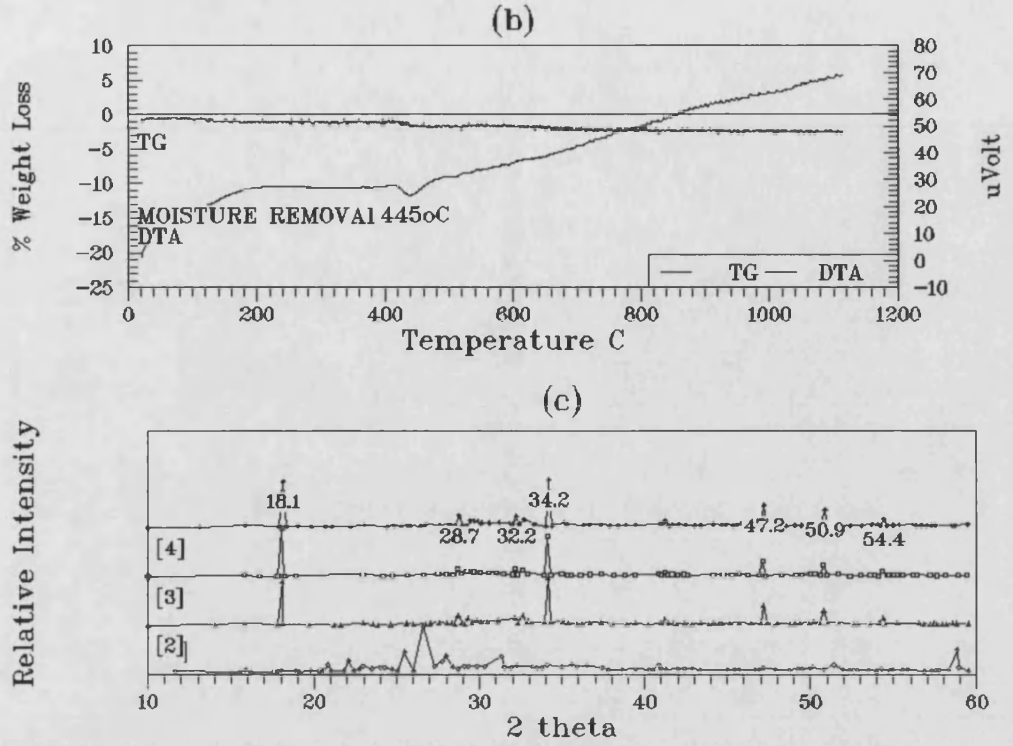

FigA.1 (cont.) (b) TG- DTA curves from OPC in as received condition , (c) XRD Diffraction patterns from OPC and Fly Ash mixtures after ageing for 28 days: [1].FA [2]OPC,[3]OOC+10% FA.

Acoustic emission examination of aged for 28 days cement and cement+fly ash specimens, under conditions similar to that of clay ceramics shows that they are relatively "quiet" materials.

The load, cumulative AE events and AE event rate as a function of deflection from a cement-5% w/w fly ash specimen aged for 28 days during 3-point bend testing is shown in fig A.3. The cumulative events (about 300 counts) and the event rate (a few counts per second) were low and in the same level to that of kaolin fired at 1000°C and. The load-deflection curve shows also an elastic behaviour familiar to brittle materials. Increase of fly ash content shows an increase of acoustic activity probably as a result of sub-critical crack growth due to fly ash particles.

Mechanical testing of aged for 28 days specimens under 3-point bending and

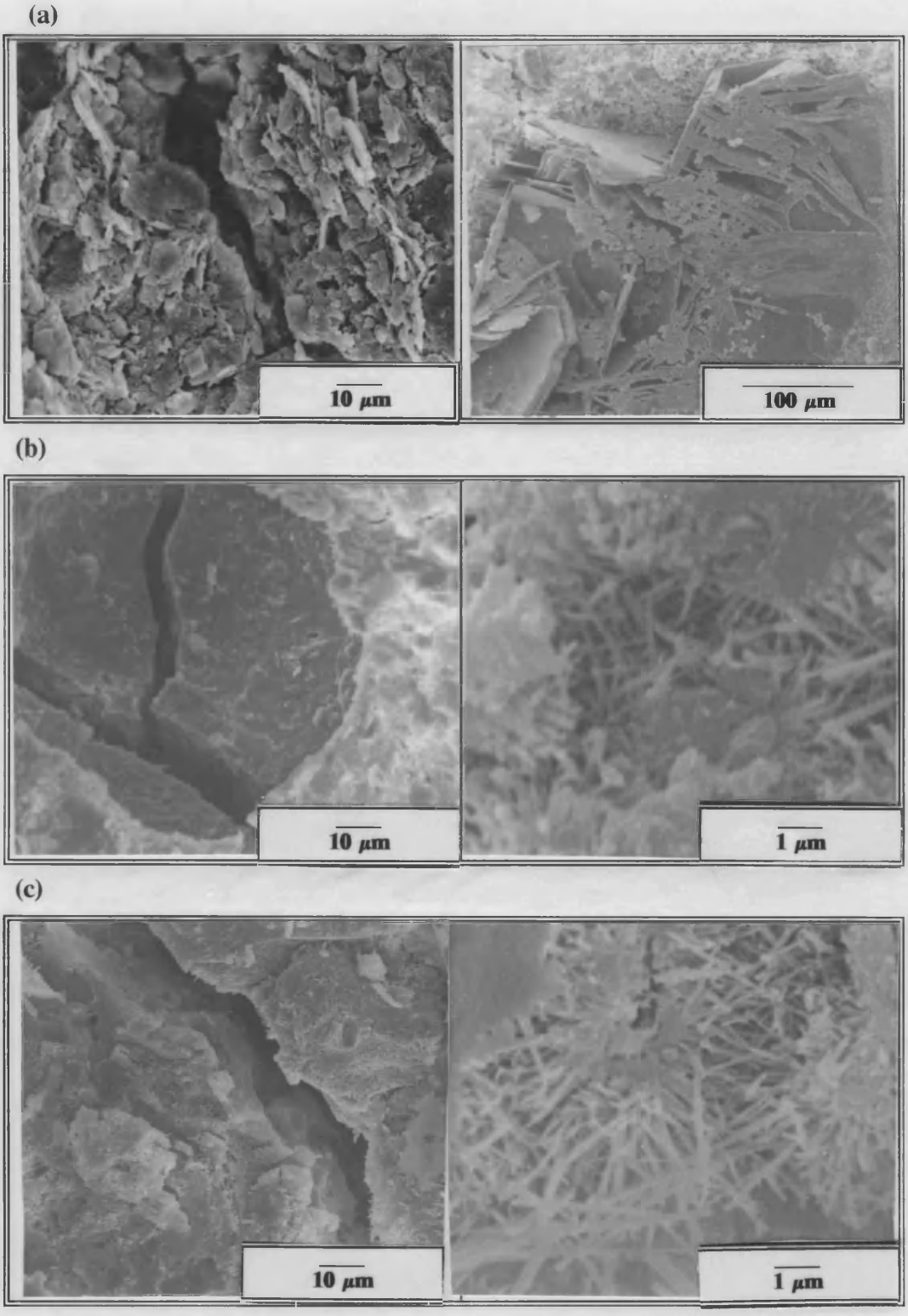

Fig. A.2 SEM micrographs from fractured surfaces of (a) OPC, (b) OPC+5%FA (c) OPC+10%FA

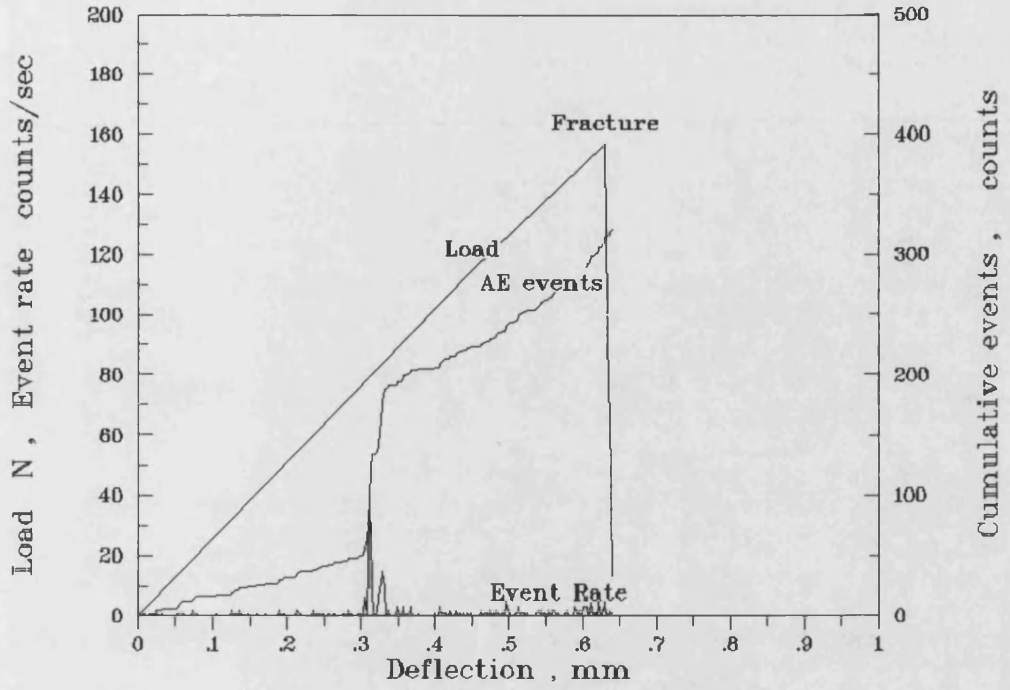

Fig A.3. Load, Cumulative AE events and AE event rate as a function of deflection from a cement-5% w/w Fly Ash specimen aged for 28 days during 3-point bend testing.

compression are shown in Tables A.2. and A.3 respectively. A graphic representation of results shows that the presence of fly ash seems to be beneficial, increasing strength in both 3-point bending and compression (fig A.4). These results are in agreement with those of Metha [A23] for high calcium fly ashes. As he suggested this effect could be attributed to the presence of reactive C_3A and calcium aluminosilicate glass. From a fracture mechanics point of view fly ash particles as SEM examination revealed could deviate crack propagation resulting in strength increase.

Statistical analysis results based on Weibull two and three parameters function and Neville function from cement (fig. A.5), and cement+fly ash composites (fig.A.6), and comparison using correlation coefficients (Table A.4) show that cement and cement-fly ash composites have similar statistical behaviour with the other ceramics.

COMPOSITE		CEMENT	CEMENT+ 5% FLY ASH	CEMENT+ 10% FLY ASH
E_b GPa	AVG	0.14	0.15	0.25
	STD	0.02	0.02	0.035
	Cv	14.2	13.3	14.0
E_d GPa	AVG	17.84	18.39	18.62
	STD	0.65	0.71	0.37
	Cv	3.67	3.8	1.98
MOR MPa	AVG	2.87	2.99	6.05
	STD	0.48	0.73	1.69
	Cv	16.6	24.6	27.93
D g/cm^3		1.75	1.82	1.82

Table A.2 Mechanical characteristics of cement and cement-fly ash composites tested under 3-point bending.

COMPOSITE		CEMENT	CEMENT+ 5% FLY ASH	CEMENT + 10% FLY ASH
COMPRES. STRENGTH	AVG	32.2	43.54	50.6
	STD	3.39	3.9	4.21
	Cv	10.5	8.95	8.3

Table A.3 Mechanical characteristics of cement and cement-fly ash composites tested in compression .

TYPE OF MATERIAL	WEIBULL MODULUS m	CORREL. COEF. IN 2-PARAME-TER WEIBULL FUNCTION r_o	CORREL. COEF. IN 3-PARAME-TER WEIBULL FUNCTION r_1	NEVILLE CORREL. COEF. r_N	MOR_{th} MPa
PURE OPC	6.52	0.9786	0.9895**	0.9890*	1.53
OPC+5% (W/W) FA	4.61	0.9443	0.9703	0.9835**	1.27
OPC+10% (w/w) FA	3.81	0.9770	0.9885**	0.9854*	1.95

Table A.4 Comparison of Statistical Characteristics of resulting from Weibull and Neville functions, using Correlation Coefficients.

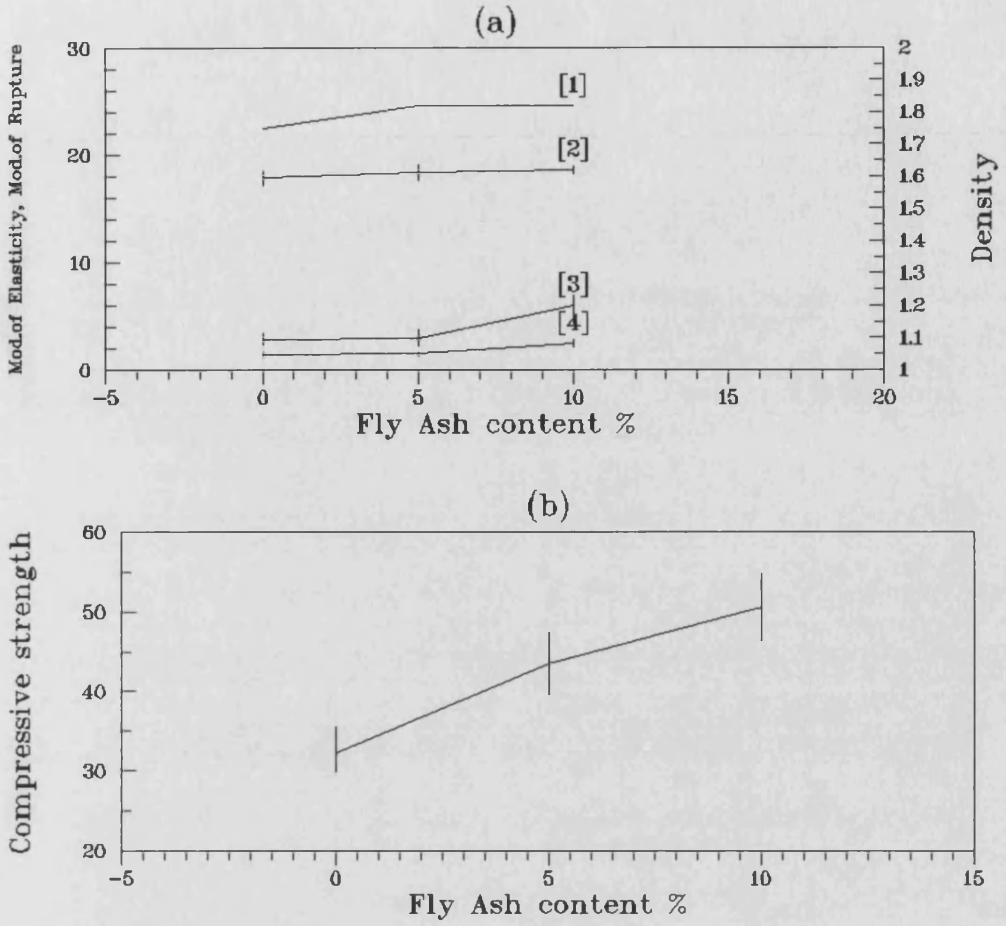

Fig. A.4 Cement and cement -fly ash composites:
(a) Variation of : [1] Density (g/cm^3), [2] M odulus of Elasticity from dynamic testing E_d (GPa) and [3] Modulus of elasticity from bending E_b (GPa) of cement with Fly Ash content, (b) Variation of compressive strength σ_c (MPa) of cement with Fly Ash content.

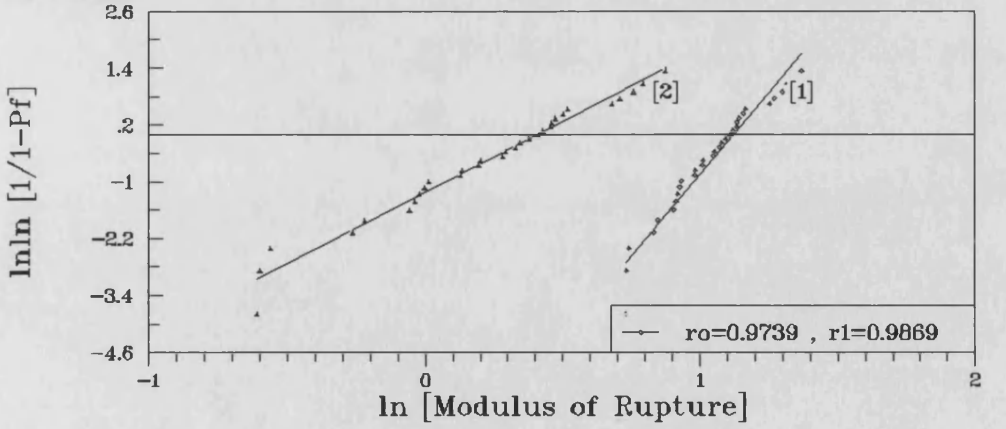

Fig.A.5 Weibull statistical distributions for OPC tested at three-point bending :
[1] 2-parameter function , [3] 3-parameter function [$MOR_{theshold}$ =1.53 MPa at Pf=0.01]

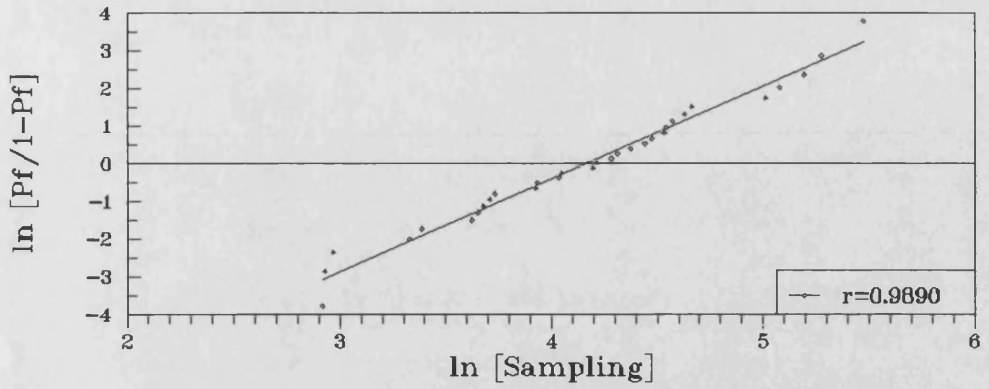

Fig. A.5(cont) Neville function.
Sampling $S=MOR^4$ [MOR in MPA]

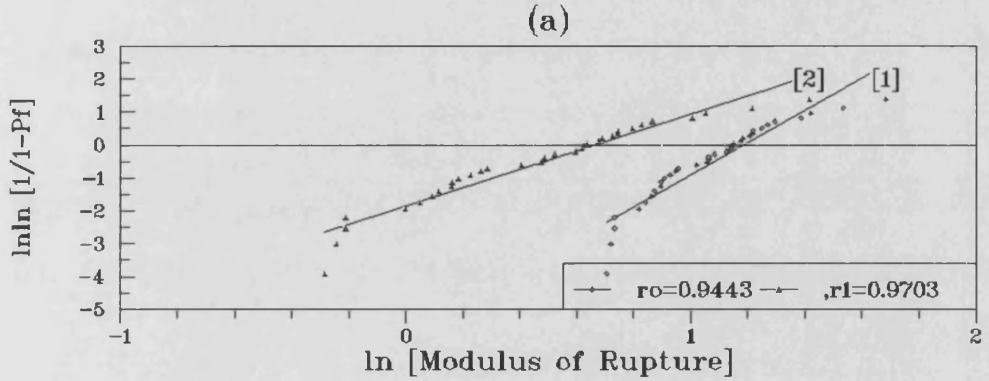

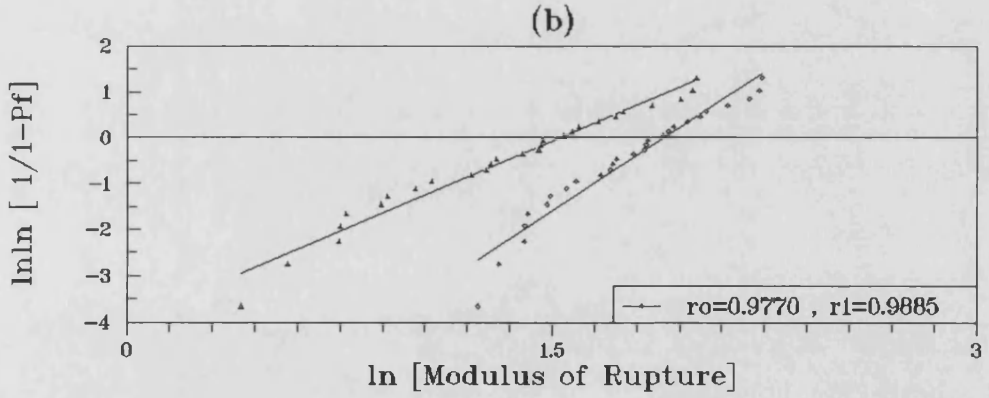

Fig. A.6 Statistical distributions for OPC+FA, tested at three-point bending ;
(a) Weibull function in 5% FA+OPC composite
(b) Weibull function a 10% FA+OPC composite
Modulus of Rupture in MPa

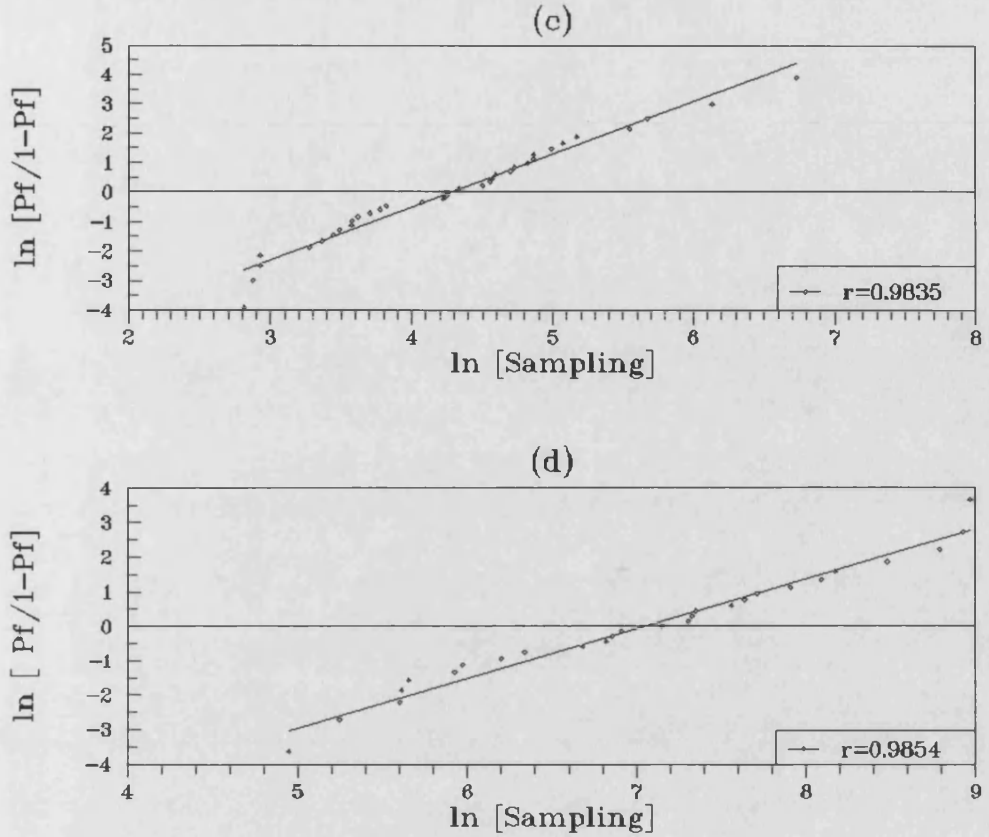

Fig. A.6 (cont.) (c) Neville function of 5% FA+OPC composite
(d) Neville function of 10%+OPC composite
Sampling S=MOR^4

REFERENCES

A1. Double D.D. and A.Hellawell, (1977),Scientific American, 237, 1, pp.82-90.

A2. Bye G.C.,(1983),"Portland Cement",The Institute of Ceramics, Pergamon press, Oxford.

A3. Skalny J.P.,Young J.F.,(1980),"Review:Mechanisms of Portland Cement Hydration", 7th ICCC (Paris Congress),Vol.I,II-1.

A4. Skalny J.,Jawed I.,and Taylor H.F.W.,(1978), World Cem.Technol. 9, p. 183.

A5. Pratt.P.L. and Jennings H.M.,(1981),Ann.Rev.Mat.Sci,11,p. 123.

A6. Lea F.M.,(1970),"The chemistry of cements and Concrete", 3rd ed.,E.Arnold Ltd.

A7. Taylor H.F.W. ed.,(1964),"The chemistry of cements", Academic Press, 1964.

A8. Diamond S., (1976), Proc. Confer.Uni.Sheffield, April 1976, pp.2-30.

A9. McCarter W.J.,(1987), Cem.Concr.Res.,17,pp. 55-64.

A10. Mills R. H., (1986), Mat.Res.Soc.Symp.Proc., Vol65, Materials Research Society, p 207.

A11. Grutzeck, M.W., Roy D.M.& Scheetz B.E., (1981), Cem.Concr.Res.,11,2, p291.

A12. Sersale R., (1980), Proc.7th Int.Cong.Chem.Cem., Paris, Vol.1, IV-1/3-1/18.

A13. Ravina D. and Mehta P.K.,(1986), Cem.Concr.Res.,16,pp 227-238.

A14. Tokyay M.,(1988),Cem.Concr.Res.,18,pp. 957-960.

A15. Halse Y.and Pratt P.L.,(1984), Cem.Concr.Res.,14,pp.491-498.

A16. Sersale R., Marchese B.& Frigione G., 7th ICCC,Paris Congress, II-III,63, 1980.

A17. Grudemo Ake , (1979), Cem.Concr.Res., 9pp. 19-34.

A18. Higgins D.D. and Bailey J.E.,(1976), Journal of Mat. Sci. 1, p.1995.

A19. Villa G. and Baretich, Proc. 7th Inter.Emis.Symp., Japan, 1984.

A20. Maji A. and Shah S.P., (1988), Exper. Mechanics, Vol 28,1, pp.27-33.

A21. McCabe W.M.,Koerner R.M., Lord A.E., (1976), ACI Journal,73, pp.367-71.

A22. Nielsen J., Griffin B., (1977), J.of Testing and Evaluation,5,(6), pp 476-483.

A23. Mehta,P.K.,(1985)Cem.Concr.Res.,15, pp.669-674.

APPENDIX 2 . GLASS

A 2.1 INTRODUCTION

Glass, the material that Griffith used to study crack propagation during brittle fracture and to develop his theory (see chapter 2.2), is the second comparison material (the first was cement) used in this work. Glass is a unique material in a sense that it is considered as a high viscosity liquid, with a structure consisting of irregular networks of silica tetrahedra bonded together with covalent bonds. This is an indication that possibly his theory is valid in cases where fracture occurs without prior plastic deformation near the crack tip.

A 2.2 EXPERIMENTAL RESULTS

A number of common soda-lime glass rods (XRF analysis shown in fig. A.7) 5.5 mm in diameter, and glass rectangular specimens of similar thickness, were used in 3-point bending and simultaneous AE testing, in order to get the statistical and acoustic behaviour of glass.

Acoustic emission, SEM examination and statistical results are shown in figs A.8 , A.9 and A.10 respectively. Glass, acoustically is a quiet material, where no Kaiser effect was found.

SEM examination reveals that glass is a homogenous material in which the fracture face has a smooth, mirror-like appearance. In accordance to LEFM, in

glass fracture occurs at the flaw whose stress intensity factor first reaches the fracture toughness of the material.

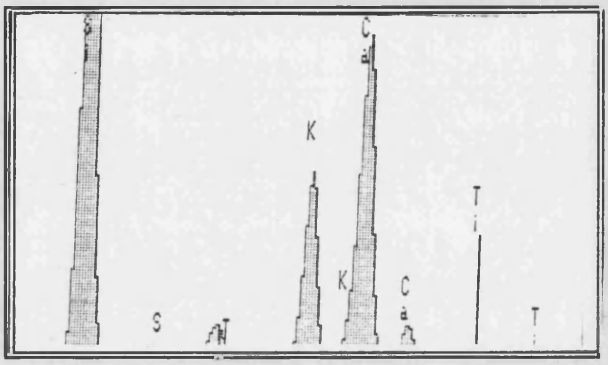

Fig. A.7 XRF spectrum of glass specimens

Comparison of the applicability of Weibull and Neville statistical functions, with the use of correlation coefficients is given in Table A.5

STATISTICAL CHARACTERISTICS OF COMPOSITE SPECIMENS					
TYPE OF MATERIAL	m	r_o	r_1	r_N	MOR_{th} MPa
GLASS	6.34	0.9741	0.9781	0.9839**	68

Table A.5 Statistical Characteristics of Glass resulting from Weibull and Neville functions, using Correlation Coefficients.

It seems that Neville function gives better results of both 2- and 3-parameter Weibull function.

Glass results and comparison with those of kaolin and composites are included in chapter 4.

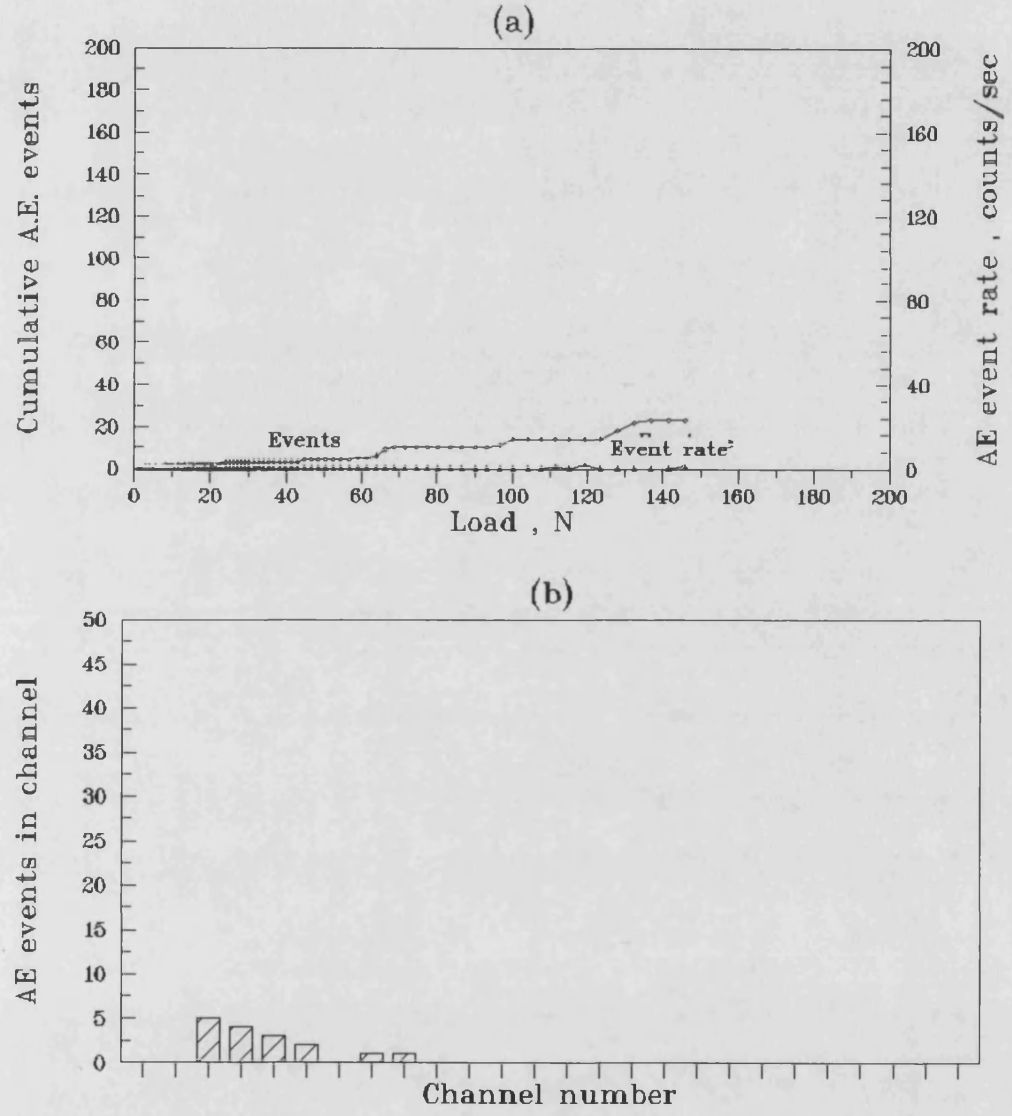

Fig. A.8 Acoustic emission from Glass specimens.

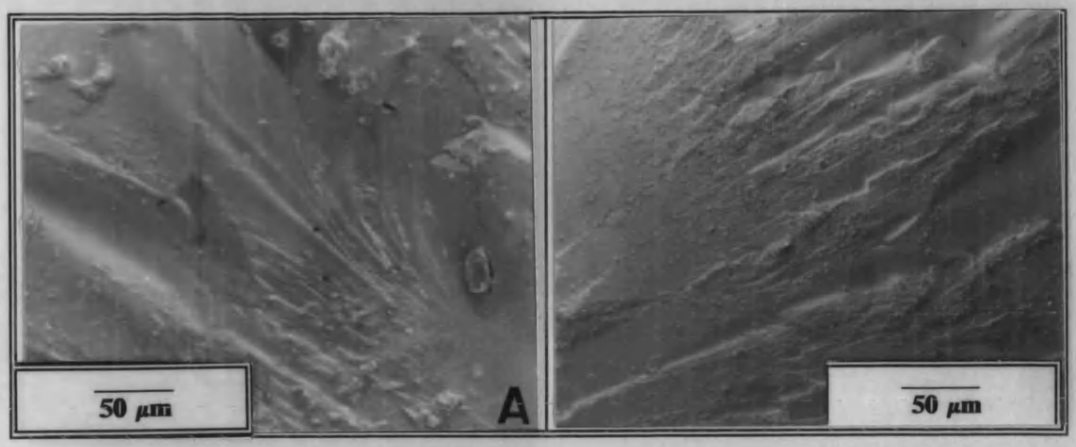

Fig. A.9 SEM examination of Glass specimens.

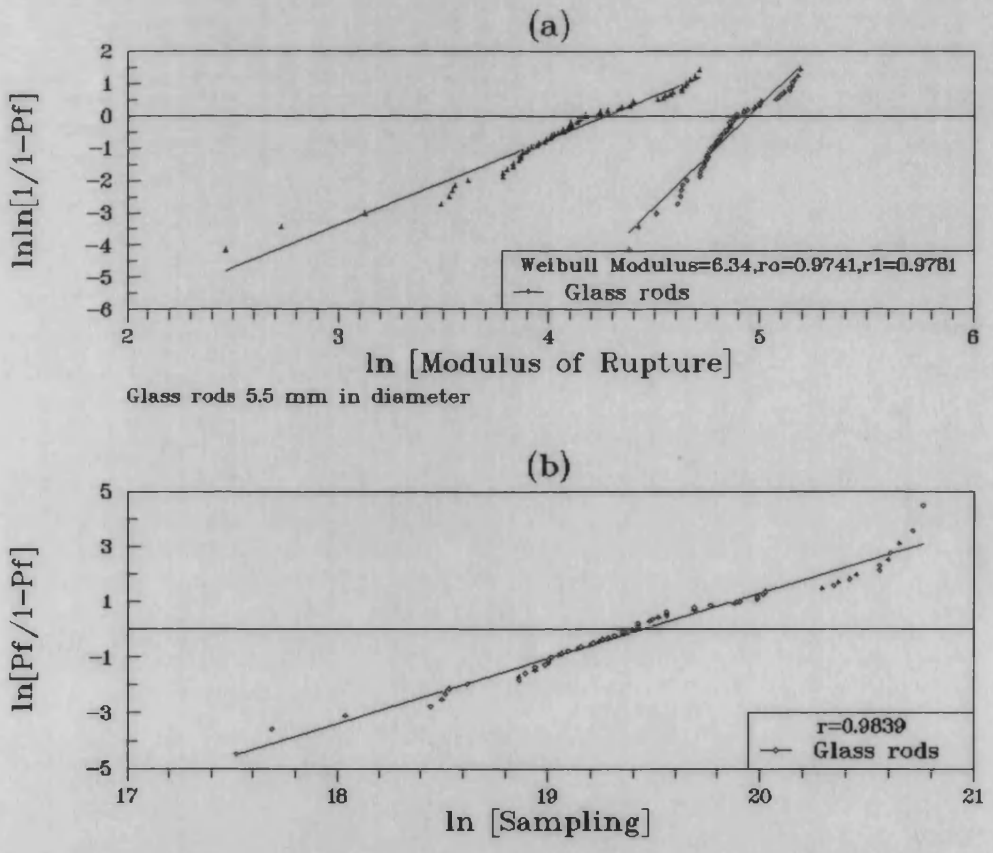

Fig. A.10 Weibull (a) and Neville (b) distributions of results from glass specimens. Modulus of Rupture MOR in MPa, Sampling $S=MOR^4$.